



Investigating Lymphatic Vascular Remodelling During Postnatal Mouse Mammary Gland Morphogenesis

KELLY LOUISE BETTERMAN

B Lab Med (Hons)

Thesis submitted for the degree of

Doctor of Philosophy

School of Medicine

Faculty of Health Sciences

The University of Adelaide

Lymphatic Development Laboratory

Division of Haematology

Centre for Cancer Biology

SA Pathology

July 2011

CONTENTS

<i>Contents</i>	<i>ii</i>
<i>Abstract</i>	<i>ix</i>
<i>Declaration</i>	<i>xi</i>
<i>Acknowledgements</i>	<i>xii</i>
<i>List of Figures</i>	<i>xiv</i>
<i>List of Tables</i>	<i>xvii</i>
<i>Abbreviations</i>	<i>xviii</i>

CHAPTER 1 **1-50**
Introduction

1.1 THE LYMPHATIC SYSTEM	2
1.1.1 Structure and function of the lymphatic system	2
1.1.2 Embryonic origin and development of the lymphatic system	6
1.1.3 Molecular markers used to identify lymphatic vessels and their role in lymphatic vascular development and function	11
1.1.3.1 Prox1	11
1.1.3.1.1 <i>Transcriptional regulation of Prox1 by Sox18 and COUP-TFII</i>	12
1.1.3.1.2 <i>Post-transcriptional regulation of Prox1 by miR-181a</i>	12
1.1.3.2 LYVE1	13
1.1.3.3 Podoplanin	14
1.1.3.4 VEGFR-3	14
1.1.3.5 Nrp2	15
1.1.3.6 CCL21	16
1.1.4 Lymphangiogenic growth factors and other molecules critical to lymphatic vascular growth, development and function	16
1.1.4.1 Lymphangiogenic growth factors	17
1.1.4.1.1 <i>VEGF-C and VEGF-D</i>	17
1.1.4.1.2 <i>Angiopoietins and Tie receptors</i>	18
1.1.4.1.3 <i>FGF-2</i>	20
1.1.4.1.4 <i>HGF</i>	20
1.1.4.1.5 <i>Insulin-like growth factors</i>	21
1.1.4.1.6 <i>PDGF-BB</i>	21
1.1.4.2 Other molecules critical to lymphatic vascular growth, development and function	21
1.1.4.2.1 <i>Adrenomedullin</i>	21
1.1.4.2.2 <i>Ccbe1</i>	22
1.1.4.2.3 <i>EphrinB2</i>	22
1.1.4.2.4 <i>Fiaf</i>	22
1.1.4.2.5 <i>FOXC2</i>	23
1.1.4.2.6 <i>Integrin-α9</i>	23
1.1.4.2.7 <i>Netrin-4</i>	24
1.1.4.2.8 <i>Sky and SLP-76</i>	24

1.2 THE MOUSE MAMMARY GLAND	25
1.2.1 Introduction to the mammary gland	25
1.2.2 Cellular composition of the mouse mammary gland	25
1.2.3 Mouse mammary gland morphogenesis	27
1.2.3.1 Embryonic mammary gland development	27
1.2.3.2 Postnatal mammary gland development	28
1.2.3.2.1 Pubertal mammary gland development	28
1.2.3.2.2 The adult nulliparous mammary gland	30
1.2.3.2.3 Mammary gland development during pregnancy and lactation	30
1.2.3.2.4 Involution	31
1.2.3.3 Key hormones involved in mouse mammary gland morphogenesis	31
1.2.3.3.1 Estrogen	31
1.2.3.3.2 Progesterone	32
1.2.3.3.3 Prolactin	32
1.2.4 A comparison of the mouse and human mammary glands	33
1.2.5 Blood vascular remodelling during postnatal mouse mammary gland morphogenesis	35
1.2.5.1 Puberty	36
1.2.5.2 Pregnancy	36
1.2.5.3 Lactation	36
1.2.5.4 Involution	38
1.2.5.5 Regulators of mammary blood vascular remodelling in the mouse	38
1.2.6 The mammary lymphatic vascular network	40
1.2.6.1 In the human breast	40
1.2.6.2 In the mouse mammary gland	42
1.3 BREAST CANCER AND LYMPHATIC VESSELS	42
1.3.1 Tumour metastasis	43
1.3.1.1 Breast cancer-related metastasis	44
1.3.1.1.1 Inhibiting lymphangiogenesis	45
1.3.2 Lymphoedema	46
1.3.2.1 Breast cancer-related lymphoedema	47
1.3.2.1.1 Therapeutic lymphangiogenesis	48
1.4 PROJECT RATIONALE AND AIMS	49

CHAPTER 2**51-71***Materials and Methods*

2.1 MATERIALS	52
2.1.1 Standard solutions	52
2.1.2 Bacterial media	52
2.1.3 Antibodies	53
2.2 METHODS	53
2.2.1 RNA analysis	53
2.2.1.1 RNA isolation	53
2.2.1.2 Determination of RNA concentration	56
2.2.1.3 First-strand cDNA synthesis	56
2.2.1.4 Real-time RT-PCR	56
2.2.2 Plasmid DNA cloning and purification	58
2.2.2.1 PCR amplification	58
2.2.2.2 DNA agarose gel electrophoresis	58

2.2.2.3 DNA extraction from agarose gels	59
2.2.2.4 Restriction enzyme digestion of DNA	59
2.2.2.5 Ligation reactions	59
2.2.2.6 Preparation of chemically-competent cells	60
2.2.2.7 Transformation of chemically-competent cells	60
2.2.2.8 Small-scale plasmid DNA production and purification	61
2.2.2.8.1 <i>Small-scale plasmid DNA production</i>	61
2.2.2.8.2 <i>Small-scale plasmid DNA purification</i>	61
2.2.2.9 Plasmid DNA sequencing	62
2.2.2.9.1 <i>DNA sequencing reaction</i>	62
2.2.2.9.2 <i>DNA sequencing product purification</i>	62
2.2.2.10 Large-scale plasmid DNA production and purification	62
2.2.2.10.1 <i>Large-scale plasmid DNA production</i>	62
2.2.2.10.2 <i>Long-term storage of plasmid DNA</i>	62
2.2.2.10.3 <i>Large-scale plasmid DNA purification</i>	63
2.2.2.11 Determination of DNA concentration	63
2.2.3 Mouse studies	63
2.2.3.1 Transgenic mice	64
2.2.4 Mammary gland collection, processing and sectioning	64
2.2.4.1 Mammary gland dissection	64
2.2.4.2 Mammary gland fixation	66
2.2.4.2.1 <i>Paraformaldehyde fixation</i>	66
2.2.4.2.2 <i>Formaldehyde fixation</i>	66
2.2.4.2.3 <i>Carnoy's solution fixation</i>	66
2.2.4.3 Mammary gland processing and sectioning	67
2.2.4.3.1 <i>Fixed-frozen mammary gland tissue</i>	67
2.2.4.3.2 <i>Paraffin-embedded mammary gland tissue</i>	67
2.2.5 Cell isolation and culture	68
2.2.5.1 Mammary gland cell isolation	68
2.2.5.2 Analysis of cell number and viability	69
2.2.5.3 Visualising cell morphology via light microscopy	69
2.2.6 Statistical analysis	69

CHAPTER 3**72-97**

Lymphatic vessels are dynamically remodelled during postnatal mouse mammary gland morphogenesis

3.1 INTRODUCTION	73
3.1.1 Lymphatic vessel patterning in other reproductive organs	73
3.1.1.1 The ovarian lymphatic vasculature	73
3.1.1.2 The uterine lymphatic vasculature	74
3.2 METHODS	75
3.2.1 Mammary gland carmine alum staining	75
3.2.2 Immunofluorescent immunostaining of mouse mammary gland sections	76
3.2.3 Lymphatic vessel quantification	76
3.2.4 Whole mount immunofluorescent immunostaining of mouse mammary glands	77
3.3 RESULTS	78
3.3.1 The ductal epithelial network is extensively remodelled during postnatal mouse mammary gland morphogenesis	78

3.3.2 Mammary lymphatic vessel density is elevated during pregnancy	78
3.3.3 Lymphatic vessels are spatially associated with mammary ducts and large blood vessels in the mouse mammary gland	80
3.3.4 Lymphatic vessel density in the mouse mammary gland correlates with density of the epithelial tree	87
3.3.5 Prox1 expression is not restricted to lymphatic vessels, but is also expressed in venous valves in the mouse mammary gland	90
3.4 DISCUSSION	92
3.5 CONCLUSION	97

CHAPTER 4

98-152

Investigating signals that regulate lymphatic vascular remodelling in the postnatal mouse mammary gland

4.1 INTRODUCTION	99
4.1.1 Biosynthesis and proteolytic processing of VEGF-C and VEGF-D	99
4.2 METHODS	103
4.2.1 Immunofluorescent immunostaining of paraffin-embedded mammary gland sections	103
4.2.2 <i>In situ</i> hybridisation	104
4.2.2.1 Production of DIG-labelled RNA probes	104
4.2.2.1.1 Generation of plasmid templates	104
4.2.2.1.2 Plasmid template linearisation	105
4.2.2.1.3 Linearised plasmid template precipitation	105
4.2.2.1.4 <i>In vitro</i> transcription of DIG-labelled RNA probes	105
4.2.2.1.5 DIG-labelled RNA probe precipitation	106
4.2.2.2 <i>In situ</i> hybridisation	106
4.2.2.2.1 Day 1 - Pre-hybridisation and hybridisation	106
4.2.2.2.2 Day 2 - Post-hybridisation washes	107
4.2.2.2.3 Day 3 - Immunological detection	107
4.2.2.2.4 Day 4 - Termination of colour development	107
4.2.3 RNA isolation from entire mouse mammary glands	107
4.2.4 Protein collection and analysis	108
4.2.4.1 Protein collection	108
4.2.4.2 Determination of protein concentration	108
4.2.4.3 Western blot analysis	108
4.2.4.3.1 SDS-PAGE	108
4.2.4.3.2 Electrophoretic transfer	109
4.2.4.3.3 Immunoblotting	109
4.2.4.3.4 Detection	109
4.2.5 <i>Ex vivo</i> lymphatic endothelial cell proliferation assay	110
4.2.5.1 Primary lymphatic endothelial cell isolation from embryonic mouse dermis	110
4.2.5.1.1 Dissection and enzymatic digestion of embryonic dermis	110
4.2.5.1.2 Depletion of contaminating macrophages	110
4.2.5.1.3 Isolation of lymphatic endothelial cells via positive selection with LYVE1	111
4.2.5.2 Mammary gland cell suspension culture and collection of conditioned media	111
4.2.5.2.1 Initial preparation and collection of first batch of conditioned media	111
4.2.5.2.2 Cell passaging and collection of second batch of conditioned media	112
4.2.5.2.3 Collection of third batch of conditioned media	112
4.2.5.2.4 Cell imaging	112

4.2.5.3 Cell proliferation assays	112
4.2.5.3.1 Conditioned media experiments	113
4.2.5.3.2 Small molecule inhibitor studies	113
4.2.6 Cell monolayer immunohistochemistry	114
4.2.7 Analysis of <i>Vegfd</i>-deficient mouse mammary glands	114
4.3 RESULTS	115
4.3.1 Lymphatic endothelial cells in the mouse mammary gland lack detectable expression of estrogen receptor alpha and progesterone receptor	115
4.3.2 <i>Vegfa</i> and <i>Pdgfa</i> are expressed in the epithelial cell compartment of the mouse mammary gland	117
4.3.3 The expression of pro-lymphangiogenic growth factors is dynamically regulated at the level of mRNA and protein during postnatal mouse mammary gland morphogenesis	119
4.3.3.1 Investigation of pro-lymphangiogenic growth factor expression by real-time RT-PCR	119
4.3.3.2 Investigation of pro-lymphangiogenic growth factors at the protein level	121
4.3.4 Myoepithelial cells are a rich source of pro-lymphangiogenic stimuli in the mouse mammary gland	125
4.3.5 Lymphatic endothelial cell proliferation <i>ex vivo</i> is promoted by conditioned media harvested from mammary gland cell suspension cultures	127
4.3.6 Mammary gland conditioned media promotes lymphatic endothelial cell proliferation <i>ex vivo</i> via VEGFR-3 and FGFR-1	131
4.3.6.1 Selection of small molecule inhibitors	131
4.3.6.2 MAZ51 and SU5416 inhibit VEGF-C- and VEGF-D-induced lymphatic endothelial cell proliferation <i>ex vivo</i>	132
4.3.6.3 MAZ51 and SU5402 inhibit mammary gland conditioned media-induced lymphatic endothelial cell proliferation <i>ex vivo</i>	134
4.3.7 <i>Vegfd</i> is dispensable for lymphangiogenesis during postnatal mouse mammary gland morphogenesis	134
4.3.8 <i>Vegfd</i>-deficiency in the pregnant mouse mammary gland has no effect on epithelial architecture	137
4.4 DISCUSSION	137
4.5 CONCLUSION	151

CHAPTER 5**153-196***Microarray analysis of isolated mammary gland cell populations*

5.1 INTRODUCTION	154
5.2 METHODS	154
5.2.1 Mammary gland FACS	154
5.2.1.1 Cell labelling	154
5.2.1.2 Flow cytometry	155
5.2.2 RNA isolation	155
5.2.2.1 DNase inactivation	157
5.2.3 Determination of isolated cell population purity	157
5.2.4 Assessment of RNA quantity and quality	157
5.2.5 Generation of samples for microarray analysis	158
5.2.5.1 RNA amplification	158
5.2.5.2 Purification of amplified cDNA	159
5.2.5.3 Generation and purification of ST-cDNA	159
5.2.5.4 Fragmentation and biotin-labelling of ST-cDNA	159

5.2.6 Microarray data analysis	160
5.3 RESULTS	160
5.3.1 FACS gating strategy optimisation	160
5.3.2 Assessment of the purity of isolated mammary gland cell populations	161
5.3.3 Microarray analyses	168
5.3.4 Validation of microarray data sets	174
5.3.4.1 Luminal epithelial cell array	174
5.3.4.2 Myoepithelial cell array	174
5.3.4.3 Haematopoietic cell array	176
5.3.4.4 Endothelial cell array	177
5.3.4.5 Pregnant epithelial cell array	178
5.3.5 Candidate genes identified from microarray analyses likely involved in vascular remodelling in the postnatal mouse mammary gland	179
5.3.6 <i>Bfk</i> is increased during pregnancy in the mouse mammary gland	182
5.4 DISCUSSION	182
5.4.1 Novel genes likely involved in vascular remodelling in the postnatal mouse mammary gland	186
5.4.1.1 <i>Cxcl15</i>	187
5.4.1.2 <i>Adam10</i>	188
5.4.1.3 <i>Anxa1</i>	190
5.4.1.4 <i>Tnc</i>	191
5.4.1.5 <i>Mmp2</i>	192
5.4.1.6 <i>Bdnf</i>	193
5.4.2 <i>Bfk</i> is an interesting gene likely involved in postnatal mouse mammary gland morphogenesis	194
5.5 CONCLUSION	195

CHAPTER 6 **197-222**

Investigating the role of Patched 1 in mammary gland lymphatic vessels

6.1 INTRODUCTION	198
6.1.1 An overview of the Hedgehog signalling pathway	198
6.1.2 Patched 1	201
6.1.2.1 Generation of <i>Ptch1^{lacZ/+}</i> mice	201
6.1.2.2 <i>Patched 1</i> mouse models	202
6.2 METHODS	203
6.2.1 Genotyping of <i>Ptch1^{lacZ/+}</i> mice	203
6.2.1.1 Genomic DNA extraction from mouse tails	203
6.2.1.2 Genotyping PCR primers	204
6.2.1.3 Genotyping PCR	204
6.2.2 Mammary gland whole mount X-gal staining	204
6.2.3 Mammary gland section DAB immunostaining	205
6.2.4 Embryonic and adult mouse tissue collection, processing and immunostaining	206
6.2.4.1 Embryonic and adult tissue collection and fixation	206
6.2.4.2 Embryonic and adult tissue whole mount X-gal staining	206
6.2.4.3 Embryonic and adult tissue cryopreservation and sectioning	207
6.2.4.4 Embryonic and adult tissue DAB immunostaining	207
6.2.4.4.1 Embryonic and adult tissue section DAB immunostaining	207
6.2.4.4.2 Adult tissue whole mount DAB immunostaining	207

6.2.4.5 Whole mount embryonic dermal skin immunofluorescent immunostaining	207
6.3 RESULTS	208
6.3.1 <i>Ptch1</i> is not expressed in mammary gland lymphatic vessels	208
6.3.2 <i>Ptch1</i> is not expressed in the lymphatic vasculature of other adult tissues	210
6.3.3 <i>Ptch1</i> is not expressed in lymphatic vessels during embryonic development	213
6.3.4 <i>Ptch1</i> haploinsufficiency does not affect lymphatic vessel patterning in embryonic skin	217
6.4 DISCUSSION	217
6.5 CONCLUSION	221
CHAPTER 7	223-233
<hr/>	
<i>Discussion</i>	
7.1 DISCUSSION	224
7.2 FUTURE DIRECTIONS	230
7.3 CONCLUSION	233
REFERENCES	234-266

ABSTRACT

The lymphatic vasculature, an essential component of the cardiovascular system, serves several functions critical to embryonic development and adult homeostasis. Lymphatic vessels return interstitial protein-rich fluid to the bloodstream, transport immune cells during immune surveillance and infection and absorb lipids from the digestive tract (Alitalo et al., 2005; Tammela and Alitalo, 2010). The aberrant growth and development of lymphatic vessels (lymphangiogenesis) is a common feature of human disorders including lymphoedema, inflammatory diseases and tumour metastasis (Alitalo et al., 2005; Tammela and Alitalo, 2010). Lymphatic vessels are of key importance to breast cancer patients. Lymphatic vessels are exploited as a key route of metastasis for tumour cells and the ability of a tumour to promote lymphangiogenesis has been linked with metastasis and poor patient prognosis (Gu et al., 2008; Nakamura et al., 2005; Nakamura et al., 2003; Ran et al., 2010; Skobe et al., 2001). Moreover, lymphatic vascular damage incurred during the surgical resection of lymph nodes commonly results in secondary lymphoedema, a debilitating complication for up to 40% of breast cancer patients (Armer et al., 2009). Despite the involvement of lymphatic vessels in breast cancer, the genes and molecular mechanisms that regulate lymphangiogenesis in the breast remain relatively uncharacterised.

The mammary epithelium and blood vasculature undergo dynamic remodelling events in response to hormonal signals and functional demands during postnatal mouse mammary gland morphogenesis (Djonov et al., 2001; Matsumoto et al., 1992; Richert et al., 2000; Watson and Khaled, 2008). The aims of this project were:

1. To investigate the spatial organisation of lymphatic vessels in the mouse mammary gland.
2. To investigate whether lymphatic vessels, like blood vessels and the mammary epithelial tree, are temporally remodelled during mouse mammary gland morphogenesis.
3. To define signals that regulate lymphangiogenesis during postnatal mouse mammary gland morphogenesis.

This study provides the first evidence demonstrating that the lymphatic vasculature is dynamically remodelled along with the mammary epithelial tree and blood vasculature during postnatal mouse mammary gland morphogenesis. In addition, this study reveals an intimate association of lymphatic vessels with epithelial ducts, a finding that has important implications for tumour metastasis, as well as the spatial organisation of lymphatic vessels in other branched epithelial tissues, including the lung, kidney, pancreas and prostate. Furthermore, we established that vascular endothelial growth factor

(Vegf) C (*Vegfc*) and *Vegfd* mRNA levels are significantly increased early during pregnancy and that proteolytically-processed, active VEGF-D is expressed selectively in pregnant, but not virgin mouse mammary glands, corresponding with the stage of peak lymphatic vessel density. In accordance with these data, we demonstrated that a tyrosine kinase inhibitor specific for VEGF receptor 3 (Kirkin et al., 2001; Kirkin et al., 2004), the principal receptor for mouse VEGF-C and VEGF-D, can block the proliferation of primary dermal lymphatic endothelial cells that is stimulated by mammary epithelial and stromal cell conditioned media *ex vivo*. These data suggest that VEGF-C and VEGF-D, two of the best characterised lymphangiogenic stimuli to date, are likely to play key roles in the stimulation of lymphangiogenesis in the pregnant mouse mammary gland. Elucidation of the molecular mechanisms controlling lymphangiogenesis in the mammary gland has the potential to reveal important targets for the future generation of pro- and anti-lymphangiogenic therapeutics, with the ultimate goal to repair surgically damaged lymphatic vessels and prevent breast cancer metastasis, respectively.

DECLARATION

This work contains no material which has been accepted for the award of any other degree or diploma in any university or other tertiary institution to Kelly Louise Betterman and, to the best of my knowledge and belief, contains no material previously published or written by another person, except where due reference has been made in the text.

I give consent to this copy of my thesis, when deposited in the University Library, being made available for loan and photocopying, subject to the provisions of the Copyright Act 1968.

I also give permission for the digital version of my thesis to be made available on the web, via the University's digital research repository, the Library catalogue and also through web search engines, unless permission has been granted by the University to restrict access for a period of time.

Kelly Louise Betterman

ACKNOWLEDGEMENTS

First and foremost, I would like to sincerely thank my supervisor, mentor and friend, Dr Natasha Harvey, for her endless guidance, encouragement, support, patience and most of all, positivity over the past four years. There have been many times when I felt beaten, but you made sure that I never lost sight of the big picture! It has been a great honour and privilege to undertake my PhD in your laboratory. Tash, you are an inspiration to any woman embarking on a career in research. I can only hope that one day I will be half as good a scientist as you!

Thank you to past and present members of the Lymphatic Development Laboratory for filling my days with gossip, laughter, food and coffee (the latter two obviously not consumed in the PC2 lab of course) and for developing my taste for wine! I am especially grateful to my two 'lab mums', Jan and Gen, for keeping me grounded, their friendship and their ever-willingness to provide assistance when needed. Jan, you are a walking scientific encyclopaedia! How can I ever repay you both?! Emma, although you are now on the other side of the world, rest assured that your pipettes are in very safe hands!

Thank you also to my co-supervisor, Dr Lisa Butler, for her valuable technical advice and constructive feedback in lab meetings, to the staff and students of the Division of Haematology and Centre for Cancer Biology for help when required and for providing a fun environment to work in, and to the National Breast Cancer Foundation for funding me with a prestigious Doctoral Research Scholarship, without which this study would not have been possible.

Last, but by all means not least, I could not have completed this PhD without the endless support of my friends and family, to whom I am most grateful!

To my APP gurlies, Darshika and Harshani, thank you for listening to my constant whinging and whining, but most of all thank you for your friendship over the past few years. I hope we can remain friends for life. This *Chief* will miss you dearly! To Diana, Chantelle, Rebecca, Tori, Felix and of course the 'Big GM' Robert, for all the laughter and lab-related shenanigans making those long nights at the lab all-the-more bearable!

To Laura and Chun Chun, *Saltcake* and *Lil' soldier*, my fellow PhD buddies who have battled alongside me from the beginning. Thank you for the laughter, your understanding, countless coffee breaks and for

the constant reminders that I am not alone...we can all have Permanent Head Damage together! Now, it's time for the *Commander* to make sure her battalion isn't left behind in combat. Girls, you can do it!!! I am eagerly awaiting sharing a drink...or two...or three...or more...with you both at the end of this 'war'. Pick up those weapons and fight...or should I say write?!

To Nas, my running buddy, how could I have made it through 'thesisanity' without all those gym sessions, 'Mt Everest' challenges, pancakes and late night motivational messages...'toughen up princess'...actually I probably would have made it through a whole lot less sore!

Most importantly, to my family, Mum, Dad and Nanna, thank you from the bottom of my heart for believing in me!

LIST OF FIGURES
CHAPTER 1

Figure 1.1	The lymphatic system	3
Figure 1.2	Characteristic features of the lymphatic vasculature	4
Figure 1.3	Development of the mammalian lymphatic vasculature	7
Figure 1.4	Populations of cells that reside in the mouse mammary gland	26
Figure 1.5	Stages of postnatal mouse mammary gland development	29
Figure 1.6	A comparison between human and mouse mammary tissue	34
Figure 1.7	Blood vascular remodelling during postnatal mouse mammary gland morphogenesis	37
Figure 1.8	Historical drawings of the human breast lymphatic network	41

CHAPTER 2

Figure 2.1	Mouse mammary gland dissection	65
Figure 2.2	Diagrammatic representation of a haemocytometer	70

CHAPTER 3

Figure 3.1	Carminium alum-stained postnatal mouse mammary glands	79
Figure 3.2	Mammary lymphatic vessel density is elevated during pregnancy	81
Figure 3.3	Lymphatic vessels are spatially associated with mammary ducts and large blood vessels in the mouse mammary gland	82
Figure 3.4	Mammary lymphatic vessels do not form 'capillary baskets' surrounding the alveoli	83
Figure 3.5	Lymphatic vessels are intimately associated with the epithelial tree in virgin, but not pubertal mouse mammary glands	85
Figure 3.6	Lymphatic vessels are intimately associated with mammary ducts, but not the alveoli, in pregnant mouse mammary glands	86
Figure 3.7	The ductal tree is dynamically remodelled during postnatal mouse mammary gland morphogenesis	88
Figure 3.8	Mammary lymphatic vessel density correlates with density of the epithelial tree	89
Figure 3.9	Prox1 is expressed in venous valves in the mouse mammary gland	91

CHAPTER 4

Figure 4.1	Schematic representation of mouse VEGF-D biosynthesis, proteolytic processing and alternatively-spliced transcripts	100
------------	---	-----

Figure 4.2	Lymphatic endothelial cells do not express estrogen receptor alpha or progesterone receptor in the mouse mammary gland	116
Figure 4.3	<i>Vegfa</i> and <i>Pdgfa</i> are expressed in mammary epithelial cells	118
Figure 4.4	The expression of pro-lymphangiogenic growth factors is dynamically regulated at the mRNA level during mouse mammary gland morphogenesis	120
Figure 4.5	<i>Reln</i> mRNA levels are increased at an early stage of pregnancy relative to virgin and late pregnant stages	122
Figure 4.6	Angpt2, but not Angpt1 protein, is increased in pregnant mouse mammary glands	123
Figure 4.7	Mature VEGF-D is present selectively in pregnant, but not virgin mouse mammary glands	124
Figure 4.8	The expression of pro-lymphangiogenic growth factors is elevated in myoepithelial cells	126
Figure 4.9	Mammary gland conditioned media promotes lymphatic endothelial cell proliferation <i>ex vivo</i>	128
Figure 4.10	The cellular composition of mammary gland cell suspension cultures is different between passages 0 and 1	129
Figure 4.11	MAZ51 and SU5416 inhibit VEGF-C- and VEGF-D-induced lymphatic endothelial cell proliferation <i>ex vivo</i>	133
Figure 4.12	Mammary gland conditioned media promotes lymphatic endothelial cell proliferation <i>ex vivo</i> via VEGFR-3 and FGFR-1	135
Figure 4.13	Lymphatic vessel patterning is unaffected in virgin <i>Vegfd</i> ^{-/-} mouse mammary glands	136
Figure 4.14	Lymphatic vessel patterning is normal in pregnant <i>Vegfd</i> ^{-/-} mouse mammary glands	138
Figure 4.15	The ductal architecture is normal in pregnant <i>Vegfd</i> ^{-/-} mouse mammary glands	139

CHAPTER 5

Figure 5.1	FACS gating strategy used for the isolation of 8 week virgin mammary gland cell populations	162
Figure 5.2	FACS gating strategy used for the isolation of 16.5 day pregnant mammary gland cell populations	164
Figure 5.3	Assessment of isolated mammary gland cell population purity	167
Figure 5.4	Principal component analysis plots	169
Figure 5.5	<i>Cxcl15</i> mRNA levels are elevated at an early stage of pregnancy relative to virgin and late pregnant stages	180
Figure 5.6	<i>Bfk</i> mRNA levels are increased in pregnant mouse mammary glands	183

CHAPTER 6

Figure 6.1	A simplified model of Hedgehog signalling in mammalian cells	200
Figure 6.2	<i>Ptch1</i> is expressed in a subset of cells associated with peripheral nerve fibres in the mouse mammary gland	209
Figure 6.3	<i>Ptch1</i> is not expressed in lymphatic vessels of adult mouse tissues	211
Figure 6.4	Expression of <i>Ptch1</i> during murine embryogenesis	214
Figure 6.5	Detailed expression analysis of <i>Ptch1</i> during murine embryogenesis	215
Figure 6.6	Dermal lymphatic vessels are patterned normally in <i>Ptch1^{lacZ/+}</i> mice	218
Figure 6.7	LYVE1-positive macrophages in the mouse mammary gland	220

LIST OF TABLES**CHAPTER 2**

Table 2.1	A list of primary antibodies and their conditions of use	54
Table 2.2	A list of directly-conjugated primary and secondary antibodies and their condition of use	55
Table 2.3	Primer pairs used for real-time RT-PCR analyses in <i>Mus musculus</i>	57

CHAPTER 5

Table 5.1	FACS gating strategy used to isolate enriched populations of cells from the mouse mammary gland	156
Table 5.2	A comparison of cell yields following FACS of virgin and pregnant mouse mammary glands	166
Table 5.3	Top 40 differentially expressed genes between endothelial cells in virgin and pregnant mouse mammary glands	170
Table 5.4	Top 40 differentially expressed genes between haematopoietic cells in virgin and pregnant mouse mammary glands	171
Table 5.5	Top 40 differentially expressed genes between luminal epithelial cells in virgin and pregnant mouse mammary glands	172
Table 5.6	Top 40 differentially expressed genes between myoepithelial cells in virgin and pregnant mouse mammary glands	173
Table 5.7	Top 40 differentially expressed genes between myoepithelial and luminal epithelial cells in pregnant mouse mammary glands	175

ABBREVIATIONS

α SMA	alpha smooth muscle actin
β -gal	beta-galactosidase
μ g	microgram
μ l	microlitre
μ m	micrometre
μ M	micromolar
ADAM10	a disintegrin and metalloproteinase 10
AGE	agarose gel electrophoresis
Angpt	angiopoietin
ANOVA	analysis of variance
AnxA1	annexin A1
AP	alkaline phosphatase
ApoER2	apolipoprotein E receptor 2
APS	ammonium persulphate
BABB	benzyl alcohol:benzyl benzoate
BC	Before Christ
BCA	bicinchoninic acid
BCIP	5-bromo-4-chloro-3-indolyl phosphate
Bcl2	B-cell lymphoma 2
BDNF	brain-derived neurotrophic factor
BEC	blood endothelial cells
Bfk	B-cell lymphoma 2 family kin
BH	Bcl2 homology
bp	base pair
BSA	bovine serum albumin
BVI	blood vascular invasion
ccbe1	collagen and calcium binding EGF domains 1
CCL21	chemokine (C-C motif) ligand 21
CD	cluster of differentiation
cDNA	complementary deoxyribonucleic acid
CLEC-2	C-type lectin-like receptor 2

cm	centimetre
CM	conditioned media
cm ²	square centimetre
CO ₂	carbon dioxide gas
COUP-TFII	chicken ovalbumin upstream promoter transcription factor 2
CXCL15	chemokine (CXC motif) ligand 15
DAB	3,3'-diaminobenzidine
Dab1	disabled homolog 1
DAPI	4',6-diamidino-2-phenylindole
DEPC	diethylpyrocarbonate
DIG	digoxigenin
DMEM	Dulbecco's Modified Eagle's Medium
DMEM-10%FBS	Dulbecco's Modified Eagle's Medium supplemented with 10% (v/v) foetal bovine serum
DMEM-20%FBS	Dulbecco's Modified Eagle's Medium supplemented with 20% (v/v) foetal bovine serum
DMEM-5%FBS	Dulbecco's Modified Eagle's Medium supplemented with 5% (v/v) foetal bovine serum
DMSO	dimethyl sulfoxide
DNA	deoxyribonucleic acid
DNase	deoxyribonuclease
dNTP	deoxyribonucleotide triphosphate
DTT	1,4-dithiothreitol
E	embryonic day
EBM®-2	Endothelial Cell Basal Medium®-2
EC	endothelial cells
ECF	enhanced chemifluorescence
EDTA	ethylenediaminetetraacetic acid
EGTA	ethylene glycol tetraacetic acid
ELISA	enzyme-linked immunosorbent assay
ELR ⁺	ELR motif; glutamic acid-leucine-arginine
EphB4	Eph receptor B4
ER α	estrogen receptor alpha
ER β	estrogen receptor beta

FACS	fluorescence-activated cell sorting
FBS	foetal bovine serum
FGF	fibroblast growth factor
FGF-1	fibroblast growth factor 1
FGF-2	fibroblast growth factor 2
FGFR-1	fibroblast growth factor receptor 1
Fiaf	fasting-induced adipose factor
FITC	fluorescein isothiocyanate
Flt4	FMS-like tyrosine kinase 4
FOXC2	forkhead box C2
G	gauge
g	gram
GFP	green fluorescent protein
Gli	glioma-associated
Gli1	glioma-associated 1
HBSS	Hank's balanced salt solution
HCl	hydrochloric acid
HEPES	4-(2-hydroxyethyl)-1-piperazineethanesulphonic acid
HGF	hepatocyte growth factor
HGFR	hepatocyte growth factor receptor
Hh	Hedgehog
HHF	Hank's balanced salt solution containing 10mM 4-(2-hydroxyethyl)-1-piperazineethanesulphonic acid and 5% (v/v) foetal bovine serum
IDC	invasive ductal carcinoma
IDL	invasive lobular carcinoma
IGF-1	insulin-like growth factor 1
IGF-2	insulin-like growth factor 2
IPTG	isopropyl- β -D-thiogalactosidase
JLS	jugular lymph sac
K14	cytokeratin 14
K18	cytokeratin 18
KCl	potassium chloride
kDa	kilodalton
KOH	potassium hydroxide

L	litre
LB	Luria Bertani
LEC	lymphatic endothelial cells
LVI	lymphatic vascular invasion
LYVE1	lymphatic vessel endothelial hyaluronan receptor 1
M	Molar
mA	milliamp
MACS	magnetic-activated cell sorting
MAZ51	3-(4-dimethylamino-naphthalen-1-ylmethylene)-1,3-dihydro-indol-2-one
mg	milligram
MgCl ₂	magnesium chloride
ml	millilitre
mm	millimetre
mM	millimolar
MMP	matrix metalloproteinase
MMTV	mouse mammary tumour virus
MQ-H ₂ O	Milli-Q water
mRNA	messenger ribonucleic acid
MTS	3-(4,5-dimethylthiazol-2-yl)-5-(3-carboxymethoxyphenyl)-2-(4-sulfophenyl)-2H-tetrazolium, inner salt
N	Normality
NaCl	sodium chloride
NaOAc	sodium acetate
NaOH	sodium hydroxide
NBT	nitro blue tetrazolium chloride
NFATc1	nuclear factor of activated T-cells, cytoplasmic, calcineurin-dependent 1
ng	nanogram
nm	nanometre
Nrp2	neuropilin 2
O.C.T	optimal cutting temperature
°C	degree Celsius
pBS	pBluescript II SK (+)
PBS	phosphate-buffered saline

PBS-0.1%TW20	phosphate-buffered saline with 0.1% (v/v) Tween@20
PBS-0.1%TX100	phosphate-buffered saline with 0.1% (v/v) Triton@X-100
PBS-0.3%TW20	phosphate-buffered saline with 0.3% (v/v) Tween@20
PBS-0.3%TX100	phosphate-buffered saline with 0.3% (v/v) Triton@X-100
PBS-0.3%TX100-1%BSA	phosphate-buffered saline with 0.3% (v/v) Triton@X-100 and 1% (w/v) bovine serum albumin
PBS-2%FBS	phosphate buffered saline with 2% (v/v) foetal bovine serum
PC	proprotein convertase
PCA	principal component analysis
PCR	polymerase chain reaction
PDGF	platelet-derived growth factor
PDGFR α	platelet-derived growth factor receptor alpha
PDGFR β	platelet-derived growth factor receptor beta
PE	phycoerythrin
PFA	paraformaldehyde
pg	picogram
pmol	picomole
PR	progesterone receptor
Prox1	Prospero-related homeobox 1
Ptch1	Patched 1
PVDF	polyvinylidene fluoride
PyMT	polyomavirus middle T antigen
RIN	RNA Integrity Number
RIPA	radioimmunoprecipitation assay
RNA	ribonucleic acid
RNase	ribonuclease
RT	room temperature
RT-PCR	reverse transcription-polymerase chain reaction
SDS	sodium dodecyl sulphate
SDS-PAGE	sodium dodecyl sulphate-polyacrylamide gel electrophoresis
Shh	sonic hedgehog
SLC	secondary lymphoid organ chemokine
SLP-76	SH2 domain containing leukocyte protein of 76kDa
Smo	smoothened

Sox18	SRY-box containing gene 18
SSC	saline-sodium citrate
ST-cDNA	sense transcript-complementary deoxyribonucleic acid
SU5402	3-[(3-(2-carboxyethyl)-4-methylpyrrol-2-yl)methylene]-2-indolinone
SU5416	3-[(2,4-dimethylpyrrol-5-yl)methylidene]-indolin-2-one
sVEGFR-2	soluble vascular endothelial growth factor receptor 2
Syk	spleen tyrosine kinase
T25	25cm ² tissue culture flask
TBE	Tris-borate-ethylenediaminetetraacetic acid
TBS	Tris-buffered saline
TBS-0.1%TW20	Tris-buffered saline with 0.1% (v/v) Tween@20
TDLU	terminal ductal lobular unit
TE	Tris-ethylenediaminetetraacetic acid
TEB	terminal end bud
TEMED	N,N,N',N'-tetramethylethylenediamine
TFB	transformation buffer
TIMP	tissue inhibitor of metalloproteinase
Tnc	tenascin C
TrkB	tropomyosin-related kinase B
tRNA	transfer ribonucleic acid
TSP1	thrombospondin 1
TSP2	thrombospondin 2
U	unit
UV	ultraviolet
V	volt
v/v	volume per volume
VE-cadherin	vascular endothelial-cadherin
VEGF	vascular endothelial growth factor
VEGF-A	vascular endothelial growth factor A
VEGF-C	vascular endothelial growth factor C
VEGF-D	vascular endothelial growth factor D
VEGFR-1	vascular endothelial growth factor receptor 1
VEGFR-2	vascular endothelial growth factor receptor 2
VEGFR-3	vascular endothelial growth factor receptor 3

VHD	VEGF homology domain
VLDLR	very low density lipoprotein receptor
w/v	weight per volume
WECH	weird chemokine
WT	wild-type
x g	relative centrifugal force
X-gal	5-bromo-4-chloro-3-indolyl- β -D-galactopyranoside

CHAPTER 1

Introduction

1.1 THE LYMPHATIC SYSTEM

1.1.1 Structure and function of the lymphatic system

The lymphatic vasculature, an essential component of the cardiovascular system, is a characteristic feature of higher order vertebrates, including fish, amphibians, reptiles and mammals. The presence of lymphatic vessels in these animals is due to a strict requirement for fluid homeostasis and can be attributed to the increased complexity of their cardiovascular systems and larger body size (Alitalo et al., 2005; Tammela and Alitalo, 2010). Lymphatic vessels are present in almost all vascularised organs and tissues within the body, with the exception of the brain, bone marrow and retina and are absent in non-vascularised tissues such as cornea, hair, nails, epidermis and cartilage (Alitalo et al., 2005; Mäkinen et al., 2007; Tammela and Alitalo, 2010). Unlike the blood vasculature, which is a closed circulatory loop, the lymphatic system lacks a central pump and thus can be considered a low flow and low pressure system. The lymphatic vascular network comprises a hierarchical, linear open-ended vascular tree; initiating as a non-contractile lymphatic capillary plexus, constituting the absorptive component, which drains lymph from the extracellular spaces of most organs and tissues and progressively joins with larger lymphatic collecting vessels; the 'drainage' component, that in turn connect to the inferior vena cava via the largest lymphatic vessel in the body, the thoracic duct (Figure 1.1). The lymphatic system also comprises lymphoid organs such as chains of lymph nodes, tonsils, Peyer's patches in the small intestine, the spleen and thymus (Oliver and Detmar, 2002).

In mammals, the blood and lymphatic vascular networks develop as anatomically separate, yet functionally-related, circulatory systems. Despite the fact that both the blood vasculature and lymphatic vasculature operate in parallel, they display distinct structural features owing to their divergent roles. Lymphatic capillaries are thin-walled, blind-ended vessels characterised by the presence of loose intercellular junctions, a single layer of overlying endothelial cells (EC) and anchoring filaments that connect the basal surface of the lymphatic endothelial cells (LEC) to the surrounding extracellular matrix, preventing vessel collapse and enabling increased uptake of fluid by virtue of vessel lumen dilatation. Furthermore, lymphatic capillaries have little or absent basement membrane and lack supporting smooth-muscle-like contractile cells which encase the outer surface of blood vessels, known as pericytes (Figure 1.2B) (Alitalo et al., 2005; Mäkinen et al., 2007; Tammela and Alitalo, 2010). All of these distinguishing features render lymphatic capillaries highly permeable to the passive uptake of fluid, large macromolecules and cells. These lymphatic capillaries successively drain into pre-collector

NOTE:
The major figure is included on page 3
of the print copy of the thesis held in
the University of Adelaide Library.

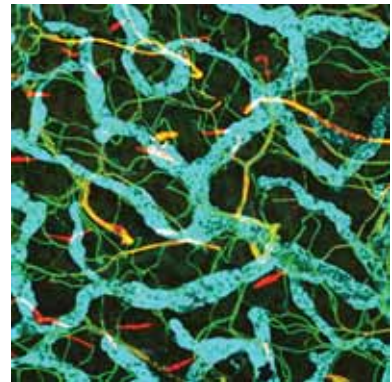


Figure 1.1 - The lymphatic system.

The lymphatic vascular network comprises a hierarchical vascular tree, which initiates as a capillary plexus (inset) specialised for collecting interstitial fluid. These lymphatic capillaries drain into larger lymphatic collecting vessels, which transport lymph through successive groups of lymph nodes to the thoracic duct. Inset demonstrates the blood (arterioles and venules) and lymphatic capillary plexuses in adult mouse ear skin. Figure adapted from Lacovara and Yoder, 2006 and inset kindly provided by Natasha L. Harvey (Centre for Cancer Biology, SA Pathology, Adelaide, Australia).

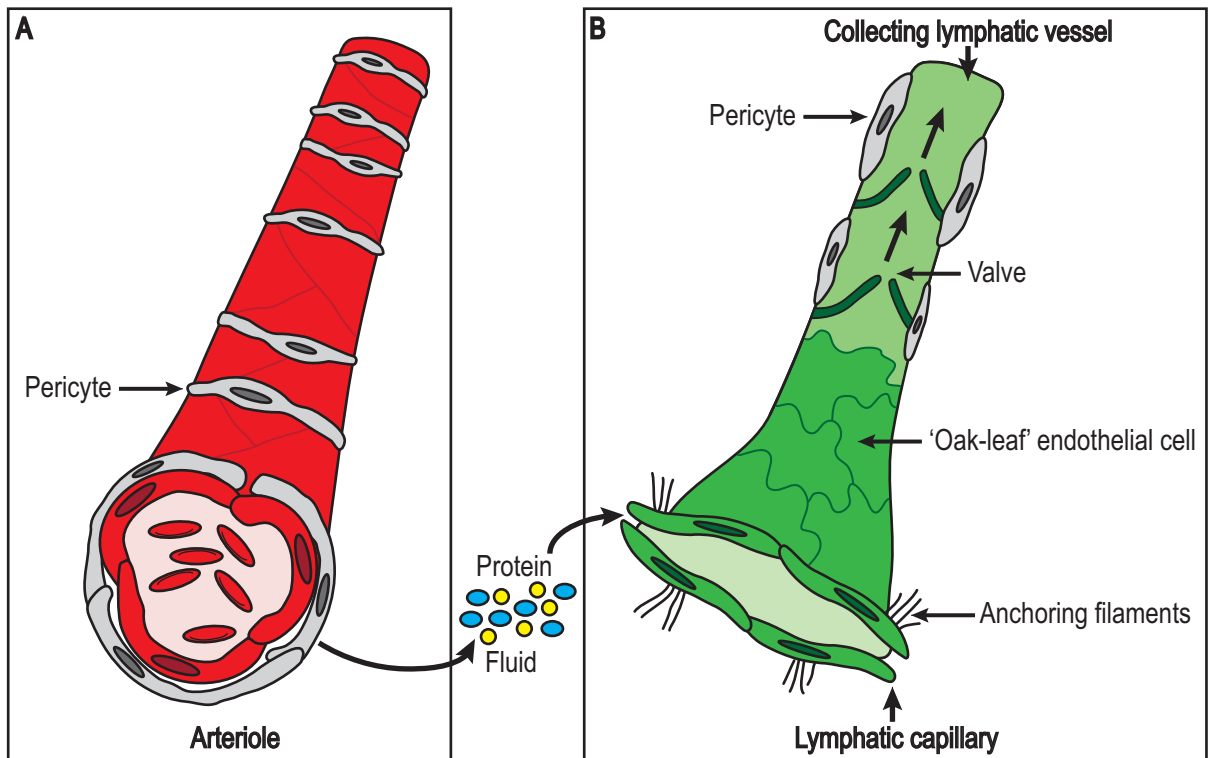


Figure 1.2 - Characteristic features of the lymphatic vasculature.

Lymphatic capillaries (**B**) differ morphologically to blood vessels of the same calibre (**A**) and are defined by the presence of a single layer of overlapping 'oak-leaf'-shaped endothelial cells and anchoring filaments, yet lack pericytes. Contrastingly, collecting lymphatic vessels (**B**) contain bi-leaflet valves enabling unidirectional propulsion of lymph flow and are invested by a layer of supporting pericytes, however, these cells form a much thinner and more disorganised layer than that seen in blood vessels (**A**) of a similar size. Figure adapted from Mäkinen et al., 2007.

and subsequently larger collecting lymphatic vessels. Collecting lymphatic vessels are surrounded by an intact, continuous basement membrane and are invested by a layer of pericytes (Figure 1.2B), however, these cells form a much thinner and more disorganised layer than that seen in blood vessels of the same calibre (Figure 1.2A). Collecting lymphatic vessels also contain bi-leaflet valves enabling unidirectional propulsion of lymph, from the periphery to the deep viscera, and prevention of back flow (Figure 1.2B) (Alitalo et al., 2005; Mäkinen et al., 2007; Tammela and Alitalo, 2010). Studies by Baluk *et al.* have demonstrated that the EC comprising these vessel subtypes are morphologically distinct. In contrast to the continuous junctions between blood endothelial cells (BEC), the EC of initial lymphatic capillaries are anchored by discontinuous 'button-like' junctions that permit fluid passage, whilst the EC of larger collecting lymphatic vessels have continuous 'zipper-like' junctions at their cell borders. Furthermore, the EC of lymphatic capillaries were observed to have a distinctive 'oak-leaf' shape permitting the overlapping of adjacent LEC flaps (Figure 1.2B) (Baluk et al., 2007).

The lymphatic vasculature serves several functions critical to both embryonic development and adult homeostasis and therefore the absence of lymphatic vessels is incompatible with life (Kajji et al., 1980). The most notable function of lymphatic vessels is the maintenance of fluid balance, whereby extravasated interstitial protein-rich fluid, known as lymph, is returned to the venous bloodstream for recirculation via the lymphatic vasculature. The lymphatic system facilitates two additional key functions in the body. Firstly, mediation of immune surveillance, whereby lymphatic vessels act as a conduit for the transportation of immune cells including lymphocytes and antigen-presenting cells, to regional lymph nodes, thus facilitating the initiation of specific immune responses. Tissues that frequently come into contact with foreign antigens, such as the skin and mucous membranes, tend to have a relatively high density of lymphatic vessels. Secondly, lymphatic vessels play a role in the absorption of dietary fats and fat-soluble vitamins. These lipid-rich molecules are released by intestinal epithelial cells in the form of chylomicrons and are absorbed by lacteals, which are specialised lymphatic capillaries within the villi of the small intestine. (Alitalo et al., 2005; Mäkinen et al., 2007; Tammela and Alitalo, 2010). In adults, similarly to blood vessels, with the exception of the female menstrual cycle, lymphatic vessels remain relatively quiescent, except in settings of tissue and organ repair, wound healing and inflammation. In addition to their physiological role, the aberrant growth and development of lymphatic vessels is instrumental in the pathogenesis of many human disorders including lymphoedema (Witte et al., 2001), inflammatory conditions, such as asthma (Baluk et al., 2005), rheumatoid arthritis (Paavonen et al., 2002; Zhang et al., 2007) and psoriasis (Kunstfeld et al., 2004), transplant rejection (Kerjaschki et al., 2004) and notably cancer and tumour metastasis (Cueni and Detmar, 2008).

1.1.2 Embryonic origin and development of the lymphatic system

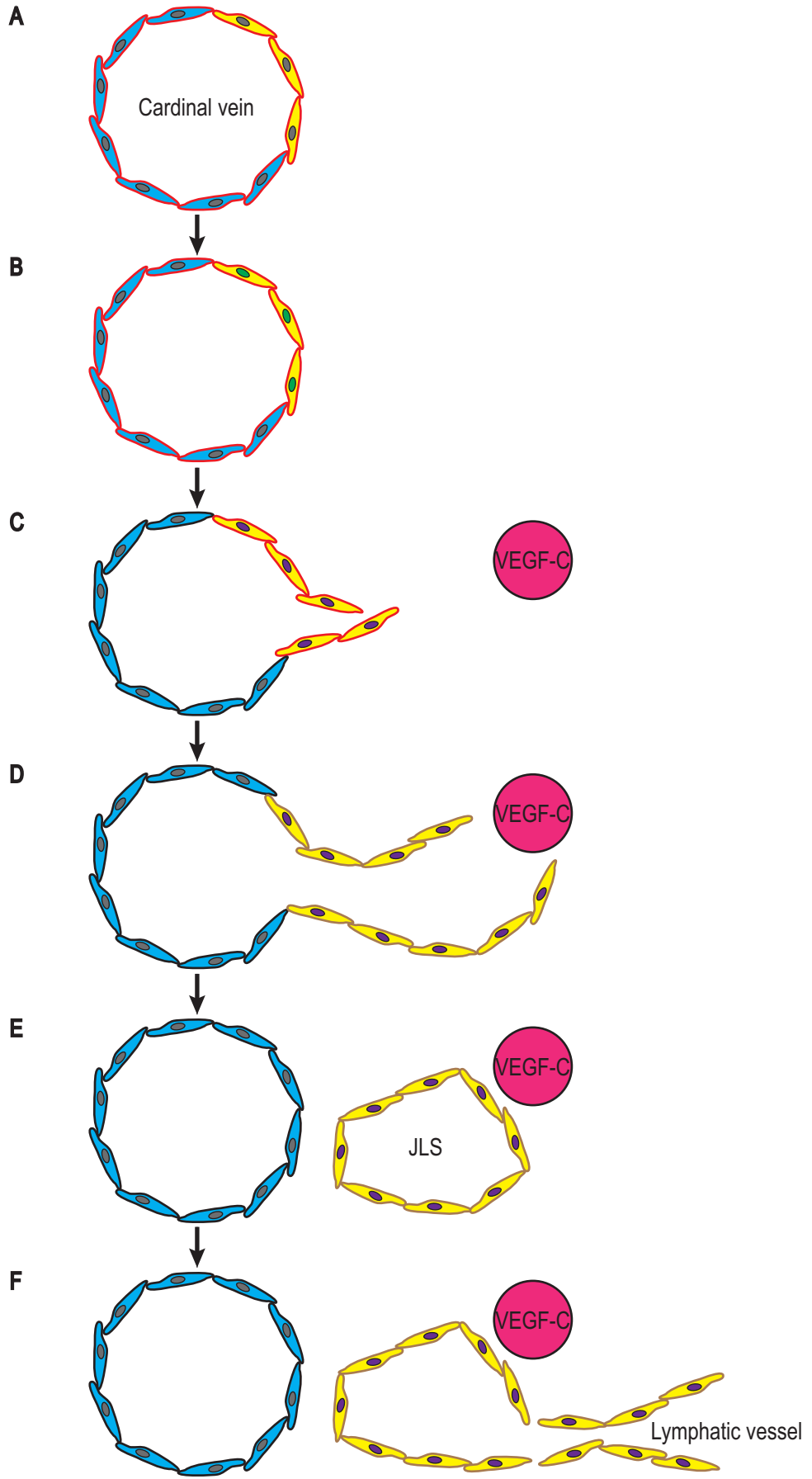
Lymphatic vessels were first described by ancient Greeks in approximately 300 BC, however, it wasn't until the seventeenth century that a functional role in lipid transport was ascribed to lymphatics by Italian anatomist, Gasparo Aselli; almost simultaneously with William Harvey's description of the blood circulation. Aselli described the lymphatic vessels in the mesentery of a recently fed dog as 'milky veins' (Asellius, 1627), a clear recognition of their structural similarity to veins and their functional role in intestinal lipid absorption and transport. Over the next 100 years, however, the field of lymphatic biology advanced rather slowly comparatively to that of the blood vasculature owing to the difficulty in observing lymphatic vessels. During this period, lymphatic vessels were distinguished from their blood vascular counterparts solely on morphological and not molecular criteria. Today, lymphatic vascular research has gathered greatly renewed interest, partly due to the identification of a handful of lymphatic-specific markers and growth factors enabling, for the first time, specific manipulation of this vascular system independent of the blood vasculature.







The development and growth of the lymphatic vascular system proceeds via a process known as lymphangiogenesis and commences considerably later than that of the blood vasculature; around embryonic weeks 6-7 in humans (van der Putte, 1975) and embryonic day (E)9.5 in mice (Wigle and Oliver, 1999). The embryonic origin of lymphatic endothelial progenitor cells has long been a controversial topic in the lymphatic field, with two models being actively debated over recent years. The first was proposed by the American anatomist, Florence Sabin, and is historically the most widely accepted theory of lymphatic development - known as the 'venous origin'. On the basis of findings from dye-injection studies on pig embryos, Sabin proposed that early during embryogenesis isolated primitive lymph sacs arise from budding venous EC and it is from these primordial structures that the peripheral lymphatic system is generated via centrifugal sprouting towards the periphery (Sabin, 1902). The second alternative and less popular model was postulated by Huntington and McClure - the 'mesenchymal origin', in which it was hypothesised that the primary lymph sacs originate from mesenchyme-derived endothelial precursors, independent of the veins and secondarily establish venous connections (Huntington and McClure, 1910). Evidence in support of both of these opposing views has been demonstrated in a variety of animal models and is discussed in more detail below.

In support of Sabin's original theory, a stepwise model of early mammalian lymphatic development was established based on molecular evidence from studies by Wigle and Oliver (Wigle and Oliver, 1999). This model depicted in Figure 1.3, in combination with more recent experimental validation and genetic

Figure 1.3 - Development of the mammalian lymphatic vasculature.

The development of the lymphatic vasculature is a stepwise process. **(A)** Embryonic veins express high levels of vascular endothelial growth factor receptor 3 (VEGFR-3), with the upregulation of lymphatic vessel endothelial hyaluronan receptor 1 (LYVE1) at embryonic day (E)9.0-9.5 in a subpopulation of venous endothelial cells. **(B)** SRY-box containing gene 18 (Sox18) is expressed in these LYVE1-positive lymphatic endothelial cell (LEC) precursors approximately half a day prior to the onset of Prospero-related homeobox 1 (Prox1) expression. **(C)** Sox18 induces Prox1 expression in this polarised population of cells at E9.5, which progressively bud from the veins by E10.5-11.5 and subsequently migrate away in response to vascular endothelial growth factor C (VEGF-C) expressed in the nearby mesenchyme. **(D)** The number and distribution of budding lymphatic precursors increases significantly between E10.5 and E12.5. During this time these cells begin to express additional LEC markers such as podoplanin, neuropilin 2 (Nrp2) and chemokine (C-C motif) ligand 21 (CCL21), whilst VEGFR-3 is simultaneously downregulated in the embryonic venous endothelium. **(E)** Further growth from the cardinal vein results in the first identifiable lymphatic structure in the mouse embryo at E11.5-12.5, the jugular lymph sac (JLS). **(F)** E12.5-14.5 results in further centrifugal sprouting of LEC, ultimately generating the entire mammalian lymphatic network via subsequent differentiation and maturation. Figure adapted from Oliver, 2004; Oliver and Harvey, 2002; Oliver and Srinivasan, 2010; Tammela and Alitalo, 2010.



 Venous endothelial cell	 Sox18
 LYVE1	 Prox1
 VEGFR-3	 VEGFR-3, podoplanin, Nrp2, CCL21

studies, currently represents the most widely accepted model (Oliver, 2004; Oliver and Harvey, 2002; Oliver and Srinivasan, 2010; Wigle et al., 2002; Wigle and Oliver, 1999). Although a functional cardinal vein is present in mice as early as E8.5, which at this time expresses vascular endothelial growth factor receptor 3 (VEGFR-3) (Kaipainen et al., 1995), the first evidence of LEC competence is the expression of lymphatic vessel endothelial hyaluronan receptor 1 (LYVE1) by a discrete few EC that line the anterior cardinal vein at E9.0-9.5 (Figure 1.3A). However, LYVE1 expression is not restricted solely to EC of the cardinal vein and is also expressed extensively throughout the embryonic blood vasculature prior to this time (Gordon et al., 2008). Following the initiation of LYVE1 in EC of the cardinal vein, the expression of the homeobox transcription factor, Prospero-related homeobox 1 (*Prox1*), is initiated in a polarised population of cells in the anterior cardinal veins at E9.5. In a recent study, François *et al.* demonstrated that SRY-box containing gene 18 (*Sox18*), is expressed in these LYVE1-positive LEC precursors approximately half a day prior to the onset of *Prox1* expression and is required to turn on *Prox1* expression in venous EC (Figure 1.3B) (François et al., 2008). *Prox1*-positive LEC progenitors begin to progressively bud from the veins by E10.5-11.5 and subsequently migrate away in a polarised manner (Figure 1.3C) to form the first discernable lymphatic structure in the mouse embryo at E11.5-12.5, the paired jugular lymph sacs (JLS) (Figure 1.3E) (Oliver, 2004; Wigle and Oliver, 1999). The distinct migratory path coursed to form the initial lymph sacs is dependent on vascular endothelial growth factor C (VEGF-C), expressed in mesenchymal cells in the vicinity of the embryonic cardinal veins (Karkkainen et al., 2004; Kukk et al., 1996). The number and distribution of budding lymphatic precursors increases significantly between E10.5 and E12.5 and during this time these cells begin to express additional LEC markers such as podoplanin, neuropilin 2 (*Nrp2*) and chemokine (C-C motif) ligand 21 (*CCL21*) (Figure 1.3D) (Oliver, 2004). Concomitantly with the acquisition of LEC markers, the expression of blood vascular markers such as CD34 and laminin is extinguished. VEGFR-3 levels are reduced in the embryonic venous endothelium around the time of LEC fate determination (Figure 1.3D) (Oliver and Harvey, 2002; Wigle et al., 2002). By E14.5, the lymphatic vasculature of the mouse embryo has spread by budding and sprouting from venous-derived lymph sacs to form a primary lymphatic plexus (Figure 1.3F). It is only near the time of birth that these lymphatic vessels fully differentiate, mature and organise into a hierarchical network of lymphatic capillaries and collectors and express a more complete profile of lymphatic markers (as described in section 1.1.3). In fact, the maturation process, including lymphatic valve development and remodelling of the superficial dermal lymphatic plexus, continues postnatally (Bazigou et al., 2009; Mäkinen et al., 2005). Recent lineage tracing experiments in mice have provided compelling evidence in support of Sabin's original model, demonstrating that the mammalian lymphatic vasculature has a mostly venous origin, arising from *Prox1*-expressing LEC progenitors in early embryonic veins (Srinivasan et al., 2007). In this study,

genetic mouse models lacking definitive haematopoiesis were used to determine that haematopoietic cells do not contribute to the developing lymph sacs (Srinivasan et al., 2007).

Controversial work generated from numerous additional research groups has suggested that other cell types, namely mesenchymal and haematopoietic cells, in addition to venous-derived EC, acquire LEC characteristics and contribute to the developing lymphatic network in mice (Buttler et al., 2008; Buttler et al., 2006). Work done in avian models has culminated in a theory for a dual origin of lymphatics, whereby the JLS arise from embryonic veins and the superficial, dermal lymphatic vessels from local scattered mesodermal precursor cells, termed mesenchymal lymphangioblasts. These two contributing compartments are proposed to fuse together to form the functional lymphatic system, at least in birds (Wilting et al., 2006). Furthermore, work in a *Xenopus laevis* tadpole model has provided additional support for a dual origin of lymphatic vessels (Ny et al., 2005). Although evidence to date illustrates that the majority of LEC are derived from Prox1-positive venous progenitors, the possibility remains that non-venous-derived populations of progenitor cells contribute to the genesis of the embryonic lymphatic vasculature.

Macrophages, via a proposed process of transdifferentiation into LEC (Maruyama et al., 2005), and bone marrow-derived circulating endothelial progenitor cells (Kerjaschki et al., 2006; Religa et al., 2005) have also been suggested to comprise a source of LEC progenitors in settings of pathological inflammation and neo-lymphangiogenesis. On the other hand, however, numerous reports exist that provide no evidence of haematopoietic contribution to the mammalian endothelial compartment during embryogenesis or in pathological settings (Gordon et al., 2010; Srinivasan et al., 2007; Stadtfeld and Graf, 2005). Macrophages have also been demonstrated to stimulate neo-lymphangiogenesis by providing a crucial source of pro-lymphangiogenic growth factors and proteases. Indeed, work from several groups has shown that macrophages in diverse settings of inflammation contribute to lymphangiogenesis, primarily by the production of vascular endothelial growth factor A (VEGF-A), VEGF-C and vascular endothelial growth factor D (VEGF-D) (Baluk et al., 2005; Cursiefen et al., 2004; Jeon et al., 2008; Kataru et al., 2009; Maruyama et al., 2007; Schoppmann et al., 2002). In contrast, recent work from our laboratory has revealed that macrophages, in the setting of developmental lymphangiogenesis, do not comprise the principal source of pro-lymphangiogenic growth factors in the embryonic dermal microenvironment and instead provide signals that regulate LEC proliferation and control the calibre of developing lymphatic vessels in the dermis (Gordon et al., 2010). Further investigation is required to define the precise role and relative contribution of myeloid cell-derived signals during developmental and inflammation-stimulated neo-lymphangiogenesis.

1.1.3 Molecular markers used to identify lymphatic vessels and their role in lymphatic vascular development and function

The identification of LEC markers has greatly facilitated our ability to study and manipulate lymphatic vessels *in vivo* and *in vitro*. The caveat to this is that many 'lymphatic-specific' markers are expressed on cells and tissues in addition to the lymphatic endothelium during embryonic development and adulthood in both normal and disease states. Therefore, it is wise to assess several lymphatic markers together in order to ascertain lymphatic identity. A panel of the most commonly used molecular markers to definitively identify lymphatic vessels from their blood vascular counterparts is discussed in detail below.

1.1.3.1 Prox1

Prox1, originally isolated due to its high homology to the *Drosophila melanogaster* homeobox gene, *prospero* (Oliver et al., 1993), is expressed in neuronal stem cells and is essential for the specification of neuronal cell fate in the *Drosophila* central nervous system (Doe et al., 1991). In mice, nuclear Prox1 can be detected in the central nervous system of the prenatal and postnatal brain, in the developing eye lens and retina, in liver, heart, pancreas and skeletal muscle (Lavado and Oliver, 2007; Oliver et al., 1993), where it plays an important role as a master regulator of cell fate decisions (Dyer et al., 2003; Hope et al., 2010; Lavado et al., 2010; Wigle et al., 1999). Prox1 is also observed in a restricted subpopulation of venous EC on the dorso-lateral side of the anterior cardinal veins at E9.5, which thereafter bud and migrate away from the vein in a polarised fashion, eventually forming lymph sacs and the superficial lymphatic vascular plexus (Oliver, 2004; Wigle and Oliver, 1999).

Studies of mice deficient in the *Prox1* homeobox transcription factor demonstrated that *Prox1* is critical for lymphatic vascular development in the mouse embryo. *Prox1*^{-/-} embryos die at approximately E14.5 and strikingly, are devoid of lymphatic vessels. *Prox1*-deficient EC initially bud and sprout from the cardinal veins, however, they never acquire markers of LEC identity and their subsequent migration is prematurely arrested at around E11.5-E12.0, resulting in the complete absence of lymphatic vessels. In contrast, blood vascular development in *Prox1*-null mice proceeds normally (Wigle and Oliver, 1999). *Prox1*-null EC fail to establish a LEC-specific gene expression profile and instead they retain a blood vascular phenotype (Wigle et al., 2002). In accordance, ectopic expression of Prox1 in differentiated blood vascular EC *in vitro* results in the upregulation of a number of LEC-specific transcripts and

concomitant suppression of blood-vascular specific genes (Hong et al., 2002; Petrova et al., 2002). *Prox1* gene dosage is critical for postnatal survival. In most genetic backgrounds *Prox1* heterozygous pups die soon after birth showing evidence of lymphatic dysfunction and develop chylous ascites, the extravasation of milky chyle from the mesenteric lymphatic vessels into the peritoneal or thoracic cavities (Harvey et al., 2005). However, Harvey *et al.* identified one genetic background in which a small number of *Prox1* heterozygous mice survived until adulthood. These mice were observed to develop adult-onset obesity, forging a link between lymph drainage and adipogenesis (Harvey et al., 2005). Recent work revealed that *Prox1* is constantly required to maintain LEC identity, illustrating that the differentiated LEC phenotype is a plastic, reversible state (Johnson et al., 2008). Taken together, these results substantiate *Prox1* as an essential regulator in the specification of LEC fate and the maintenance of LEC identity; thus *Prox1* is considered a 'master regulator' of LEC phenotype. To this end, *Prox1* can be considered as a 'gold-standard' LEC marker.

1.1.3.1.1 Transcriptional regulation of *Prox1* by *Sox18* and COUP-TFII

Despite the importance of *Prox1* for lymphangiogenesis, very little is actually known about the mechanisms by which *Prox1* expression is controlled in EC, although recent work has demonstrated that the transcription factors *Sox18*, which directly activates *Prox1* expression by binding to its proximal promoter (François et al., 2008) and chicken ovalbumin upstream promoter transcription factor 2 (COUP-TFII) (Srinivasan et al., 2010), are critical for the induction of *Prox1* expression in lymphatic endothelial progenitor cells within the embryonic venous endothelium. Studies by François *et al.* established that lack of *Sox18* function results in the complete arrest of embryonic lymphatic vascular development, resulting in oedema and embryonic lethality (François et al., 2008). Mutations in the human *SOX18* gene were recently identified to cause both recessive and dominant forms of hypotrichosis-lymphoedema-telangiectasi syndrome; a condition characterised by hair (hypotrichosis), lymphatic (lymphoedema) and blood vascular (telangiectasia) malformations (Irrthum et al., 2003). Studies by Srinivasan *et al.* demonstrated that COUP-TFII, a regulator of venous identity, is necessary for the activation of *Prox1* in embryonic veins. COUP-TFII directly binds to the *Prox1* regulatory region and up until E13.5 COUP-TFII function is required for the maintenance of *Prox1* expression. After this time, *Prox1* expression in LEC becomes independent of COUP-TFII (Srinivasan et al., 2010).

1.1.3.1.2 Post-transcriptional regulation of *Prox1* by *miR-181a*

Novel data recently generated in our laboratory has uncovered a novel mechanism by which *Prox1* is post-transcriptionally regulated via the microRNA, *miR-181a*, which is expressed more highly in embryonic BEC compared to LEC. *miR-181a* binds to the 3'-untranslated region of *Prox1*, leading to

transcript degradation and translational inhibition, therefore providing a mechanism by which *Prox1* expression is post-transcriptionally regulated in EC and normally silenced in the blood vasculature (Kazenwadel et al., 2010).

1.1.3.2 LYVE1

LYVE1 is one of the most commonly used markers to identify lymphatic endothelium. LYVE1 is a cell surface transmembrane glycoprotein receptor for hyaluronan expressed abundantly on lymphatic vessels, that was identified on the basis of shared structural and functional similarity with the hyaluronan receptor, CD44 (Banerji et al., 1999; Prevo et al., 2001). In contrast to the model of embryonic lymphatic development proposed by Wigle *et al.* (Wigle et al., 2002), work from our laboratory demonstrated that LYVE1 is expressed broadly on intra-embryonic blood vessels prior to the induction of *Prox1* in the cardinal veins. Following the specification of LEC fate, however, the expression of LYVE1 is upregulated in *Prox1*-positive LEC progenitors in the cardinal veins (Gordon et al., 2008). Postnatally, LYVE1 levels are progressively downregulated in collecting lymphatic vessels, yet remain high on EC of lymphatic capillaries (Mäkinen et al., 2005). It is well-established in the literature that LYVE1 expression is not restricted solely to the lymphatic vasculature, LYVE1 is also detected on endothelial sinusoids of lymph nodes, liver, spleen and a small proportion of blood vessels in the lung (Banerji et al., 1999; Mouta Carreira et al., 2001; Prevo et al., 2001) and by a subpopulation of activated tissue macrophages (Lee et al., 2011; Schledzewski et al., 2006). Recent work from our laboratory has revealed that LYVE1 is also expressed on blood vessels of the yolk sac, inter-somitic vessels and endocardium during mouse embryogenesis (Gordon et al., 2008) and by a discrete population of macrophages that are intimately associated with the developing embryonic lymphatic vasculature (Gordon et al., 2010).

Initial functional studies demonstrated that LYVE1 acts as an endocytic receptor for the extracellular matrix glycosaminoglycan, hyaluronan, ascribing a putative role for LYVE1 in facilitating hyaluronan transport from tissues, via the lymph, to lymph nodes where it is degraded (Prevo et al., 2001). The exact physiological role of LYVE1 in the regulation of lymphatics, however, remains to be elucidated. Recent studies using *Lyve1*-null mice, which are viable, have demonstrated that LYVE1 is dispensable for both hyaluronan transport and for normal lymphatic vascular development (Gale et al., 2007; Huang et al., 2006).

1.1.3.3 Podoplanin

Podoplanin, historically known by a host of synonymous names including E11 antigen and T1 α , is a small transmembrane mucin-type glycoprotein that is highly expressed by embryonic and adult LEC; as early as E10.5-11.5 in budding Prox1-positive lymphatic progenitor cells (Schacht et al., 2003). Intriguingly, podoplanin is not expressed in Prox1-positive lymphatic endothelial progenitors located within the veins, but is turned on once these cells exit the cardinal veins (Natasha L. Harvey and Mathias François, unpublished observations). During mouse embryonic development, podoplanin expression can also be detected in the central nervous system and foregut around E9.0 (Schacht et al., 2003). Podoplanin, as its name suggests, is also expressed by kidney podocytes (Breiteneder-Geleff et al., 1997) and a host of other cell types, such as keratinocytes, osteoblasts and osteocytes, epithelial cells of the choroid plexus, glandular myoepithelial cells, ciliary epithelial cells of the eye and type 1 alveolar lung cells (Schacht et al., 2005; Wetterwald et al., 1996; Williams et al., 1996).

Targeted inactivation of *Pdpn* results in perinatal lethality, caused by abnormal lung development and these mice display defects in lymphatic vascular, but not blood vascular, patterning, resulting in diminished lymphatic transport and function, congenital lymphoedema and dilation of cutaneous and intestinal lymphatic vessels (Schacht et al., 2003). *In vitro*, podoplanin has been demonstrated to promote LEC adhesion, migration and tube formation (Schacht et al., 2003). In addition, podoplanin has been shown to play a critical role in the activation of platelets via the C-type lectin-like receptor 2 (CLEC-2) during the process of blood and lymphatic vessel separation (see section 1.1.4.2.8) (Suzuki-Inoue et al., 2007). Together, these findings suggest a role for podoplanin in the normal patterning and function of lymphatic vessels and in separation of the blood and lymphatic vascular networks.

1.1.3.4 VEGFR-3

VEGFR-3, also known as FMS-like tyrosine kinase 4 (Flt4), was the first gene shown to have a restricted expression profile in lymphatic vessels (Kaipainen et al., 1995). VEGFR-3 is structurally related to vascular endothelial growth factor receptor 1 (VEGFR-1), which is required for the recruitment of haematopoietic precursors and migration of monocytes, and vascular endothelial growth factor receptor 2 (VEGFR-2), which is primarily expressed by blood vascular EC and has an essential role in vasculogenesis (the *de novo* formation of blood vessels) and angiogenesis (the process by which new blood vessels develop from pre-existing vessels) (Olsson et al., 2006; Shalaby et al., 1995). Although VEGFR-2 has also been documented to be expressed by LEC *in vitro* (Hirakawa et al., 2003; Kriehuber

et al., 2001), the role of VEGFR-2 signalling in LEC is not well-defined. However, VEGFR-2 and VEGFR-3 have been reported, at least *in vitro*, to heterodimerise (Dixelius et al., 2003). Unlike VEGFR-1 and VEGFR-2 that largely interact with VEGF-A, VEGFR-3 binds two predominantly lymphangiogenic ligands, VEGF-C and VEGF-D (section 1.1.4.1.1) (Olsson et al., 2006). From E8.5 onwards, VEGFR-3 is expressed in all vascular EC, but later becomes downregulated on BEC and subsequently more restricted to the lymphatic endothelium in most adult tissues (Kaipainen et al., 1995). However, VEGFR-3 is highly expressed on angiogenic tip cells and plays a critical role in blood vascular sprouting (Tammela et al., 2008) and some tumour-associated blood vessels have been shown to express VEGFR-3 (Kubo et al., 2000; Partanen et al., 1999; Valtola et al., 1999; Witmer et al., 2001).

Vegfr3^{-/-} mouse embryos die mid-gestation (approximately E9.5) due to defective blood vascular remodelling and extensive cardiovascular defects, indicating a critical role for VEGFR-3 in the early embryonic cardiovascular system, prior to the development of the lymphatic vasculature (Dumont et al., 1998). Studies by Veikkola *et al.* using transgenic mice with overexpression of a VEGFR-3-specific mutant of VEGF-C revealed that activation of the VEGFR-3 signal transduction pathway was sufficient to promote lymphangiogenesis *in vivo* (Veikkola et al., 2001). Fittingly, a missense point mutation in the region of the *FLT4* gene encoding the tyrosine kinase domain, resulting in tyrosine kinase inactivation, has been found in human patients with Milroy disease; a rare hereditary form of lymphoedema presenting at birth and characterised by a phenotypic pattern of hypoplastic cutaneous lymphatic vessels (Karkkainen et al., 2000). Studies in zebrafish (Hogan et al., 2009b) and *Xenopus* tadpoles (Ny et al., 2008) have determined a critical role for VEGFR-3 in developmental lymphangiogenesis, however, due to the embryonic lethality of *Vegfr3*-null mice prior to lymphatic vessel development, the precise role of VEGFR-3 signalling in developmental lymphangiogenesis has not been conclusively defined. Nonetheless, all of the data generated to date are supportive of a central role for this tyrosine kinase receptor.

1.1.3.5 Nrp2

Nrp2 is a non-kinase type 1 transmembrane glycoprotein, originally identified as an axonal guidance receptor for the class three family of semaphorins and certain members of the vascular endothelial growth factor (VEGF) family (Neufeld et al., 2002). Nrp2 expression can be detected as early as E10.0 in the mouse in EC of the cardinal vein and budding LEC. The floor plate, neurons of the ventral spinal cord, dorsal root and sympathetic ganglia also express Nrp2 at this time. During subsequent development, Nrp2 expression becomes constrained to embryonic and adult LEC, as well as venous

EC, albeit at a much reduced level to that in lymphatic vessels (Yuan et al., 2002). *Nrp2* knockout mice exhibit hypoplasia of small lymphatic vessels and capillaries during embryogenesis, whereas arteries, veins and larger collecting lymphatic vessels develop normally, exposing a selective requirement for *Nrp2* in lymphatic vessel development (Yuan et al., 2002). A more specific role for *Nrp2* in lymphangiogenesis has recently been described by Xu *et al.*, whereby *Nrp2*, through interaction with VEGFR-3, modulated endothelial tip cell extension and prevented tip cell stalling and retraction in lymphatic vascular sprouts formed in response to VEGF-C (Xu et al., 2010). In addition, the transcription factor, COUP-TFII has been demonstrated to play a critical role in mediating multiple steps in both developmental and pathological lymphangiogenesis in mice, at least in part, by stimulating the direct transcription of *Nrp2* (Lin et al., 2010). Interestingly, *Nrp2* has also been identified as a co-receptor for VEGF-C and VEGF-D (Karpanen et al., 2006).

1.1.3.6 CCL21

CCL21, also known as secondary lymphoid organ chemokine (SLC), is a chemo-attractant expressed by secondary lymphoid organs, particularly high endothelial venules and T-cell areas of lymph nodes, spleen and Peyer's patches. CCL21 is also expressed on embryonic and adult lymphatic endothelium, but not blood vessel endothelium, from approximately E12.5 onwards (Gunn et al., 1998; Wigle et al., 2002). No obligatory functional role during lymphangiogenesis has been ascribed to CCL21 to date, however, an essential role in inflammatory conditions and in the homing of immune cells to lymphoid organs has been established (Gunn et al., 1999; Gunn et al., 1998).

1.1.4 Lymphangiogenic growth factors and other molecules critical to lymphatic vascular growth, development and function

To date, a number of growth factors have been implicated in multiple aspects of lymphatic vessel biology; from their initial development, to their subsequent growth, guidance, remodelling and functionality. A brief description of the best characterised of these molecules is provided below.

1.1.4.1 Lymphangiogenic growth factors

It is likely that several lymphangiogenic growth factors, factors that induce lymphangiogenesis, act in a coordinated way to control the process of lymphatic vessel growth and development in physiological and pathological settings.

1.1.4.1.1 VEGF-C and VEGF-D

To date, the best characterised lymphangiogenic stimuli are the VEGFR-3 activating ligands, VEGF-C and VEGF-D, which induce proliferation, migration and survival of LEC in a variety of *in vivo* and *in vitro* contexts. Both of these growth factors are highly homologous from a structural viewpoint; each possessing a bioactive central VEGF homology domain (VHD) containing the binding sites for VEGFR-2 and VEGFR-3, flanked by long N- and C-terminal propeptides. VEGF-C and VEGF-D are initially secreted from the cell as homodimers of the full-length glycoprotein, known as precursor proteins, and are subsequently proteolytically-processed in the extracellular environment to release the mature, fully-processed 21kDa VHD domain (see section 4.1.1) (Joukov et al., 1997; Stacker et al., 1999). So far, the serine protease, plasmin (McColl et al., 2003) and proprotein convertases (PC); furin, PC5 and PC7 have been shown to cleave VEGF-C (Siegfried et al., 2003) and VEGF-D (McColl et al., 2007).

As discussed above, VEGF-C is expressed in regions where the lymphatic vessels develop during embryogenesis, but expression can also be detected weakly in the spinal cord, lymph nodes, heart, lung, kidney, placenta, skeletal muscle and ovary (Karkkainen et al., 2004; Kukk et al., 1996). VEGF-C is also expressed by BEC and vascular smooth muscle cells, which likely represent important sources of VEGF-C in physiological and pathological lymphangiogenesis (Joory et al., 2006; Karkkainen et al., 2004). Homozygous deletion of *Vegfc* in mice leads to an arrest in lymphatic vascular development, resulting in embryonic death at around E15. Interestingly, EC in *Vegfc*^{-/-} mice commit to the lymphatic lineage but do not sprout and migrate away from the cardinal veins; one of the first crucial steps in the development of the lymphatic vascular system. Mice heterozygous for *Vegfc* survive into adulthood but display severe lymphatic hypoplasia (Karkkainen et al., 2004). Not only is VEGF-C essential for embryonic lymphatic development, but its signalling through VEGFR-3 has been shown to selectively induce lymphatic, but not blood vessel growth, in the skin of transgenic mice overexpressing VEGF-C (Jeltsch et al., 1997). In contrast, inactivation of *Vegfd*, the second activating ligand for VEGFR-3, which is highly expressed in embryonic and adult lung tissue, does not disrupt lymphatic vascular development, suggesting that VEGF-D is dispensable for embryonic lymphangiogenesis, perhaps due to compensation by VEGF-C (Baldwin et al., 2005). Furthermore, VEGF-D was shown to be expendable

in settings of postnatal and adult lymphangiogenesis (Koch et al., 2009). The lack of a profound lymphatic vessel defect in *Vegfd*-deficient mice may reflect a subtle, functionally-redundant, or non-existent role for this growth factor during embryonic and postnatal development. Nevertheless, VEGF-D has been shown to induce pathological lymphangiogenesis and metastasis in mouse tumour models (Koch et al., 2009; Stacker et al., 2001) and the overexpression of VEGF-D in the skin of transgenic mice results in lymphatic hyperplasia (Veikkola et al., 2001). The functional redundancy between VEGF-C and VEGF-D, due to their high homology, can be appreciated from studies involving the overexpression of VEGF-D in the skin of *Vegfc*^{+/-} mice, in which rescue of lymphatic hypoplasia was observed (Haiko et al., 2008). Fascinatingly, compound deletion of both *Vegfc* and *Vegfd* fails to recapitulate the early embryonic lethality observed in *Vegfr3*-null mice, suggesting the existence of perhaps another unidentified compensatory factor(s) capable of activating the VEGFR-3 signalling pathway (Haiko et al., 2008).

The receptor binding, affinity and consequently, the biological activity of VEGF-C and VEGF-D, are mediated by the stepwise proteolytic processing of the precursor proteins (as discussed in detail in section 4.1.1). Following proteolytic cleavage, the fully-processed forms have a greatly increased affinity for VEGFR-3 and acquire the ability to interact with VEGFR-2 (Joukov et al., 1997; Stacker et al., 1999). A novel alternatively spliced, soluble form of VEGFR-2 (designated sVEGFR-2) was recently identified and reported to be essential for maintaining the alymphatic state of the cornea. A study by Albuquerque *et al.* demonstrated that sVEGFR-2 inhibited both developmental and reparative lymphangiogenesis by blocking VEGF-C function; therefore, attributing a unique and selective anti-lymphangiogenic property to sVEGFR-2 (Albuquerque et al., 2009). sVEGFR-2, by sequestering endogenously-available VEGF-C (Albuquerque et al., 2009), functions in an analogous fashion to the previously identified anti-angiogenic molecule; soluble VEGFR-1, which acts as a trap for endogenous VEGF-A, resulting in corneal avascularity (Ambati et al., 2006). The sVEGFR-2 variant has already been proven to be of high clinical significance in the treatment of tumour metastasis in a mouse model (Shibata et al., 2010). sVEGFR-2 therefore holds future therapeutic potential for the treatment of human lymphatic vascular malformations, cancer and transplant rejection.

1.1.4.1.2 Angiopoietins and Tie receptors

The angiopoietin (Angpt) growth factors, Angpt1 and Angpt2, act as ligands for the tyrosine kinase receptor, Tie2, which is expressed almost exclusively on the surface of EC (Dumont et al., 1993). The role of Angpt-Tie signalling in vascular development has been extensively studied using a number of genetic mouse models and is critical for blood vascular remodelling, maturation and stabilisation

(Dumont et al., 1994; Maisonpierre et al., 1997; Suri et al., 1996). It is generally accepted that Angpt1 is associated with blood vessel stabilisation and recruitment of perivascular cells, whereas Angpt2 acts to counter these actions.

The role of this signalling axis in lymphangiogenesis has only been unravelled recently and much remains to be determined. Both Tie1 (Qu et al., 2010), a close homologue of Tie2, and Tie2 (Morisada et al., 2005; Tammela et al., 2005) have been demonstrated to be expressed at detectable levels in LEC, whilst Angpt2 is most highly expressed in the smooth muscle cells covering the surface of large arteries and the vascular endothelium of veins and venules (Gale et al., 2002; Maisonpierre et al., 1997). In mouse models lacking *Tie1*, *Tie2* or *Angpt1*, initial blood vascular development proceeds normally but the subsequent remodelling and maturation during embryogenesis is perturbed. Mice deficient in *Tie1* die around E13.5-14.5 due to severe oedema, haemorrhage and microvessel rupture (Puri et al., 1995). Recently, it has been demonstrated that *Tie1*-deficient embryos exhibit lymphatic vascular abnormalities that precede the blood vessel phenotype, indicating that the Tie1 receptor is dispensable for LEC commitment but is required for normal embryonic lymphangiogenesis (D'Amico et al., 2010; Qu et al., 2010). Similarly, *Tie2*^{-/-} mice die around E9.5-12.5 due to cardiac defects and a failure in the primary capillary plexus to remodel (Dumont et al., 1994). *Angpt1*^{-/-} mice die by E12.5 showing a disrupted vascular pattern and cardiac defects reminiscent of *Tie2*^{-/-} mice (Suri et al., 1996). Overexpression of Angpt1 *in vivo*, however, stimulates LEC proliferation and promotes vessel enlargement and the generation of new lymphatic sprouts, and thus Angpt1 can be considered to have potent lymphangiogenic activity (Morisada et al., 2005; Tammela et al., 2005).

Angpt2^{-/-} mice develop normally embryonically but demonstrate defective postnatal blood and lymphatic remodelling, characterised by incomplete regression of the hyaloid blood vasculature and defective lymphatic vessel maturation, including impaired pericyte investment of the collecting vessels and abnormal patterning of lymphatic capillaries. As a result these mice develop peripheral oedema and chylous ascites and die neonatally (Gale et al., 2002). In combination with work from Dellinger *et al.*, the phenotypic analysis of *Angpt2*^{-/-} mice implies that Angpt2 is dispensable for embryonic vascular development, but has a requisite role in postnatal vessel remodelling and maturation (Dellinger et al., 2008; Gale et al., 2002). Remarkably, the lymphatic, but not the blood vascular, phenotype can be rescued by replacement of the *Angpt2* gene with *Angpt1*, indicating that Angpt2 acts as a Tie2 agonist in LEC, but as an antagonist in BEC (Gale et al., 2002). Taken together, these data suggest differential requirements for the Angpt-Tie signalling axis in the two vascular compartments.

1.1.4.1.3 FGF-2

Fibroblast growth factors (FGF) and in particular, fibroblast growth factor 2 (FGF-2), are potent stimulators of angiogenesis *in vivo* and *in vitro* (Auguste et al., 2003). However, the role of FGFs in lymphangiogenesis is less well-established. FGF-2, an angiogenic heparin binding protein, promotes the growth of lymphatic vessels in a mouse corneal assay, most likely through VEGFR-3, via the induction of VEGF-C expression in BEC and supporting perivascular cells (Kubo et al., 2002). Using a mouse corneal assay, Chang *et al.* have demonstrated that low doses of FGF-2 selectively stimulates lymphangiogenesis (Chang et al., 2004). It is conceivable that FGF-2, which enhances the migration and proliferation of LEC *in vitro*, might also act directly through fibroblast growth factor receptor 3, which has been shown to be upregulated by Prox1 in lymphatic endothelium (Shin et al., 2006). Studies by Shin *et al.* also revealed that two specific FGF ligands, fibroblast growth factor 1 (FGF-1) and FGF-2, promoted the proliferation, migration, and survival of cultured LEC in a VEGFR-3-independent manner; further strengthening a role for FGF signalling in lymphangiogenesis (Shin et al., 2006). Recent work in our laboratory has revealed that fibroblast growth factor receptor 1 (FGFR-1) is important for mediating FGF-2-induced proliferation, migration and tube formation in primary embryonic LEC *ex vivo* (Jan Kazenwadel, Genevieve Secker and Natasha L. Harvey, unpublished data).

1.1.4.1.4 HGF

Hepatocyte growth factor (HGF), a heparin-binding glycoprotein produced by various mesenchymal cells, has also been shown to act as a lymphangiogenic factor by directly promoting the proliferation, migration and tube formation of cultured human LEC, as well as promoting the formation of new lymphatic vessels *in vivo* when overexpressed in transgenic mice or delivered subcutaneously (Kajiyama et al., 2005). HGF mediates its lymphangiogenic role via a membrane-spanning receptor tyrosine kinase, the hepatocyte growth factor receptor (HGFR), independently of the VEGFR-3 pathway (Kajiyama et al., 2005). Furthermore, Kajiyama *et al.* found that HGFR was more highly expressed on LEC than by BEC *in vitro* and was preferentially expressed by activated, proliferating lymphatic endothelium *in vivo*, as opposed to quiescent lymphatic vessels in normal skin (Kajiyama et al., 2005). A subsequent independent study by Cao *et al.* demonstrated that HGF promoted lymphangiogenesis in mouse corneal and tumour models, however, they proposed an indirect mechanism of action due to a lack of detectable HGFR on newly-formed lymphatic vessels in the mouse cornea (Cao et al., 2006). Further experimental investigation is not only required to determine the discrepancy between these two reports, but to clarify the precise role of HGF in lymphangiogenesis.

1.1.4.1.5 Insulin-like growth factors

Insulin-like growth factor 1 (IGF-1) and 2 (IGF-2), secreted protein hormones that share structural similarity to insulin, have also been reported to exhibit lymphangiogenic capabilities. IGF-1 and IGF-2 promoted proliferation and chemotaxis of cultured primary LEC, which express the insulin-growth factor transmembrane receptors 1 and 2, *in vitro* (Björndahl et al., 2005). Both IGF-1 and IGF-2 have been shown to promote lymphatic vessel growth in a mouse corneal assay (Björndahl et al., 2005), however, the roles of these growth factors during developmental lymphangiogenesis *in vivo* is not established.

1.1.4.1.6 PDGF-BB

The platelet-derived growth factor (PDGF) family of secreted glycoproteins have well-established and diverse roles in a variety of cell types during development and in adulthood. The PDGF family consists of four members, PDGF-A, -B, -C and -D, which form either homo- or heterodimers (Hoch and Soriano, 2003). Of particular interest in lymphangiogenesis is PDGF-B and its receptor, platelet-derived growth factor receptor beta (PDGFR β), which have long been established as critical regulators of vascular mural cell recruitment during embryogenesis (Hellström et al., 1999). Cao *et al.* demonstrated that expression of PDGF-BB in murine fibrosarcoma cells induced tumour lymphangiogenesis in mice and promoted enhanced metastasis to lymph nodes. In addition to this *in vivo* role for PDGF-BB, Cao *et al.* further showed that PDGF-BB is a chemo-attractant for primary LEC and that PDGF receptors are expressed by newly formed lymphatic vessels in a corneal model; thus implicating a role for PDGF-BB in lymphangiogenesis (Cao et al., 2004).

1.1.4.2 Other molecules critical to lymphatic vascular growth, development and function

1.1.4.2.1 Adrenomedullin

Mice deficient in the vasodilator and diuretic peptide, adrenomedullin, or components of its receptor complex are perinatal lethal due to the development of severe generalised oedema without the presence of haemorrhage by mid-gestation; indicating a necessary role for these class of genes in the development of the lymphatic system (Fritz-Six et al., 2008). Adrenomedullin is also recognised as an important vascular factor involved in blood vessel development and function (Ribatti et al., 2005). The phenotype of adrenomedullin-deficient mice likely reflects its function in both blood and lymphatic vessel compartments.

1.1.4.2.2 *Ccbe1*

A recent study in zebrafish using a forward genetic screening approach identified collagen and calcium binding EGF domains 1 (*ccbe1*) as a critical regulator of lymphatic vessel formation in zebrafish; ascribing a role to *ccbe1* in the budding of lymphangioblasts and angiogenic sprouting from the venous endothelium (Hogan et al., 2009a). Recently, mutations in the human ortholog, *CCBE1*, have been linked with recessively-inherited generalised lymphatic dysplasia in humans (Alders et al., 2009; Connell et al., 2010). These linkage-studies demonstrate that *ccbe1* is critical for lymphangiogenesis; however, its mechanism of action remains to be determined.

1.1.4.2.3 *EphrinB2*

The transmembrane ligands, ephrins, and their cognate Eph tyrosine kinase receptors, are well-established regulators of axonal guidance in the nervous system (Flanagan and Vanderhaeghen, 1998) and more recently, have been shown to play a crucial role in remodelling of the blood vasculature (Kuijpera et al., 2007). In the embryonic blood vasculature, ephrinB2 and its receptor, Eph receptor B4 (EphB4), are specifically expressed in arterial and venous EC, respectively (Wang et al., 1998). A functional requirement of ephrinB2 during postnatal remodelling of the primary lymphatic capillary plexus has recently been demonstrated. Mice expressing a mutant C-terminal PDZ domain of ephrinB2 display a normal blood vascular network, but perturbed postnatal remodelling of the lymphatic vasculature, characterised by hyperplasia of collecting lymphatic vessels, lack of luminal valve formation and a failure of the primary lymphatic plexus to remodel into a hierarchical network (Mäkinen et al., 2005). In these studies by Mäkinen *et al.* it was also noted that collecting lymphatic vessels maintain expression of both ephrinB2 and EphB4, whilst the newly formed lymphatic capillaries lost expression of ephrinB2, but retained expression of EphB4; suggesting a further role for ephrinB2-EphB4 interactions in the establishment of the distinction between a capillary versus a collecting lymphatic vessel (Mäkinen et al., 2005).

1.1.4.2.4 *Fiaf*

A novel role for fasting-induced adipose factor (Fiaf), a glycosylated, proteolytically-processed protein produced by small intestinal enterocytes, in the regulation of postnatal lymphatic partitioning from the blood vasculature in the small intestine has been documented. *Fiaf*-deficient mice develop normally until birth, but die postnatally exhibiting dilated, blood-filled intestinal lymphatic vessels (Bäckhed et al., 2007).

1.1.4.2.5 FOXC2

The fourth transcription factor, in addition to Prox1, Sox18 and COUP-TFII, implicated in lymphangiogenesis is the forkhead transcription factor, forkhead box C2 (FOXC2). FOXC2 is highly expressed in developing lymphatic vessels, as well as in lymphatic valves (Dagenais et al., 2004; Petrova et al., 2004). *Foxc2*^{-/-} mice die due to severe cardiovascular defects. The initial development of lymphatic vessels proceeds normally in these mice, yet the collecting lymphatic vessels lack valves and the lymphatic capillaries acquire ectopic coverage of basement membrane and pericytes (Petrova et al., 2004); a clear indication that FOXC2 has an important role in the maturation of collecting lymphatic vessels. FOXC2 represents the second gene to be associated with hereditary lymphoedema, with mutations in the human gene linked to lymphoedema-distichiasis; a rare autosomal dominant syndrome characterised by late-onset lymphoedema, a double row of eyelashes (distichiasis) and varicose veins (Brice et al., 2002; Fang et al., 2000; Finegold et al., 2001). Unlike in Milroy disease, the lymphatic vasculature in lymphoedema-distichiasis patients is often normal or hyperplastic, but with abnormal patterning and retrograde lymph flow due to defective lymphatic valves (Brice et al., 2002; Petrova et al., 2004). A functional role for FOXC2 in the development and maintenance of venous valves has also been established (Mellor et al., 2007). Furthermore, in a recent study, a novel link between nuclear factor of activated T-cells, cytoplasmic, calcineurin-dependent 1 (NFATc1) and FOXC2 in the regulation of lymphatic maturation was found (Norrmén et al., 2009).

1.1.4.2.6 Integrin- α 9

The molecular mechanisms underlying the anchorage of LEC to the extracellular matrix are largely unknown. Targeted inactivation of the cell-matrix adhesion receptor, integrin- α 9, which forms heterodimers with integrin- β 1, is causative of foetal bilateral chylothorax, the accumulation of chyle in the pleural cavity, in mice (Huang et al., 2000). Accordingly, heterozygous missense mutations in the *ITGA9* gene have been recently documented to underlie congenital chylothorax in humans foetuses (Ma et al., 2008). Integrin- α 9 has been shown to be highly expressed in the EC that constitute lymphatic valves and EC-specific deletion of this integrin results in defective formation of luminal valve leaflets and retrograde lymphatic flow (Bazigou et al., 2009). A similar phenotype was observed in mice lacking the EIIIA domain of the integrin- α 9-specific ligand, fibronectin (Bazigou et al., 2009). Collectively, these results support a role for integrin signalling and LEC interaction with the extracellular matrix in lymphatic valve morphogenesis.

1.1.4.2.7 Netrin-4

Very recently, netrin-4 was implicated in lymphangiogenesis as a pro-lymphangiogenic growth factor (Larrieu-Lahargue et al., 2010). This laminin-like secreted protein has previously been demonstrated to play a vital role in axonal guidance, its founding role, and blood vascular endothelial biology (Cirulli and Yebra, 2007). Larrieu-Lahargue *et al.* showed that netrin-4 induced proliferation, migration and survival of LEC (Larrieu-Lahargue et al., 2010). Neogenin and Unc5b, two putative receptors of netrins, are expressed by LEC and netrin-4-overexpressing human breast tumours in mice develop a greater number of metastases owing to increased lymphatic vessel density and permeability (Larrieu-Lahargue et al., 2010).

1.1.4.2.8 Syk and SLP-76

During developmental progression, the majority of connections between the blood and lymphatic networks are lost, except at the point where the thoracic duct empties into the subclavian vein, enabling the return of lymph to the bloodstream. Two key molecular players; the tyrosine kinase, spleen tyrosine kinase (Syk) and its adaptor molecule, SH2 domain containing leukocyte protein of 76kDa (SLP-76), have been identified to play an essential role in the separation of the blood and lymphatic vasculature. Mice with homozygous mutations in either of these molecules develop arterio-venous shunts and abnormal lymphatico-venous communications, resulting in the presence of blood-filled lymphatic vessels and haemorrhage (Abtahian et al., 2003). Both Syk and SLP-76 are highly and almost exclusively expressed in haematopoietic cells, suggesting that a haematopoietic signalling pathway contributes to the disconnection of lymphatic from blood vessels (Sebzda et al., 2006). Indeed, it has been recently demonstrated that podoplanin expressed on the surface of LEC binds CLEC-2 on platelets and activates Syk and SLP-76 signalling to regulate embryonic blood and lymphatic vascular separation (Bertozzi et al., 2010; Suzuki-Inoue et al., 2010; Uhrin et al., 2010). The finding that *Clec2*^{-/-} mice develop a vascular mixing phenotype (Bertozzi et al., 2010; Suzuki-Inoue et al., 2010) similar to mice lacking *Pdpr* (Uhrin et al., 2010), *Syk* and *SLP-76* (Abtahian et al., 2003) is in support of this novel separation mechanism mediated by platelets.

1.2 THE MOUSE MAMMARY GLAND

1.2.1 Introduction to the mammary gland

The mammary gland can be thought of as the one anatomical structure that distinguishes mammals from all other animals (Sternlicht et al., 2006) and unlike most other mammalian organs, development of the mammary gland is almost exclusively postnatal. Mammary glands are epidermal appendages that can be considered a dynamic, complex secretory tissue that undergo extensive hormonally-induced changes in conjunction with the female reproductive cycle. Despite many similarities existing between human and rodent mammary glands (as discussed in section 1.2.4), the number and location of the glands themselves varies among different species. Mice have five pairs of mammary glands, the rat six, whilst in humans only one pair develops in the thoracic region (Hennighausen and Robinson, 2005; Maller et al., 2010). In the mouse, all five pairs of mammary fat pads lie just below the skin, located along what is known as the 'mammary line' and are named according to their anatomical location as thoracic (three pairs) or inguinal (2 pairs) (Richert et al., 2000). The primary evolutionary function of the mammary gland is to secrete milk protein and fats during lactation to support suckling young. To this end, in mice, the mammary gland is capable of producing up to 20% of the dam's body weight in milk (Hennighausen and Robinson, 2005).

1.2.2 Cellular composition of the mouse mammary gland

From a macroscopic perspective, each mammary fat pad in the mouse has a centrally-located lymph node and an external nipple to which the primary epithelial duct is connected to allow for the release of milk to the body's surface during lactation (Richert et al., 2000). Branching morphogenesis and repeated bifurcations ultimately form an arborised 'tree-like' epithelial architecture in the mouse mammary gland (Silberstein, 2001). Microscopically, two cellular compartments constitute the mammary gland, the epithelia and the surrounding mammary stroma, which are derived during embryogenesis from the ectoderm and mesoderm, respectively (Parmar and Cunha, 2004). These compartments consist of a number of different cell types which interact closely with one another. Epithelial cells form the ductal network, consisting of two discrete populations of epithelial cells that form a bi-layered structure; the inner luminal epithelial cells, which form the ducts and terminally differentiate to generate the secretory alveoli, and the contractile myoepithelial cells which form a continuous, basal layer surrounding these luminal cells and directly contact the basement membrane (Figure 1.4) (Hennighausen and Robinson,

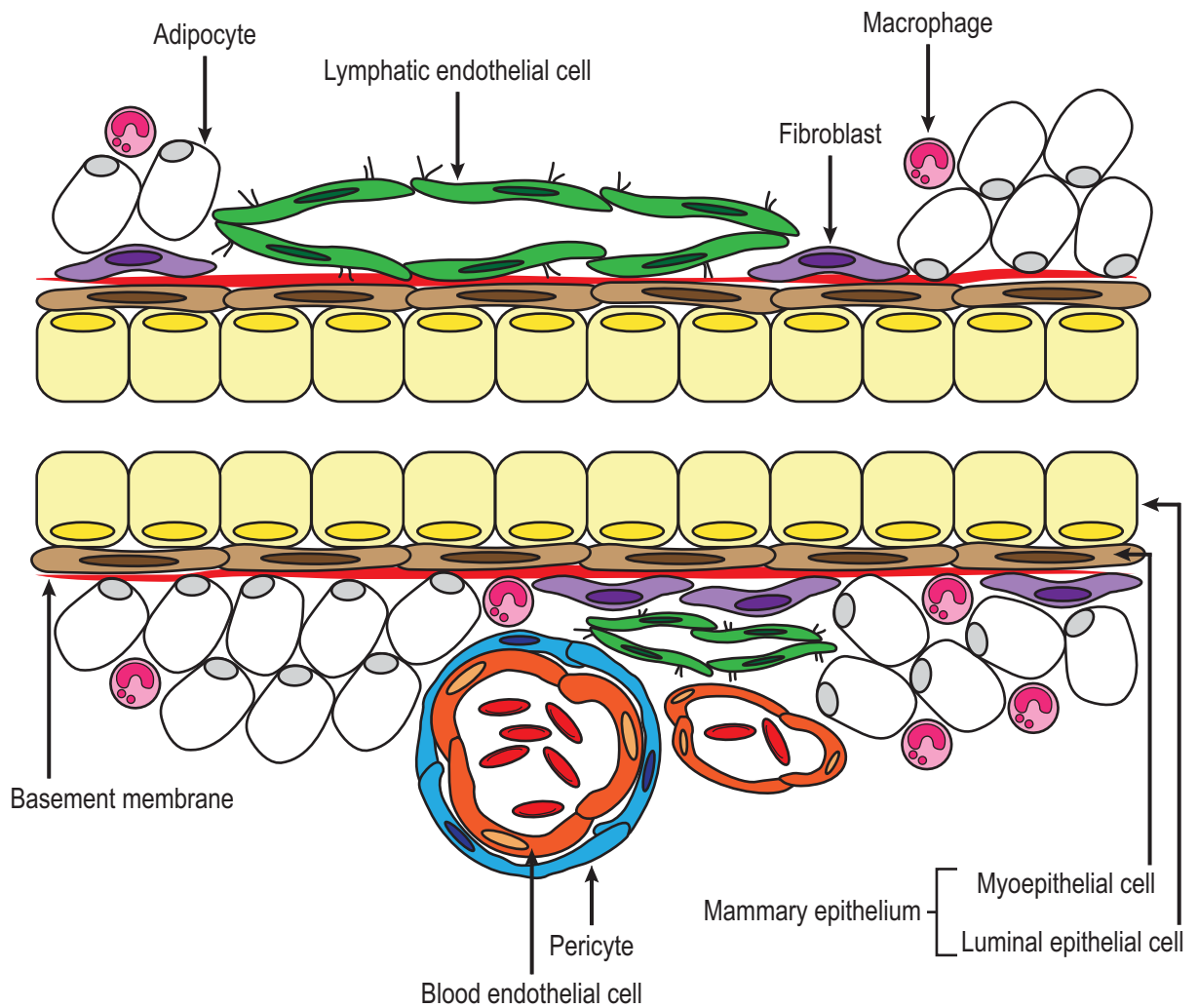


Figure 1.4 - Populations of cells that reside in the mouse mammary gland.

The mouse mammary gland milieu comprises numerous cell types which interact closely with one another: epithelial cells (luminal and myoepithelial) that form the ductal epithelia, adipocytes which constitute the fat pad into which the ductal epithelium is embedded, blood endothelial cells and their associated supporting pericytes, stromal cells, including fibroblasts and macrophages, and lymphatic endothelial cells.

2005; Watson and Khaled, 2008). On the other hand, the stromal compartment consists of adipocytes which constitute the fat pad into which the expansive ductal network is embedded; BEC and associated supporting pericytes that form the blood vasculature; stromal cells including fibroblasts and a range of immune and haematopoietic cells such as macrophages, neuronal cells which innervate the mammary gland; and last but by no means least, LEC which comprise the lymphatic vascular network (Figure 1.4) (Watson and Khaled, 2008). The latter are frequently overlooked as comprising part of the cellular pool in the mouse mammary gland milieu.

1.2.3 Mouse mammary gland morphogenesis

Mouse mammary gland morphogenesis occurs in distinct embryonic and postnatal stages that are inherently linked to sexual maturity and reproduction of the animal. Postnatal mammary gland morphogenesis encompasses both puberty and the adult female mammary gland developmental cycle consisting of pregnancy, lactation and involution. Whilst the focus of this study was on postnatal mouse mammary gland development, for the purpose of completeness, a brief explanation of the sequential processes involved in embryonic mammary gland development is included.

1.2.3.1 Embryonic mammary gland development

The first indication of the initiation of mammary gland morphogenesis in the mouse embryo occurs as early as E10.5, with the formation of two 'mammary lines' or 'milk lines' of ectodermal origin, which extend in an anteroposterior direction along both lateral flanks in the developing embryo (Richert et al., 2000; Veltmaat et al., 2003; Watson and Khaled, 2008). By E11.5, the mammary glands can be detected as individual structures in the form of five pairs of round, multi-layered ectodermal, symmetrically positioned mammary placodes (Watson and Khaled, 2008); each pair developing in an asynchronous temporal fashion (Mailleux et al., 2002). Between E12.5-13.5 these mammary placodes subsequently transform into elevated bulb-shaped buds of epithelial cells that can be distinguished morphologically from the surrounding epidermis and by E14.5 these distinct epithelial buds penetrate into the underlying dermal mesenchyme (Veltmaat et al., 2003). It is here that further mammary gland development is temporarily arrested in female mice, whilst androgen receptor activation in male embryos results in epithelial bud degeneration by E15.5. This testosterone-mediated destruction of mammary buds in male mice is unique to murine embryonic development (Veltmaat et al., 2003). At this point, further development resumes in female embryos whereby each mammary bud elongates to form a sprout that begins to penetrate the underlying mammary fat pad precursor tissue; with each sprout

subsequently forming a lumen that eventually opens onto the surface of the skin where a nipple forms via epidermal invagination (Veltmaat et al., 2003). Rudimentary ductules begin to develop around E16.0 and by E18.5 these ductules have established a small, simple network of between 10-15 branches that occupy a minor proportion of the overall fat pad at birth. At this stage of embryonic development, additional growth of the mammary gland is halted, where the gland remains quiescent until puberty, at around three weeks of age, when hormonal-derived signals drive a rapid growth spurt in the mammary gland parenchyma (Watson and Khaled, 2008).

1.2.3.2 Postnatal mammary gland development

1.2.3.2.1 Pubertal mammary gland development

In the first few postnatal weeks, the rudimentary mammary ductal tree undergoes allometric growth until puberty (approximately three weeks of age) when ovarian steroid hormones, particularly estrogen, initiate peak ductal growth from 3-6 weeks of age (Richert et al., 2000). Pubertal mammary gland development can be considered an active phase of proliferation. During this time, terminal end buds (TEB), which are bulbous structures that contain highly proliferative cells, appear at the tips of growing ducts enabling the elongation and branching of these ducts into the surrounding fat pad stroma (Figure 1.5A). Proliferation within these TEBs results in ductal elongation, whilst cleaving of TEBs yield bifurcation of the ducts to form branches (Richert et al., 2000; Watson and Khaled, 2008). This process is known as 'branching morphogenesis', a common developmental process shared by several tissues, including the lung, salivary gland and kidney (Silberstein, 2001). Around five weeks of age the mammary ducts have characteristically filled two-thirds of the surrounding fat pad tissue (Silberstein, 2001) and eventually by 10-12 weeks of age, the TEBs have regressed as the limits of the mammary fat pad are reached and the entire adult female nulliparous gland becomes filled with a regularly-spaced branched network of primary and secondary ducts lacking alveoli (Figure 1.5B); as a result growth ceases (Watson and Khaled, 2008).

As a means of elucidating the molecular mechanisms involved in pubertal branching morphogenesis, a myriad of mouse models with overt ductal phenotypes during puberty have been investigated. Regulators identified to date, as reviewed by Howlin *et al.*, include the hormones, estrogen and progesterone, growth factors and their respective receptors such as epidermal growth factor and HGF, transcription factors and co-activators, cell cycle regulators, adhesion molecules, cytokines and extracellular matrix molecules and matrix metalloproteinases (MMP) (Howlin et al., 2006). Nevertheless

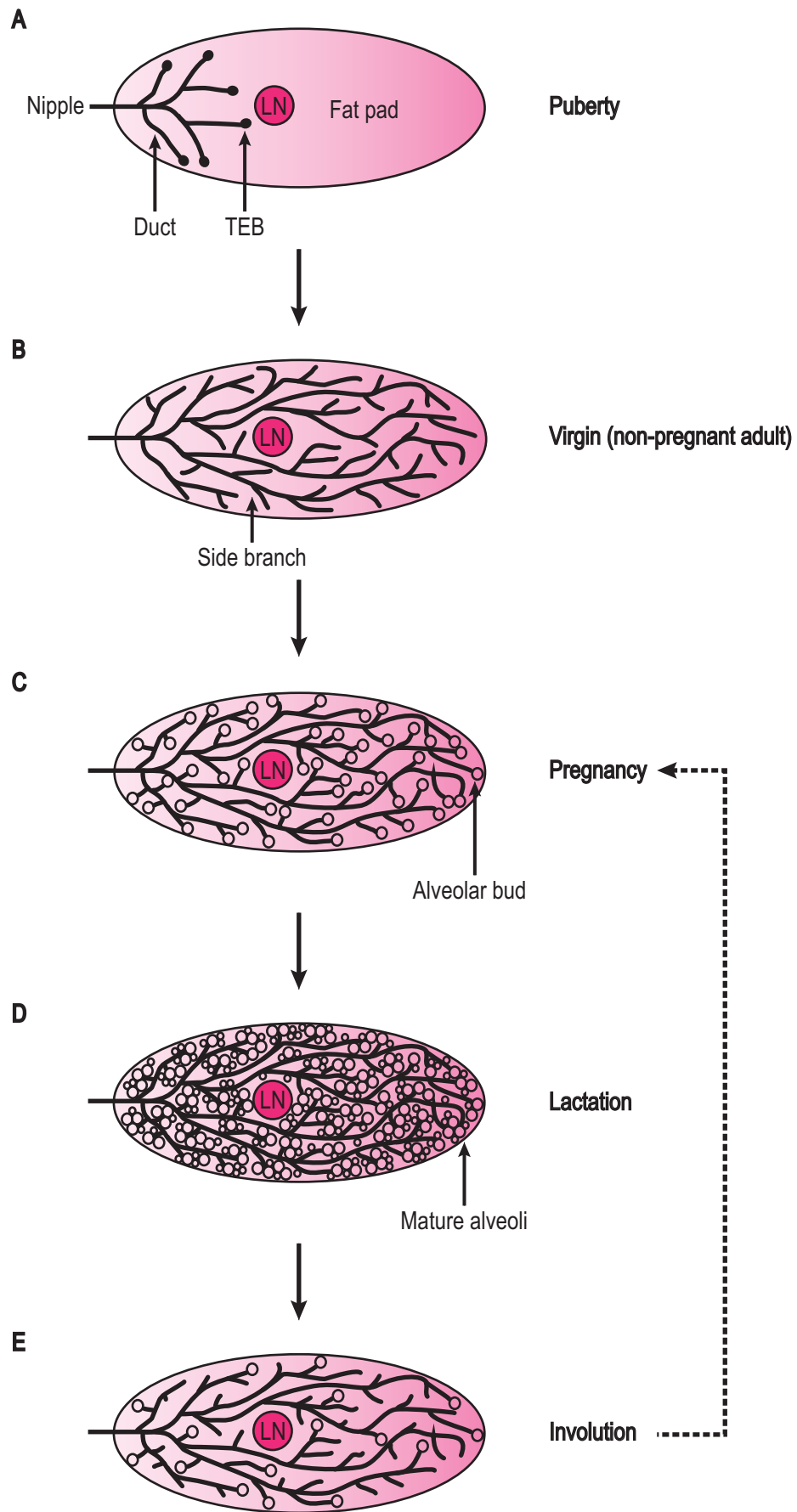


Figure 1.5 - Stages of postnatal mouse mammary gland development.

Schematic representation of the different stages of postnatal mouse mammary gland development; from a pubertal state (A), to a mature nulliparous adult gland (B) which subsequently undergoes major hormonal-induced changes during pregnancy (C), lactation (D) and involution (E). LN - lymph node, TEB - terminal end bud. Figure adapted from Hennighausen and Robinson, 2005; Watson and Khaled, 2008.

a great deal more insight is required to completely understand the regulatory mechanisms controlling this important period of mouse mammary gland development.

1.2.3.2.2 The adult nulliparous mammary gland

In the absence of pregnancy, the adult nulliparous, or virgin mammary gland is generally considered to be relatively inactive or held in a 'resting' state. However, the post-pubertal mouse mammary gland is exposed to cyclic hormonally-induced fluctuations that constitute the estrous cycle; the equivalent of the menstrual cycle in humans (Andres and Strange, 1999; Fata et al., 2001). The murine estrous cycle, controlled by an elaborate interplay between ovarian and pituitary hormones, spans 4-5 days and can be divided into four discrete phases: proestrus, estrus, metestrus and diestrus (Andres and Strange, 1999). During these stages, extensive cycles of secondary branching (proliferation) and lobuloalveolar formation (differentiation), followed by apoptosis (programmed cell death) have been shown to occur concurrently with each resultant estrous cycle (Andres and Strange, 1999; Fata et al., 2001). It is not until pregnancy, however, that full lobuloalveolar development occurs.

1.2.3.2.3 Mammary gland development during pregnancy and lactation

During the 18-21 days of pregnancy, the mouse mammary gland undergoes further developmental changes to give rise to tertiary branches and the formation of alveolar buds (Figure 1.5C). This phase of morphological change represents a peak in mammary differentiation and ultimately culminates in the formation of a fully lactating gland at parturition (Richert et al., 2000). In the initial stages of pregnancy, the epithelial to adipocyte ratio increases due to the vast proliferation of ductal branches, whilst during the second half of pregnancy alveolar buds cleave and differentiate into individual fully mature secretory alveoli; a process known as the lobuloalveolar phase of mammary gland development. These individual alveoli, which eventually become milk-secreting lobules on lactation, gradually expand to fill the majority of the fat pad by late pregnancy, where they persist until the cessation of lactation (Figure 1.5D) (Richert et al., 2000). Myoepithelial cells remain surrounding the alveoli but rather than forming a continuous sheath, as they do in the pubertal gland, they form a discontinuous layer, with their contractility assisting in the movement of milk proteins and lipids along the mammary ducts (Richert et al., 2000). As lactation proceeds, adipocytes become metabolised allowing for the widespread expansion of the mature secretory alveolar subunits into the entire surrounding mammary fat pad (Richert et al., 2000). The process of lactation itself, involving the manufacturing and secretion of milk, continues for around three weeks until the suckling pups are weaned.

1.2.3.2.4 Involution

Following weaning, the mammary gland undergoes post-lactational regression, commonly termed involution, which utilises a highly coordinated process of programmed cell death, known as apoptosis. This stage of postnatal mammary gland development involves the greatest degree of remodelling and remarkably, 80% of the surplus epithelium is removed within just a few days (Watson and Khaled, 2008). Initially, involution is reversible and lactation can be reinitiated upon suckling, however, after two days the mammary gland undergoes an irreversible sequence of cellular death (Richert et al., 2000). Involution itself involves many tightly regulated processes including the suspension of milk protein gene expression; the collapse, asynchronous apoptosis and subsequent phagocytosis of secretory alveolar epithelial cells; extensive rearrangement of the rather chaotic ductal-tree morphology and ultimately the refilling of the gland by adipocytes (Richert et al., 2000). By day 21 of involution, the parous mammary gland resembles an almost 'pre-pregnant' state, somewhat more differentiated, with a more extensive framework of side-branching and the presence of isolated alveoli distributed throughout the gland (Figure 1.5E) (Richert et al., 2000). With each ensuing pregnancy a new round of alveolar expansion, maturation and regression are initiated.

1.2.3.3 Key hormones involved in mouse mammary gland morphogenesis

It is a well-known fact that almost all aspects of mammary gland biology and development are strictly dependent upon and coordinated by a complex interplay between systemic hormones. The minimal hormonal requirements necessary for maintenance of mammary gland morphogenesis are the steroid hormones, estrogen and progesterone, and the peptide hormone, prolactin. These hormones elicit local paracrine interactions between the epithelia and surrounding mammary stroma and undoubtedly themselves control a multitude of mammogenic growth factors (Fendrick et al., 1998; Hennighausen and Robinson, 1998; Parmar and Cunha, 2004). These hormones are instrumental in the dynamic remodelling that occurs in the epithelial and stromal tissue compartments in the mouse mammary gland, during each cycle of pregnancy, lactation and involution.

1.2.3.3.1 Estrogen

Estrogen, produced by the ovaries, is largely responsible for the ductal outgrowth into the surrounding mammary fat pad in the pubertal mouse mammary gland (Silberstein et al., 1994). Prior to puberty, however, the mammary gland remains refractory to the effect of exogenous estrogen (Fendrick et al., 1998). In order to mediate its action, estrogen binds two distinct cognate nuclear receptors encoded by separate genes, estrogen receptor alpha (ER α) and estrogen receptor beta (ER β). Studies from ER α

knockout mouse models have established that embryonic mammary gland development is independent of ER α , rather ER α is required for the subsequent ductal elongation and outgrowth during puberty (Bocchinfuso et al., 2000). In stark contrast, despite detectable levels of expression of ER β in the mouse mammary gland, albeit at low levels (Tremblay et al., 1998; Zeps et al., 1999), deletion of ER β has no adverse effect on ductal development during puberty (Förster et al., 2002). It was observed, however, that ER β knockout glands failed to develop ductal side branches and alveoli following puberty, emphasising the importance of ER β for the complete differentiation of the mouse mammary gland during pregnancy and lactation (Förster et al., 2002).

1.2.3.3.2 Progesterone

The physiological effects of progesterone are mediated through interaction with a specific intracellular receptor, the progesterone receptor (PR). Two isoforms exist, PRA and PRB, which display differential activities as transcription factors. These distinct protein receptor isoforms are encoded by two separate transcripts generated via differential transcription from alternative promoters on the same gene (Conneely et al., 2003). Despite structural similarities, PRA and PRB display divergent functionality *in vitro* and *in vivo* and in the mouse are expressed in a distinct spatial and temporal pattern. PRA is the predominant isoform expressed in the pubertal and virgin mammary gland, whereas PRB is the main isoform detected in pregnancy (Aupperlee et al., 2005). Unlike ER, whose presence is required in the mammary stroma in addition to the epithelia (Mueller et al., 2002), the primary target of progesterone is mammary epithelial-expressed PR, both before and during pregnancy (Briskin et al., 1998). Progesterone, through interaction with its receptor, is essential for the extensive side-branching and alveologenesis that occurs during early pregnancy, however, the contribution of this ligand-receptor interaction in the initial ductal growth and branching in the pubertal gland is minor (Briskin et al., 1998).

1.2.3.3.3 Prolactin

Prolactin is a peptide hormone which is produced and secreted by lactotroph cells in the anterior pituitary. Prolactin mediates its function via binding to the prolactin receptor, a transmembrane protein belonging to the class I cytokine receptor family. This peptide hormone has two essential roles in reproduction. Firstly, it is responsible for the maintenance of the corpus luteum during early pregnancy, which ensures the secretion of both estrogen and progesterone. Secondly, and more importantly, prolactin is critical for the proliferation and functional differentiation of the lobuloalveoli in the mammary gland; constituting maintenance of lactation (Hennighausen and Robinson, 2005). Around mid-gestation, both functions of prolactin are replaced until birth of the young by placental lactogens; peptide

hormones which bind to the prolactin receptor, but are instead produced by the placenta during pregnancy (Hennighausen and Robinson, 2005).

1.2.4 A comparison of the mouse and human mammary glands

Profound similarities exist between the development, hormone-responsiveness and function of the mammary gland in mice and humans, making the mouse an excellent model to study postnatal mammary gland function and dysfunction. Nevertheless, a few notable differences need to be considered. While mouse and human mammary glands have comparable rudimentary parenchyma, which consists of a bi-layered epithelial tree, in the mouse this arborised ductal network arises from a single elongated duct, whereas in humans, multiple branching ductal networks are present that converge at the nipple (Maller et al., 2010; Sternlicht et al., 2006). However, both the human and mouse mammary ducts contain similar populations of epithelial cells, including luminal and myoepithelial subtypes, which express identical markers; cytokeratins 8 and 18 and cytokeratins 5, 14 and alpha smooth muscle actin (α SMA), respectively (Parmar and Cunha, 2004).

The key functional components of the mouse and human mammary gland differ morphologically, despite both being hormone-responsive, dynamically active during the estrous and menstrual cycles and producing milk (Cardiff, 1998). In the human breast, the functional unit is termed the 'terminal ductal lobular unit' (TDLU). The TDLU consists of a small group of blind-ended lobules, or acini, emanating from a terminal duct which are encased by loose intralobular connective tissue that in turn is surrounded by a denser connective tissue layer (Figure 1.6A), effectively resembling a cluster of grapes at the end of a stem (Parmar and Cunha, 2004). On the other hand, in mice, the major functional entities are referred to as 'lobuloalveolar units', which lack this intralobular loose connective tissue constituent (Cardiff, 1998; Parmar and Cunha, 2004).

Furthermore, the relative abundance and nature of the stromal connective tissue differs substantially between the human and mouse mammary gland. The mouse mammary gland is predominantly adipose tissue interspersed with a small acellular fibrous tissue component, whilst the human breast is primarily fibroblastic (Parmar and Cunha, 2004). In the mouse mammary gland the stroma surrounding the ducts (periductal stroma) is relatively sparse. Instead, the mouse mammary gland is characterised by an abundance of adipose tissue that lies in very close proximity to the ductal epithelium (Figure 1.6B). In the human breast, an abundance of fibrous connective tissue and fibroblasts exist surrounding the ducts and alveoli (Figure 1.6A). Despite the human breast containing a substantial fat component to a similar

NOTE:
This figure is included on page 34
of the print copy of the thesis held in
the University of Adelaide Library.

Figure 1.6 - A comparison between human and mouse mammary tissue.

Schematic representation of the human breast illustrating a terminal ductal lobular unit (TDLU) in close association with interstitial fibrous connective tissue stroma and not the distant adipose tissue (**A**), and the mouse mammary gland showing the spatial localisation of the ductal epithelium with adjacent fibroblasts and adipocytes (**B**). Figure adapted from Parmar and Cunha, 2004.

degree to that found in the mouse mammary gland, the difference lies in its distant spatial locality compared to the ductal epithelium (Maller et al., 2010; Parmar and Cunha, 2004).

From a developmental biology perspective, the formation of the human breast proceeds in a similar stepwise fashion to that in the mouse, just at a more measured rate owing to the differential gestation periods; 9 months versus 18-21 days, respectively. By around day 35 (4th week of gestation) the first visible indication of human mammary gland development can be detected, however, it is not until six months of gestation that the basic tubular architecture of the human mammary gland is established (Parmar and Cunha, 2004). In contrast to murine mammary gland development, in which testosterone initiates destruction of the mammary bud in males during embryogenesis (Veltmaat et al., 2003), glands develop similarly in both male and female human fetuses until puberty (Parmar and Cunha, 2004). Nonetheless, similarly to mice, puberty results in drastic changes in the human breast and strikingly, the adult, non-lactating human breast consists of greater than 80% stromal tissue (Parmar and Cunha, 2004).

1.2.5 Blood vascular remodelling during postnatal mouse gland morphogenesis

For obvious reasons, studies investigating changes in the microvasculature in the adult human breast over the course of the female reproductive cycle are not feasible; therefore the majority of mammary gland biology data is generated from animal studies, primarily the mouse.

Normal mouse mammary epithelial tissue undergoes extensive morphological changes, including growth, differentiation and reorganisation, in response to hormonal signals and functional demands beginning at puberty and encompassing the complete adult female reproductive cycle, as detailed in sections 1.2.3.2.2-4. These dynamic remodelling events are not restricted to the mammary epithelia and extend to the mammary endothelium, which undergoes repeated cycles of angiogenic expansion during pregnancy and lactation, followed by a concomitant ordered regression at involution (Djonov et al., 2001; Matsumoto et al., 1992; Pepper et al., 2000). These necessary recurring modifications in the mammary vasculature ensure that the functional capacity and homeostatic-state of the mammary gland is maintained. In particular, during pregnancy and lactation, a time when the epithelial parenchyma expands dramatically at the expense of the surrounding stromal and adipose tissue, there is a need for an increased supply of oxygen, nutrients and fluid to sustain the raised secretory and metabolic activity of the mammary epithelial cells themselves (Andres and Djonov, 2010).

1.2.5.1 Puberty

At the onset of puberty in the mouse, the microvasculature of the mammary gland is composed primarily of a periductal capillary plexus (Figure 1.7A), which subsequently expands slightly in both size and complexity in the mature virgin gland (Figure 1.7B). During these developmental stages the blood vascular capillaries, which rarely extend into nearby adipose tissue alone, have been demonstrated to run either in parallel or encircle the limited mammary ducts (Djonov et al., 2001; Matsumoto et al., 1992). These microvessels are characterised by the presence of abundant capillary sprouts (arrows, Figure 1.7A) indicative of sprouting angiogenesis (Djonov et al., 2001).

1.2.5.2 Pregnancy

During pregnancy, the mammary vasculature rapidly expands, giving rise to an increase in the number of capillaries and the formation of additional capillary sprouts, which intricately intertwine with one another to form 'capillary baskets' (dashed outline, Figure 1.7C) surrounding the developing alveoli. A switch from sprouting angiogenesis to intussusception, a process by which new blood vessels arise from the splitting of pre-existing blood vessels, occurs in the last phase of pregnancy (Djonov et al., 2001; Matsumoto et al., 1992). Furthermore, Pepper *et al.* demonstrated via quantification of capillary density in the mouse mammary gland, that just prior to parturition the mammary blood vascular network reaches its maximal density (Figure 1.7F) (Pepper et al., 2000).

1.2.5.3 Lactation

On lactation, the size of the 'capillary baskets' or 'vascular honeycomb' structures increases further in parallel with the extensive proliferation of the alveoli that occurs during this stage of the reproductive cycle; therefore the vasculature of the lactating mammary gland is characterised by a well-established capillary meshwork encasing the alveolar units (Figure 1.7D) (Djonov et al., 2001). Accompanying the expansion of the vascular network is an increase in the surface area of the individual EC (Matsumoto et al., 1992). Consequently, the endothelium in the lactating mammary gland can be considered fully developed, both morphologically and metabolically.

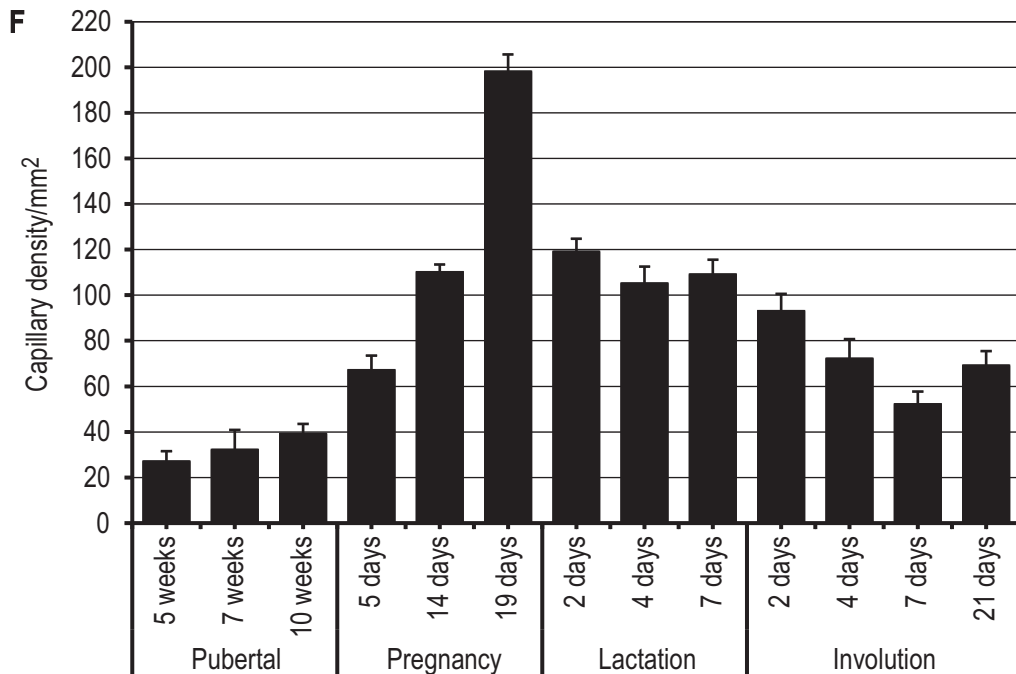
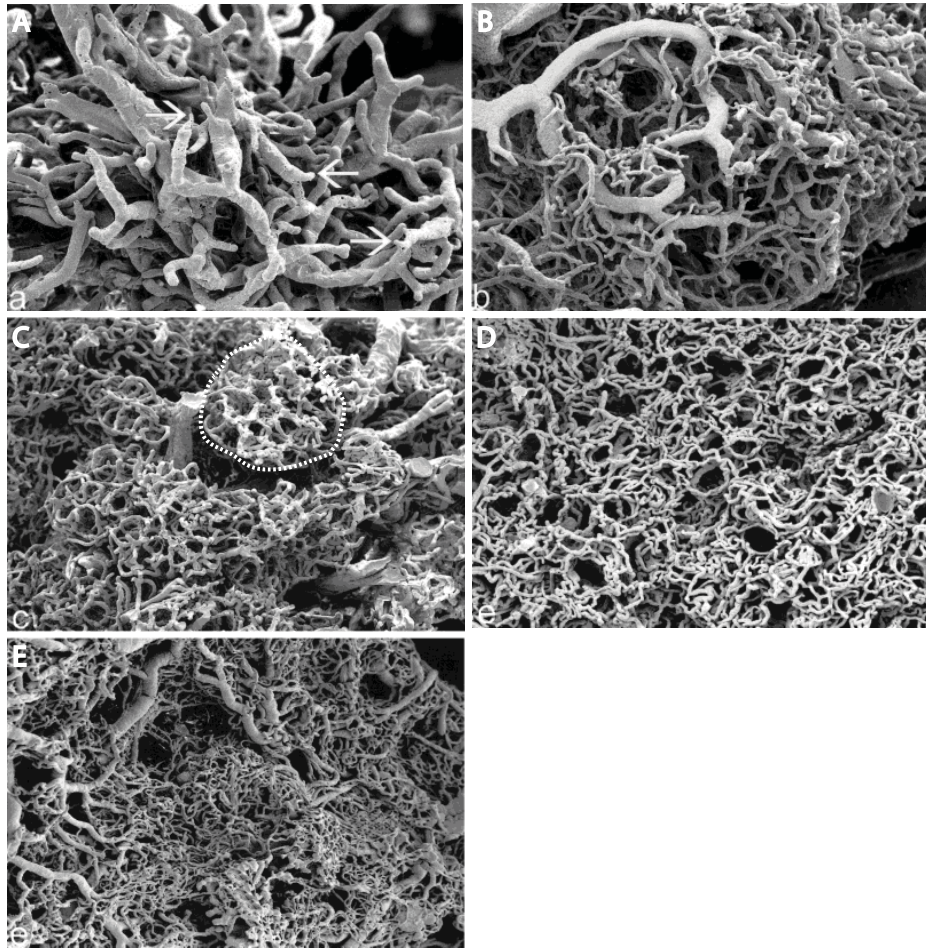


Figure 1.7 - Blood vascular remodelling during postnatal mouse mammary gland morphogenesis.

Scanning electron micrographs of methyl methacrylate corrosion casts of the mouse mammary gland vasculature; at 5 weeks puberty (A), in a 12 week virgin mouse (B), 19 days pregnancy (C), 10 days lactation (D) and 6 days involuting (E). Images (A-E) from Djonov et al., 2001. (F) Quantification of capillary density in the mouse mammary gland. Error bars represent \pm standard deviation. Data adapted from Pepper et al., 2000.

1.2.5.4 Involution

Following the cessation of lactation, regression of the mammary blood vasculature occurs in conjunction with apoptosis of the secretory alveoli. Regression of the vasculature is achieved by regional collapse of the 'basket-like' vascular networks, capillary retraction and endothelial attenuation (Djonov et al., 2001). As the alveoli asynchronously involute, the blood vessel network appears quite disorganised and it is not uncommon for well-preserved 'capillary baskets' to be detected adjacent to regions of collapsed or contracted vasculature (Figure 1.7E) (Djonov et al., 2001). It has been observed that the mammary vasculature just ten days into the involuting process has already reverted to a similar degree of vascular complexity to that seen in the virgin mammary gland (Matsumoto et al., 1992; Pepper et al., 2000). At this stage, the mammary blood vascular network remains in a steady-state, prior to a subsequent round of expansion with the succeeding pregnancy.

1.2.5.5 Regulators of mammary blood vascular remodelling in the mouse

Despite the well-documented cyclical reorganisation of the mammary gland blood vasculature, surprisingly little is known about the signals and molecular mechanisms that control physiological vascular remodelling in the mammary gland. VEGF-A, the founding member of the VEGF family and a potent angiogenic stimulus (Ferrara and Davis-Smyth, 1997), is the best characterised mediator to date. Previous studies have demonstrated that *Vegfa* expression is differentially regulated at the transcriptional level throughout the adult mouse reproductive cycle (Hovey et al., 2001; Pepper et al., 2000). Furthermore, Islam *et al.* have recently shown that VEGF-A protein levels also fluctuate during murine postnatal mammary gland development with highest levels detected late in pregnancy, prior to a gradual decline in expression during lactation and involution (Islam et al., 2010), corresponding to a similar peak and trough observed in vascular density at these stages (Pepper et al., 2000). A study by Rossiter *et al.* further addressed the role of VEGF-A via conditional inactivation of *Vegfa* in the mammary epithelia, postulated to be the major source of mammary gland-derived *Vegfa* (Islam et al., 2010; Pepper et al., 2000). The ablation of *Vegfa* in the epithelial cellular pool resulted in partial disruptions in the spatial organisation of the blood microvasculature; not only were these vessels less abundant, less branched and less convoluted, they failed to retain their proximity to the alveoli, nor did they form the characteristic 'capillary baskets' (Djonov et al., 2001; Matsumoto et al., 1992) observed in the normal mammary gland setting (Rossiter et al., 2007). Intriguingly, there was no significant overall reduction in the density of the microvasculature in these mice before or during pregnancy, suggesting

that mammary epithelial-derived *Vegfa* is partially dispensable for angiogenesis in the mammary gland vasculature (Rossiter et al., 2007).

As previously discussed, hormones are instrumental for all aspects of epithelial development and function in the mouse mammary gland. It is therefore conceivable that these sex steroid hormones may also be involved in the modulation of mammary vascularisation. Indeed, it has been proposed that the effects of estrogen in relation to the vascular endothelium involve its direct and/or indirect regulation of pro- and anti-angiogenic growth factor production by mammary epithelial cells (Dabrosin, 2005). Interestingly, a direct target of estrogen is the rat *Vegfa* gene, which has been found to contain a functional estrogen response element, suggesting an estrogen-mediated regulation of *Vegfa* transcription (Hyder et al., 2000). In accordance with this and as previously mentioned, the highest levels of VEGF-A are found in late pregnancy in normal mouse mammary gland development (Islam et al., 2010), whilst in human breast tissue it has been observed that extracellular levels of VEGF-A *in vivo* increase two-fold during the luteal phase of the menstrual cycle (Dabrosin, 2003). These two windows are characterised by high levels of both estrogen and progesterone, suggestive of a role for progesterone acting in collaboration with estrogen to induce the cyclic variation in VEGF-A expression; a theory that has since been substantiated (Wu et al., 2004). A more definitive role for progesterone in the dynamic changes in the mammary gland blood vasculature is yet to be documented. In addition to the mammary epithelial cells, human EC have been demonstrated, somewhat ambiguously, to express functional estrogen receptors (Cid et al., 2002; Kim-Schulze et al., 1996). Taken together, these data allude to the role of estrogen in potentiating the complex process of angiogenesis in one of two ways, either by inducing the epithelium to impart angiogenic stimulation or by acting directly on EC themselves.

In addition to steroid hormones, prolactin, another potent mediator of the growth and differentiation of the mammary gland, has been shown to have angiogenic activity. However, on proteolytic cleavage of full-length prolactin, anti-angiogenic proteolytic fragments, known as vaso-inhibins, are generated (Struman et al., 1999). These contradictory roles for prolactin still remain under debate, largely due to the conflicting reports on the expression and molecular heterogeneity of the prolactin receptor in EC of different vascular beds (Ochoa et al., 2001; Ricken et al., 2007) and whether the action of prolactin on EC is direct or indirect. A thought-provoking review by Clapp *et al.* summarises the possible interplay of these opposing roles of prolactin in the normal mammary gland. Clapp *et al.* hypothesised that low levels of both cathepsin D and MMPs; proteases which have previously been shown to be involved in mammary gland tissue remodelling processes (Benaud et al., 1998; Green and Lund, 2005) and that

have the ability to generate vasoinhibins (Baldocchi et al., 1993; Macotela et al., 2006) are not present in sufficient quantities to generate vasoinhibins during pregnancy and lactation, thus prolactin is largely left intact, supporting mammary gland angiogenesis and blood flow during lactation (Clapp et al., 2008). Alternatively, high levels of proteolytic activity during the involuting phase of mammary gland development would favour the production of vasoinhibins, thereby inhibiting blood vessel growth and stimulating vascular regression (Clapp et al., 2008). Despite offering a novel mechanism by which prolactin could regulate the balance of positive and negative factors controlling blood vascular remodelling in the postnatal mammary gland, this hypothesis remains to be authenticated experimentally. It has, however, been shown that the expression of prolactin, and its cathepsin D-mediated cleavage, vary with the estrous cycle in the bovine corpus luteum (Erdmann et al., 2007), another organ that undergoes physiological angiogenesis during adulthood.

To date, the aforementioned factors are recognised as playing a key role in mammary gland vascular remodelling; nevertheless this catalogue is by no means exhaustive. As reviewed by Dabrosin *et al.*, considerably less is known about a number of other factors with established roles in angiogenesis, including IGF-1, growth hormone, FGF-2, thrombospondin 1 (TSP1), interleukin-8 and soluble VEGFR-1, in the setting of the breast (Dabrosin, 2005). Studies by Haldimann *et al.* have recently revealed a putative role for ephrinB2 in the remodelling of the mammary gland vasculature (Haldimann et al., 2009). Much remains to be discovered in terms of additional growth factors that act in concert to regulate vascular remodelling in the setting of postnatal mouse mammary gland morphogenesis.

1.2.6 The mammary lymphatic vascular network

1.2.6.1 In the human breast

The gross anatomy of the lymphatic system in the adult female human breast and the signals that regulate changes in the lymphatic vasculature are poorly understood. Historical studies do exist, however these are predominantly anatomical observations based largely on post-mortem injection studies. Our current anatomical knowledge of human breast lymphatics still depends on studies that date back to the mid-nineteenth century, which were derived primarily from initial observations made by a French anatomist, Sappey (Figure 1.8A), and subsequently summarised in drawings by Poirier and Cuneo (Figure 1.8B). These diagrams, which remain in press today, portray a sub-areolar lymphatic plexus and a small number of larger lymphatic vessels which drain to axillary lymph nodes (Suami et al., 2008; Suami et al., 2009). Despite the revolution in surgical techniques, the advent of sentinel lymph

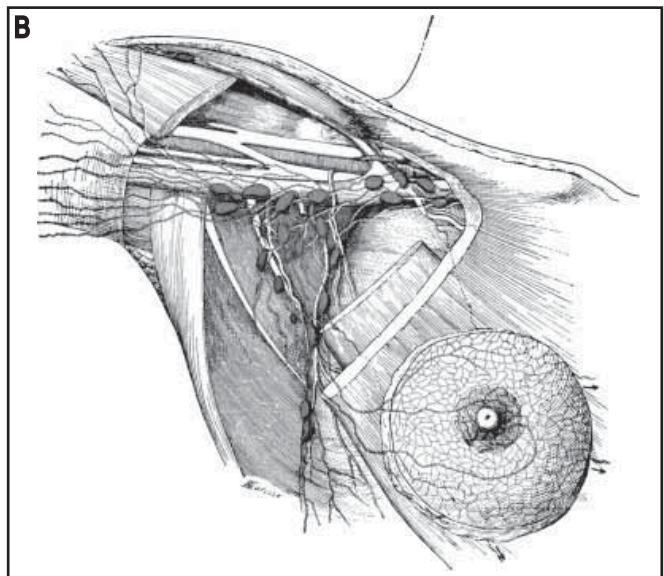
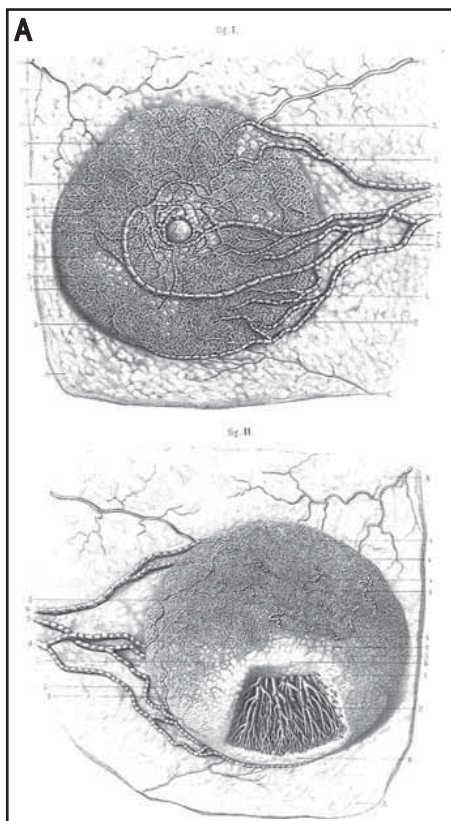


Figure 1.8 - Historical drawings of the human breast lymphatic network.

(A) Sappey's drawing of the lymphatics in the female breast from 1874. (B) Poirier and Cuneo's summary diagram of lymphatic drainage in the human breast. Images from Suami et al., 2008 (A); Suami et al., 2009 (B).

node detection and the implementation of intravital dyes to visualise lymphatic vessels, there has been no real advance in the understanding of the lymphatic vasculature in the human breast.

1.2.6.2 In the mouse mammary gland

As discussed above, the murine mammary blood vasculature is constantly remodelled during physiological mammary gland morphogenesis, undergoing repeated cycles of expansion and regression in parallel with the dynamic, hormonally-stimulated growth and differentiation of the mammary epithelia (Djonov et al., 2001; Matsumoto et al., 1992). The patterning of lymphatic vessels in the normal mouse mammary gland, however, has received little such attention over the years, evidenced by limited publications within the field. The identity and source of lymphangiogenic stimuli that drive the development of the lymphatic network in the mouse mammary gland is even more poorly understood.

The best reported documentation on the subject of the mammary lymphatic vasculature is a rodent study published over a decade ago (Ohtani et al., 1998). In this study Ohtani *et al.*, utilising a rat model, investigated the distribution and ultrastructure of lymphatic vessels in virgin, pregnant, lactating and involuting rat mammary glands via light microscopy and found that across all stages analysed, lymphatic vessels resided within the interlobular connective tissue and along the mammary ducts. During lactation most of the interlobular lymphatic vessels were demonstrated to be expanded and positioned in close proximity to the alveoli, with no accompanying relationship to blood vessels. Ohtani *et al.* proposed that the interlobular lymphatic capillaries drain into larger lymphatic collecting vessels, which were shown to either follow the path of adjacent arteries and veins or large mammary ducts (Ohtani et al., 1998). Besides this elementary investigation, no current documentation exists which serves to further explore lymphatic vascular growth and remodelling and the signals that regulate lymphangiogenesis in the mouse mammary gland; thus forming the underlying rationale for this project.

1.3 BREAST CANCER AND LYMPHATIC VESSELS

Hippocrates, the father of Western Medicine, first described breast cancer in 460 BC. Breast cancer is a disease in which abnormal cells in the breast tissue multiply and form an '*in situ*' or invasive tumour, most commonly originating from the ductal or lobular tissue (Australian Institute of Health and Welfare & National Breast and Ovarian Cancer Centre, 2009). Today, more than a million women worldwide are newly diagnosed with breast cancer every year (Armer et al., 2009). In Australia, breast cancer is now

recognised as the most common cancer in women, excluding cancers of the skin, accounting for over a quarter (ie. 28%) of all reported cancer cases in women in 2006. Breast cancer affects as many as one in nine Australian women and one in 38 women will lose their battle with this disease before the age of 85. Although much less common in males, men also develop breast cancer (Australian Institute of Health and Welfare & National Breast and Ovarian Cancer Centre, 2009).

Whilst lymphatic vessels have been inextricably linked with the progression of many forms of human epithelial cancers, for the purpose of this study, the role of the lymphatic vasculature will be discussed in relation to breast cancer. Lymphatic vessels can be considered of fundamental importance in breast cancer in at least two ways. Firstly, lymphatic vessels can facilitate metastasis; a leading cause of mortality in breast cancer patients, by providing an accessible route for the dissemination of tumour cells (Ran et al., 2010). Metastasis to the lymph nodes represents the single most important prognostic indicator in breast cancer patients (Fisher et al., 1983). Secondly, secondary lymphoedema is a frequent complication for up to 40% of breast cancer patients following surgical resection of axillary lymph nodes (Armer et al., 2009) and is a disabling condition for which there is currently very little effective treatment. Despite the involvement and importance of lymphatic vessels in breast cancer, very little is known about the genes and molecular mechanisms that regulate their growth and development in the human breast and many of the mechanisms underlying the ability of breast cancer cells to metastasise remain poorly understood.

1.3.1 Tumour metastasis

Metastasis is the leading cause of mortality in patients diagnosed with a range of human cancers, accounting for approximately 90% of cancer-related deaths (Eccles and Welch, 2007; Gupta and Massagué, 2006). Tumours can metastasise to distant sites in the body via three main routes; the blood vasculature (haematogenous spread), the lymphatic system (lymphogenous spread) or more rarely, directly into tissues and body cavities (Stacker et al., 2002). Compared to haematogenous spread, little is known about the biology of lymphatic vessels within tumours, the regulation of tumour lymphangiogenesis and the molecular mechanisms that malignant tumour cells use to exploit the lymphatic vasculature in order to metastasise. It is generally accepted that some of the most common forms of solid tumours, including melanoma (Dadras et al., 2003), breast (Fisher et al., 1983; Schoppmann et al., 2004), prostate (Jennbacken et al., 2005), colorectal (Barresi et al., 2011), lung (Harada et al., 2011) and head and neck squamous cell carcinomas (Kyzas et al., 2005), preferentially spread from the site of origin to invade regional and distal draining lymph nodes via the lymphatic

vessels, where they can subsequently enter the systemic circulation and eventually disseminate to distant tissues and organs in the body. The extent of lymph node metastases, an early and common event in metastatic disease, and lymphatic vessel density thus represents a major determinant for the staging and prognosis of many of these human malignancies and most frequently guides therapeutic options. Despite the fact that poor patient prognosis has been correlated with increased lymphatic vessel density and the incidence of lymph node metastases in many human tumours; major conjecture still exists, however, regarding the presence and functionality of lymphatic vessels within tumours (intratumoural lymphatic vessels). In some experimental systems it has been shown that intratumoural lymphatic vessels are present, but are poorly functional and conduct no fluid, due to high intratumoural pressure (Padera et al., 2002; Wong et al., 2005); compared with lymphatic vessels located at the tumour periphery (peritumoural lymphatic vessels) which have been demonstrated to be fully functional (Padera et al., 2002).

Lymphatic vessels may be favourably selected over the blood vasculature as a portal for metastasis as they seem to offer many advantages for the invasion and trafficking of tumour cells, such as, they are naturally equipped for the transportation of cells around the body; the nature of the vessels themselves, which are considered 'leakier' than blood vessels due to a discontinuous basement membrane and loose intercellular junctions; a reduced flow rate and corresponding reduction in shear stress leading to an increase in cell survival; and a dramatically higher concentration of hyaluronan in the lymph, a molecule known to elicit strong cellular protective properties (Laurent and Fraser, 1992; Ran et al., 2010). The exact mechanism(s) by which tumour cells metastasise via the lymphatic vessels currently remain enigmatic. It is plausible that tumour cells stimulate the formation and invasion of newly-induced intratumoural and peritumoural lymphatic vessels by the production of lymphangiogenic growth factors. However, the invasion of pre-existing lymphatic vessels residing at the tumour margins may equally contribute to metastatic potential. It is also possible that the propensity of a tumour to metastasise involves a complex interplay between both pathological and physiological lymphatic vascular networks.

1.3.1.1 Breast cancer-related metastasis

Mounting clinical and experimental data suggest that lymphatic vessels function as a critical transport route for the metastasis of breast cancer cells (Ran et al., 2010; Skobe et al., 2001). Accordingly, the major cause of death from breast cancer is the dissemination of the primary breast tumour to form distant metastases that interfere with the function of vital organs, namely the lung, bone, brain and other visceral organs (Ran et al., 2010; Schoppmann et al., 2004). Lymph drainage from the breast is

therefore of paramount importance in relation to metastasis; the axillary lymph nodes receive about 75% of the total lymph drainage from the breast. This is reflected by the increased frequency of tumour metastases to these nodes, which are ineffective barriers to the spread of cancer (Bundred et al., 1994). The presence or absence of involved axillary lymph nodes is ultimately the single best prognostic predictor of breast cancer survival in clinical use, to date, independent of tumour size, histological grade and other clinicopathological parameters (Fisher et al., 1983).

In addition to the reasons mentioned above in section 1.3.1, the preferential metastasis via lymphatic vessels of breast cancer cells is likely a result of the high frequency of lymphatic vascular invasion (LVI) observed in breast cancer as compared with blood vascular invasion (BVI) (Ran et al., 2010). Despite the fact that vascular invasion encompassing both types of vessels has been reported in breast cancer and is a poor prognostic marker (Lauria et al., 1995), the vast majority of studies have only identified LVI as a significant predictor of poor patient prognosis and disease outcome (Marinho et al., 2008; Mohammed et al., 2007a; Schoppmann et al., 2004; Woo et al., 2002). One of the largest studies conducted to date, involving a cohort of 1408 subjects, detected LVI in 34.2% of all breast cancer cases, whilst the prevalence of BVI was particularly low, identified in only 4.2% of patients (Lauria et al., 1995). A similar predilection for increased LVI was demonstrated in a separate study of 177 invasive breast carcinomas, in which LVI was detected in 96.4% of all specimens, whereas BVI was detected in only a meagre 3.5% (Mohammed et al., 2007a). Hence, the tendency for LVI over BVI is strong evidence to support the preferential nature of breast cancer for lymphogenous spread. Factors underlying the preferential lymphogenous spread remain to be identified.

1.3.1.1.1 Inhibiting lymphangiogenesis

The inhibition of tumour lymphangiogenesis can be considered one of the most attractive targets in the fight against tumour metastasis and notably breast cancer metastasis. Currently, no clinical therapeutic strategy that specifically targets the development and subsequent progression of metastasis exists. In light of this, the causality between tumour-induced lymphangiogenesis and lymph node metastasis has been demonstrated in a variety of experimental mouse tumour models. The forced expression of either VEGF-C (Karpanen et al., 2001; Mattila et al., 2002; Skobe et al., 2001) or VEGF-D (Stacker et al., 2001) in tumour xenografts and transgenic mouse models promotes tumour lymphangiogenesis and greatly facilitates tumour metastasis. Conversely, inhibiting the VEGFR-3 signalling pathway through the use of various fusion proteins and blocking antibodies has shown promise as a strategy to reduce metastasis, as indicated by a reduction in tumour lymphangiogenesis and dramatic suppression of lymph node metastasis in a variety of mouse tumour models (Burton et al., 2008; He et al., 2002;

Karpanen et al., 2001; Stacker et al., 2001). A similar correlative relationship between expression of VEGF-C and VEGF-D, an induction of lymphangiogenesis, elevated LVI, increased frequency of lymph node metastasis and poor patient prognosis has been documented in several studies of human breast cancer patients (Choi et al., 2005; Gu et al., 2008; Mohammed et al., 2007b; Nakamura et al., 2005; Nakamura et al., 2003).

The growth factors Angpt1 and Angpt2 have also been implicated in the pathogenesis of breast cancer owing firstly, to their elevated levels in the plasma of breast cancer patients (Caine et al., 2003), and secondly, to their apparent association with tumour metastasis and short survival observed in both human breast cancer patient samples and experimentally in mouse models (Holopainen et al., 2009; Imanishi et al., 2007; Sfiligoi et al., 2003). Therefore, Angpt1 and Angpt2 are plausible targets for the modulation of tumour metastasis. More recently, a Nrp2-blocking antibody that inhibits binding of VEGF-C has been shown to reduce tumour lymphangiogenesis and metastasis to sentinel lymph nodes and distant organs, but did not affect quiescent, established lymphatic vessels (Caunt et al., 2008). Consequently, Nrp2 may comprise yet another avenue for anti-lymphangiogenic therapeutic intervention. To date, VEGF-C and VEGF-D represent two of the most logical targets for pharmacological inhibition, however, the role of additional factors in physiological and pathological lymphangiogenesis (as detailed in section 1.1.4.1) remain to be identified. It is perhaps conceivable that in the not so distant future, some of these growth factors will prove to be promising anti-metastatic therapeutic targets to be utilised for the prevention and treatment of human cancer progression.

1.3.2 Lymphoedema

Lymphoedema is a general term encompassing a spectrum of pathological conditions in which there is excessive regional accumulation of protein-rich fluid, or lymph, in the soft tissues. Lymphoedema is caused by a reduction, or stasis, in lymphatic vascular transport, generally as a result of lymphatic vessel hypoplasia or functional insufficiency of the lymphatics. Typically, this manifests as generalised uni- or bilateral swelling of the upper or lower extremities, however, visceral lymphatic abnormalities and swelling of the head, abdomen and genitalia can also occur (Rockson, 2001). Common complications of lymphoedema include the inability to use the affected limb(s), progressive dermal fibrosis, accumulation of adipose and connective tissue, impaired wound healing, compromised immune defence, increased susceptibility to infections and subsequent cellulitis (Rockson, 2001). Lymphoedema can be simplistically classified as primary (hereditary) or secondary (acquired). Secondary lymphoedema is much more prevalent than the primary form and develops as a consequence of lymphatic vascular

damage or obstruction caused by various surgical, traumatic, inflammatory, or neoplastic insults (Loudon and Petrek, 2000; Rockson, 2001). The most common form of secondary lymphoedema worldwide is filariasis, an infection of lymphatic vessels caused by the parasitic worms, *Wuchereria bancrofti* and *Brugia malayi/timori*, which results in obstruction and scarring of the lymphatic vessels culminating in chronic lymphoedema of the lower limbs and genitalia (Pfarr et al., 2009). In developed countries, however, post-operative lymphoedema in breast cancer patients accounts for the majority of secondary lymphoedema cases, with a reported average incidence of 40% (Armer et al., 2009).

Regardless of the cause, once lymphoedema has developed it is essentially incurable and becomes a chronic, potentially debilitating condition for the afflicted individual, requiring lifelong attention. To date, very few effective therapeutic approaches exist for lymphoedema patients. The limited treatment options that are available, however, are based primarily on the control and management of the condition through elevation and massage of the grossly-swollen limb, exercise, physiotherapy, occasional surgery, manual lymphatic drainage and the application of compression garments (Loudon and Petrek, 2000; Rockson, 2001).

1.3.2.1 Breast cancer-related lymphoedema

Breast cancer surgery for axillary lymph node clearance or mastectomy, is the leading cause of secondary lymphoedema in developed countries and manifests as oedema of the arm post-operatively, often with a latent onset. However, lymphoedema can also develop in breast cancer patients from the formation of fibrosis around lymphatic vessels induced by infection, thereby restricting lymph flow, or from the physical obstruction of lymphatic vessels and nodes by the growth of a metastatic tumour (Loudon and Petrek, 2000; Rockson, 2001). The reported incidence of oedema in breast cancer patients following surgery varies substantially in the published literature, reported anywhere from 6% to 80% (Rockson, 2001); with an average incidence of 40% (Armer et al., 2009). This disparity is likely a reflection of differential criteria and measurement techniques applied to define lymphoedema.

The aetiology of breast cancer-related lymphoedema is not fully understood. However, it is generally accepted that the incidence and degree of arm lymphoedema correlates with the extent of axillary clearance, owing to the fact that all of the lymphatic vessels of the upper limb drain either directly, or indirectly, into a terminal group of lymph nodes in the axilla (Loudon and Petrek, 2000). Historically, in the classical Halstedian radical mastectomy, essentially all lymphatic vessels were dissected and removed along with the adjacent chest wall muscles and breast(s). This technique was subsequently

replaced by a more conservative procedure involving the removal of most of the lymphatic vessels and lymph nodes in the axilla of the affected side, known as complete axillary lymph node dissection or clearance (Loudon and Petrek, 2000). Because dissemination to regional lymph nodes via lymphatic vessels is a common first step in breast cancer metastasis, and indeed a variety of other solid human cancers (as previously listed in section 1.3.1), nodal status remains the most important prognostic indicator in breast cancer patients (Fisher et al., 1983). Thus, sentinel lymph node biopsy, first reported in 1993, was developed to accurately predict the spread of tumour cells to regional nodes and to stage patients more precisely. Here lymphatic vessels are followed to the first node, or nodes, to which the lymphatic vessels from the breast drain, that collect an injected dye or isotope, known as the sentinel node(s). If this node(s) is malignancy-free, it predicts negativity in the remainder of the axillary lymphatic vessels, thereby reducing the need for complete axillary dissection of the lymphatic vessels and hence minimising the associated chances of developing lymphoedema (Loudon and Petrek, 2000).

1.3.2.1.1 Therapeutic lymphangiogenesis

There are very few known molecular players that regulate the lymphatic vasculature in the adult; therefore therapeutic options for the reconstitution of damaged lymphatic vessels, enabling restoration of lymphatic flow post-surgery are currently extremely limited. Studies trialling the microsurgical transplantation of autologous lymph nodes as a means of overcoming post-mastectomy-related lymphoedema have had minimal efficacy (Becker et al., 2006). Hence, it has been proposed that local stimulation of lymphangiogenesis, in the vicinity of the area of tumour resection, by the carefully controlled temporal and spatial administration of lymphangiogenic stimuli could be one potential mechanism to facilitate lymphatic vessel growth and functionality. On this front, the ability of viral-mediated gene delivery of VEGF-C to promote the re-growth of hypoplastic lymphatic vessels in a mouse model of lymphoedema has been shown to restore lymphatic vascular development and function (Karkkainen et al., 2001). As a therapeutic advance, Tammela *et al.* recently showed that lymphatic capillaries, induced by adenovirally-delivered VEGF-C or VEGF-D, gradually underwent intrinsic remodelling, differentiation and maturation into functional collecting lymphatic vessels in a mouse model of axillary lymph node dissection (Tammela et al., 2007). Additionally, in order to restore the anatomy of the axilla following surgery in mice, VEGF-C therapy was combined with lymph node transplantation, yielding promising results (Tammela et al., 2007). A similar finding was demonstrated in a rabbit model of popliteal lymph node removal, whereby mature collecting vessels regenerated in response to recombinant VEGF-C (Ikomi et al., 2006). These results indicate that growth factor-induced regeneration of lymphatic vessels is plausible, and in combination with lymph node transplantation, could provide a solid foundation for the future treatment of lymphoedema in humans. One potential risk

associated with these approaches, however, particularly in patients who have undergone surgery to remove primary tumours and affected lymphatic vessels, is that newly-induced lymphangiogenesis occurring near the site of tumour removal could facilitate subsequent metastatic spread of residual tumour cells. Therefore, it will be of utmost importance to test these approaches exhaustively in appropriate mouse models prior to proceeding to the clinic (Stacker et al., 2002).

1.4 PROJECT RATIONALE AND AIMS

While the epithelial tree and blood vasculature are dynamically remodelled during postnatal mouse mammary gland morphogenesis (Andres and Djonov, 2010; Djonov et al., 2001; Matsumoto et al., 1992; Richert et al., 2000), little is known regarding the growth, remodelling and spatial organisation of lymphatic vessels in the mouse mammary gland. This is emphasised by a single, decade-old publication by Ohtani *et al.* analysing lymphatic vessels in the rat mammary gland (Ohtani et al., 1998).

Lymphatic vessels play at least two key roles in breast cancer. Firstly, lymphatic vessels function as a critical transport route for the metastasis of breast cancer cells (Ran et al., 2010; Skobe et al., 2001) and the ability of a tumour to promote lymphangiogenesis has been correlated with metastasis and poor patient prognosis in breast cancer (Gu et al., 2008; Nakamura et al., 2005; Nakamura et al., 2003; Ran et al., 2010; Skobe et al., 2001). Secondly, lymphatic vascular damage incurred during the surgical resection of axillary lymph nodes commonly results in secondary lymphoedema, a disabling problem for a large proportion of breast cancer patients (Armer et al., 2009). Despite the involvement of lymphatic vessels in breast cancer, the genes and molecular mechanisms that regulate lymphangiogenesis in the breast remain relatively uncharacterised.

By expanding our understanding of the molecular mechanisms important for lymphatic vessel growth and development in breast tissue, we will be afforded the opportunity to understand how they are 'hijacked' to facilitate tumour metastasis in breast cancer. The identification of lymphangiogenic regulators in the breast has the potential to reveal important targets for the future generation of therapeutics to either ablate, or stimulate lymphangiogenesis; with the ultimate goal of halting breast cancer metastasis, or repairing surgically damaged lymphatic vessels and reconstituting lymphatic flow in lymphoedema patients, respectively.

The intended aims of this project were as follows:

- 1. To investigate the spatial organisation of lymphatic vessels in the mouse mammary gland.**
- 2. To investigate whether lymphatic vessels, like blood vessels and the mammary epithelial tree, are temporally remodelled during mouse mammary gland morphogenesis.**
- 3. To define signals that regulate lymphangiogenesis during postnatal mouse mammary gland morphogenesis.**

Collectively, this project represents the first specific analysis of lymphangiogenesis during postnatal mammary gland morphogenesis in the mouse.

CHAPTER 2

Materials and Methods

2.1 MATERIALS

General laboratory chemicals were of analytical research grade and were purchased from a range of manufacturers. All oligonucleotides were purchased from GeneWorks (GeneWorks Pty Ltd, Adelaide, Australia) and all tissue culture plasticware, unless otherwise stated, was purchased from BD (Franklin Lakes, NJ). Milli-Q water (MQ-H₂O) was produced by a Milli-Q Ultrapure Water System (Millipore, Billerica, MA). Specialist reagents and their respective sources are detailed below.

2.1.1 Standard solutions

A number of commonly used standard solutions were utilised throughout this study and include: maleate buffer (used as a 1x solution containing 100mM maleic acid and 150mM sodium chloride (NaCl), pH adjusted to 7.5 using 10M sodium hydroxide (NaOH)); phosphate-buffered saline (PBS) (used as a 1x solution containing 137mM NaCl, 2.7mM potassium chloride (KCl), 10mM disodium hydrogen phosphate and 2mM potassium dihydrogen phosphate, pH adjusted to 7.4 using hydrochloric acid (HCl)); 4% weight per volume (w/v) phosphate-buffered paraformaldehyde (PFA) (referred to as 4% PFA) (40g PFA dissolved in 1L of PBS, pH adjusted to 7.4 using HCl); saline-sodium citrate (SSC) buffer (used as a 1x solution containing 150mM NaCl and 15mM trisodium citrate); Tris-borate-ethylenediaminetetraacetic acid (EDTA) (TBE) buffer (used as a 0.5x solution containing 44.5mM Tris, 44.5mM boric acid and 1mM EDTA); Tris-buffered saline (TBS) (used as a 1x solution containing 10mM Tris (pH 7.5) and 150mM NaCl) and Tris-EDTA (TE) buffer (used as a 1x solution containing 10mM Tris-HCl (pH 8.0) and 1mM EDTA (pH 8.0)).

2.1.2 Bacterial media

All bacteria was cultured in Luria Bertani (LB) broth consisting of 1% (w/v) Bacto™ tryptone (BD, Sparks, MD), 0.5% (w/v) Bacto™ yeast extract (BD) and 1% (w/v) NaCl, pH adjusted to 7.2 using 1M NaOH, prior to sterilisation via autoclaving. For bacterial colony growth, LB agar was used (LB broth with the addition of 1.5% (w/v) Bacto™ agar (BD)). LB agar was sterilised via autoclaving, prior to the addition of required antibiotics. LB agar was poured into sterile 100mm petri dishes. LB agar plates were stored for up to 1 month at 4°C.

2.1.3 Antibodies

A comprehensive list of the antibodies utilised throughout all experimental protocols are listed in Table 2.1 (primary antibodies) and Table 2.2 (directly-conjugated primary and secondary antibodies).

2.2 METHODS

2.2.1 RNA analysis

2.2.1.1 RNA isolation

All ribonucleic acid (RNA) procedures were performed using ART® aerosol resistant filter tips (Molecular BioProducts, Inc., San Diego, CA). Total RNA was isolated from cells using TRIzol® Reagent (Invitrogen, Carlsbad, CA) according to the manufacturer's instructions. All volumes listed are given per 1ml of TRIzol® Reagent used for the initial sample lysis. Briefly, cells were lysed in 1ml of TRIzol® Reagent and homogenised using a 25G needle and syringe. Homogenised samples were incubated at room temperature (RT) for 5 minutes to allow complete dissociation of nucleoprotein complexes, prior to the addition of 0.2ml of chloroform. Samples were vigorously mixed for 15 seconds, incubated at RT for 3 minutes and then phase separation carried out via centrifugation at 12,000 x g for 15 minutes at 4°C. The aqueous phase containing RNA was transferred to a clean microcentrifuge tube and the organic phase stored at -20°C for future protein extraction as required. RNA was precipitated via the addition of 0.5ml of isopropanol, mixed well and incubated at RT for 10 minutes, prior to centrifugation at 12,000 x g for 10 minutes at 4°C. To facilitate isolation of RNA from small samples (< 10⁶ cells), 10µg nuclease-free glycogen (Roche, Roche Diagnostics GmbH, Mannheim, Germany) was added to the aqueous phase as a carrier prior to precipitation. Following centrifugation, the supernatant was removed and the resulting RNA pellet was washed once with 1ml 75% volume per volume (v/v) ethanol, mixed and then centrifuged at 7,500 x g for 5 minutes at 4°C. The supernatant was removed and the RNA pellet briefly air-dried before being redissolved in an appropriate volume of diethylpyrocarbonate (DEPC)-treated MQ-H₂O and stored at -70°C, avoiding repeated freeze-thaw cycles.

ANTIBODY	SUPPLIER	APPLICATION	DILUTION
goat anti-mouse CCL21	R&D Systems	mWM-IF	1:250
goat anti-mouse E-cadherin	R&D Systems	C, IF(FF), mWM-IF	1:500, 1:500, 1:500
goat anti-mouse VEGF-D	R&D Systems	WB	1:500
goat anti-mouse VEGFR-3	R&D Systems	IF(FF)	1:200
goat anti-rat neuropilin-2	R&D Systems	sWM-IF	1:500
hamster anti-mouse podoplanin (clone 8.1.1)	Developmental Studies Hybridoma Bank	DAB, IF(P)	1:500, 1:5000
mouse monoclonal anti- β -actin	Sigma	WB	1:5000
rabbit anti-class III β -tubulin	Covance	DAB, sWM-IF	1:1000, 1:2000
rabbit anti-ER α (MC-20)	Santa Cruz	IF(P)	1:1000
rabbit anti-human progesterone receptor	DakoCytomation	IF(P)	1:500
rabbit anti-keratin 14	Covance	C	1:2000
rabbit anti-mouse angiopoietin-1	Alpha Diagnostic International	WB	1:500
rabbit anti-mouse angiopoietin-2	Calbiochem	WB	1:500
rabbit anti-mouse LYVE-1	AngioBio	DAB, IF(FF), MACS	1:1000 (sections)/ 1:500 (WM), 1:500, 1:200
rabbit anti-Prox1	AngioBio	C, DAB, IF(FF), mWM-IF, sWM-IF	1:1000, 1:1000, 1:500, 1:500, 1:500
rabbit monoclonal anti- cytokeratin 18	Abcam (Cambridge, UK)	C	1:100
rat anti-mouse CD31	BioLegend	C, DAB, IF(FF), mWM-IF, sWM-IF	1:500, 1:500, 1:500, 1:500, 1:500
rat anti-mouse CD45	BD Pharmingen (San Diego, CA)	C	1:250
rat anti-mouse F4/80	Invitrogen	MACS	1:100
rat anti-mouse PDGFR β	eBioscience (San Diego, CA)	C	1:250

Table 2.1 - A list of primary antibodies and their conditions of use.

C - cell monolayer immunocytochemistry, DAB - 3,3'-diaminobenzidine (DAB) immunostaining, IF(FF) - immunofluorescent immunostaining of fixed-frozen sections, IF(P) - immunofluorescent immunostaining of paraffin-embedded sections, MACS - magnetic-activated cell sorting, mWM-IF - whole mount immunofluorescent immunostaining of mouse mammary glands, sWM-IF - embryonic dermal skin whole mount immunofluorescence, WB - Western blot, WM - whole mount.

ANTIBODY	SUPPLIER	APPLICATION	DILUTION
Alexa Fluor® 488 donkey anti-goat	Invitrogen	C, IF(FF), mWM-IF	1:500, 1:500, 1:500
Alexa Fluor® 488 donkey anti-rabbit	Invitrogen	IF(FF)	1:500
Alexa Fluor® 488 donkey anti-rat	Invitrogen	C, mWM-IF, sWM-IF	1:500, 1:500, 1:500
Alexa Fluor® 488 goat anti-hamster	Invitrogen	IF(P)	1:500
Alexa Fluor® 555 donkey anti-rabbit	Invitrogen	C, IF(FF), mWM-IF, sWM-IF	1:500, 1:500, 1:500, 1:500
Alexa Fluor® 555 goat anti-rabbit	Invitrogen	IF(P)	1:500
Alexa Fluor® 555 goat anti-rat	Invitrogen	IF(FF)	1:500
Alexa Fluor® 647 chicken anti-rat	Invitrogen	IF(FF), mWM-IF	1:500, 1:500
Alexa Fluor® 647 donkey anti-goat	Invitrogen	IF(FF), mWM-IF, sWM-IF	1:500, 1:500, 1:500
Alexa Fluor® 647 donkey anti-rabbit	Invitrogen	sWM-IF	1:500
Alexa Fluor® 647 rat anti-mouse CD45	BioLegend	FC	0.25µg per 10 ⁶ cells
Alexa Fluor® 647 rat anti-mouse F4/80	Invitrogen	FC	0.25µg per 10 ⁶ cells
Alexa Fluor® 700 hamster anti-mouse/rat CD29	BioLegend	FC	0.5µg per 10 ⁶ cells
alkaline phosphatase goat anti-rabbit	GE Healthcare	WB	1:5000
alkaline phosphatase rabbit anti-goat	Invitrogen	WB	1:1000
biotinylated goat anti-hamster IgG	Vector Laboratories	DAB	1:400
biotinylated goat anti-rabbit IgG	Vector Laboratories	DAB	1:400 (sections)/ 1:1000 (WM)
biotinylated rabbit anti-rat IgG	Vector Laboratories	DAB	1:400
Cy3-conjugated mouse monoclonal anti-α-smooth muscle actin	Sigma-Aldrich	C, mWM-IF, sWM-IF	1:1000, 1:1000, 1:1000
Cy5-linked goat anti-mouse	GE Healthcare	WB	1:2000
PE/Cy5 rat anti-mouse CD24	BioLegend	FC	0.25µg per 10 ⁶ cells
PE/Cy7 rat anti-mouse CD31	BioLegend	FC	0.25µg per 10 ⁶ cells
sheep anti-digoxigenin-AP, Fab fragments	Roche	ISH	1:5000

Table 2.2 - A list of directly-conjugated primary and secondary antibodies and their conditions of use.

C - cell monolayer immunocytochemistry, DAB - 3,3'-diaminobenzidine (DAB) immunostaining, FC - flow cytometry, IF(FF) - immunofluorescent immunostaining of fixed-frozen sections, IF(P) - immunofluorescent immunostaining of paraffin-embedded sections, ISH - *in situ* hybridisation, mWM-IF - whole mount immunofluorescent immunostaining of mouse mammary glands, sWM-IF - embryonic dermal skin whole mount immunofluorescence, WB - Western blot, WM - whole mount.

2.2.1.2 Determination of RNA concentration

RNA samples were diluted 1:1 with 2x TE buffer (pH 8.0) and the resulting RNA concentrations were determined based on the absorbance of the sample at 260nm on a NanoDrop™ 1000 spectrophotometer and version 3.7 software (NanoDrop Technologies, Inc., Wilmington, DE). A ratio of sample absorbance at 260nm to 280nm of approximately 2.0 and a ratio of sample absorbance at 260nm to 230nm of approximately 1.8-2.2 were accepted as indicators of high purity RNA. The presence of protein, phenol or other contaminants was indicated by an appreciably lower ratio in either case.

2.2.1.3 First-strand cDNA synthesis

For investigation of messenger RNA (mRNA), isolated total RNA, as detailed above in section 2.2.1.1, was reverse transcribed to form complementary deoxyribonucleic acid (cDNA) using SuperScript™ III First-Strand Synthesis SuperMix (Invitrogen) as per manufacturer's instructions, in a total reaction volume of 20µl. RNA (0.1-1µg) was combined with a mix of 2.5µM oligo(dT)₂₀ and 50ng random hexamer primers and incubated in an Eppendorf Mastercycler (Eppendorf, Hamburg, Germany) at 65°C for 5 minutes, then immediately chilled on ice for at least 1 minute. This RNA-primer mixture was subsequently combined with First-Strand Reaction Mix and SuperScript™ III/RNaseOUT™ Enzyme Mix and incubated at 25°C for 10 minutes, followed by 50 minutes at 50°C. Reactions were terminated via a 5 minute incubation at 85°C, followed by cooling to 4°C. cDNA was diluted as necessary using DEPC-treated MQ-H₂O and stored at -20°C.

2.2.1.4 Real-time RT-PCR

Real-time reverse transcription-polymerase chain reaction (RT-PCR) was performed in triplicate on each individual gene analysed using RT² Real-Time™ SYBR Green/Rox Master Mix (SABiosciences, Frederick, MD). Primers were designed with the aid of Primer3 software version 4.0 (Rozen and Skaletsky, 2000) to flank an intron-exon boundary, in order to prevent amplification of genomic deoxyribonucleic acid (DNA), to be 20-22bp in length and to yield a product size between 150-300bp. The resultant primer pairs used for real-time RT-PCR amplification are shown in Table 2.3. Real-time RT-PCRs were performed in 0.1ml polymerase chain reaction (PCR) tubes in a 15µl total reaction volume containing 2µl of cDNA (generated as per section 2.2.1.3), 7.5pmol of both forward and reverse primers and 1x RT² Real-Time™ SYBR Green/Rox Master Mix. Amplification was performed using a

GENE	FORWARD PRIMER	REVERSE PRIMER
<i>Acta2</i>	5'-GCATCCACGAAACCACCTAT-3'	5'-TGGAAGGTAGACAGCGAAGC-3'
<i>Actb</i>	5'-GATCATTGCTCCTCCTGAGC-3'	5'-GTCATAGTCCGCCTAGAAGCAT-3'
<i>Angpt1</i>	5'-CAGCATCTGGAGCATGTGAT-3'	5'-AACATCTGTCAGCTTTCGGG-3'
<i>Angpt2</i>	5'-GATCTTCCTCCAGCCCCTAC-3'	5'-CAGCAAGCTGGTCCAATCT-3'
<i>Bfk</i>	5'-GGCCGCCTTCGAATACTGGG-3'	5'-GCCACCTGTCTTGCCACGTT-3'
<i>Cxcl15</i>	5'-CCATGCTCCTGCTGGCTGTCC-3'	5'-GGGCCAACAGTAGCCTTCACCC-3'
<i>Fgf1</i>	5'-AGCCCAAAGTCTACTGC-3'	5'-GGTTTTCTCCAGCCTTCC-3'
<i>Fgf2</i>	5'-AGCGGCTCTACTGCAAGAAC-3'	5'-GCCGTCCATCTTCCTCATA-3'
<i>Hgf</i>	5'-TGCCAGAAAGATATCCCGAC-3'	5'-CTTCTCCTTGGCCTTGAATG-3'
<i>Krt18</i>	5'-CCTTGCCGCCGATGACTTTA-3'	5'-CAGCCTTGTGATGTTGGTGT-3'
<i>Pdgfa</i>	5'-GAGATACCCCGGGAGTTGAT-3'	5'-TCTTGCAAAGTGCAGGAATG-3'
<i>Pdgfb</i>	5'-CCTCGGCCTGTGACTAGAAG-3'	5'-GGGGCAATACAGCAAATACC-3'
<i>Pecam1</i>	5'-AACAGAAACCCGTGGAGATG-3'	5'-GTCTCTGTGGCTCTCGTTCC-3'
<i>Ptprc</i>	5'-GGTTGTTCTGTGCCTTGTT-3'	5'-GGATAGATGCTGGCGATGAT-3'
<i>Reln</i>	5'-CGTCCCCTGGAAGCTCGGA-3'	5'-TGCCTGAGCCCATGTTGCCG-3'
<i>Vegfa</i>	5'-TGAGACCCTGGTGGACATCT-3'	5'-TATGTGCTGGCTTTGGTGAG-3'
<i>Vegfc</i>	5'-GCAGCTAACAAAGACATGTCAA-3'	5'-CCACAAGTATGGCCGAAG-3'
<i>Vegfd</i>	5'-TGCAAGACGAGACTCCACTG-3'	5'-GCAGCAGCTCTCCAGACTTT-3'

Table 2.3 - Primer pairs used for real-time RT-PCR analyses in *Mus musculus*.

Corbett Research Rotor-Gene™ 6000 real-time rotary analyser (QIAGEN, QIAGEN GmbH, Hilden, Germany) according to the following parameters: 95°C for 15 minutes, followed by cycling at 95°C for 15 seconds, 60°C for 25 seconds and 72°C for 10 seconds, for a maximum of 40 cycles, followed by a final extension at 72°C for 3 minutes and melt from 72-99°C. Data were collected and analysed using Rotor-Gene™ 6000 Series Software version 1.7 (QIAGEN) and melt curves examined to validate the generation of single product amplicons following every real-time RT-PCR amplification run. Data were normalised to *Actb* as previously described (Livak and Schmittgen, 2001).

2.2.2 Plasmid DNA cloning and purification

2.2.2.1 PCR amplification

Primers for cloning purposes were designed with the aid of Primer3 software version 4.0 (Rozen and Skaletsky, 2000). Primer sequences are listed in the body of the text as required. All PCR amplifications were performed using ART® aerosol resistant filter tips (Molecular BioProducts) and thermally cycled on an Eppendorf Mastercycler (Eppendorf). PCR amplifications were performed in a 20µl total reaction volume containing 1x ThermoPol Reaction Buffer (New England BioLabs, Inc., Ipswich, MA), 3-5µl of cDNA (generated as per section 2.2.1.3), 0.2mM deoxyribonucleotide triphosphates (dNTPs), 1U *Taq* DNA polymerase (New England BioLabs) and 10pmol of both forward and reverse primers. Typical amplification parameters were as follows: an initial denaturation step of 95°C for 5 minutes, followed by 35 cycles of denaturation at 95°C for 45 seconds, primer annealing at an optimised temperature for each individual primer set for 45 seconds and extension at 72°C for 1 minute, followed by a final extension at 72°C for 5 minutes and cooling to 4°C. PCR products were separated via agarose gel electrophoresis (AGE), as described in detail below in section 2.2.2.2. PCR templates were extracted from agarose gels as per section 2.2.2.3 for use in subsequent cloning procedures.

2.2.2.2 DNA agarose gel electrophoresis

DNA was analysed via horizontal AGE using 1% (w/v) agarose gels prepared using 0.5x TBE buffer containing 0.5µg/ml ethidium bromide (Fluka Biochemika, Steinheim, Germany). DNA samples were loaded using an appropriate volume of 6x gel-loading buffer (0.25% (w/v) bromophenol blue, 0.25% (w/v) xylene cyanol FF and 30% (v/v) glycerol in MQ-H₂O) to achieve a final concentration of 1x. Samples were electrophoresed alongside 500ng of SPP1/*EcoRI* DNA molecular weight markers (GeneWorks). Gels were run in 0.5x TBE buffer at 100-150V for 0.5-1 hour depending on the size of

DNA fragments to be resolved, with subsequent visualisation using an UVItec Gel Documentation System and associated UVIPhotoMW version 11.01 software (UVItec Limited, Cambridge, UK).

2.2.2.3 DNA extraction from agarose gels

DNA fragments, separated via AGE as described above in section 2.2.2.2, were visualised briefly using ultraviolet (UV) light and excised from the agarose gels using a scalpel blade. DNA was extracted from excised portions of agarose using a QIAquick® Gel Extraction Kit (QIAGEN) as per the manufacturer's handbook, with all incubations at RT unless otherwise stated. Briefly, 3 volumes of Buffer QG was added to 1 volume of agarose gel (100mg \approx 100 μ l) and incubated at 50°C for 10 minutes or until the gel slice containing the DNA had completely dissolved. Following gel dissolution, 1 volume of isopropanol was added to the sample and mixed. The sample was subsequently loaded onto a QIAquick spin column and centrifuged for 1 minute at 1,500 x g. The flow through was discarded, followed by the addition of 0.5ml Buffer QG to the column and centrifugation for 1 minute at 16,000 x g. Samples were washed twice with 0.75ml Buffer PE and centrifuged for 1 minute at 16,000 x g. The column was transferred to a clean microcentrifuge tube and the membrane allowed to air-dry, prior to the elution of DNA via the addition of 30 μ l Buffer EB directly onto the membrane. The column was incubated for 1 minute and then centrifuged at 16,000 x g for 1 minute. The extracted DNA was stored at -20°C. Confirmation of the purification procedure was determined via AGE analysis, as previously described (section 2.2.2.2).

2.2.2.4 Restriction enzyme digestion of DNA

Vectors, plasmids and DNA templates were digested with a variety of restriction enzymes sourced from New England BioLabs and were carried out according to the manufacturer's instructions. All analytical restriction endonuclease DNA digests were performed using 0.5-2.0 μ l template DNA (up to 1 μ g) and 5-25U of enzyme in the supplied NE Buffer 1-4 in a total reaction volume of 20 μ l and incubated for 1 hour at 37°C. Digested DNA plasmids and fragments were subsequently analysed via AGE, as described in section 2.2.2.2, to verify complete digestion and fragment sizes.

2.2.2.5 Ligation reactions

Ligation reactions were performed using the pGEM®-T Easy Vector System I kit (Promega, Promega Corporation, Madison, WI) as per the manufacturer's recommendations, which utilises T4 DNA ligase

and the pGEM®-T Easy vector. Briefly, 10µl ligation reactions were prepared containing 5µl of 2x Rapid Ligation Buffer, 1µl (50ng) of pGEM®-T Easy vector, 0.8µl (2.4U) of T4 DNA ligase and 3.2µl (15-150ng) of purified DNA fragment (from section 2.2.2.3) and incubated overnight at 4°C.

2.2.2.6 Preparation of chemically-competent cells

The method used to prepare chemically-competent cells was adapted from a previously established protocol (Sambrook and Russel, 2001). *Escherichia coli* DH5α cells were streaked out on a LB agar plate and grown overnight at 37°C. A single colony was aseptically selected and inoculated into 5ml Ψ broth (containing 2% (w/v) tryptone, 0.5% (w/v) yeast extract and 0.5% (w/v) magnesium sulphate, with pH adjusted to 7.6 using 0.5M potassium hydroxide (KOH) and sterilised via autoclaving), which was incubated overnight at 37°C with shaking. The overnight culture was subcultured 1:20 into 100ml pre-warmed Ψ broth and incubated at 37°C with shaking until an optical density of between 0.5 and 0.6 at 600nm was reached (typically 1.5-2 hours). Cells were subsequently chilled on ice for 5 minutes with frequent mixing to facilitate uniform cooling of the cells, prior to centrifugation in a Beckman Coulter Avanti™ J-25I High-Performance Centrifuge using a JA-25.50 rotor (Beckman Coulter, Inc., Brea, CA) at 4,500 x g for 5 minutes at 4°C. The supernatant was aspirated and the cell pellet was resuspended in 40ml ice-cold transformation buffer (TFB)I (containing 30mM potassium acetate, 100mM KCl, 10mM calcium chloride dihydrate, 50mM manganese chloride tetrahydrate and 15% (v/v) glycerol, with pH adjusted to 5.8 with 0.2M acetic acid and filter-sterilised with a 0.22µm filter). Cells were incubated on ice for 5 minutes and centrifuged as per previous conditions. The supernatant was carefully removed and the pellet gently resuspended in 4ml ice-cold TFBII (containing 10mM 3-(N-morpholino)propanesulphonic acid, 75mM calcium chloride dihydrate, 10mM KCl and 15% (v/v) glycerol, with pH adjusted to 6.5 with 0.5M KOH and filter-sterilised through a 0.22µm filter) and incubated on ice for 15 minutes. Cells were aliquoted into pre-chilled 1.5ml microcentrifuge tubes on dry ice and stored indefinitely at -70°C.

2.2.2.7 Transformation of chemically-competent cells

For transformation, 10µl ligation reactions (from section 2.2.2.5) were gently mixed with a 50µl aliquot of chemically-competent DH5α cells (prepared as above in section 2.2.2.6) and incubated on ice for 30 minutes. Samples were heat-shocked at 42°C for exactly 1.5 minutes, followed by an immediate cold-shock on ice for 2 minutes, prior to recovery in 800µl antibiotic-free LB broth at 37°C for 45 minutes. For blue-white colour selection, a LB agar plate containing 50µg/ml ampicillin (Sigma, Sigma-Aldrich Co.,

St. Louis, MO) was coated with 40µl of 20mg/ml 5-bromo-4-chloro-3-indolyl-β-D-galactopyranoside (X-gal) solution and 10µl of 1M isopropyl-β-D-thiogalactosidase (IPTG) using a sterile glass spreader, prior to plating 200µl of the transformation mix. Blue-white colour selection enabled easy detection of successful ligations (white colonies). Plates were allowed to dry prior to overnight incubation at 37°C.

2.2.2.8 Small-scale plasmid DNA production and purification

2.2.2.8.1 Small-scale plasmid DNA production

Small-scale plasmid DNA purification was used solely for the purpose of screening colonies following transformation, prior to performing large-scale bacterial cultures. Following overnight incubation, single white colonies of interest were selected and inoculated into 2ml LB broth cultures containing 50µg/ml ampicillin and incubated overnight at 37°C with shaking.

2.2.2.8.2 Small-scale plasmid DNA purification

The protocol used for plasmid DNA purification from bacteria was a modified version of the alkaline lysis method of Birnboim and Doly (Birnboim and Doly, 1979), utilising solutions from the QIAGEN Plasmid Midi Kit (QIAGEN). In brief, 1ml of overnight bacterial cultures were pelleted at 16,000 x g for 1 minute, supernatant removed and the pellet resuspended in 150µl Buffer P1, followed by the addition of 150µl Buffer P2 to facilitate cell lysis. The samples were vigorously mixed by inversion 4-6 times and left at RT for 5 minutes, prior to the addition of 150µl ice-cold Buffer P3, mixed again by inversion and incubated on ice for a further 5 minutes. Genomic DNA and protein were pelleted via centrifugation at 16,000 x g for 15 minutes. The resulting supernatant was transferred to a fresh microcentrifuge tube and plasmid DNA was precipitated on ice for 15 minutes via the addition of 0.1 volumes 3M sodium acetate (NaOAc) (pH 5.2) and 2.5 volumes 100% (v/v) ethanol. Plasmid DNA was pelleted at 16,000 x g for 15 minutes, washed with 70% (v/v) ethanol and centrifuged again at 16,000 x g for a further 1 minute. The resulting plasmid DNA pellet was air-dried, resuspended in 100µl MQ-H₂O and stored at -20°C. Putative plasmid clones were subsequently restriction enzyme digested (section 2.2.2.4) and analysed via AGE (section 2.2.2.2) to enable selection of clones for further manipulation (see section 2.2.2.9-11). Remaining bacterial cultures were stored at 4°C awaiting clone confirmation via restriction enzyme digestion and DNA sequencing, prior to large-scale plasmid DNA production.

2.2.2.9 Plasmid DNA sequencing

2.2.2.9.1 DNA sequencing reaction

The sequence of plasmid DNA templates were analysed via a fluorescence-based dye-terminator sequencing reaction, prior to large-scale production of plasmid DNA. Sequencing reactions were performed in a 20µl total reaction volume containing 4µl of BigDye® Terminator Ready Reaction Mix version 3.1 (Applied Biosystems, Foster City, CA), 4µl (100-300ng) of small-scale purified plasmid DNA (from section 2.2.2.8.2), 100ng of T7 sequencing primer (5'-TAATACGACTCACTATAGGG-3') and 11µl MQ-H₂O. Amplification was performed in an Eppendorf Mastercycler (Eppendorf) with the following cycling conditions: an initial denaturation step at 96°C for 1 minute, followed by 35 cycles of denaturation at 96°C for 10 seconds, primer annealing at 50°C for 5 seconds and extension at 60°C for 4 minutes, followed by cooling to 4°C.

2.2.2.9.2 DNA sequencing product purification

Following the completion of the sequencing reaction, samples were purified via an isopropanol precipitation method. Briefly, 80µl of 75% (v/v) isopropanol was added to the 20µl sequencing reaction, samples vortexed and sequencing products precipitated at RT for 15 minutes, followed by centrifugation at 16,000 x g for 20 minutes. Supernatant was removed and the pellet washed with 250µl of 75% (v/v) isopropanol, prior to centrifugation for a further 5 minutes at 16,000 x g. Upon removal of the supernatant, pellets were dried for 2-3 minutes at 55°C and submitted to the Division of Molecular Pathology (SA Pathology, Adelaide, Australia) for analysis on an ABI PRISM® 3700 DNA analyser (Applied Biosystems).

2.2.2.10 Large-scale plasmid DNA production and purification

2.2.2.10.1 Large-scale plasmid DNA production

Plasmid DNA clones, previously verified two-fold via restriction enzyme digestion and sequencing, were cultured large-scale using 1ml of overnight bacterial culture (generated in section 2.2.2.8.1) in 50ml LB broth supplemented with 50µg/ml ampicillin and incubated overnight at 37°C with shaking.

2.2.2.10.2 Long-term storage of plasmid DNA

Bacterial cultures containing plasmids of interest were stored in glycerol at -70°C indefinitely. Glycerol stocks were prepared in 2ml cryogenic screw-top vials containing 1:3 mix of 60% (v/v) glycerol and large-scale overnight bacterial culture as produced above (section 2.2.2.10.1).

2.2.2.10.3 Large-scale plasmid DNA purification

Plasmid DNA was purified from the 50ml overnight bacterial cultures using a QIAGEN Plasmid Midi Kit (QIAGEN), as per the manufacturer's instructions. Bacterial cultures were pelleted in a Beckman Coulter Avanti™ J-25I High-Performance Centrifuge using a JA-25.50 rotor (Beckman Coulter) at 6,000 x g for 15 minutes at 4°C and the resulting bacterial pellets resuspended in 4ml Buffer PI, prior to the addition of 4ml Buffer P2 to facilitate cell lysis. Samples were mixed by inversion 4-6 times and incubated at RT for 5 minutes. 4ml of chilled Buffer P3 was added, mixed by inversion 4-6 times and incubated on ice for a further 15 minutes, prior to centrifugation at 20,000 x g for 30 minutes at 4°C. Meanwhile, a QIAGEN-tip 100 was equilibrated with 4ml Buffer QBT and the column allowed to empty via gravity flow. Following centrifugation, the supernatant was removed promptly and applied to the equilibrated column. The column was washed twice with 10ml of Buffer QC. Plasmid DNA was then eluted from the column into a high-speed centrifuge tube via the addition of 5ml of Buffer QF to the column and precipitated by the addition of 3.5ml 100% (v/v) isopropanol. Samples were vigorously mixed and centrifuged at 15,000 x g for 30 minutes at 4°C. Supernatant was removed and the plasmid DNA pellet washed with 2ml of 70% (v/v) ethanol, prior to centrifugation at 15,000 x g for 10 minutes at 4°C. Supernatant was carefully decanted and the plasmid DNA pellet allowed to air-dry for 15 minutes before being redissolved in 100µl Buffer EB. Plasmid DNA was stored at -20°C. Plasmid DNA clones were digested with restriction enzymes (section 2.2.2.4) and analysed via AGE (section 2.2.2.2) as a final means of clone validation, prior to proceeding with plasmid linearisation and ultimately digoxigenin (DIG)-labelled RNA probe synthesis (see section 4.2.2.1.2-5).

2.2.2.11 Determination of DNA concentration

The concentration of double-stranded DNA was routinely determined using a NanoDrop™ 1000 spectrophotometer and version 3.7 software (NanoDrop Technologies). The concentration of DNA in samples was determined based on the absorbance of neat samples at 260nm. A ratio of sample absorbance at 260nm to 280nm of approximately 1.8 and a ratio of sample absorbance at 260nm to 230nm of approximately 1.8-2.2 were accepted as indicators of DNA purity. The presence of protein, phenol or other contaminants was indicated by an appreciably lower ratio in either case.

2.2.3 Mouse studies

Experiments using mice were performed using C57BL/6 and Patched 1 (*Ptch1*)^{lacZ/+} mice. E12.5, E14.5 and E16.5 embryos were obtained from crosses between C57BL/6 mice and C57BL/6 with *Ptch1*^{lacZ/+}

mice. Adult female mice were subjected to timed pregnancies and were scored by the presence of vaginal plugs with 8am on the day of vaginal plug detection designated as 0.5 days post coitum. All animal procedures were approved and conducted in accordance with SA Pathology Animal Ethics Committee, the University of Adelaide Animal Ethics Committee and the Australian National Health and Medical Research Council guidelines.

2.2.3.1 Transgenic mice

Ptch1^{lacZ/+} mice were obtained from the University of Queensland (Brisbane, Australia) as characterised previously (Goodrich et al., 1997) (for further details see section 6.1.2.1). Mammary gland tissue from mice containing a floxed *Gata-3* allele with *cre*-recombinase expressed under the control of the mouse mammary tumour virus (MMTV) promoter (referred to as *MMTV-creD;Gata-3*), as previously described (Asselin-Labat et al., 2007) and mice expressing the oncoprotein, polyomavirus middle T antigen (PyMT), under the control of MMTV (Guy et al., 1992) (denoted *MMTV-PyMT*) were kindly provided by Marie-Liesse Asselin-Labat and Jane E. Visvader (Victorian Breast Cancer Research Consortium Laboratory, The Walter and Eliza Hall Institute of Medical Research, Melbourne, Australia). In addition, mammary gland tissue from *Vegfd*-deficient mice (denoted *Vegfd^{-/-}*) and corresponding wild-type (WT) control mice (denoted *Vegfd^{+/+}*) were generously provided by Marc G. Achen and Sophie Paquet-Fifield (Tumour Angiogenesis Program, Peter MacCallum Cancer Centre, Melbourne, Australia) as previously described (Baldwin et al., 2005).

2.2.4 Mammary gland collection, processing and sectioning

2.2.4.1 Mammary gland dissection

Following humane killing of mice, the fourth pair of inguinal mammary fat pads (both left and right) were dissected from female mice at various postnatal stages, as depicted in Figure 2.1. Briefly, a small incision was made in the middle of the mouse with scissors, ensuring that the underlying peritoneum remained intact. From this initial incision, a 'T-shaped' cut was made down the centre of the mouse towards the tail and across the middle, followed by a diagonal cut made across the middle of each hind leg between the fourth and fifth nipple as indicated in Figure 2.1A,C. The skin was then lifted away from the peritoneum using a pair of forceps until the mammary fat pads were visible (Figure 2.1B,D). Skin flaps were then peeled away from the body of the mouse using a cotton applicator and subsequently pinned out onto the foam board to enable the nipple end of the mammary fat pad to be detached from

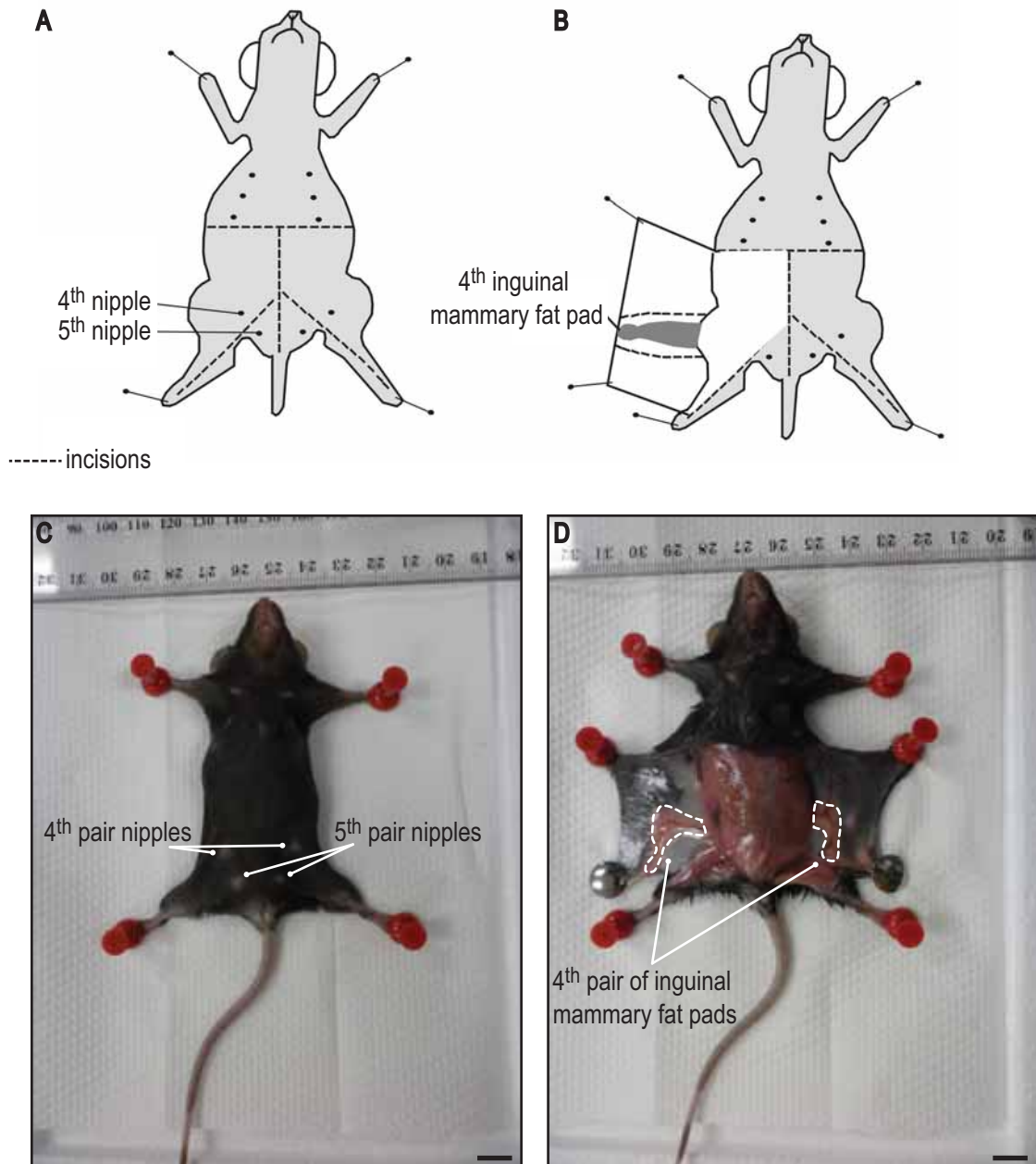


Figure 2.1 - Mouse mammary gland dissection.

Diagrammatic representation of the incisions made to enable dissection of the fourth pair of inguinal mammary fat pads (**A**) and of the skin flap peeled back revealing one of the fourth pair of inguinal mammary fat pads (**B**). A 10 day involuting wild-type C57BL/6 mouse demonstrating the fourth and fifth pairs of nipples (**C**) and the fourth pair of inguinal mammary fat pads with the skin flaps peeled back from the mouse's body (**D**). Scale bars represent 1cm. (**A**) and (**B**) were kindly provided by Amelia A. Peters (The University of Queensland, Brisbane, Australia).

the mouse. If required, inguinal lymph nodes were further dissected from mammary fat pads. Mammary fat pads were released from associated skin flaps using small dissecting scissors.

2.2.4.2 Mammary gland fixation

Following dissection, whole mouse mammary glands were fixed using a variety of methods dependent on the analyses being performed.

2.2.4.2.1 Paraformaldehyde fixation

For cryosectioning and immunofluorescent immunostaining, as well as for whole mount immunofluorescent immunostaining (see section 3.2.4), glands were washed three times in PBS for 10 minutes each on ice, prior to fixation in 4% PFA overnight at 4°C with gentle agitation. Following fixation, glands were washed 3 x 10 minutes in PBS on ice and stored at 4°C in PBS containing 0.01% (w/v) of the antibacterial agent, thimerosal.

2.2.4.2.2 Formaldehyde fixation

Prior to paraffin-embedding, mammary glands were spread onto glass slides immediately after dissection and immersed into a Coplin jar containing neutral-buffered formaldehyde (10% (v/v) formalin solution) overnight (no longer than 30 hours) at RT. Following fixation, glands were removed from the glass slides and placed into tissue embedding cassettes and stored in 70% (v/v) ethanol (up to 36 hours) prior to further processing of the tissue (see section 2.2.4.3.2).

2.2.4.2.3 Carnoy's solution fixation

For glands requiring carmine alum staining post-fixation, glands were spread onto glass slides immediately after dissection and incubated in Coplin jars for 2-4 hours at RT in Carnoy's solution containing 60% (v/v) ethanol, 30% (v/v) chloroform and 10% (v/v) glacial acetic acid. Carnoy's solution-fixed glands were transferred to MQ-H₂O via a graded ethanol series (70% and 30% (v/v) ethanol, diluted using MQ-H₂O) and MQ-H₂O for 15 minutes each, prior to staining in carmine alum (see section 3.2.1).

2.2.4.3 Mammary gland processing and sectioning

2.2.4.3.1 Fixed-frozen mammary gland tissue

Following fixation in 4% PFA and washing in PBS as described in section 2.2.4.2.1, glands were cryopreserved in PBS containing 30% (w/v) sucrose for 24-48 hours at 4°C with gentle agitation. Samples were embedded in Tissue-Tek® Cryomolds® (ProSciTech, Queensland, Australia) using Tissue-Tek® Optimal Cutting Temperature (O.C.T) Compound (Sakura, Sakura Finetek Europe B.V., Zoeterwoude, The Netherlands) and left to completely freeze on dry ice. Once the samples were adequately frozen they were stored at -70°C until required for cryosectioning. Unstained fixed-frozen mammary tissue (for immunofluorescent immunostaining) and X-gal-stained mammary tissue (for DAB immunostaining) samples were cryosectioned at a thickness of 45µm and 30µm, respectively, using a Leica CM1950 cryostat (Leica Microsystems, Leica Microsystems GmbH, Wetzlar, Germany) set to an optimal working temperature of -26°C. Sections were placed on SuperFrost Ultra Plus® slides (Menzel-Gläser, Menzel GmbH & Co. KG, Braunschweig, Germany) and left to air-dry at RT for 2 hours, prior to storage in slide boxes at -70°C.

2.2.4.3.2 Paraffin-embedded mammary gland tissue

Once glands were formaldehyde-fixed and transferred to 70% (v/v) ethanol as detailed in section 2.2.4.2.2, glands were processed on a routine overnight cycle in a Tissue-Tek® VIP™ vacuum infiltration tissue processor (Sakura). Glands were subsequently embedded into molten paraffin wax using a Tissue-Tek® TEC™ tissue embedding console system (Sakura). Following hardening of the paraffin, moulds were removed and paraffin blocks stored at RT until required for sectioning. Paraffin sections, 4µm in thickness, were obtained on a Leica RM2235 rotary microtome (Leica Microsystems) and floated on a 42°C water bath, where they were collected onto SuperFrost Ultra Plus® slides (Menzel-Gläser) and left to adhere overnight at 60°C on a heating block. Sections were stored in slide boxes at 4°C for future immunostaining. For mRNA *in situ* hybridisation analyses, paraffin blocks were freshly prepared and sectioned as soon as practical with no long-term storage, in order to minimise degradation of mRNA within tissue samples. Sections for *in situ* hybridisation were stored in slide boxes at 4°C and used within 1 month.

2.2.5 Cell isolation and culture

2.2.5.1 Mammary gland cell isolation

Cells were isolated from mouse mammary gland tissue following digestion according to a previously established protocol (Shackleton et al., 2006). Briefly, inguinal mammary fat pads were dissected from female mice as described in detail in section 2.2.4.1 (with inguinal lymph nodes removed) and placed on ice in Dulbecco's Modified Eagle's Medium (DMEM) (Sigma) supplemented with 5% (v/v) foetal bovine serum (FBS) (SAFC Biosciences, Inc., Lenexa, KS) (DMEM-5%FBS). Typically 2-10 mice were used, depending on the postnatal stage of the mice and on the experimental analyses being performed. Glands were manually dissociated using scalpel blades to form a tissue slurry prior to enzymatic digestion in DMEM-5%FBS, 150U/ml of both collagenase type 1 and collagenase type 3 (Worthington Biochemical, Worthington Biochemical Corporation, Lakewood, NJ) and 100U/ml hyaluronidase (Worthington Biochemical) for 50 minutes at 37°C with frequent agitation using a transfer pipette (usually 2-8 mammary fat pads per 5ml of digestion mix subject to postnatal stage of mice). 10ml of PBS with 2% (v/v) FBS (PBS-2%FBS) was added to the resultant organoid suspension and pelleted at 300 x g for 5 minutes. The pellet was then resuspended in 0.25% (w/v) trypsin (Worthington Biochemical) reconstituted in DMEM supplemented with 0.0005N HCl and 1mM ethylene glycol tetraacetic acid (EGTA) briefly for 1-2 minutes at RT, prior to addition of 10ml PBS-2%FBS to stop the reaction. The cell suspension was pelleted at 300 x g for 5 minutes and resuspended in DMEM-5%FBS containing 5mg/ml neutral protease (dispase) (Worthington Biochemical) and 0.1mg/ml deoxyribonuclease (DNase) I (Worthington Biochemical) for 5 minutes at 37°C. 10ml PBS-2%FBS was then added to the cell suspension and cells pelleted at 300 x g for 5 minutes. Following centrifugation, cells were resuspended very briefly (approximately 1 minute) in 1:4 mix of PBS-2%FBS and red cell lysis buffer (containing 155.2mM ammonium chloride and 10mM potassium bicarbonate) to facilitate red cell lysis, prior to the addition of 5 volumes PBS-2%FBS to halt the reaction. The resultant cell suspension was filtered through a BD Falcon™ 40µm nylon cell strainer (BD) to remove any residual cell debris and fibrous strands, rinsed with 1 volume DMEM-5%FBS and centrifuged at 300 x g for 5 minutes, followed by resuspension of cell pellets in an appropriate volume of DMEM-5%FBS (usually 1ml). At this time an aliquot was removed for cell counting as per section 2.2.5.2 and cells stored on ice prior to further manipulation.

2.2.5.2 Analysis of cell number and viability

Cell counts were performed using a haemocytometer to assess cell number and viability for routine passaging and experimental analyses. Following the trypsinisation of cells, 10µl of cell suspension was mixed with an equal volume of 0.4% (w/v) Trypan Blue Solution (Sigma) to assess cell viability. Viable cells (ie. cells that had not taken up Trypan Blue) were counted within the haemocytometer grid, as depicted in Figure 2.2, using an Olympus CX41 microscope (Olympus, Olympus Corporation, Tokyo, Japan). Cell number was determined as the number of cells counted, divided by the number of squares (labelled 1-9 in Figure 2.2) that the cells were counted in. This was multiplied by the dilution factor of the Trypan Blue (ie. 2) and by 10⁴ to express the cell number as cells per ml. This can be summarised by the following equation:

$$\text{Cell number (cells/ml)} = (\text{number of cells counted/number of squares counted}) \times 2 \times 10^4$$

2.2.5.3 Visualising cell morphology via light microscopy

Cultured cells were visualised using an inverted phase contrast Olympus CKX41 microscope (Olympus) at 10x or 20x magnification.

2.2.6 Statistical analysis

The majority of data analysis was performed by the Data Management and Analysis Centre (The University of Adelaide, Adelaide, Australia) using SAS® version 9.2 software (SAS Institute Inc., Cary, NC).

For the analysis of lymphatic vessel number (Figure 3.2A), log-linear modelling was used, according to a Poisson distribution with a log link. Conversely, a mixed model approach, analogous to analysis of variance (ANOVA), was used for the statistical analysis of mammary gland section area (Figure 3.2B) and lymphatic vessel density (Figure 3.2C). If a significant difference between postnatal stages was detected ($P < 0.05$), then pair-wise comparisons using a Sidak adjustment for multiple comparisons were used to determine differences between means.

For *ex vivo* LEC proliferation assays with multiple treatments (Figure 4.9; Figure 4.12), data was analysed using ANOVA, assuming a randomised complete block design, with at least three data points

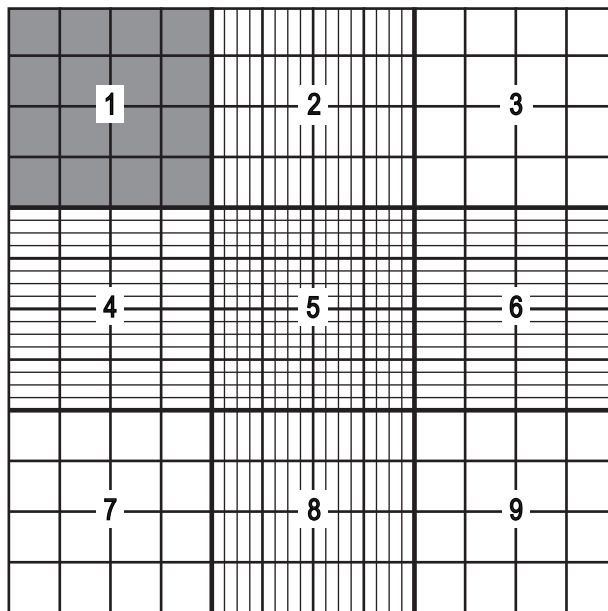


Figure 2.2 - Diagrammatic representation of a haemocytometer.

obtained for each condition. If a significant difference between treatments was detected at the 5% significance level ($P < 0.05$), then pair-wise comparisons using a Sidak adjustment for multiple comparisons were used to determine differences between means.

Alternatively, P -values were calculated using the two-tailed Student's t -test.

For all statistical analyses, a P -value < 0.05 was considered to be statistically significant.

CHAPTER 3

Lymphatic vessels are dynamically remodelled during postnatal mouse mammary gland morphogenesis

3.1 INTRODUCTION

It is well-established that normal mammary tissue undergoes dramatic morphological changes, including growth, differentiation and reorganisation, in response to hormonal signals and functional demands during postnatal mouse mammary gland morphogenesis; beginning at puberty and encompassing the complete adult female reproductive cycle (Richert et al., 2000; Watson and Khaled, 2008). These dynamic remodelling events are not solely restricted to the mammary epithelia and extend to the mammary gland blood vasculature, which undergoes repeated cycles of angiogenic expansion during pregnancy and lactation, followed by a concomitant ordered regression at involution (Djonov et al., 2001; Matsumoto et al., 1992; Pepper et al., 2000). Whilst blood vascular remodelling in the mouse mammary gland has been well documented, the growth and remodelling of lymphatic vessels has received little such attention; only a single publication investigating the lymphatic vasculature in the rat mammary gland has been published (Ohtani et al., 1998). We hypothesised that the mammary gland lymphatic vasculature would be subject to dynamic remodelling stimuli, in conjunction with the hormonally-stimulated expansion and regression of mammary epithelial and stromal tissue components, during postnatal mouse mammary gland morphogenesis.

3.1.1 Lymphatic vessel patterning in other reproductive organs

Whilst limited data exists on the growth, remodelling and patterning of lymphatic vessels in the mouse mammary gland, recent work has studied the process of lymphangiogenesis in mammalian reproductive organs, including the ovary and uterus.

3.1.1.1 The ovarian lymphatic vasculature

The remodelling capacity of the blood vasculature has been well described within the ovary; however, the location and morphological changes in the ovarian lymphatic vasculature and the factors responsible for the growth and regulation of these vessels remain largely unknown. Although the exact function of the lymphatic vessels within the ovary is not well-defined, it is assumed that they play a role in fluid homeostasis and immune cell trafficking, akin to their major function in other organs. A recent study by Brown *et al.* illustrated that lymphatic vessels in the ovary are spatially associated with estrogenic secondary ovarian follicles, yet do not form a thecal capillary network analogous to that of the blood vasculature, nor were they present in the corpus luteum (Brown et al., 2010). In accordance

with the distinct spatial patterning of ovarian lymphatic vessels, Brown *et al.* demonstrated that ovarian lymphangiogenesis is dynamically regulated in response to hormonal cues, such as follicle-stimulating hormone and estradiol, that regulate the expression of pro-lymphangiogenic growth factors, including *Vegfc* and *Vegfd* (Brown *et al.*, 2010). It is interesting to note that lymphatic vessels are absent from ovaries during early postnatal mouse development and it is not until postnatal day 8.5 that a small number of lymphatic vessels are identified in the stalk region of the ovary. By postnatal day 12.5, when the antral stage of folliculogenesis is first evident, lymphatic vessels had expanded entirely throughout the ovarian tissue (Brown *et al.*, 2010).

3.1.1.2 The uterine lymphatic vasculature

In a similar fashion to the ovary, blood vascular growth and remodelling has been studied extensively in the human and rodent endometrium during the menstrual and estrous cycles, respectively, however, only limited information exists pertaining to lymphatic vessels in the uterus. It is generally accepted that the middle layer of the uterine wall, known as the myometrium, in both humans and rodents contains a rich network of lymphatic vessels (Donoghue *et al.*, 2007; Girling *et al.*, 2010; Koukourakis *et al.*, 2005; Rogers *et al.*, 2008), however, numerous conflicting reports exist on the distribution of lymphatic vessels within the inner lining of the uterus, known as the endometrium. Several studies detected lymphatics in both the functionalis and basalis layers of the human endometrium, with the basalis region exhibiting larger lymphatic vessels and an increased lymphatic vessel density, compared to the small and sparsely distributed lymphatics of the functionalis. However, there was no significant difference observed between the proliferative and secretory phase lymphatic vessel density with respect to the functionalis, basalis and myometrial layers (Donoghue *et al.*, 2007; Rogers *et al.*, 2008). In contrast, a recent study by Girling *et al.* demonstrated that lymphatic vessels are extremely rare within the mouse endometrium (Girling *et al.*, 2010). Additional studies in rat observed lymphatic vessels selectively in the basalis layer of the endometrium (Uchino *et al.*, 1987), whilst several studies in humans noted a complete absence of lymphatic vessels in the endometrium (Koukourakis *et al.*, 2005; Red-Horse *et al.*, 2006). The reasons for these observed differences in endometrial lymphatic vessel density remain unclear, but could lie in the structural and functional variations across species, or in the methods of detection of the vessels themselves. Interestingly, two studies observed that lymphatic vessels were commonly found encircling spiral arteries in the basalis layer, forming intimate contacts with the vascular smooth muscle cells surrounding these arteries (Donoghue *et al.*, 2007; Volchek *et al.*, 2010). Once the stromal cells had decidualised, however, lymphatic vessels were no longer found to be associated with these spiral arteries (Volchek *et al.*, 2010). Furthermore, Volchek *et al.* noted that lymphatic vessels were also

located immediately adjacent to endometrial glands in the human uterus (Volchek et al., 2010). Taken together, these data demonstrate that like the ovary, endometrial lymphatic vessels are temporally regulated and display a distinct organ-specific spatial distribution. Of interest is the identity of signals that regulate lymphangiogenesis in these reproductive organs and how they are controlled by circulating hormones.

As discussed previously, lymphatic vessels play a key role in breast cancer in at least two ways. Firstly, lymphatic vessels can facilitate metastasis, particularly to axillary lymph nodes, which represents the single best prognostic predictor of breast cancer survival in clinical use (Fisher et al., 1983). Secondly, secondary lymphoedema, a common complication for up to 40% of breast cancer patients following surgical excision of axillary lymph nodes (Armer et al., 2009), is a debilitating condition for which very few effective therapeutic approaches currently exist. Despite the fundamental importance of lymphatic vessels in breast cancer, very little is known about the genes and molecular mechanisms that regulate their growth and development in the human breast. The aim of this chapter was to investigate the pattern of lymphatic vessels in the mouse mammary gland and in addition, to determine whether, like blood vessels, they were temporally remodelled during postnatal mouse mammary gland morphogenesis.

3.2 METHODS

3.2.1 Mammary gland carmine alum staining

Following the fixation of mouse mammary glands in Carnoy's solution (section 2.2.4.2.3), glands were stained overnight at RT in carmine alum stain. Carmine alum stain was prepared using 0.2% (w/v) carmine (Sigma) and 0.5% (w/v) aluminium potassium sulphate in MQ-H₂O, which was boiled with a magnetic stirrer in a fume hood for 20 minutes. The stain was left to cool and then filtered using Whatman paper, prior to the addition of thimerosal to a final concentration of 0.01% (w/v) and storage for up to 6 months in the dark at 4°C. Following staining in carmine alum, glands were rinsed in MQ-H₂O and dehydrated through a graded ethanol series (70%, 90% and 100% (v/v) ethanol, diluted using MQ-H₂O) for at least 15 minutes for each step. Glands were then cleared in xylene overnight, using at least 2 changes of fresh xylene. Once sufficiently cleared, glands were overlayed with DePeX mounting medium (BDH, BDH Limited, Poole, UK) and mounted using a 24mm x 50mm glass coverslip. Any gaps that appeared on drying were filled with fresh DePeX mounting medium the following day and left to set

completely for a further 2 days. Carmine alum-stained glands were imaged using an Olympus DP20-5E digital camera (Olympus) attached to an Olympus SZX7 stereo microscope (Olympus). Images were processed using DP20-DRV version 1.1 software (Olympus) and Adobe Photoshop CS5 version 12.0 (Adobe, Adobe Systems Incorporated, San Jose, CA).

3.2.2 Immunofluorescent immunostaining of mouse mammary gland sections

Immunofluorescent immunostaining was performed on fixed-frozen cryosections of mouse mammary gland tissue, as previously described in section 2.2.4.3.1. All incubations were at RT unless otherwise indicated. Selected slides were removed from -70°C storage, labelled and framed with an ImmEdge™ Pen (Vector Laboratories, Inc., Burlingame, CA) and left to air-dry for 2 hours. Slides were washed for 15 minutes in TBS with 0.1% (v/v) Tween@20 (Sigma) (TBS-0.1%TW20), prior to blocking in a humidified chamber for 3 hours with a blocking solution containing a mixture of 20% (v/v) newborn bovine serum (SAFC Biosciences), 60% (v/v) maleate buffer (pH 7.5) and 2% (w/v) Blocking Reagent (Roche). Samples were then incubated in a humidified chamber overnight with primary antibodies (see Table 2.1) diluted in the aforementioned blocking solution, followed by 3 x 10 minute washes in TBS-0.1%TW20. This was followed by incubation with the corresponding Alexa Fluor® secondary antibodies (Invitrogen) (see Table 2.2), also diluted in blocking solution, for 3 hours in a light-proof humidified chamber to avoid photo-bleaching. Slides were washed 3 x 10 minutes in TBS-0.1%TW20, rinsed in MQ-H₂O to remove residual salt, air-dried for 15 minutes and then mounted in ProLong® Gold antifade reagent (Invitrogen). Edges of the coverslip were sealed with nail polish to prevent leakage of the mounting reagent. Slides were stored in the dark at 4°C. Immunostaining was analysed at the Detmold Family Trust Cell Imaging Centre (Centre for Cancer Biology, SA Pathology, Adelaide, Australia) using a Bio-Rad Radiance 2100 confocal microscope (Bio-Rad Laboratories, Hercules, CA) equipped with 3 lasers (488nm Argon ion, 543nm Green HeNe and 637nm Red Diode) attached to an Olympus IX70 inverted microscope (Olympus). Adobe Photoshop CS5 version 12.0 (Adobe) was used for subsequent image processing.

3.2.3 Lymphatic vessel quantification

Mammary glands from a range of postnatal stages were cryosectioned the entire way through the fat pad as detailed in section 2.2.4.3.1, and 6-8 slides per gland were chosen at evenly-spaced intervals. Staining was performed as previously described in section 3.2.2 using a combination of rabbit anti-

Prox1 (AngioBio, AngioBio Co., Del Mar, CA), rat anti-mouse CD31 (BioLegend, San Diego, CA) and goat anti-mouse E-cadherin (R&D Systems, Minneapolis, MN) antibodies. The corresponding Alexa Fluor®-conjugated secondary antibodies (Invitrogen) were incubated in a sequential manner to avoid cross-reactivity; Alexa Fluor® 488 donkey anti-rabbit and Alexa Fluor® 647 donkey anti-goat, followed by Alexa Fluor® 555 goat anti-rat. See Table 2.1 and 2.2 for the antibody dilutions used. The number of lymphatic vessels per mammary gland section was counted at the time of imaging. Lymphatic vessel counts were averaged across sections to obtain a mean lymphatic vessel count per mammary gland. Section area (cm²) was subsequently determined using ImageJ version 1.41 software (Abràmoff et al., 2004). Three mice for each postnatal stage were analysed and data was expressed as lymphatic vessels per section or lymphatic vessels per cm².

3.2.4 Whole mount immunofluorescent immunostaining of mouse mammary glands

Mammary glands from various postnatal stages were subjected to whole mount immunofluorescent immunostaining. Glands were dissected as detailed in section 2.2.4.1 and fixed as per section 2.2.4.2.1, with the inguinal lymph nodes left intact to ensure the morphological integrity of the dissected mammary fat pads. 24 well flat-bottomed tissue culture plates were used for subsequent immunostaining steps and all steps were carried out at RT unless stated otherwise. Whole mammary glands were permeabilised in PBS with 0.3% (v/v) Triton®X-100 (Sigma) (PBS-0.3%TX100) for 15 minutes, prior to blocking in PBS-0.3%TX100 containing 1% (w/v) bovine serum albumin (BSA) (Sigma) (PBS-0.3%TX100-1%BSA) for a period of 6 hours to overnight at 4°C with gentle agitation. Following blocking, primary antibodies (listed in Table 2.1) were diluted in PBS-0.3%TX100-1%BSA and incubated with the glands for 1 hour at RT to allow for initial antibody binding, followed by overnight incubation at 4°C with gentle agitation. Glands were washed extensively for 5 x 1 hour in PBS-0.3%TX100, followed by the addition of Alexa Fluor®-conjugated secondary antibodies (Invitrogen) (listed in Table 2.2) diluted in PBS-0.3%TX100-1%BSA. Secondary antibodies were incubated with tissues overnight at 4°C with gentle agitation. All subsequent steps were carried out in the dark to avoid photo-bleaching. Unbound secondary antibody was removed by 5 x 1 hour washes in PBS-0.3%TX100, followed by an extended overnight wash in PBS-0.3%TX100 at 4°C with gentle agitation. Glands were post-fixed using 4% PFA for 1 hour, washed 3 x 10 minutes in PBS and then dehydrated via a graded methanol series (25%, 50% and 100% (v/v) methanol, diluted using PBS) for 45 minutes each step. Next, the mammary glands were subjected to a graded benzyl alcohol:benzyl benzoate (BABB) (mixed at a ratio of 1:2) series (50%

and 100% (v/v) BABB, diluted using methanol) for 45 minutes each. Due to the adipose-rich nature of the mammary fat pads, the glands were replaced with fresh 100% (v/v) BABB and left to clear further overnight. Following clearing, mouse mammary glands were mounted in 100% (v/v) BABB in ibidi uncoated μ -Dish^{35mm, low} petri dishes (ibidi, ibidi GmbH, Martinsried, Germany) with a 22mm x 22mm glass coverslip and stored at 4°C. Confocal images taken through the entire thickness of the mammary fat pads were acquired as per section 3.2.2.

3.3 RESULTS

3.3.1 The ductal epithelial network is extensively remodelled during postnatal mouse mammary gland morphogenesis

To become familiar with the gross morphology of the ductal tree in the mouse mammary gland at the outset of this project, we initially performed carmine alum stains on mouse mammary glands from a variety of stages of postnatal development. It is evident from these whole mount preparations that the epithelial tree undergoes extensive and rapid morphological changes over the course of postnatal mammary gland morphogenesis. This dynamic process begins at puberty with the presence of a regularly-spaced network of ductal branches that each terminate in a bulbous structure, known as the terminal end bud (TEB) (Figure 3.1A,B). By the time the mouse has reached adulthood, the gland is filled with an arborised network of primary ducts and secondary side branches lacking TEBs (Figure 3.1C,D). As pregnancy advances, tertiary ductal branches and alveolar buds form (Figure 3.1E-H), which ultimately culminate in the formation of mature secretory alveoli that expand to fill the entire mammary fat pad during lactation (Figure 3.1I,J). Upon weaning, the mammary gland undergoes the greatest degree of remodelling during involution, whereby surplus epithelium is gradually removed and the gland becomes repopulated by adipocytes (Figure 3.1K,L).

3.3.2 Mammary lymphatic vessel density is elevated during pregnancy

In order to investigate lymphatic vessel density in the postnatal mouse mammary gland, we analysed inguinal mammary fat pads from WT C57BL/6 female mice across the reproductive cycle; from a virgin state through pregnancy, lactation and involution. This was achieved via immunofluorescent immunostaining of frozen mammary gland sections with the following antibodies: rat anti-mouse CD31 (BioLegend), a commonly used pan-endothelial marker, rabbit anti-Prox1 (AngioBio) to definitively

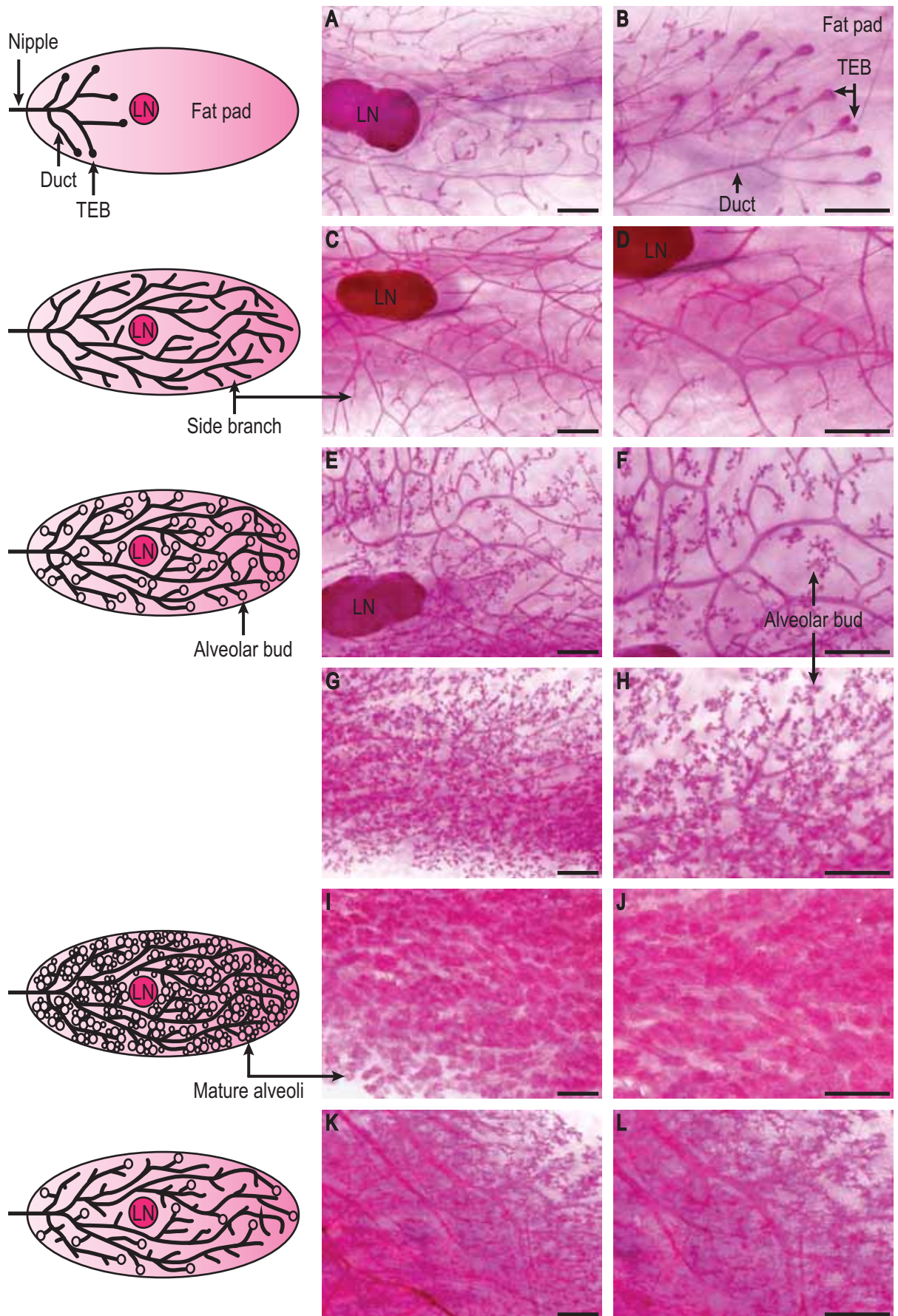


Figure 3.1 - Carmine alum-stained postnatal mouse mammary glands.

Carmine alum-stained whole mount mammary glands from 6 week virgin (A,B), 6 month (C,D), 11.5 day pregnant (E,F), 14.5 day pregnant (G,H), 10 day lactating (I,J) and 4 day involuting (K,L) mice show the extensive remodelling of the ductal network that occurs during postnatal mouse mammary gland morphogenesis. LN - lymph node, TEB - terminal end bud. Scale bars represent 1mm.

identify lymphatic vessels from blood vessels and goat anti-mouse E-cadherin (R&D Systems) to detect mammary epithelial cells, both luminal and myoepithelial subtypes. The number of lymphatic vessels was quantified per section and found to be increased significantly during lactation when compared to virgin and involuting stages (Figure 3.2A). During the quantification process it was observed that the size of the mammary gland fluctuated dramatically across the stages analysed, with the mammary gland reaching a maximal size during lactation (Figure 3.2B). This is consistent with maturation and engorgement of the alveoli, the milk-producing component of the gland, with milk protein and lipids (Richert et al., 2000). Therefore, the number of lymphatic vessels per section was normalised to account for the area of the corresponding tissue section using ImageJ version 1.41 software (Abràmoff et al., 2004). Upon normalisation to the area of the section, lymphatic vessel density, indicated by lymphatic vessels per cm², was significantly increased in the pregnant state, compared to virgin and involuting stages (Figure 3.2C). These quantification analyses indicate that the mammary gland lymphatic network undergoes a transient temporal expansion and then subsequently regresses following pregnancy and lactation, reverting to a density comparable to the 'pre-pregnant' or 'virgin-like' state.

3.3.3 Lymphatic vessels are spatially associated with mammary ducts and large blood vessels in the mouse mammary gland

To ascertain the spatial location of lymphatic vessels within the mouse mammary gland, immunofluorescent immunostaining was performed on mammary gland tissue sections, as detailed above in section 3.3.2. In order to achieve the best view of lymphatic vessels possible, the thickness of mammary gland sections was extensively optimised from 4µm (thin) paraffin sections to 60µm (thick) frozen sections (data not shown). Cryopreserved tissue sectioned at 45µm was determined to be the optimal section thickness for immunostaining analyses. Mammary glands from 3 mice were analysed for each morphogenetic time point. We observed that lymphatic vessels (arrowheads) were intimately spatially associated with both mammary ducts (Figure 3.3A,C,E,G) and large blood vessels (Figure 3.3B,D,F,H) during all stages of mammary gland development analysed, suggesting that signals derived from the ductal epithelia and/or the blood vasculature may provide cues that pattern the mammary lymphatic vessel network. Closer analysis revealed that, unlike the well-characterised blood vascular 'capillary baskets' that elaborately encapsulate the alveoli during pregnancy and lactation (Djonov et al., 2001; Matsumoto et al., 1992), as evidenced by CD31 staining (Figure 3.4A,C,E,G), lymphatic vessels (arrowheads) were not observed encasing the alveoli during pregnancy (Figure 3.4B,D) or lactation

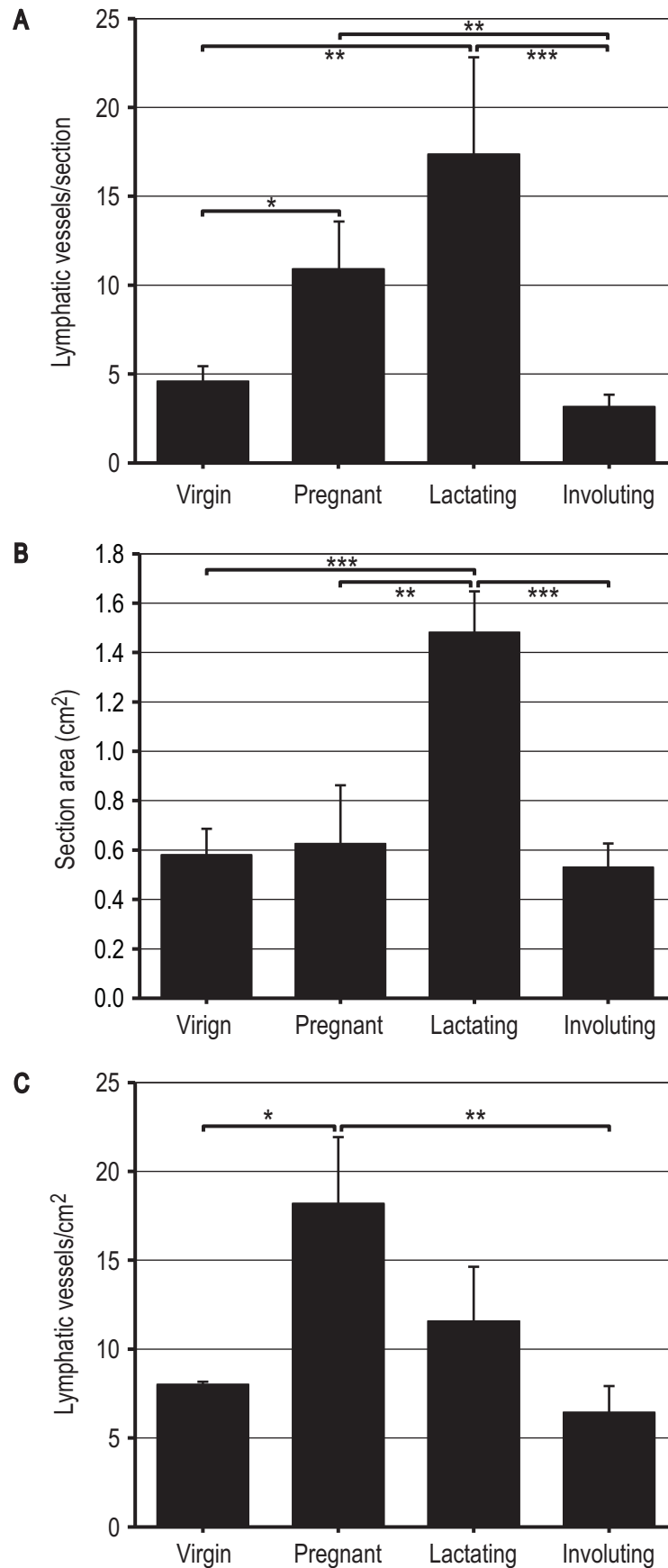


Figure 3.2 - Mammary lymphatic vessel density is elevated during pregnancy.

Lymphatic vessel quantification in 8 week virgin, 14.5 day pregnant, 10 day lactating and 11 day involuting mice reveals that mammary lymphatic vessel density is elevated during pregnancy (C). Data is represented graphically as lymphatic vessels per section (A), section area (cm²) (B) and lymphatic vessels per cm² (C). Data shown represent the mean \pm standard error of the mean of three independent mice. *P*-values were calculated using a log-linear (A) or mixed (B,C) modelling approach, with a Sidak adjustment for multiple comparisons, **P*<0.05, ***P*<0.001, ****P*<0.0001.

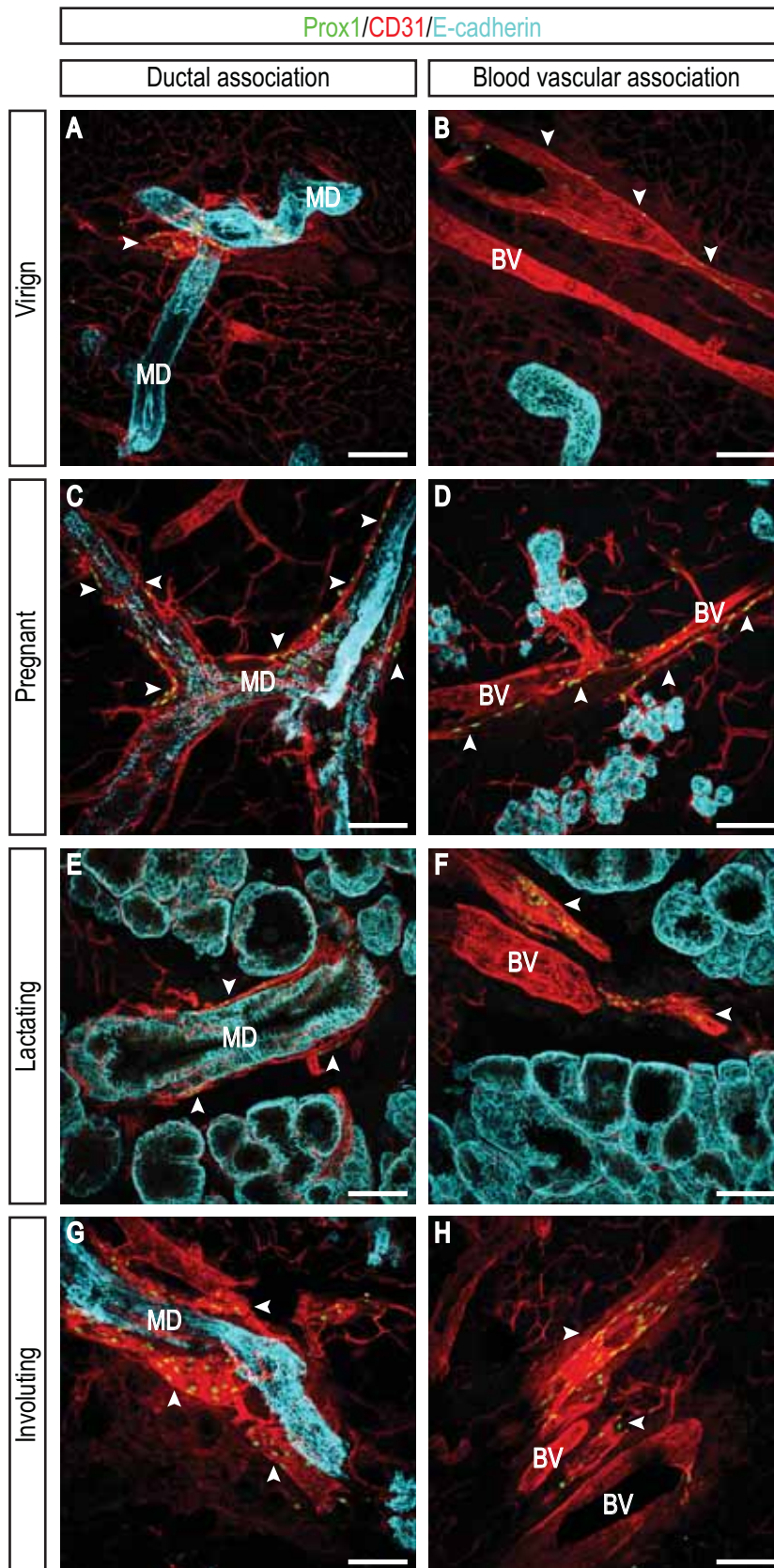


Figure 3.3 - Lymphatic vessels are spatially associated with mammary ducts and large blood vessels in the mouse mammary gland.

Confocal z-stack images of 45 μ m sections demonstrating the close association of lymphatic vessels (arrowheads) with mammary ducts (MD; **A,C,E,G**) and large blood vessels (BV; **B,D,F,H**) in 8 week virgin (**A,B**), 14.5 day pregnant (**C,D**), 10 day lactating (**E,F**) and 11 day involuting (**G,H**) mammary glands. Images are representative of three mice. Scale bars represent 100 μ m.

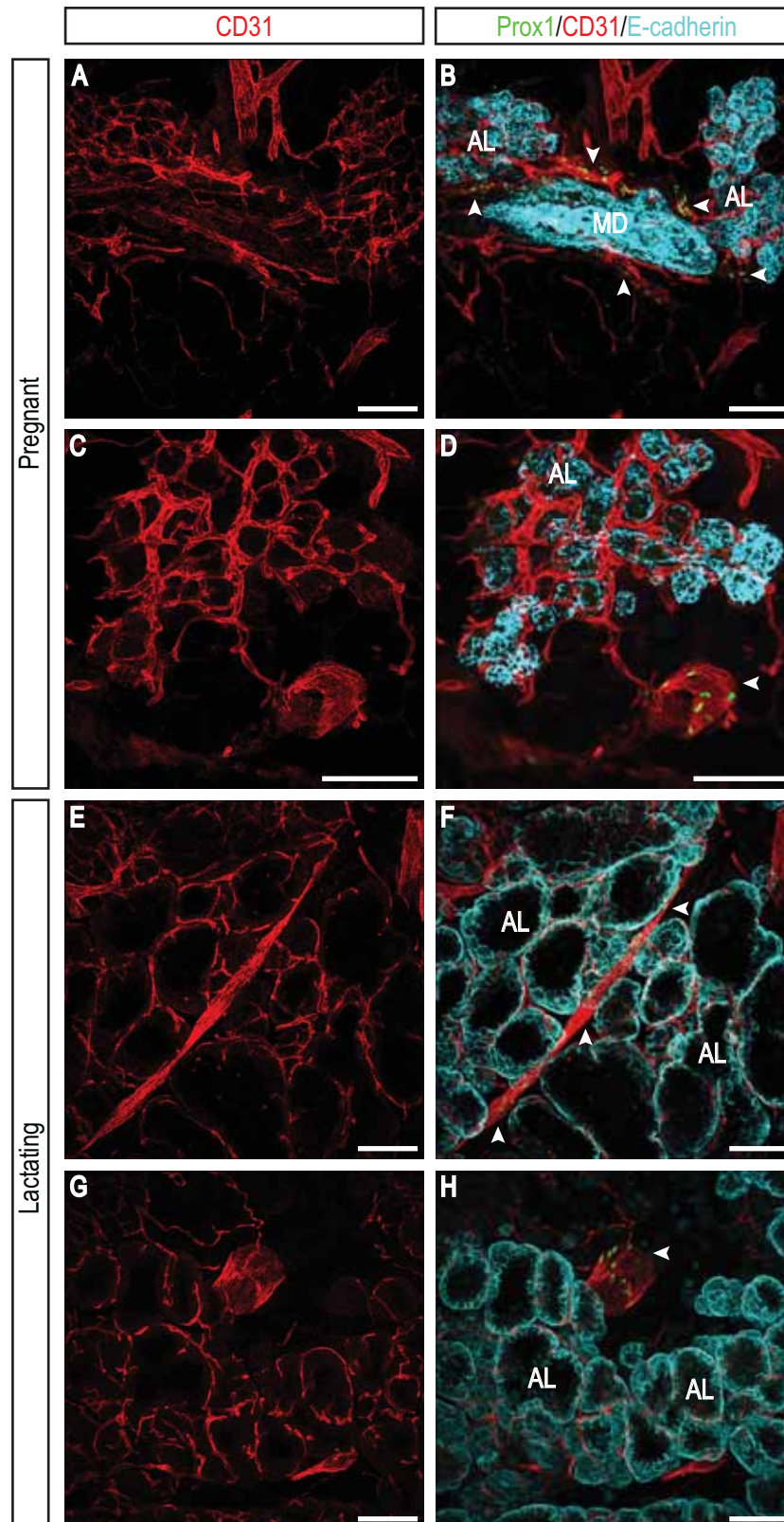


Figure 3.4 - Mammary lymphatic vessels do not form 'capillary baskets' surrounding the alveoli.

Confocal z-stack images of 45 μ m sections demonstrating the absence of lymphatic vessels (arrowheads) around the alveoli (AL) in 14.5 day pregnant (**B,D**) and 10 day lactating (**F,H**) mammary glands. **A,C,E,G** are single-channel images of **B,D,F,H**, respectively, demonstrating blood vascular 'capillary baskets'. Images are representative of three mice. MD - mammary duct. Scale bars represent 100 μ m.

(Figure 3.4F,H). Instead lymphatic vessels were spatially associated with larger mammary ducts (Figure 3.3A,C,E,G).

In order to further investigate the distinct patterning of lymphatic vessels in the mouse mammary gland, we optimised a whole mount immunofluorescent immunostaining protocol. This approach provided a three-dimensional view of the intact fat pad microenvironment, without compromising on clarity and resolution. Two combinations of primary antibodies were found to be optimal for these analyses. The first combination was that used previously in section 3.3.2, consisting of rat anti-mouse CD31 (BioLegend), a commonly used pan-endothelial marker, rabbit anti-Prox1 (AngioBio) to distinguish lymphatic vessels from blood vessels and goat anti-mouse E-cadherin (R&D Systems) to detect the mammary epithelia. The second triple-labelling combination included rat anti-mouse CD31 (BioLegend), to detect blood and lymphatic vessels, goat anti-mouse CCL21 (R&D Systems) to detect lymphatic vessels and Cy3-conjugated mouse monoclonal anti- α -smooth muscle actin (Sigma-Aldrich, Sigma-Aldrich Co., St. Louis, MO) to detect the ductal and alveolar epithelia and large blood vessels by virtue of binding to myoepithelial cells and the vascular smooth muscle sheath investing blood vessels, respectively. Unlike the nuclear localisation of Prox1, CCL21 displayed a punctate staining pattern in lymphatic vessels (Figure 3.5A,B,D-I; Figure 3.6A-D) and is likely indicative of secretory vesicles, analogous to that observed in neurons (de Jong et al., 2008).

Whole mount immunostaining analyses revealed a similar spatial relationship between lymphatic vessels and the mammary ducts in both virgin (Figure 3.5F-I) and pregnant (Figure 3.6) stages to that previously seen in sections (Figure 3.3A,C,E,G), whilst offering further insight into the nature of mammary lymphatic vascular patterning. Intriguingly, lymphatic vessels were not observed in close proximity to the rudimentary epithelial tree in 3 week old pubertal mammary glands, as evidenced by a lack of Prox1 staining in close proximity to these ducts (d; Figure 3.5C). However, lymphatic vessels were intimately associated with the mammary ducts (d) by 8 weeks of age (Figure 3.5F-I). In a similar fashion to that observed in sections (Figure 3.3B,D,F,H), lymphatic vessels were also found to follow the path of some large blood vessels, most likely arteries (a), based on their morphology and extensive expression of α SMA and CD31, in both pubertal (Figure 3.5A,B) and virgin (Figure 3.5D,E) mammary glands.

In a manner similar to the way that blood vascular capillary plexuses run in parallel or encircle the mammary ducts in the virgin gland (Matsumoto et al., 1992), lymphatic capillaries were observed to track alongside the mammary ducts (outlined by dashed lines), or alternatively, spiral around the ducts

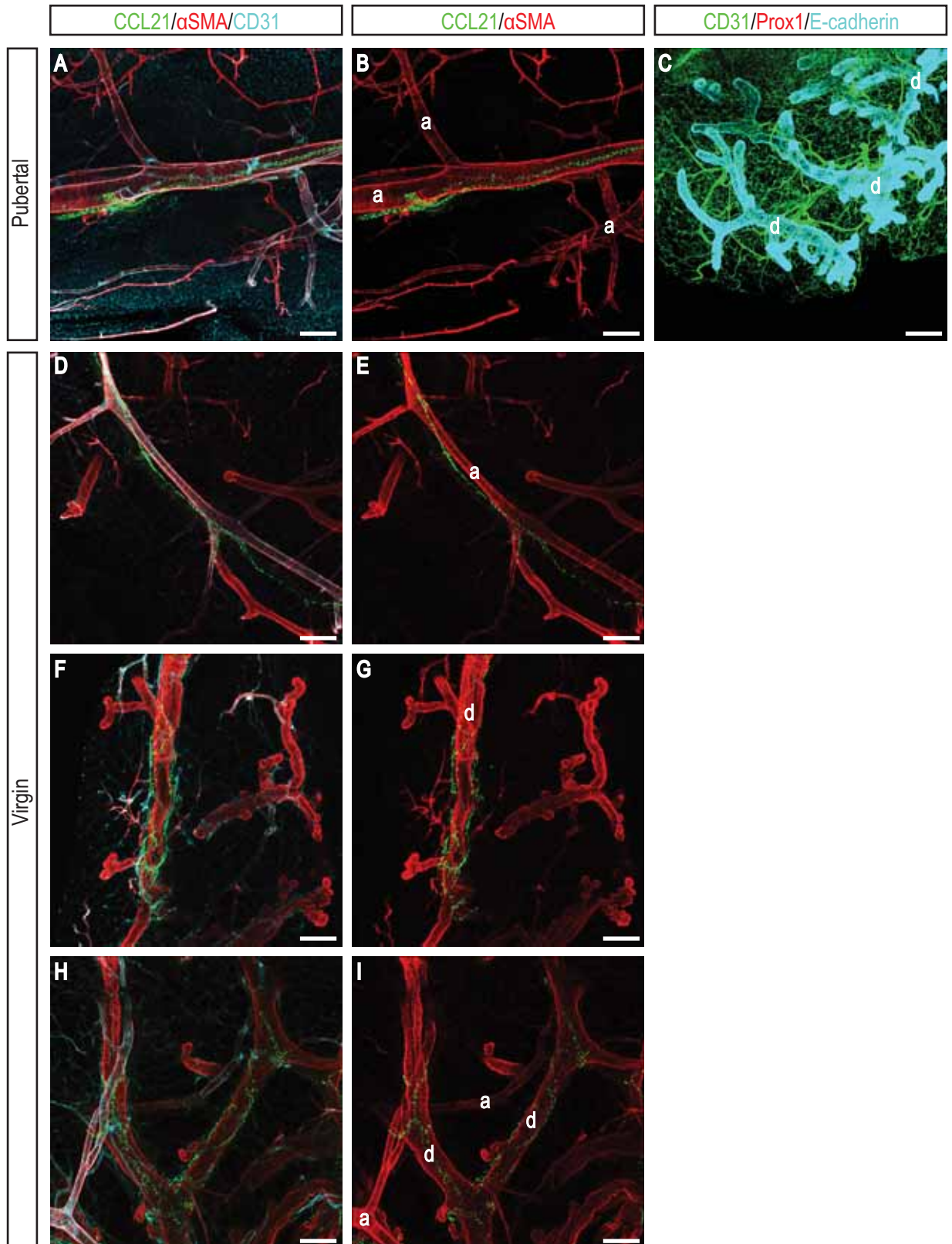


Figure 3.5 - Lymphatic vessels are intimately associated with the epithelial tree in virgin, but not pubertal mouse mammary glands.

Confocal z-stack images of 3 week pubertal (**A-C**) and 8 week virgin (**D-I**) whole mount mammary glands reveal that mammary lymphatic vessels are not associated with the epithelial tree during puberty (**C**), but are however, intimately associated with the mammary ducts (**d**) by 8 weeks of age (**F-I**). Lymphatic vessels are also spatially localised along some major blood vessels, most likely arteries (**a**), based on their co-expression of CD31 and alpha smooth muscle actin (α SMA), in both pubertal (**A,B**) and virgin (**D,E**) mammary glands. **B,E,G,I** illustrate double-channel images of **A,D,F,H**, respectively. Images are representative of two mice. Scale bars represent 150 μ m.

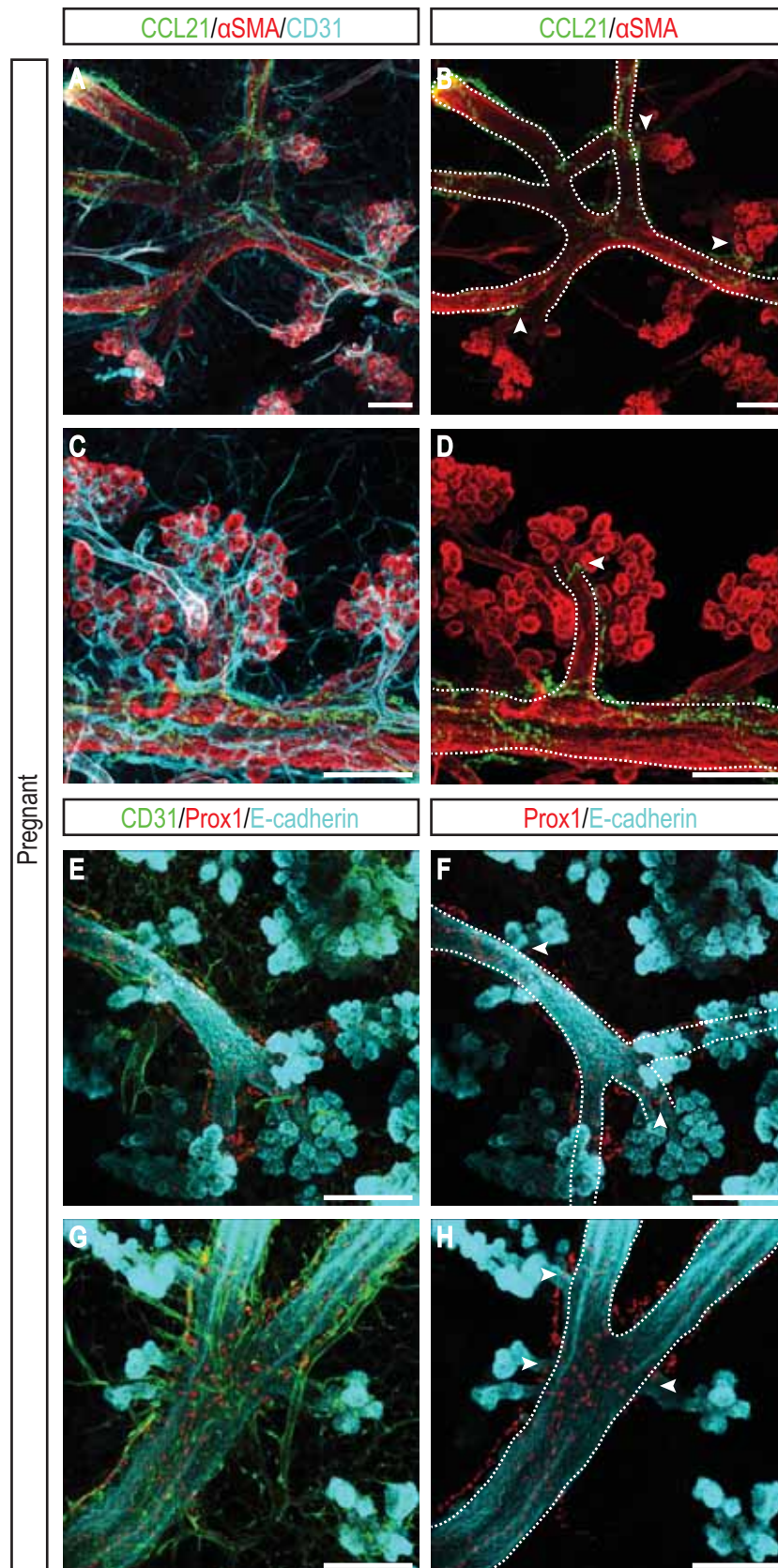


Figure 3.6 - Lymphatic vessels are intimately associated with mammary ducts, but not the alveoli, in pregnant mouse mammary glands.

Confocal z-stack images of 14.5 day pregnant whole mount mammary glands reveal that lymphatic vessels are intimately associated with mammary ducts (outlined by dashed lines), but do not extend into the protruding alveolar clusters. **B,D,F,H** represent dual-channel images of **A,C,E,G**, respectively. Images are representative of two mice. α SMA - alpha smooth muscle actin. Scale bars represent 150 μ m.

in the pregnant mammary gland (Figure 3.6). As observed in mammary gland sections (Figure 3.4B,D,F,H), lymphatic vessels were not present in the vicinity of alveoli (Figure 3.6B,D,F,H). Rather, the lymphatic capillaries appeared to traverse some distance along minor ductal side branches or 'alveolar stalks' (arrowheads), before ceasing further extension into protruding alveolar clusters (Figure 3.6B,D,F,H).

Whole mount staining of lactating and involuting glands was also performed, however due to the thickness of the gland and the presence of autofluorescent apoptotic cells, respectively; it was extremely difficult to detect lymphatic vessels readily using this approach. It was possible, however, to image the epithelial tree and blood vessels at these developmental stages, further highlighting the dramatic morphological changes that the mammary gland ductal tree undergoes during postnatal mouse mammary gland morphogenesis (Figure 3.7).

3.3.4 Lymphatic vessel density in the mouse mammary gland correlates with density of the epithelial tree

Based on our observations that lymphatic vessel density in the mouse mammary gland is increased during pregnancy and that lymphatic vessels are spatially associated with the ductal epithelia, we sought to determine whether lymphatic vascular density correlated with epithelial density. To address this question, we investigated lymphatic vessel density and patterning in inguinal mammary fat pads from transgenic mouse models displaying either a hypo- or hyperplastic epithelial tree; *MMTV-creD;Gata-3* (Asselin-Labat et al., 2007) and *MMTV-PyMT* (Guy et al., 1992; Lin et al., 2003) mice, respectively. In these mouse models, the mouse mammary tumour virus (MMTV)-long terminal repeat promoter/enhancer is used to excise/drive transgene expression specifically in mammary gland epithelial cells (Cardiff and Muller, 1993). As previously detailed, triple-labelling using rat anti-mouse CD31 (BioLegend), rabbit anti-Prox1 (AngioBio) and goat anti-mouse E-cadherin (R&D Systems) were used to detect blood and lymphatic vessels, lymphatic vessels and mammary epithelial cells, respectively. Mammary gland lymphatic vessel density was measured by counting lymphatic vessels in multiple immunostained mammary gland tissue sections (section 3.2.3). Analysis of mammary lymphatic vessel density in mammary glands from 8 week old *MMTV-creD;Gata-3* mice, which show limited expansion of the ductal tree compared to control littermates (Asselin-Labat et al., 2007), revealed a trend towards a reduction in lymphatic vascular density (Figure 3.8A). Unfortunately, only one mouse per genotype was available for these analyses, therefore we analysed lymphatic vessel density in both

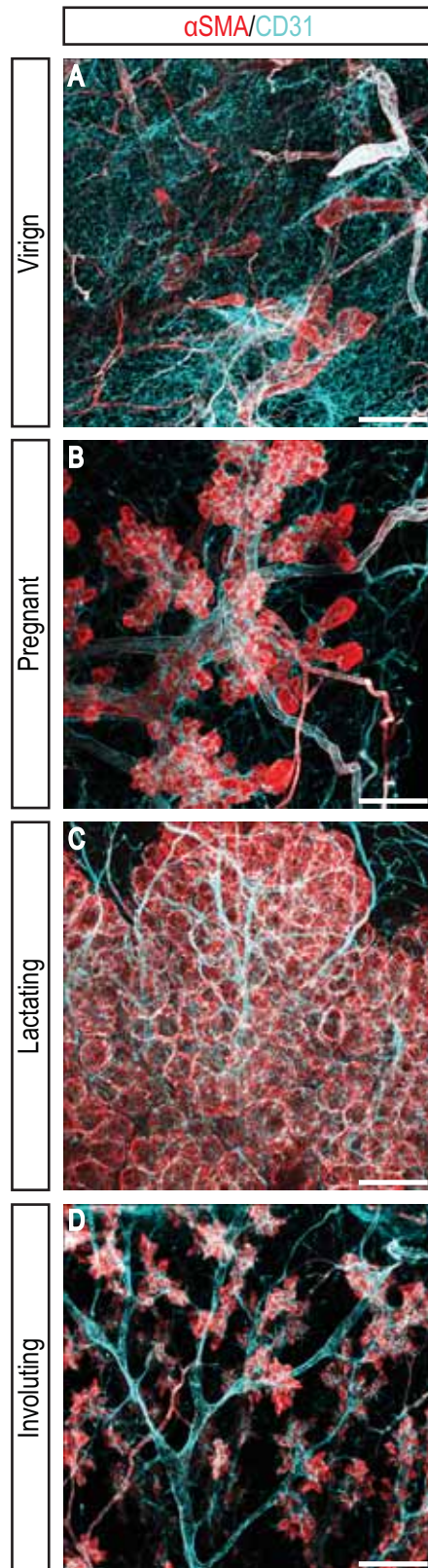


Figure 3.7 - The ductal tree is dynamically remodelled during postnatal mouse mammary gland morphogenesis. Confocal z-stack images of whole mount 8 week virgin (**A**), 14.5 day pregnant (**B**), 10 day lactating (**C**) and 10 day involuting mammary glands (**D**) stained with alpha smooth muscle actin (α SMA) and CD31. Scale bars represent 150 μ m.

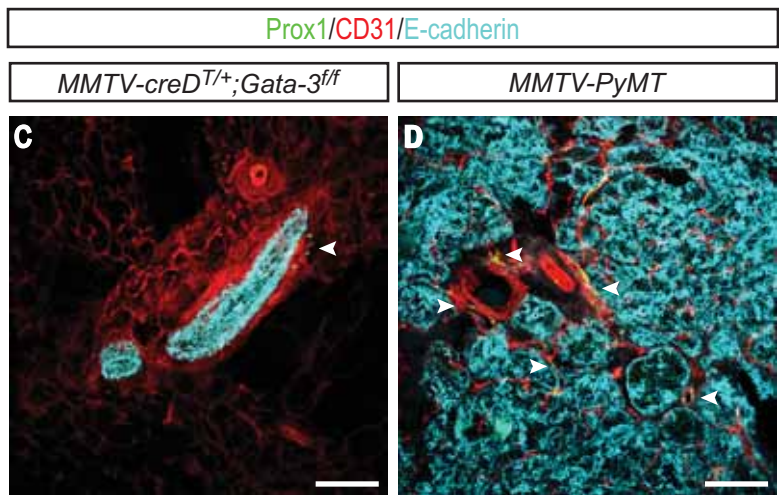
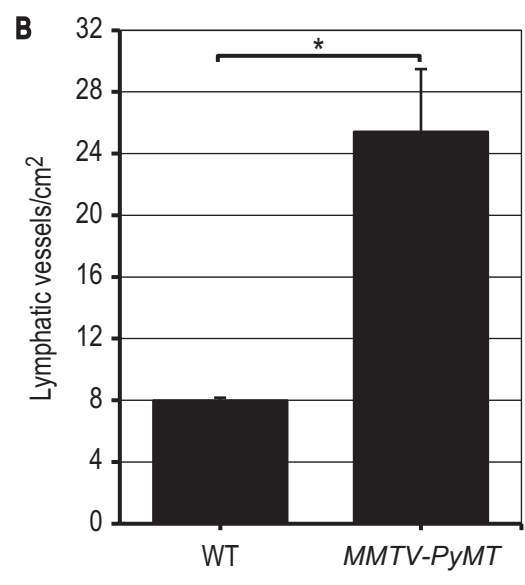
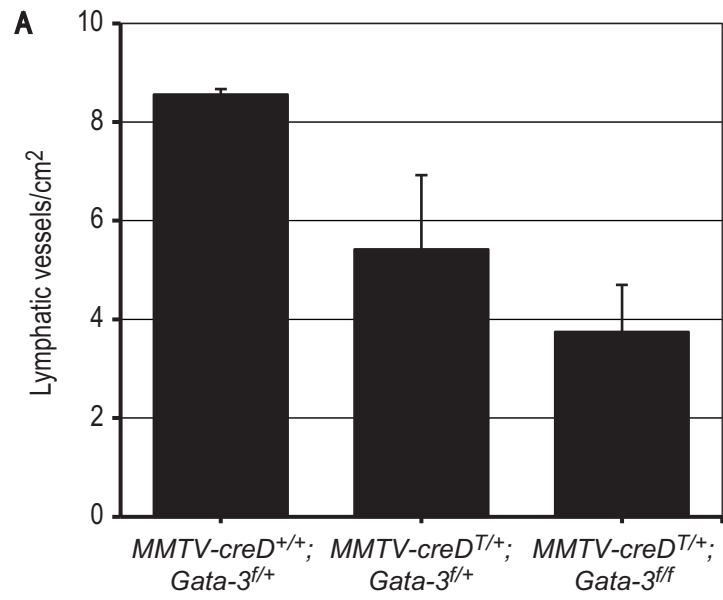


Figure 3.8 - Mammary lymphatic vessel density correlates with density of the epithelial tree. Mammary lymphatic vessel quantification in 8 week *MMTV-creD;Gata-3* (A), wild-type (WT) and *MMTV-PyMT* (B) mice. Error bars represent the mean \pm standard error of the mean of three independent experiments (B) and one experiment (A). *P*-values were calculated using the two-tailed Student's *t*-test, **P*<0.01. Confocal z-stack images of 45 μ m sections comparing lymphatic vessel (arrowheads) and epithelial tree density in *MMTV-creD^{T/+};Gata-3^{ff}* (C) and *MMTV-PyMT* (D) mammary glands. MMTV - mouse mammary tumour virus, PyMT - polyomavirus middle T antigen. Scale bars represent 100 μ m.

left and right inguinal mammary fat pads in these mice. Figure 3.8C is representative of the reduced lymphatic vessel density observed in *MMTV-creD^{T/+};Gata-3^{fl/fl}* mice.

In the *MMTV-PyMT* mouse model of breast cancer, expression of the oncoprotein, polyomavirus middle T antigen (PyMT), is under the control of MMTV and is therefore restricted to the mammary epithelium. As a result, epithelial hyperplasia can be detected as early as 4 weeks of age and eventually by around 14 weeks of age, progresses to overt mammary carcinoma (Guy et al., 1992; Lin et al., 2003). Quantification of lymphatic vessel density in 8 week old *MMTV-PyMT* mice revealed a significant increase in lymphatic vascular density compared to WT counterparts (Figure 3.8B). Figure 3.8D is representative of the increased lymphatic vessel density observed in *MMTV-PyMT* mice.

Taken together, our data demonstrates a strong correlation between lymphatic vessel density and density of the epithelial tree in the mouse mammary gland. Whilst these data do not dissect out the relative contribution of the mammary blood vasculature, which may also be altered in these mouse models, they do suggest that the mammary gland epithelium is a potential source of lymphangiogenic signals that contribute to the regulation of lymphatic vascular growth and remodelling in the postnatal mouse mammary gland.

3.3.5 Prox1 expression is not restricted to lymphatic vessels, but is also expressed in venous valves in the mouse mammary gland

Throughout our extensive analyses of the mammary gland via whole mount immunostaining and immunostaining of sections, it became increasingly apparent that Prox1, a commonly used LEC marker, was also expressed in what appeared to be venous valves in the mouse mammary gland, based on their morphology and location in blood vessels. Venous valves (double arrowheads) were morphologically distinct from lymphatic valves (arrow), appearing as discrete clusters of Prox1-positive cells, rather than a bicuspid valve leaflet (Figure 3.9A-C). This unexpected observation was validated by triple immunofluorescent-labelling using rabbit anti-Prox1 (AngioBio), rat anti-mouse CD31 (BioLegend) and goat anti-mouse VEGFR-3 (R&D Systems) primary antibodies to further discriminate lymphatic vessels from blood vessels. This analysis demonstrated that discrete clusters of Prox1-positive cells (double arrowheads) were indeed present in large blood vessels (Figure 3.9D-L) and on the basis of morphology, lack of VEGFR-3 expression, lack of Prox1 expression in non-valve EC and the documented restriction of valves to veins, not arteries (dela Paz and D'Amore, 2009), we concluded that

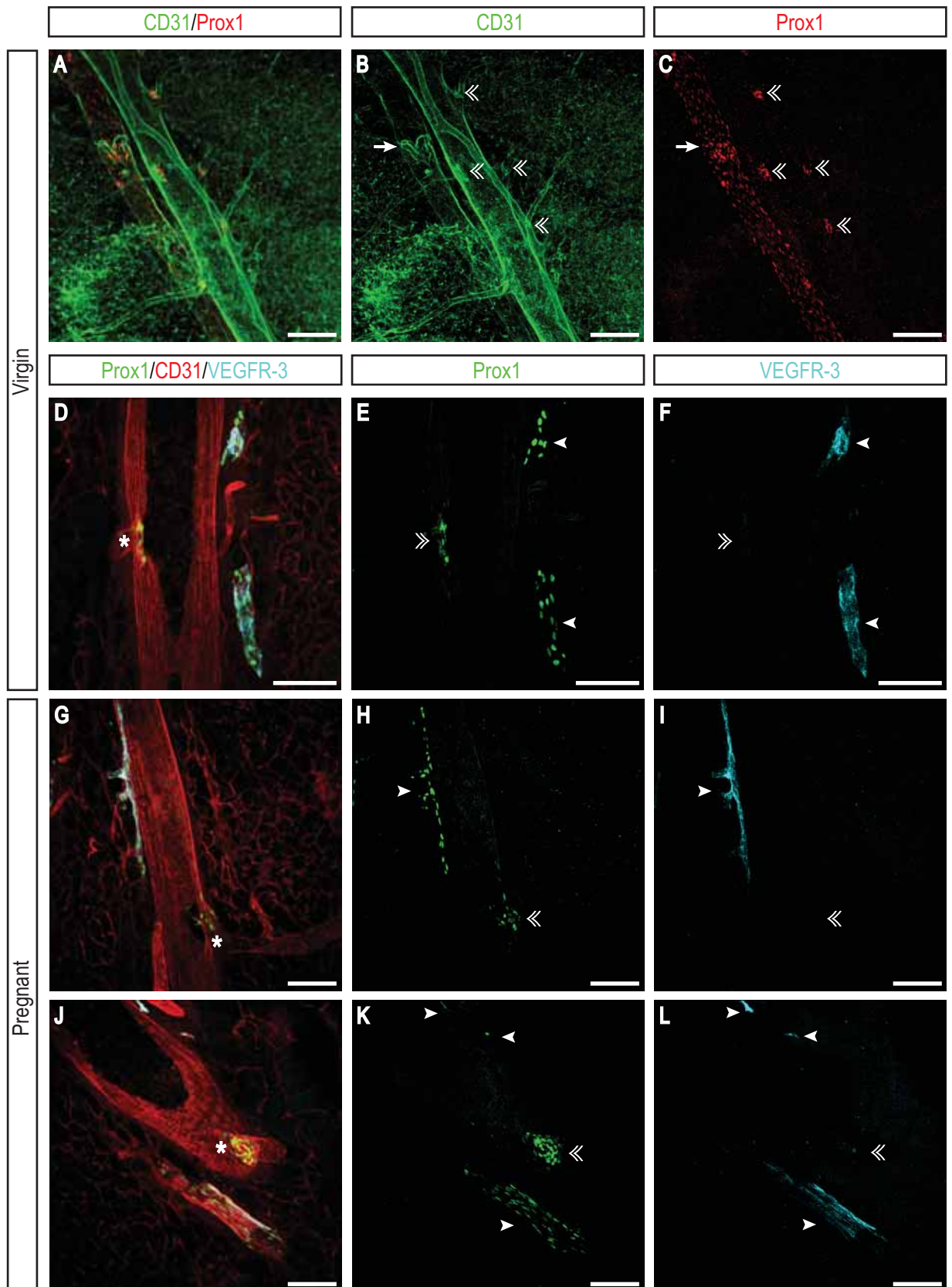


Figure 3.9 - Prox1 is expressed in venous valves in the mouse mammary gland.

Confocal z-stack images of 8 week virgin whole mount mammary glands reveal that Prox1 is expressed in blood vasculature valves (double arrowheads), which are distinct from lymphatic valve leaflets (arrow) (A-C). Triple immunofluorescent-labelling of mammary gland sections from 6 week virgin (D-F) and 6.5 day pregnant (G-L) mice demonstrate that venous valves (double arrowheads) are located at sites of bifurcation (*) and express Prox1 at comparable levels to mammary lymphatic vessels (arrowheads). B,C;E,F;H,I;K,L illustrate single colour panels of A,D,G,J, respectively. Scale bars represent 100 μ m.

these blood vessels were veins. In venous valves (double arrowheads), Prox1 was apparent at levels comparable to that seen in lymphatic vessels (arrowheads; Figure 3.9E,H,K). Interestingly, we also noted that venous valves only appeared at sites of bifurcation along the length of the vein (*; Figure 3.9D,G,J). To our knowledge, and with the exception of the earliest stages of lymphatic vascular development, this is the first evidence that Prox1 is expressed in the blood vasculature and specifically, restricted to venous valves.

3.4 DISCUSSION

Our data demonstrates that along with the mammary epithelial tree and blood vasculature, the lymphatic vascular network is dynamically remodelled during mammary gland morphogenesis; with a peak in lymphatic vessel density observed in the pregnant state, followed by a concomitant reduction during involution to a density that is comparable to a 'pre-pregnant' or 'virgin-like' state. A similar pattern of expansion and regression has been previously documented in the mouse mammary gland blood microvasculature (Figure 1.7F) (Pepper et al., 2000). The increase in mammary gland lymphatic vessel density observed during pregnancy is in accordance with pregnancy being a period involving extensive proliferation of ductal branches and a dramatic increase in the epithelial to adipocyte ratio (Richert et al., 2000). This is further corroborated by our finding in transgenic mouse models exhibiting epithelial hypoplasia and hyperplasia that lymphatic vessel density in the mouse mammary gland correlates with the density of the epithelial tree. Taken together, these data suggest that epithelial-derived growth factors are likely to be a major source of lymphangiogenic stimuli accounting for the growth, patterning and remodelling of the lymphatic vasculature during postnatal mouse mammary gland morphogenesis. Our data demonstrating that lymphatic vessels share a close spatial association with large ducts, often encircling and tracking along the length of these structures, provides further evidence in support of the mammary gland epithelium acting as a source of pro-lymphangiogenic growth factors. Additional sources of lymphangiogenic growth factors in the mouse mammary gland may also exist, and include the blood vasculature (either the EC themselves or the supporting pericytes), resident and circulating haematopoietic cells, such as macrophages, peri-ductal stromal cells and hormonal influences. The analysis of these potential sources will be addressed in Chapters 4 and 5.

Despite the prominent spatial relationship of the mammary lymphatic vasculature with the ductal tree, we did however, observe a smaller proportion of lymphatic vessels in close proximity to large blood vessels, most likely arteries (Figure 3.3B,D,F,H; Figure 3.5A,B,D,E). This finding is in agreement with

studies from Bussmann *et al.* which demonstrate that intersegmental lymphatic vessels have a striking tendency to align with arterial, rather than venous, intersegmental vessels in the zebrafish trunk, suggesting that arteries provide critical guidance cues for LEC migration and patterning (Bussmann *et al.*, 2010). It is hypothesised that arterial EC may secrete particular lymphangiogenic growth factors, such as VEGF-C, or deposit extracellular matrix components that provide an essential substrate for directed LEC migration (Bussmann *et al.*, 2010). In accordance with this data, blood vessels, particularly vascular smooth muscle cells surrounding arteries, are a source of VEGF-C (Karkkainen *et al.*, 2004; Kubo *et al.*, 2002) and VEGF-D (Rutanen *et al.*, 2003), during early stages of mouse embryogenesis, in mouse models of inflammation and in human atherosclerotic lesions, respectively. Therefore, the blood vasculature cannot be discounted as a potential source of lymphangiogenic stimuli in the postnatal mouse mammary gland. Taken together, our data suggest that lymphatic vessels in the early pubertal mouse mammary gland might first enter the mammary gland following the path of large blood vessels and progressively expand to become intimately associated with the growing ductal epithelium. We would therefore predict that the large collecting lymphatics, including the afferent and efferent lymphatics emanating from the central inguinal lymph node, are independent of the temporally-regulated ductal-associated lymphatic capillaries.

Intriguingly, we observed a distinct lack of association of lymphatic vessels with alveoli in the pregnant and lactating mouse mammary gland; unlike the well-characterised blood vascular 'capillary baskets' that elaborately encapsulate the alveoli during these developmental stages (Djonov *et al.*, 2001; Matsumoto *et al.*, 1992). This observation may not be completely surprising given the disparate functions of the alveoli and lymphatic vessels. Alveolar epithelial cells are the site of active milk protein and lipid synthesis and secretion in the mammary gland (Richert *et al.*, 2000); whilst the major role of lymphatic vessels is fluid homeostasis, returning extravasated interstitial protein-rich fluid back to the venous bloodstream for recirculation (Alitalo *et al.*, 2005; Mäkinen *et al.*, 2007; Tammela and Alitalo, 2010). Therefore, the presence of lymphatic vessels in close proximity to the milk-secreting alveoli would more than likely limit milk and nutrient supply to suckling young. The distinctive absence of lymphatic vessels in conjunction with the alveoli may result as a consequence of differentially regulated gene expression between ductal and alveolar epithelial cells. One such candidate for 'repelling' lymphatic vascular growth is soluble VEGFR-2 (sVEGFR-2). Albuquerque *et al.* recently demonstrated that sVEGFR-2 is expressed specifically in epithelial cells comprising the cornea and is responsible for maintaining the alymphatic state of the cornea by sequestering endogenously-available VEGF-C (Albuquerque *et al.*, 2009). This function is analogous to that of soluble VEGFR-1, which acts as a trap for endogenous VEGF-A, resulting in corneal avascularity (Ambati *et al.*, 2006). It is conceivable that

sVEGFR-2 may be expressed specifically in the alveolar epithelia, where it functions to sequester any endogenously-available VEGF-C, or its close homologue, VEGF-D; thus accounting for the lack of lymphatic vessels associated with the alveoli in the mouse mammary gland. The analysis of sVEGFR-2 expression levels and cellular localisation in the postnatal mouse mammary gland is currently ongoing.

Studies investigating the distribution of lymphatic vessels in the rat mammary gland by Ohtani *et al.* highlight several key similarities and differences when compared with our data in the mouse mammary gland. Interestingly, Ohtani *et al.* concluded that during lactation lymphatic vessel number was maximal (Ohtani *et al.*, 1998). This is in accordance with our finding that peak lymphatic vessel number occurs during lactation; however, this was prior to normalising lymphatic number to section area (Figure 3.2A). Furthermore, whilst Ohtani *et al.* observed that larger lymphatic collecting vessels are found adjacent to mammary ducts during all developmental stages; during lactation however, most of the lymphatics were found to be positioned in close proximity to the alveoli with no accompanying relationship to blood vessels (Ohtani *et al.*, 1998). This observation is in contrast to our data which reveals a tendency for lymphatic vessels to be in close association with mammary ducts and blood vessels, with a distinct lack of affinity for the alveoli. In this rat study, however, only light microscopy of semi-thin sections and transmission electron microscopy were used to determine lymphatic vessel localisation. From our studies, it is clear that sections alone offer limited information when compared to whole mount immunostaining analyses, which offer a three-dimensional representation of the mammary gland environment. In addition, Ohtani *et al.* used enzyme histochemistry for 5'-nucleotidase, a widely employed method at the time of their study to identify lymphatic vessels in many tissues and organs, as specific markers of the lymphatic vasculature were limited. Therefore, it is difficult to determine whether these discrepancies are related to variation across species or due to technical limitations of the study by Ohtani *et al.*

Our observation that lymphatic vessels are precisely patterned and temporally remodelled during postnatal mouse mammary gland morphogenesis is comparable to the lymphatic vasculature in other murine reproductive organs, such as the ovary and uterus. Unlike the ovarian blood vasculature, which develops a fine capillary network within the thecal layers during follicle growth, lymphatic vessels are larger and lie in close proximity to growing estrogenic ovarian follicles in the mouse ovary (Brown *et al.*, 2010). This spatial separation of blood and lymphatic vessels within the thecal layers of the ovary is similar to the lack of lymphatic capillaries observed around the alveoli in the mammary gland and may reflect the divergent roles of these two distinct vascular systems at these precise anatomical locations. In addition, two studies of the human endometrium noted that lymphatic vessels were commonly

observed surrounding spiral arteries in the basalis layer, forming intimate contact with the vascular smooth muscle cells which encase these vessels (Donoghue et al., 2007; Volchek et al., 2010). A similar phenomenon is observed in the mouse mammary gland, whereby lymphatic vessels are found following the path of arteries and large ducts; the latter of which are surrounded by a continuous layer of contractile myoepithelial cells, akin to vascular smooth muscle cells, with their contractility assisting in the movement of milk proteins and lipids along the mammary ducts (Richert et al., 2000). It is therefore plausible that vascular smooth muscle cells and myoepithelial cells could be a common source of lymphangiogenic stimuli accounting for the precise patterning of lymphatic vessels in the postnatal mouse mammary gland. In comparison, the alveoli are surrounded by a discontinuous sheath of myoepithelial cells (Richert et al., 2000), which could provide further justification for the lack of observed association of these structures with lymphatic vessels.

A key issue that has not been addressed experimentally in this study is the mechanism by which lymphatic vessels grow in the mouse mammary gland. It is plausible that lymphatic vessels follow a similar mechanism of growth to blood vessels in the mouse mammary gland during pregnancy; whereby concomitant with epithelial cell expansion, blood vessels grow during the first half of pregnancy by sprouting angiogenesis, whilst in the last half of pregnancy and lactation, non-proliferative intussusceptive angiogenesis is the predominant form of angiogenesis responsible for the expansion of the mammary vascular plexus (Djonov et al., 2001). Even more intriguing is the process of vascular regression, which to date remains enigmatic. Corrosion cast studies by Djonov *et al.* revealed that the ordered regression of the capillary bed observed post-weaning not only parallels that of the parenchyma, but is a result of capillary retraction and progressive vascular obliteration, as evidenced by blind-ended stumps and capillaries of extremely thin calibre (Djonov et al., 2001). Morphological criteria, such as condensed chromatin and the appearance of apoptotic bodies, support the suggestion that a proportion of BEC undergo apoptosis during mammary gland involution (Walker et al., 1989). Whether an analogous sequence of sprouting lymphangiogenesis and intussusceptive lymphangiogenesis, followed by capillary retraction and LEC death are responsible for the observed expansion and regression of the mammary lymphatic vasculature, respectively, remains to be elucidated. Real-time imaging of lymphatic vessel growth in the mouse mammary gland *ex vivo* could be one approach to address these questions.

Analysis of whole mount immunostained mammary glands from 8 week old virgin mice revealed that the number of lymphatic vessels per gland varied slightly from mouse-to-mouse (data not shown), despite the overall patterning of the lymphatic vessels appearing comparable. Initially, this observation was

attributed to normal physiological and biological variation, but in retrospect this disparity in lymphatic vessel density may be related to the estrous cycle. Studies by Fata *et al.* revealed that specific changes at the morphological and cellular level in mammary epithelial branches and alveolar development in nulliparous mice led to extensive mouse-to-mouse variations. These differences were shown to correspond with the murine estrous cycle and fluctuating physiological levels of steroid hormones (Fata *et al.*, 2001). Furthermore, it is well-established that extensive cycles of regional secondary branching, lobuloalveolar formation and apoptosis occur in the mouse mammary gland concurrently with each estrous cycle (Andres and Strange, 1999; Fata *et al.*, 2001). Again, fluctuating hormone levels account for these transient changes in the ductal epithelia and could potentially influence the mammary lymphatic vascular network in a similar fashion. In future experiments utilising nulliparous female mice it may be necessary to determine the estrous stage of each mouse via cytological evaluation of vaginal smears as previously described (Inderdeo *et al.*, 1996), prior to further analyses. In addition, based on the hormonally-induced fluctuations in the ductal epithelia across the murine estrous cycle (Andres and Strange, 1999; Fata *et al.*, 2001) and the proposed link between ovarian lymphangiogenesis and hormonal regulation (Brown *et al.*, 2010); it may also be interesting to perform lymphatic vessel quantification analyses in the nulliparous adult female mouse mammary gland at proestrus, estrus, metestrus and diestrus. Such data could assist in dissecting out the relative contribution of steroid hormone control on the mammary lymphatic network.

Our surprising observation that Prox1 is expressed in venous valves of the mammary gland blood vasculature, at a level comparable to lymphatic vessels (Figure 3.9), is intriguing. Prox1 has been documented to be highly expressed in developing and adult murine intraluminal lymphatic valves, along with FOXC2 and VEGFR-3; the latter of which is characteristically down-regulated on collecting lymphatic vessels (Bazigou *et al.*, 2009; Norrmén *et al.*, 2009). This suggests that LEC comprising the valve leaflets are molecularly distinct from adjacent cells in the collecting lymphatic vessel trunk. The mechanisms of lymphatic valve morphogenesis, however, have remained poorly characterised until recently. Studies by Bazigou *et al.* revealed a novel role for integrin- $\alpha 9$ and its specific ligand, fibronectin-E111A, in the process of lymphatic valve leaflet formation (Bazigou *et al.*, 2009). During embryogenesis, lymphatic valve formation is initiated by upregulation of the transcription factors, Prox1 and FOXC2, in distinct clusters of EC in collecting lymphatics, which ultimately define the position of future valve development (Norrmén *et al.*, 2009). This is subsequently followed by the increased expression of integrin- $\alpha 9$ in cells constituting the luminal valves and deposition of extracellular matrix containing fibronectin-E111A (Bazigou *et al.*, 2009). It is intriguing to note, that whilst lymphatic luminal valves are located within the walls of collecting lymphatic vessels to facilitate unidirectional lymph flow;

the Prox1-positive valves detected in the blood vasculature of the mouse mammary gland appear morphologically and spatially distinct to those in lymphatic vessels. Venous valves appear as discrete clusters of Prox1-positive cells, rather than bicuspid valve leaflets, and are located exclusively at sites of bifurcation along the length of the blood vessel (Figure 3.9A-C). A tendency for venous valves to form at such sites was documented by Kampmeier and Birch, who found that the majority of valves in human venous trunks were located just distal to the connection points of minor venous branches (Kampmeier and Birch, 1927). The unique spatial location of these blood vascular valves is suggestive of a role for fluid hydrodynamics in regulating their precise formation; just as the function of lymphatic valves is thought to be driven by the pressures and flow of fluid across them (Zawieja, 2009). In addition to lymphatic valves, Prox1 expression has also been reported in cardiac valves in the chick and mouse during early embryonic heart development (Risebro et al., 2009; Rodriguez-Niedenführ et al., 2001; Wilting et al., 2007). Therefore, the presence of Prox1 in EC comprising lymphatic, venous and cardiac valves suggests that similar molecular mechanisms drive valve morphogenesis in lymphatic vessels, veins and the heart, respectively.

3.5 CONCLUSION

The data presented in this chapter provides the first specific analysis of lymphangiogenesis in the postnatal mouse mammary gland and illustrate that lymphatic vessels are dynamically remodelled, both spatially and temporally, in conjunction with the mammary epithelial tree and blood vasculature, during postnatal mouse mammary gland morphogenesis. Our extensive analyses have demonstrated that mammary lymphatic vessel density is increased significantly in the pregnant state, compared to virgin and involuting stages, indicating that the mammary lymphatic network undergoes a transient temporal expansion during pregnancy and subsequently regresses during involution. Furthermore, we have established that lymphatic vessels in the mouse mammary gland share an intimate spatial association with mammary ducts, but not with alveoli and to a lesser extent, are spatially associated with large blood vessels. Concomitant with these studies, we made the serendipitous discovery that Prox1 is expressed in the mammary blood vasculature, being specifically restricted to venous valves. In combination with lymphatic vessel quantification data from transgenic mouse models, our data illustrate that lymphatic vessel density correlates with density of the epithelial tree; thus suggesting that mammary gland epithelial cells are a probable source of lymphangiogenic stimuli in the mouse mammary gland. Studies described in Chapters 4 and 5 investigate the potential signals and growth factors involved in the regulation of this dynamic process.

CHAPTER 4

Investigating signals that regulate lymphatic vascular remodelling in the postnatal mouse mammary gland

4.1 INTRODUCTION

Having established that the lymphatic vascular network in the mouse mammary gland is dynamically remodelled along with the mammary epithelial tree and blood vasculature during postnatal mammary gland morphogenesis, we sought to determine the identity and source of lymphangiogenic stimuli that drive lymphatic vascular growth and remodelling in the postnatal mouse mammary gland. We hypothesised that the signals that regulate lymphangiogenesis in the mammary gland could either be direct; involving the interaction of steroid hormones such as estrogen and progesterone, acting via their cognate receptors expressed by LEC; or indirect, encompassing signals arising from nearby mammary epithelial, blood vascular or stromal tissue components in response to these hormone signalling events.

The growth factors VEGF-C and VEGF-D represent the foremost candidates likely to regulate lymphangiogenesis in the mouse mammary gland, evidenced by their well-established role in settings of physiological and pathological lymphangiogenesis in several mouse models (Jeltsch et al., 1997; Karkkainen et al., 2004; Karpanen et al., 2001; Koch et al., 2009; Mattila et al., 2002; Skobe et al., 2001; Stacker et al., 2001; Tammela et al., 2007; Veikkola et al., 2001). Moreover, a strong correlative relationship between the expression of VEGF-C and VEGF-D with increased lymphangiogenesis, elevated lymphatic vascular invasion (LVI), increased incidence of lymph node metastasis and poor patient prognosis has been documented in numerous clinical studies of human breast cancer patients (Choi et al., 2005; Gu et al., 2008; Mohammed et al., 2007b; Nakamura et al., 2005; Nakamura et al., 2003).

4.1.1 Biosynthesis and proteolytic processing of VEGF-C and VEGF-D

Members of the VEGF family are potent EC mitogens known to stimulate both angiogenesis and lymphangiogenesis in a range of biological settings via activation of the tyrosine kinase receptors, VEGFR-2 and VEGFR-3, expressed on the surface of vascular EC. VEGF-C and VEGF-D, first described as *c-fos* induced growth factor, are two such family members (previously discussed in section 1.1.4.1.1). VEGF-C and VEGF-D are initially secreted from the cell as non-covalently-linked, anti-parallel homodimers of the full-length glycoprotein, which are post-translationally processed by stepwise proteolytic cleavage of N- and C-terminal propeptides, generating a mature form that exists as a non-covalent VHD dimer (Figure 4.1A) (Joukov et al., 1997; Stacker et al., 1999). This process is conserved across humans and mice (Baldwin et al., 2001b) and has been shown to be catalysed by a number of

NOTE:

This figure is included on page 100 of the print copy of the thesis held in the University of Adelaide Library.

Figure 4.1 - Schematic representation of mouse VEGF-D biosynthesis, proteolytic processing and alternatively-spliced transcripts.

(A) VEGF-D is initially secreted from the cell as a non-covalent, disulphide-linked homodimer of the full-length glycoprotein, which is processed extracellularly by stepwise proteolytic cleavage of flanking N- and C-terminal propeptides to generate a mature form that exists as a non-covalent dimer of the VHD (VEGF homology domain). All combinations of subunits with no or partial processing are possible but for simplicity purposes are not shown. Dashed lines - non-covalent interactions between domains, scissors - sites of proteolytic cleavage, -S-S- - inter-subunit disulphide bridges. (B) Alternative RNA splicing of the mouse *Vegfd* transcript generates two distinct VEGF-D isoforms, designated VEGF-D₃₅₈ and VEGF-D₃₂₆. The transcripts for both isoforms contain a sequence derived from exon 1 to the splice acceptor site of exon 6. The transcript for VEGF-D₃₅₈ lacks the sequence encoded by the 3' region of exon 6 and includes a sequence derived from exon 7, whilst the VEGF-D₃₂₆ transcript contains a sequence derived from the entire coding (grey) and untranslated (white) regions of exon 6. (A) and (B) derived from Baldwin et al., 2001b.

proteolytic enzymes *in vitro*, including the serine protease, plasmin, which cleaves both N- and C-terminal propeptides of VEGF-C and VEGF-D (McColl et al., 2003) and members of the proprotein convertase (PC) family of serine proteases such as furin, PC5 and PC7; the latter of which promotes cleavage at the C-terminal end only (McColl et al., 2007; Siegfried et al., 2003). An added level of complexity is that plasmin and PCs are synthesised as inactive precursors, known as zymogens, which themselves require specific cleavage by enzymes and autocatalytic events, respectively, to acquire their proteolytic activity (Andreasen et al., 2000; Seidah et al., 2008). The proteolytic enzymes involved in activating VEGF-C and VEGF-D *in vivo* are less well-characterised. Nevertheless, the importance of proteolytic cleavage *in vivo* is emphasised by the capacity of mature VEGF-D, in contrast to full-length unprocessed VEGF-D, to promote tumour growth and lymph node metastasis in a mouse tumour model (Harris et al., 2011). Proteolytic cleavage is also essential for the receptor binding specificity, affinity and consequent biological activity of VEGF-C and VEGF-D *in vivo*. Numerous *in vitro* studies have demonstrated that removal of both propeptide extensions greatly increases the propensity for VEGF-C and VEGF-D to bind to VEGFR-2 and VEGFR-3, indicating that mature VEGF-C and VEGF-D bind both VEGFR-2 and VEGFR-3 with high affinity, whilst the full-length counterparts bind only to VEGFR-3 with high affinity (Joukov et al., 1997; McColl et al., 2003; McColl et al., 2007; Stacker et al., 1999). This is consistent with *in vivo* studies by Rissanen *et al.* whereby adenoviral delivery of full-length VEGF-D into rabbit hind limb skeletal muscle promoted lymphangiogenesis, whereas mature VEGF-D stimulated both angiogenesis and lymphangiogenesis (Rissanen et al., 2003). Surprisingly, unlike human VEGF-D that binds both human and mouse VEGFR-2 and VEGFR-3, it has been reported that mouse VEGF-D is specific for VEGFR-3 and does not bind mouse VEGFR-2, but can bind human VEGFR-2 (Achen et al., 1998; Baldwin et al., 2001a). This finding suggests that the biological functions of VEGF-D may differ across species. This difference in specificity, however, is not observed for the closely-related growth factor, VEGF-C, as human VEGF-C activates human VEGFR-2 (Joukov et al., 1996) and mouse VEGF-C has been reported to bind and cross-link mouse VEGFR-2 (Baldwin et al., 2001a).

Studies have revealed that the proteolytic processing of VEGF-D in mouse is mostly analogous to that in humans; mouse VEGF-D is reported to be processed solely in the extracellular environment, with no intracellular processing observed to date (Baldwin et al., 2001b; Stacker et al., 1999). However, unlike VEGF-D, the initial cleavage event for VEGF-C has been reported to occur near the end of the secretory pathway or at the plasma membrane (Joukov et al., 1997). In addition to proteolysis, RNA splicing and differential protein glycosylation add a further level of complexity to the bioactivity of VEGF-D in the mouse. Alternative RNA splicing of the *Vegfd* transcript generates two VEGF-D isoforms with distinct C-terminal propeptides, designated VEGF-D₃₂₆ and VEGF-D₃₅₈, differing in size by 32 amino acids. The

transcripts for both isoforms contain a sequence derived from exon 1 to the splice acceptor site of exon 6. However, the transcript for VEGF-D₃₅₈ is generated by a splice event from within exon 6 to the beginning of exon 7 and thus lacks the sequence encoded by the 3' region of exon 6 and includes a sequence derived from exon 7; whereas the VEGF-D₃₂₆ transcript arises in the absence of this splice event and contains a sequence derived from the entire coding (grey) and untranslated (white) regions of exon 6 (Figure 4.1B) (Baldwin et al., 2001b). Both VEGF-D isoforms have been shown to exhibit similar receptor binding affinities for VEGFR-3, but consistent with previous findings, neither bind mouse VEGFR-2 (Baldwin et al., 2001a; Baldwin et al., 2001b).

As a direct result of RNA splicing and proteolysis, multiple forms of VEGF-D can exist in the extracellular milieu. The numbers denote the proposed size (in kDa) of murine VEGF-D protein peptides when separated via sodium dodecyl sulphate-polyacrylamide gel electrophoresis (SDS-PAGE) under reducing conditions. VEGF-D can exist as a polypeptide of 21kDa, corresponding to the completely processed form (ie. with both the N- and C-terminal propeptides cleaved), which represents the mature, bioactive form of VEGF-D consisting only of the VHD. Numerous partially-processed forms of VEGF-D can also exist, including 48kDa and 45kDa peptides corresponding to the C-terminal propeptide and the VHD of VEGF-D₃₅₈ and VEGF-D₃₂₆, respectively; a 36kDa species representing the N-terminal propeptide and the VHD; a 36kDa form that represents the C-terminal propeptide of VEGF-D₃₅₈; and 34kDa and 31kDa polypeptides corresponding to two differentially glycosylated forms of the C-terminal propeptide of VEGF-D₃₂₆. Alternatively, VEGF-D can remain completely unprocessed at 58kDa and 55kDa, representing full-length VEGF-D₃₅₈ and VEGF-D₃₂₆, respectively (Baldwin et al., 2001b; Stacker et al., 1999). However, it is not known what proportion, if any, of these freely-diffusible proteins remain associated with the extracellular matrix or bound to the cell surface.

In addition to VEGF-C and VEGF-D, the PDGF family represents another group of growth factors that are initially synthesised as precursor proteins and then post-translationally, proteolytically-processed. However, in contrast to VEGF-C and VEGF-D, PDGF-AA and PDGF-BB are cleaved exclusively intracellularly; PDGF-BB is proteolytically cleaved at two sites by PCs and N-terminal cleavage is required for the C-terminal cleavage event (Östman et al., 1992; Siegfried et al., 2005). Neuropilins have recently been shown to act as co-receptors for VEGFR-3 and can bind partially-processed forms of VEGF-C and VEGF-D (Karpanen et al., 2006). The regulation of VEGF-C and VEGF-D biosynthesis and bioactivity, and the roles of individual partially-processed propeptides in signalling *in vivo* is a complex process, of which much still remains to be elucidated.

The aim of this chapter was to identify and characterise signals that drive lymphatic vascular growth and remodelling during postnatal mouse mammary gland morphogenesis. In particular, we sought to characterise the roles of VEGF-C and VEGF-D in mammary gland lymphangiogenesis.

4.2 METHODS

4.2.1 Immunofluorescent immunostaining of paraffin-embedded mammary gland sections

Immunofluorescent immunostaining was also performed on paraffin-embedded sections of mammary gland tissue, as prepared in section 2.2.4.3.2. All incubations were performed at RT unless otherwise indicated. Sections were dewaxed 2 x 5 minutes in xylene, rehydrated 2 x 5 minutes in 100% (v/v) ethanol and rinsed 2 x 5 minutes in MQ-H₂O, prior to citrate buffer (pH 6.5) and heat-mediated antigen retrieval. For antigen retrieval, slides were placed into two polypropylene slide dishes (ProSciTech) containing freshly prepared citrate buffer (10.9mM citric acid, pH adjusted to 6.5 using 5M NaOH) and microwaved (using a Panasonic Inverter Microwave Oven, model NN-S454WF, Panasonic, Osaka, Japan) on high power for 3-4 minutes to ensure boiling, followed by a further 15 minutes on low power. Following antigen retrieval, slides were gradually cooled at RT for 30 minutes. Sections were then washed 3 x 5 minutes in MQ-H₂O, 1 x 5 minutes in PBS and framed with an ImmEdge™ Pen (Vector Laboratories), prior to blocking for 1 hour in a humidified chamber with PBS with 0.3% (v/v) Tween®20 (Sigma) (PBS-0.3%TW20) containing 1% (w/v) BSA. Primary antibodies (listed in Table 2.1) diluted in PBS-0.3%TW20 were added and incubated overnight at 4°C in a humidified chamber and then slides were washed 3 x 5 minutes in PBS. Next, sections were incubated for 2 hours with Alexa Fluor®-conjugated secondary antibodies (Invitrogen) (see Table 2.2) diluted in PBS-0.3%TW20, in a light-proof humidified chamber to avoid photo-bleaching. Slides were subsequently washed 3 x 5 minutes, air-dried for 5 minutes, mounted using Gel/Mount™ Aqueous Mounting Medium with Anti-Fading Agents (Biomed, Biomed Corp., Foster City, CA) and stored indefinitely at 4°C. Images were obtained using an Olympus DP-70 camera (Olympus) attached to an Olympus BX51 upright microscope (Olympus) and processed with the aid of OLYSIA BioReport version 3.2 software (Olympus) and Adobe Photoshop CS5 version 12.0 (Adobe).

4.2.2 *In situ* hybridisation

4.2.2.1 Production of DIG-labelled RNA probes

4.2.2.1.1 Generation of plasmid templates

Small fragments of the coding region of *Mus musculus Pdgfa* and *Vegfa* were amplified from E11.5 lung cDNA (generated previously by Natasha L. Harvey) using the following primer sets: *Pdgfa* forward primer 5'-GATGAGGACCTGGGCTTG-3' and reverse primer 5'-CTCATCTCACCTCACATC-3' (generating a 600bp fragment); *Vegfa* forward primer 5'-TGGAGCGTTCCTGTGAG-3' and reverse primer 5'-GGTGTGTCTACAGGAATC-3' (generating a 490bp fragment). PCR amplification was performed as previously described (section 2.2.2.1) using the primer annealing temperatures, 50°C and 52°C, respectively. PCR fragments were separated via AGE (section 2.2.2.2), purified (section 2.2.2.3) and ligated into pGEM®-T Easy vector (Promega) (section 2.2.2.5). The resulting plasmid constructs were transformed into chemically-competent cells (section 2.2.2.7) and clones containing inserts subsequently screened via blue-white colour selection. Plasmids isolated from white colonies (section 2.2.2.8) were confirmed two-fold using sequencing (section 2.2.2.9) (orientation of the inserted PCR fragment was also determined in this manner) and analytical *EcoRI* (New England BioLabs) digests (section 2.2.2.4).

Due to the presence of an internal *NcoI* restriction site in the *Pdgfa* PCR fragment, this fragment required sub-cloning, using *EcoRI* (New England BioLabs), into the pBluescript II SK (+) (referred to as pBS) vector (Stratagene, La Jolla, CA) (sections 2.2.2.5-9). *NcoI* was the only restriction enzyme found in the multiple cloning site of the pGEM®-T Easy vector that could be used to linearise plasmid templates to generate a 5' overhang, enabling efficient *in vitro* transcription via SP6 RNA polymerase. Therefore, pBS was *EcoRI* restriction enzyme digested (as per section 2.2.2.4) and treated with 10U of calf intestinal alkaline phosphatase (AP) (Finnzymes, Espoo, Finland) for 1 hour at 37°C to promote dephosphorylation of the *EcoRI* cut ends, preventing re-ligation of the pBS vector. The *EcoRI*-digested and dephosphorylated pBS vector was then run on an agarose gel (section 2.2.2.2) and gel purified (section 2.2.2.3), prior to utilisation for sub-cloning.

Large-scale plasmid production and purification was performed for both pGEM®-T Easy-VEGF-A and pBS-PDGF-A constructs, as previously described in section 2.2.2.10.

4.2.2.1.2 Plasmid template linearisation

Plasmid templates were linearised via restriction enzyme digestion in 100µl total reaction volumes, containing 12µg of purified plasmid DNA (quantified as per section 2.2.2.11), 25U *NcoI*, *SpeI*, *XhoI* or *NotI* restriction enzymes (New England BioLabs), 1x the appropriate NE Buffer (New England BioLabs) and 1x BSA (excluding reactions involving *NcoI*), made to volume with MQ-H₂O. Double-digests enabling excision of the cloned fragment for size confirmation were performed simultaneously in 20µl total reaction volumes, containing 1µg of purified plasmid DNA, 2.5U *NcoI* and *SpeI* (pGEM®-T Easy-VEGF-A) or *XhoI* and *NotI* (pBS-PDGF-A), 1x NE Buffer 2 or 3, respectively, and 1x BSA, made to volume using MQ-H₂O. All restriction enzyme digests were incubated at 37°C for 2 hours. Following digestion, 2µl of linearised template reactions and 5µl of double-digest reactions were run via AGE (section 2.2.2.2) to verify complete enzymatic digestion and confirm the size of cloned fragments, respectively. Linear templates were stored at -20°C.

4.2.2.1.3 Linearised plasmid template precipitation

Linearised templates were purified as follows: 100µl TE buffer (pH 8.0) was added to the 100µl digest reactions (section 4.2.2.1.2), mixed, followed by the addition of 50µl phenol-chloroform (1:1) and centrifuged at 16,000 x g for 5 minutes. Following phase separation, the aqueous phase was transferred to a clean microcentrifuge tube and DNA precipitated for 1-3 hours at -20°C via the addition of 1/10th volume 3M NaOAc and 2.5 volumes 100% (v/v) ethanol. Precipitated DNA was pelleted at 16,000 x g for 15 minutes and washed with 200µl 70% (v/v) ethanol and centrifuged for a further 1 minute at 16,000 x g. Samples were air-dried at RT for 5-10 minutes, resuspended in 20µl TE buffer (pH 8.0) and the DNA concentration determined (section 2.2.2.11). Purified plasmid templates were stored at -20°C.

4.2.2.1.4 *In vitro* transcription of DIG-labelled RNA probes

Sense and anti-sense digoxigenin (DIG)-labelled, single-stranded RNA probes were synthesised from purified *SpeI*-linearised pGEM®-T Easy-VEGF-A templates and *NotI*-linearised pBS-PDGF-A templates using T7 RNA Polymerase (Roche) and *NcoI*-linearised pGEM®-T Easy-VEGF-A templates using SP6 RNA Polymerase (Roche) or *XhoI*-linearised pBS-PDGF-A templates using T3 RNA Polymerase (Roche), respectively. Reactions consisted of 1µg of purified linearised DNA template (from section 4.2.2.1.3), 20U of the corresponding RNA polymerase, 1x Transcription Buffer (Roche), 10mM 1,4-dithiothreitol (DTT), 1x DIG RNA Labelling Mix (Roche) and 10U Protector RNase Inhibitor (Roche), made up to a total reaction volume of 20µl with DEPC-treated MQ-H₂O. *In vitro* transcription reactions utilising T3 or T7 RNA polymerase were incubated at 37°C for 2 hours, whilst reactions involving SP6 RNA polymerase were incubated at 40°C for 2 hours.

4.2.2.1.5 DIG-labelled RNA probe precipitation

Following *in vitro* transcription, DIG-labelled RNA probes were purified as follows: 80µl TE buffer (pH 8.0) was added to the 20µl synthesis reactions (section 4.2.2.1.4), mixed, followed by the addition of 10µl of 4M lithium chloride and 300µl 100% (v/v) ethanol. Samples were mixed and RNA precipitated at -20°C for 2 hours, prior to pelleting the precipitated RNA via centrifugation at 16,000 x g for 15 minutes. Pelleted RNA was washed with 200µl 75% (v/v) ethanol and spun for a further 1 minute at 16,000 x g. The supernatant was removed and samples air-dried for 5-10 minutes. RNA pellets were resuspended in 50µl TE buffer (pH 8.0) and quantified (section 2.2.1.2). DIG-labelled RNA probes were stored at -20°C.

4.2.2.2 *In situ* hybridisation

The subsequent procedures were performed following treatment of surfaces and equipment with RNase AWAY® (Invitrogen) and using ART® aerosol resistant filter tips (Molecular BioProducts). All solutions were made using DEPC-treated MQ-H₂O.

4.2.2.2.1 Day 1 - Pre-hybridisation and hybridisation

Sections (as per section 2.2.4.3.2) were dewaxed in xylene for 2 x 5 minute washes and then rehydrated in 1 x 5 minute wash for each solution of 100% (v/v) ethanol and 90% (v/v) ethanol, followed by 2 x 5 minute washes in PBS. Sections were framed using an ImmEdge™ Pen (Vector Laboratories). Sections were treated with 5µg/ml of proteinase K (Roche) for 30 minutes at 37°C in pre-warmed digestion buffer (50mM Tris (pH 7.5) and 5mM EDTA), post-fixed in 4% PFA for 5 minutes at RT and washed thrice for 3 minutes in PBS. Acetylation was carried out for 10 minutes at RT in 0.1M triethanolamine with the addition of 0.178% (v/v) concentrated HCl and 0.254% (v/v) acetic anhydride (Sigma), followed by 3 x 5 minute washes in PBS. Following acetylation, sections were pre-hybridised in a humidified (using 50% (v/v) formamide and 5x SSC) chamber for 2 hours at RT in pre-warmed (to 55°C) hybridisation buffer containing 50% (v/v) deionised formamide (Sigma), 5x SSC (pH 4.5), 50µg/ml yeast transfer RNA (tRNA) (Ambion, Inc., Austin, TX), 1% (w/v) sodium dodecyl sulphate (SDS) and 50µg/ml heparin (Sigma-Aldrich). 50µl of hybridisation buffer per section was prepared containing 4ng/µl sense or anti-sense DIG-labelled RNA probes and heated to 80°C for 5 minutes prior to cooling and applying to the pre-hybridised sections. Sections were subsequently covered with parafilm to prevent evaporation and hybridised overnight at 72°C in a humidified chamber within a Hybaid Shake 'n' Stack Hybridisation Oven (Thermo Electron Corporation, Waltham, MA).

4.2.2.2.2 Day 2 - Post-hybridisation washes

Slides were transferred to pre-warmed (to 72°C) 5x SSC (pH 4.5) and gently agitated at RT for 20-30 minutes to remove parafilm coverslips. Slides were subsequently washed with 0.2x SSC at 72°C for 3 hours, followed by a 5 minute rinse in 0.2x SSC at RT. Sections were then washed in Buffer 1 containing 100mM Tris (pH 7.5), 150mM NaCl and 0.24mg/ml levamisole (used to block endogenous AP activity) for 5 minutes at RT, followed by blocking using a mixture of 20% (v/v) newborn bovine serum (SAFC Biosciences), 60% (v/v) maleate buffer (pH 7.5) and 2% (w/v) Blocking Reagent (Roche), for 1 hour at RT in a humidified chamber. For immunological detection, sections were incubated with a 1:5000 dilution of AP-conjugated anti-DIG Fab fragment antibody (Roche) in blocking solution and incubated overnight at RT in a humidified chamber.

4.2.2.2.3 Day 3 - Immunological detection

Sections were washed 3 x 5 minutes at RT in Buffer 1, followed by a 10 minute wash in freshly made Buffer 3 containing 100mM Tris (pH 9.5), 100mM NaCl, 50mM magnesium chloride (MgCl₂), 0.24mg/ml levamisole and 1% (v/v) Tween®20 (Sigma). Buffer 3 was replaced with 80µl of Buffer 4 (50:1 mix of Buffer 3 and nitro blue tetrazolium chloride/5-bromo-4-chloro-3-indolyl phosphate (NBT/BCIP) Stock Solution (Roche)) per section. Sections were covered with parafilm and left for overnight RT colour development in a light-proof, humidified chamber.

4.2.2.2.4 Day 4 - Termination of colour development

Colour development was ceased via a 5 minute wash in TE buffer (pH 8.0). Sections were air-dried and subsequently dipped in xylene and mounted permanently using DePeX mounting medium (BDH). Images were captured as previously described in section 4.2.1.

4.2.3 RNA isolation from entire mouse mammary glands

Whole mouse inguinal mammary fat pads, with the central lymph nodes removed, were dissected as per section 2.2.4.1 from 2-4 x mice and digested for 50 minutes at 37°C in DMEM-5%FBS containing 150U/ml of both collagenase type 1 and collagenase type 3 (Worthington Biochemical) and 100U/ml hyaluronidase (Worthington Biochemical) with frequent agitation, prior to the addition of 5ml PBS-2%FBS and centrifugation at 300 x g for 5 minutes. Cells were resuspended in 500µl DMEM-5%FBS, an aliquot taken for cell counting and viability analysis (section 2.2.5.2) and re-pelleted at 300 x g for 5 minutes. The resulting heterogeneous mammary gland cell suspensions were processed using TRIzol® Reagent (Invitrogen) (section 2.2.1.1).

4.2.4 Protein collection and analysis

4.2.4.1 Protein collection

Mammary gland protein lysates were prepared from cell suspensions generated as described in section 4.2.3. The resulting cell pellets were lysed on ice for 1 hour with radioimmunoprecipitation assay (RIPA) buffer consisting of 150mM NaCl, 50mM Tris (pH 7.4), 10mM EDTA, 1% (v/v) Igepal CA-630 (Sigma-Aldrich), 0.5% (w/v) sodium deoxycholate, 0.1% (w/v) SDS supplemented with 1x Protease Inhibitor Cocktail (Roche) and centrifuged at 16,000 x g for 15 minutes at 4°C to pellet any cell debris. RIPA buffer protein lysates were stored at -70°C until required for analysis.

4.2.4.2 Determination of protein concentration

Protein concentration was determined using the Pierce Bicinchoninic Acid (BCA) Protein Assay Kit (Pierce Biotechnology, Rockford, IL), as per the manufacturer's instructions. This assay utilises the property of Cu^{2+} , which is reduced to Cu^{1+} by proteins in an alkaline solution. Cu^{1+} can subsequently be detected via a colorimetric reaction following the addition of BCA reagent. Briefly, protein lysates were thawed on ice and 1/5 and 1/10 dilutions were prepared in MQ-H₂O. 10µl of neat protein samples, diluted samples and a 0-2mg/ml titration of BSA protein standards were pipetted in duplicate into a flat-bottomed 96 well microplate, prior to the addition of 200µl BCA working reagent per well, consisting of a 50:1 mix of BCA Reagent A and BCA Reagent B. The protein and reagents were gently mixed and incubated at 37°C for 30 minutes to allow for colour development. Absorbance was measured at 562nm using a FLUOstar OPTIMA microplate reader (BMG LABTECH, Offenburg, Germany). The concentration of protein in the sample lysates was determined following the construction of a standard curve generated from the absorbance readings of the BSA protein standards.

4.2.4.3 Western blot analysis

4.2.4.3.1 SDS-PAGE

SDS-PAGE gels were prepared consisting of a lower 10% resolving gel (10% (w/v) acrylamide/bis (19:1), 375mM Tris-HCl (pH 8.8), 0.1% (w/v) SDS, 0.05% (w/v) ammonium persulphate (APS) and 0.05% (v/v) N,N,N',N'-tetramethylethylenediamine (TEMED) (Sigma)) and an upper 5% stacking gel (5% (w/v) acrylamide/bis (19:1), 125mM Tris-HCl (pH 6.8), 0.1% (w/v) SDS, 0.05% (w/v) APS and 0.1% (v/v) TEMED (Sigma)). The Mini-PROTEAN® Tetra Cell electrophoresis tank apparatus (Bio-Rad

Laboratories) was used for protein electrophoresis according to the manufacturer's instructions. 20µg of protein lysates (section 4.2.4.1) were diluted using 1% (w/v) SDS in a final volume of 20µl in protein loading buffer (31.25mM Tris (pH 6.8), 0.1M DTT, 0.01% (w/v) bromophenol blue, 1.25% (w/v) SDS and 10% (v/v) glycerol) and heated at 99°C for 10 minutes. Protein samples were loaded into the SDS-PAGE lanes in conjunction with 5µl of Precision Plus Protein Kaleidoscope™ standards (Bio-Rad Laboratories) and run under reducing conditions in SDS running buffer (25mM Tris, 191.8mM glycine and 0.1% (w/v) SDS) at a constant 200V for 55 minutes.

4.2.4.3.2 Electrophoretic transfer

Proteins resolved by SDS-PAGE were subsequently transferred to polyvinylidene fluoride (PVDF) membranes (PerkinElmer Life Sciences, Boston, MA). Briefly, PVDF membranes were soaked in 100% (v/v) methanol for 5 minutes, rinsed in MQ-H₂O and then equilibrated for a further 10 minutes in chilled transfer buffer (189.8mM glycine and 25mM Tris). SDS-PAGE gels were removed from the electrophoresis tank apparatus, the stacking portion of the gels were removed and discarded, whilst the resolving portion of the gels were rinsed in MQ-H₂O and equilibrated in chilled transfer buffer for 10 minutes. The Criterion™ Blotter electrophoretic transfer cell (Bio-Rad Laboratories) was assembled as per the manufacturer's instructions and run for 2 hours at a constant 300mA in cold transfer buffer.

4.2.4.3.3 Immunoblotting

Following electrophoretic transfer, membranes were washed 3 x 10 minutes in PBS with 0.1% (v/v) Tween®20 (Sigma) (PBS-0.1%TW20) prior to blocking for 1 hour with 5% (w/v) skim milk powder in PBS-0.1%TW20. Membranes were incubated with one or more primary antibodies (see Table 2.1) diluted in PBS-0.1%TW20 overnight at 4°C with gentle agitation. Following overnight incubation, membranes were washed 3 x 10 minutes in PBS-0.1%TW20 and incubated with appropriate secondary antibodies (see Table 2.2) diluted in PBS-0.1%TW20 for 1 hour at RT. Prior to detection, membranes were washed 3 x 10 minutes in PBS-0.1%TW20.

4.2.4.3.4 Detection

Signal was detected using either enhanced chemifluorescence (ECF)™ Western Blotting Reagent (GE Healthcare, Waukesha, WI) or by Cy5-directly-conjugated secondary antibodies, depending on the primary antibodies used. Membranes were scanned on a Typhoon™ 9410 Variable Mode Imager (GE Healthcare) using associated software, with densitometry analyses performed using ImageQuant TL version 7.0 software (GE Healthcare).

4.2.5 *Ex vivo* lymphatic endothelial cell proliferation assay

4.2.5.1 Primary lymphatic endothelial cell isolation from embryonic mouse dermis

Primary LEC were isolated from E16.5 mouse dermis using a novel method developed in our laboratory by Jan Kazenwadel (Centre for Cancer Biology, SA Pathology, Adelaide, Australia) (Kazenwadel et al., 2010).

4.2.5.1.1 Dissection and enzymatic digestion of embryonic dermis

E16.5 embryos (approximately 17-20 embryos pooled) were harvested from C57BL/6 pregnant mice and dissected in DMEM. Pieces of embryonic dermal skin were removed with the aid of an Olympus SZX7 stereo microscope (Olympus) and transferred into ice-cold HHF (Hank's balanced salt solution (HBSS) (Sigma) containing 10mM 4-(2-hydroxyethyl)-1-piperazineethanesulphonic acid (HEPES) and 5% (v/v) FBS). Dissected skin was rinsed twice in DMEM containing 20% (v/v) FBS (DMEM-20%FBS), prior to digestion in 10ml DMEM-20%FBS containing 2.5mg/ml collagenase type 2 (Worthington Biochemical), 2.5mg/ml collagenase type 4 (Worthington Biochemical) and 1mg/ml DNase I (Worthington Biochemical) at 37°C for 30 minutes with frequent agitation. Digested skin was filtered through a BD Falcon™ 40µm nylon cell strainer (BD) and rinsed twice with DMEM-20%FBS. The filtrate was centrifuged at 300 x g for 10 minutes and the resulting cell pellet resuspended in 5-10ml HHF. Cells were counted (as per section 2.2.5.2), centrifuged for a second time at 400 x g for 5 minutes and resuspended at a final concentration of 10⁸ cells per ml of HHF.

4.2.5.1.2 Depletion of contaminating macrophages

A magnetic-activated cell sorting (MACS) procedure utilising a MiniMACS™ Separation System (Miltenyi Biotec, Miltenyi Biotec GmbH, Bergisch Gladbach, Germany) was subsequently employed to purify LEC from digested embryonic skin preparations. Macrophages were depleted from the dermal cell mixture via the addition of 10µl per ml of cell suspension of purified rat anti-mouse F4/80 antibody (Invitrogen) and rotation on a MACSmix™ tube rotator (Miltenyi Biotec) at 4°C for 5 minutes. Following antibody incubation, 10-20 volumes of MACS buffer (PBS containing 2mM EDTA and 5% (v/v) FBS, filter-sterilised through a 0.22µm filter) was added and cells pelleted at 400 x g for 5 minutes. Cells were resuspended in 80µl of MACS buffer with the addition of 20µl goat anti-rat IgG MicroBeads (Miltenyi Biotec) per 10⁷ cells and incubated at 4°C on the MACSmix™ (Miltenyi Biotec) for 15 minutes. 10-20 volumes of MACS buffer was added and cells pelleted as above, prior to magnetic separation of cells using a MACS® MS column (Miltenyi Biotec) and associated apparatus as per the manufacturer's

instructions. Following washing and elution from the column, the resultant flow-through contained a crude mixture of cells including the desired LEC, whilst macrophages were retained on the column. The aforementioned step was repeated on the flow-through fraction to ensure minimal contamination of subsequent isolated LEC with LYVE1-positive macrophages, as previously documented (Gordon et al., 2010).

4.2.5.1.3 Isolation of lymphatic endothelial cells via positive selection with LYVE1

Macrophage-depleted cell suspensions were resuspended at a concentration of 10^8 cells per ml of HHF and 5 μ l of rabbit anti-mouse LYVE-1 antibody (AngioBio) was added per ml of cell suspension. Goat anti-rabbit IgG MicroBeads (Miltenyi Biotec) were then used to purify LYVE1-labelled LEC as detailed above (4.2.5.1.2). LYVE1-positive LEC were subsequently eluted from the column as per the manufacturer's instructions and reapplied to a second MACS[®] MS column (Miltenyi Biotec) to increase the purity of the isolated LEC population. LEC were counted (section 2.2.5.2) and stored on ice prior to seeding for subsequent *ex vivo* assays.

4.2.5.2 Mammary gland cell suspension culture and collection of conditioned media

4.2.5.2.1 Initial preparation and collection of first batch of conditioned media

Mammary glands from 2-3 x 16.5 day pregnant WT female mice were dissected and digested as previously described in section 4.2.3. Following digestion, 1ml of the crude cell suspension (approximately $2-3 \times 10^6$ cells) was plated in an uncoated CELLSTAR[®] 25cm² tissue culture flask (referred to as T25) (Greiner Bio-One, Greiner Bio-One GmbH, Frickenhausen, Germany) and grown in 5ml DMEM supplemented with 10% (v/v) FBS (DMEM-10%FBS), 50U/ml penicillin and 50 μ g/ml streptomycin (Gibco, Paisley, UK). At the same time, cells were seeded into an ibidi ibiTreat tissue culture treated μ -Slide 8 well slide (ibidi) at approximately $0.8-1.2 \times 10^5$ cells per well (ie. 1/25th of the T25 flask seeding density). Mammary gland cell suspensions were left to adhere for 6 hours at 37°C/5% carbon dioxide gas (CO₂). After this time, the media (referred to as conditioned media (CM)₁) was collected, centrifuged at 400 x g for 5 minutes to pellet any cellular debris and non-adherent cells, syringe-filtered through a 0.2 μ m sterile filter and stored in aliquots at -70°C. Viable, adherent cells were rinsed with DMEM-10%FBS and fresh DMEM-10%FBS supplemented with 50U/ml penicillin and 50 μ g/ml streptomycin (Gibco) was added and incubated with cells for 72 hours at 37°C/5% CO₂.

4.2.5.2.2 Cell passaging and collection of second batch of conditioned media

Following 72 hours in culture, the CM (referred to as CM2) was harvested and processed as detailed above in section 4.2.5.2.1. Cells were passaged using 0.25mg/ml Trypsin/EDTA Solution (Lonza, Walkersville, MO) and seeded into a second T25 flask at a density of 2.0×10^5 cells and an ibidi ibiTreat tissue culture treated μ -Slide 8 well slide (ibidi) at 2.0×10^4 cells per well in DMEM-10%FBS supplemented with 50U/ml penicillin and 50 μ g/ml streptomycin (Gibco). Cells were incubated at 37°C/5% CO₂ for a further 96 hours. The initial ibidi μ -Slide 8 well slide was treated for immunocytochemistry (section 4.2.6).

4.2.5.2.3 Collection of third batch of conditioned media

After a further 96 hours in culture the final batch of CM (referred to as CM3) was collected and processed as above in section 4.2.5.2.1, whilst the second ibidi μ -Slide 8 well slide was simultaneously treated for immunocytochemistry (section 4.2.6).

4.2.5.2.4 Cell imaging

Every 24 hours in culture, cells were imaged using phase contrast on an Olympus DP20-5E digital camera (Olympus) attached to an inverted Olympus CKX41 microscope (Olympus). Images were processed using DP20-DRV version 1.1 software (Olympus) and Adobe Photoshop CS5 version 12.0 (Adobe).

4.2.5.3 Cell proliferation assays

Cell proliferation was monitored using CellTiter 96® AQueous One Solution Cell Proliferation Assay reagent (Promega) according to the manufacturer's instructions. Briefly, primary LEC were freshly isolated from E16.5 mouse dermis, as described above in section 4.2.5.1. Cells were seeded in flat-bottomed 96 well microplates coated with 50 μ g/ml fibronectin (Roche) at a density of 1×10^4 cells per well in 100 μ l Endothelial Cell Basal Medium®-2 (EBM®-2) (Lonza) supplemented with Microvascular Endothelial Cell Growth Medium®-2 SingleQuots® (Lonza). Day 0 and Day 2 microplates were prepared in this fashion with the inclusion of blank wells (ie. media in the absence of cells) in duplicate for each treatment group, to allow subtraction of any background absorbance associated with the media. Cells were left to adhere overnight at 37°C/5% CO₂ and then cells were serum-starved in 100 μ l per well of EBM®-2 (Lonza) supplemented with either 0.5% (v/v) FBS (for CM experiments - section 4.2.5.3.1) or 0.5mg/ml ALBUMAX™ I (Gibco) (for small molecule inhibitor studies - section 4.2.5.3.2) and incubated for 4 hours at 37°C/5% CO₂. Following serum-starvation, 100 μ l of control/treatment media

was added to cells and blank wells of the Day 2 microplate(s) and cells were left to proliferate for 48 hours at 37°C/5% CO₂. Each treatment was performed in quadruplicate. To determine the baseline absorbance readings, 20µl of CellTiter 96® AQ_{ueous} One Solution Cell Proliferation Assay reagent (Promega) was added to each well of the Day 0 microplate and incubated for 4 hours at 37°C/5% CO₂ to allow colour development. Absorbance was then measured at 490nm on a FLUOstar OPTIMA microplate reader (BMG LABTECH). The CellTiter 96® AQ_{ueous} One Solution Cell Proliferation Assay reagent contains a tetrazolium compound, 3-(4,5-dimethylthiazol-2-yl)-5-(3-carboxymethoxyphenyl)-2-(4-sulfophenyl)-2H-tetrazolium, inner salt (MTS), which is bio-reduced by living cells into a coloured formazan product. Thus, the quantity of formazan product, as measured by the absorbance at 490nm, is directly proportional to the number of viable, metabolically active cells in culture, providing a measure of cellular proliferation. Day 2 microplate(s) were processed and absorbance readings measured as for Day 0 following a further 48 hours in culture from the addition of treatment groups.

4.2.5.3.1 Conditioned media experiments

For the investigation of LEC proliferation *ex vivo* in the presence of CM harvested from pregnant mouse mammary glands, treatment groups consisted of EBM®-2 (Lonza) supplemented with 30% (v/v) CM1, CM2 or CM3 (from section 4.2.5.2.1-3). Control groups were cultured in EBM®-2 (Lonza) supplemented with 30% (v/v) of the corresponding base media that the CM was produced in (ie. DMEM-10%FBS containing 50U/ml penicillin and 50µg/ml streptomycin (Gibco)), resulting in a final FBS concentration of 3% (v/v).

4.2.5.3.2 Small molecule inhibitor studies

For optimisation of these assays, LEC were cultured in the presence or absence of growth factors with/without inhibitors in EBM®-2 (Lonza) supplemented with 0.5mg/ml ALBUMAX™ I (Gibco), whereas for the investigation of inhibitors in the presence and/or absence of CM, LEC were cultured as described in section 4.2.5.3.1. Recombinant human VEGF-C (R&D Systems) and recombinant mouse VEGF-D (R&D Systems) were used at 200ng/ml (Jan Kazenwadel, Genevieve Secker and Natasha L. Harvey, unpublished data) and 200ng/ml and 1µg/ml (Marconcini et al., 1999), respectively. The small molecule inhibitors were used at the following concentrations: 3-(4-dimethylamino-naphthalen-1-ylmethylene)-1,3-dihydro-indol-2-one (MAZ51) (Sigma) (Kirkin et al., 2001; Kirkin et al., 2004) and 3-[(2,4-dimethylpyrrol-5-yl)methylidene]-indolin-2-one (SU5416) (Sigma) (Fong et al., 1999) at 5µM, and InSolution™ 3-[(3-(2-carboxyethyl)-4-methylpyrrol-2-yl)methylene]-2-indolinone (SU5402) (Calbiochem, Merck KGaA, Darmstadt, Germany) at 10µM (Jan Kazenwadel, Genevieve Secker and Natasha L. Harvey, unpublished data). All small molecule inhibitors were reconstituted in dimethyl sulfoxide (DMSO),

aliquoted and stored at -70°C. The final concentration of DMSO was kept consistent across all control and treatment groups at 0.2% (v/v).

4.2.6 Cell monolayer immunocytochemistry

Cells of interest were trypsinised and plated onto ibidi ibiTreat tissue culture treated μ -Slide 8 well slides (ibidi), at the seeding densities detailed in section 4.2.5.2.1-2. Cells were cultured at 37°C/5% CO₂ until the required confluence was reached. Cells were fixed in 4% PFA for 10 minutes. All incubations were performed at RT unless stated otherwise. Following fixation, cells were permeabilised in PBS with 0.1% (v/v) Triton®X-100 (Sigma) (PBS-0.1%TX100) for 3 x 10 minutes. Samples were blocked for 30 minutes in PBS-0.1%TX100 containing 0.2% (w/v) BSA, prior to incubation overnight in one or more primary antibodies (see Table 2.1) diluted in the aforementioned blocking solution. Cells were then washed with PBS-0.1%TX100 for 3 x 10 minutes, prior to addition of suitable Alexa Fluor® secondary antibodies (Invitrogen) (see Table 2.2) diluted in PBS-0.1%TX100 and incubated for 3 hours in the dark to avoid photo-bleaching. Samples were again washed with PBS-0.1%TX100 for 3 x 10 minutes, rinsed in MQ-H₂O and mounted in ProLong® Gold antifade reagent with 4',6-diamidino-2-phenylindole (DAPI) (Invitrogen), then stored at 4°C in the dark. Images were obtained at the Detmold Family Trust Cell Imaging Centre (Centre for Cancer Biology, SA Pathology, Adelaide, Australia) using a Nikon C1-Z confocal microscope (Nikon, Nikon Corporation, Tokyo, Japan) equipped with 3 solid lasers (Sapphire 488nm, Compass 532nm and Compass 405nm) attached to a Nikon Eclipse TE2000 inverted microscope (Nikon). Images were processed using EZ-C1 FreeViewer Gold version 3.90 software (Nikon) and Adobe Photoshop CS5 version 12.0 (Adobe).

4.2.7 Analysis of *Vegfd*-deficient mouse mammary glands

Lymphatic vascular patterning in left and right inguinal mammary glands from 13 week old virgin and 14.5 day pregnant female *Vegfd*^{+/+} and *Vegfd*^{-/-} mice, provided by Marc G. Achen and Sophie Paquet-Fifield (Tumour Angiogenesis Program, Peter MacCallum Cancer Centre, Melbourne, Australia) was assessed by whole mount immunofluorescent immunostaining, as detailed in section 3.2.4. Two combinations of antibodies were used: firstly, rat anti-mouse CD31 (BioLegend), rabbit anti-Prox1 (AngioBio) and goat anti-mouse E-cadherin (R&D Systems) and secondly, rat anti-mouse CD31 (BioLegend), goat anti-mouse CCL21 (R&D Systems) and Cy3-conjugated mouse monoclonal anti- α -smooth muscle actin (Sigma-Aldrich).

4.3 RESULTS

4.3.1 Lymphatic endothelial cells in the mouse mammary gland lack detectable expression of estrogen receptor alpha and progesterone receptor

It is well-established that the normal growth and development of the mouse mammary gland from birth is dependent on, and coordinated by a complex interplay between hormones; namely the ovarian steroid hormones, estrogen and progesterone, and prolactin, along with a multitude of local growth factors (Fendrick et al., 1998; Hennighausen and Robinson, 1998; Parmar and Cunha, 2004). In the mammary gland, estrogen and progesterone have been shown to regulate ductal (Silberstein et al., 1994) and alveolar morphogenesis (Fendrick et al., 1998), respectively, through the interaction with their cognate nuclear receptors. Owing to the importance of estrogen and progesterone in the dynamic restructuring of the postnatal mammary epithelial tree, we sought to determine whether estrogen and progesterone might directly regulate the remodelling of the mammary lymphatic vasculature via acting through their receptors expressed by LEC. Due to the minor documented role of ER β in the mammary gland (Förster et al., 2002) compared to the striking phenotypes of ER α knockout mice (Bocchinfuso et al., 2000), our subsequent expression analysis was restricted to ER α and PR. ER α was detected by immunostaining using rabbit anti-ER α (MC-20) (Santa Cruz, Santa Cruz Biotechnology, Inc., Santa Cruz, CA), while both isoforms of PR were detected using a rabbit anti-human progesterone receptor antibody (DakoCytomation, Dako Denmark A/S, Glostrup, Denmark). LEC were detected using hamster anti-mouse podoplanin (clone 8.1.1) (developed by Andrew Farr, Developmental Studies Hybridoma Bank, Iowa City, IA), which is also expressed by myoepithelial cells in the mammary gland (Schacht et al., 2005). Whilst these nuclear hormone receptors were detected in mammary gland epithelial cells (double arrowheads), neither ER α , nor PR were detected in lymphatic vessels (arrowheads) at any stage of mammary gland development analysed; from puberty, through pregnancy, lactation and involution (Figure 4.2). These observations suggest that lymphatic vessels in the mammary gland do not respond directly to estrogen and progesterone via the action of these steroid hormones binding to their cognate receptors on LEC. However, these data do not exclude the possibility that LEC in the mammary gland may be responsive to these hormones in an ER α /PR-independent manner. In summary, our data suggests that the growth, remodelling and patterning of the lymphatic vasculature in the mouse mammary gland is likely under the influence of mammary gland-derived lymphangiogenic signals, rather than steroid hormones directly.

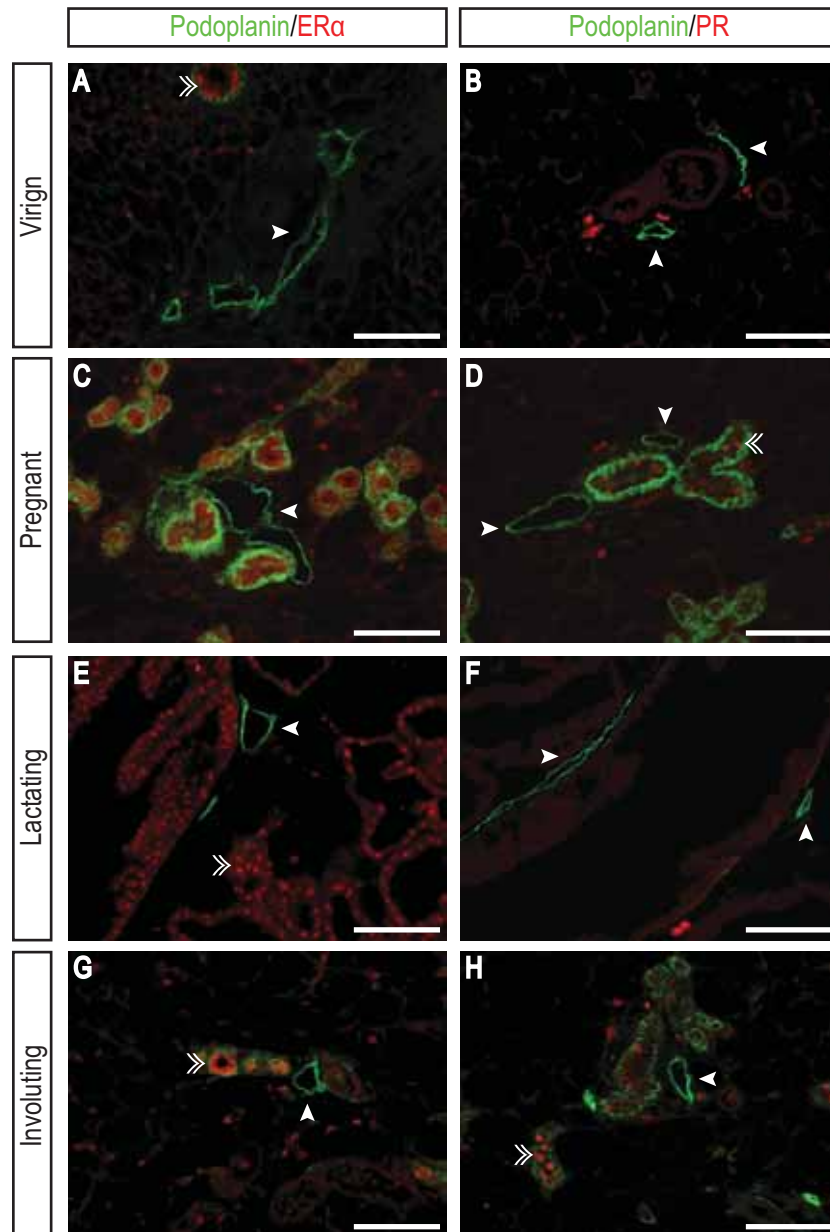


Figure 4.2 - Lymphatic endothelial cells do not express estrogen receptor alpha or progesterone receptor in the mouse mammary gland.

Immunostaining of 4 μ m paraffin sections reveal that lymphatic vessels (arrowheads) do not express estrogen receptor alpha (ER α ; **A,C,E,G**) or progesterone receptor (PR; **B,D,F,H**) in 6 week virgyn (**A,B**), 16.5 day pregnant (**C,D**), 10 day lactating (**E,F**) and 10 day involuting (**G,H**) mammary glands. However, epithelial expression of both ER α and PR is evident (double arrowheads). Images are representative of at least two mice. Scale bars represent 100 μ m.

4.3.2 *Vegfa* and *Pdgfa* are expressed in the epithelial cell compartment of the mouse mammary gland

As a preliminary method of investigating candidate genes likely to be important for mammary gland lymphangiogenesis, we analysed the precise expression pattern of a panel of established pro-lymphangiogenic growth factors in the mouse mammary gland via mRNA *in situ* hybridisation. *Vegfc*, *Vegfd*, *Pdgfb*, *Fgf1*, *Fgf2* and *Hgf* showed no detectable expression via this method at virgin and pregnant stages (data not shown). However, *Vegfa* and *Pdgfa* demonstrated robust expression in mammary epithelial cells. *Vegfa* expression was detected in luminal and myoepithelial cell subtypes in virgin and pregnant mammary glands (Figure 4.3A,C), whereas during lactation only a discrete subset of luminal epithelial cells displayed prominent *Vegfa* expression (Figure 4.3E). These cells may reflect a more differentiated phenotype, such as a secretory alveolar epithelial cell. Interestingly, *Vegfa* expression was also detected in a distinct population of cells interspersed amongst the surrounding adipocytes in virgin and pregnant mammary glands (arrowheads; Figure 4.3A,C). The exact identity of these cells currently remains enigmatic. In contrast, *Pdgfa* was found to be most highly expressed in the myoepithelial cell layer compared to luminal epithelial cells in the virgin and pregnant mammary gland (Figure 4.3B,D); whilst during lactation expression of *Pdgfa* was no longer detectable (Figure 4.3F). Expression of *Vegfa* and *Pdgfa* were reduced to below the level of detection in 10 day involuting mammary gland sections (data not shown). Corresponding sense probes for both genes displayed negligible reactivity (insets; Figure 4.3A-F). Taken together, these data demonstrate that the expression of *Vegfa* and *Pdgfa* are temporally and spatially regulated during postnatal mouse mammary gland morphogenesis. Due to the possibility that the levels of expression of other pro-lymphangiogenic growth factors assessed may have been below the threshold level of detection by *in situ* hybridisation, at the stages of mammary gland morphogenesis analysed, the expression levels of candidate pro-lymphangiogenic growth factors was investigated further using real-time RT-PCR.

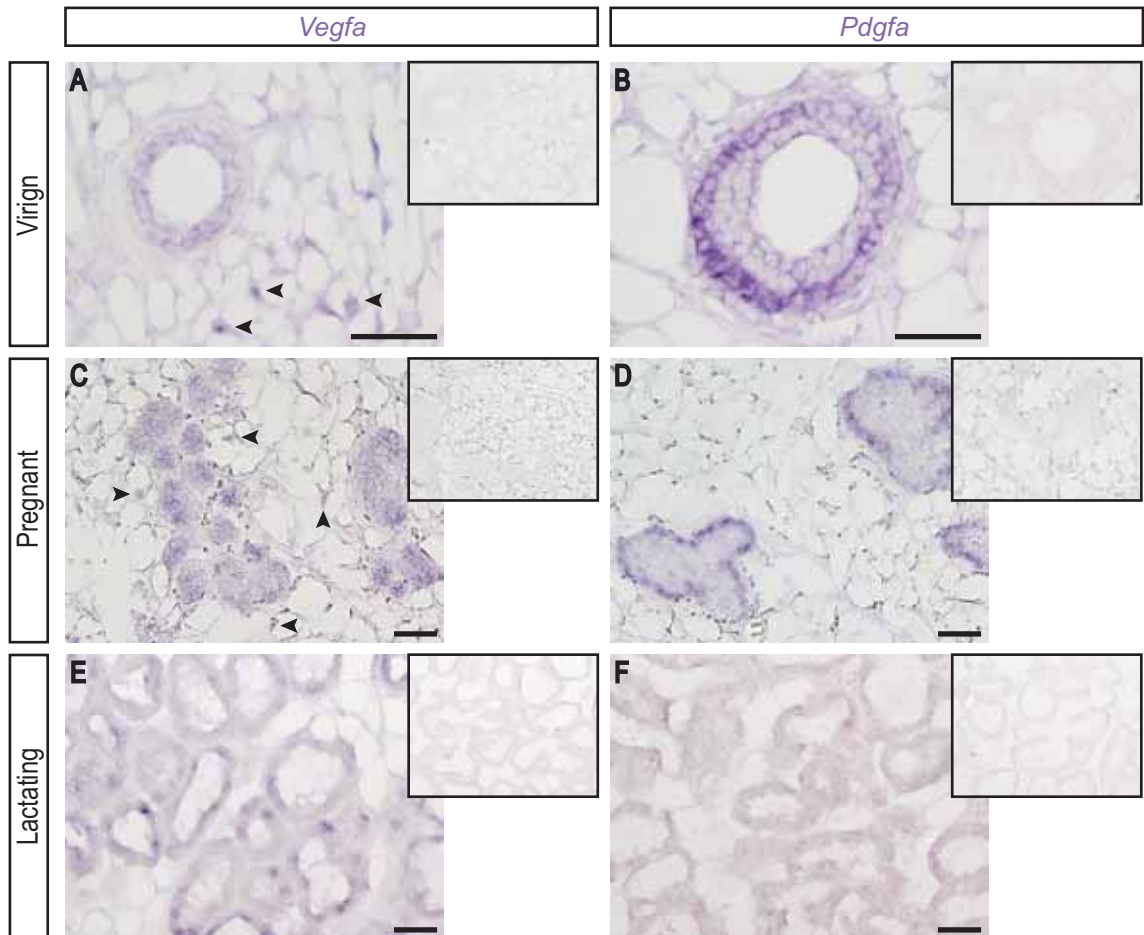


Figure 4.3 - *Vegfa* and *Pdgfa* are expressed in mammary epithelial cells.

In situ hybridisation analyses on 4 μ m 6 week virgin (**A,B**), 14.5 day pregnant (**C,D**) and 10 day lactating (**E,F**) paraffin sections reveal that *Vegfa* is expressed in luminal and myoepithelial subtypes and a discrete population of cells (arrowheads) distributed throughout the surrounding adipose tissue in virgin (**A**) and pregnant (**C**) states, with expression appearing restricted to a discrete subset of epithelial cells during lactation (**E**). *Pdgfa* is expressed most highly in myoepithelial cells in virgin (**B**) and pregnant states (**D**), with expression undetectable during lactation (**F**). Insets demonstrate negligible reactivity with sense probes. Scale bars represent 50 μ m.

4.3.3 The expression of pro-lymphangiogenic growth factors is dynamically regulated at the level of mRNA and protein during postnatal mouse mammary gland morphogenesis

4.3.3.1 Investigation of pro-lymphangiogenic growth factor expression by real-time RT-PCR

To further elucidate the identity of lymphangiogenic signals that drive the growth and remodelling of the lymphatic vasculature in the postnatal mouse mammary gland, the relative expression of a panel of established pro-lymphangiogenic factors was quantified from RNA prepared from whole mammary glands (section 4.2.3) harvested from 9 week virgin, early (4.5 day) and late-stage (16.5 day) pregnant female WT mice using real-time RT-PCR. This more sensitive approach enabled the analysis of genes previously undetectable via *in situ* hybridisation. Furthermore, an earlier (4.5 day) stage of pregnancy was included in these analyses owing to the lack of detectable expression of many of these candidate lymphangiogenic growth factors during late pregnancy using *in situ* hybridisation and to ensure that potential peaks in expression of these growth factors were not missed by restricting our analyses solely to a later stage of pregnancy. Strikingly, we observed a significant increase at the mRNA level in the two key lymphangiogenic growth factors, *Vegfc* (Jeltsch et al., 1997) and *Vegfd* (Stacker et al., 2001), at an early stage of pregnancy relative to both virgin (*Vegfc* - 15.2-fold, *Vegfd* - 9.5-fold) and late pregnant stages (*Vegfc* - 57.7-fold, *Vegfc* - 146.4-fold) (Figure 4.4A), potentially explaining the lack of detection of these growth factors by *in situ* hybridisation. Elevated *Vegfc* and *Vegfd* expression correlates with our observation that peak lymphatic vessel density is achieved during pregnancy (Figure 3.2C). In stark contrast, the expression of *Vegfa* was not markedly altered (Figure 4.4A), negating a global temporal effect across the VEGF family. Levels of other established pro-lymphangiogenic stimuli were also found to be temporally regulated at the mRNA level in the mouse mammary gland. These included *Pdgfb* (Cao et al., 2004), elevated in virgin (8.0-fold) and late pregnant (4.0-fold) stages relative to early pregnancy; a progressive increase in *Angpt1* (5.2-fold) (Morisada et al., 2005; Tammela et al., 2005) and concomitant decrease in *Angpt2* (3.9-fold) (Gale et al., 2002) during pregnancy compared to virgin stages; increased *Fgf1* (3.6-fold) (Shin et al., 2006) and correspondingly, decreased *Fgf2* (13.9-fold) (Kubo et al., 2002; Shin et al., 2006) during the late stage of pregnancy relative to an earlier pregnant time point (Figure 4.4B).

As part of these analyses we also investigated mRNA levels of *Reln*, recognised as a key signalling molecule involved in neuronal cell migration and positioning (Förster et al., 2010). More recently, reelin

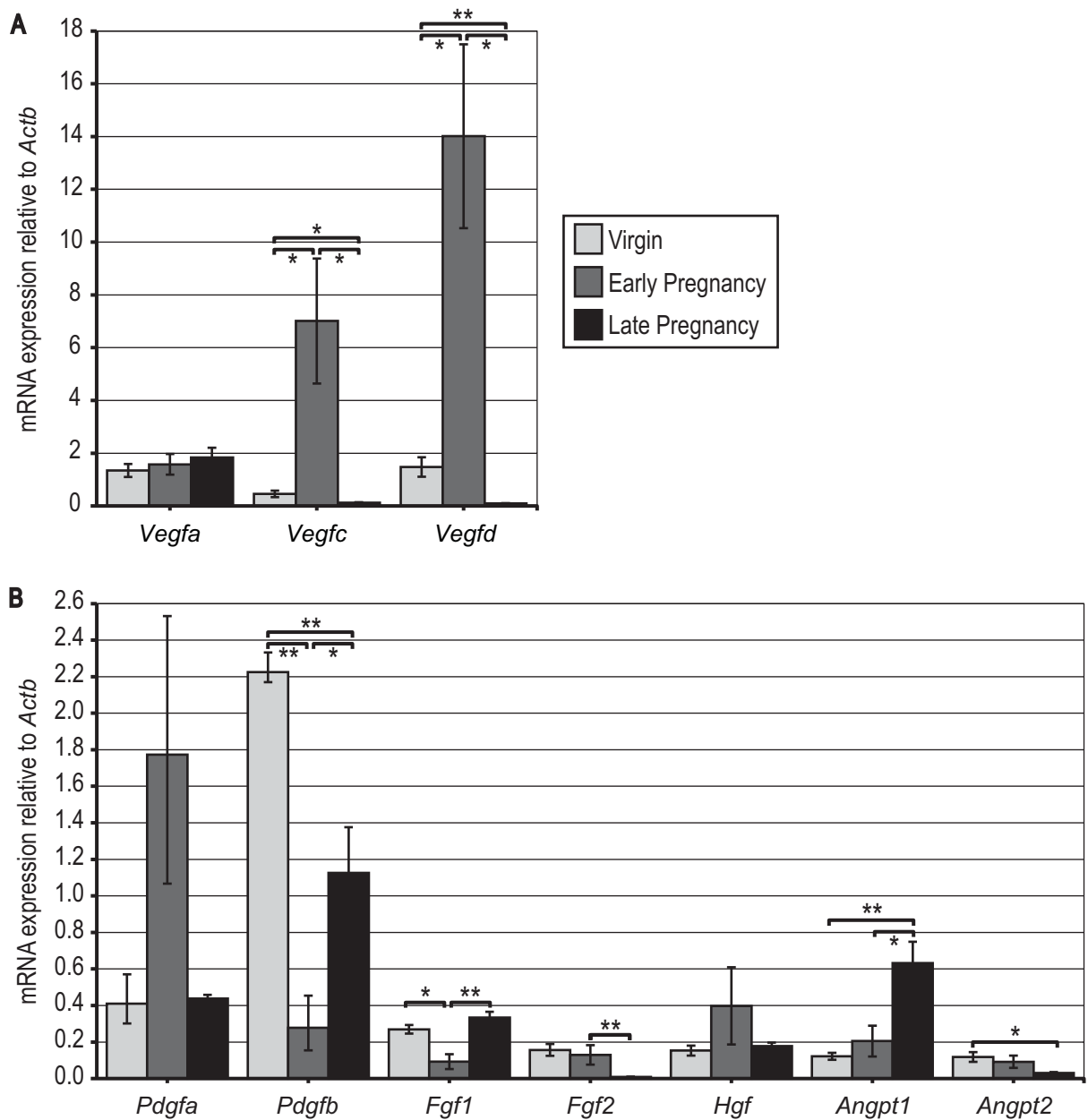


Figure 4.4 - The expression of pro-lymphangiogenic growth factors is dynamically regulated at the mRNA level during mouse mammary gland morphogenesis.

Real-time RT-PCR was used to determine the relative level of gene expression in mammary glands harvested from 9 week virgin compared with early (4.5 day) and late (16.5 day) pregnant wild-type female mice (A,B). Samples were pooled from at least two mice. Data shown represent the mean \pm standard error of the mean of three (9 week virgin, 16.5 day pregnant) or four (4.5 day pregnant) independent experiments. *P*-values were calculated using the two-tailed Student's *t*-test, **P*<0.05, ***P*≤0.01. RT-PCR - reverse transcription-polymerase chain reaction.

signalling has been implicated in normal mammary gland morphogenesis (Khialeeva et al., 2011). Recent data from our laboratory indicate that *Reln* and the reelin receptors, very low density lipoprotein receptor (*Vldlr*) and apolipoprotein E receptor 2 (*Apoer2*) are highly expressed in primary dermal embryonic LEC (Jan Kazenwadel and Natasha L. Harvey, unpublished data), suggesting a potential role for reelin signalling in mammary gland lymphangiogenesis. Intriguingly, we found that *Reln* mRNA levels were significantly increased 27.4-fold and 20.4-fold in early pregnancy, compared to virgin and late pregnant stages, respectively (Figure 4.5). Taken together, these data illustrate that pro-lymphangiogenic growth factors are temporally regulated at the mRNA level during mammary gland morphogenesis and suggest that the increase in lymphatic vascular density during pregnancy might occur as a direct result of elevated gene expression of pro-lymphangiogenic stimuli, including *Vegfc*, *Vegfd* and *Angpt1*, in the pregnant mouse mammary gland.

4.3.3.2 Investigation of pro-lymphangiogenic growth factors at the protein level

As a means of further investigating the levels of candidate pro-lymphangiogenic growth factors at various stages of mammary gland morphogenesis, we analysed protein levels via Western blot analysis using mammary gland protein lysates (section 4.2.4.1). Whilst *Angpt1* was significantly increased in 16.5 day pregnant relative to 9 week virgin mammary glands at the mRNA level, interestingly no corresponding increase was observed at the level of protein, upon blotting with a rabbit anti-mouse angiopoietin-1 antibody (Alpha Diagnostic International, San Antonio, TX) (Figure 4.6A,C). However, a 2.1-fold increase in *Angpt2* protein levels was observed in 16.5 day pregnant mammary glands compared to 9 week virgin glands (Figure 4.6B,D).

In conjunction with the temporal regulation of *Vegfd* mRNA levels, we detected a 21kDa band corresponding to the VHD subunit of mature, fully-processed VEGF-D (Baldwin et al., 2001b; Stacker et al., 1999), selectively in 16.5 day pregnant, but not 9 week virgin mouse mammary glands (arrow; Figure 4.7). Whilst we are currently unable to definitively determine the exact size of additional protein bands present on Western blots (*; Figure 4.7), which are nonetheless comparable across virgin and pregnant stages, they likely represent numerous partially-processed VEGF-D peptides (section 4.1.1) (Baldwin et al., 2001b; Stacker et al., 1999). The presence of mature VEGF-D selectively in pregnant, but not virgin, mouse mammary glands suggests that VEGF-D may be one of the key growth factors responsible for stimulating lymphangiogenesis during pregnancy in the postnatal mouse mammary gland.

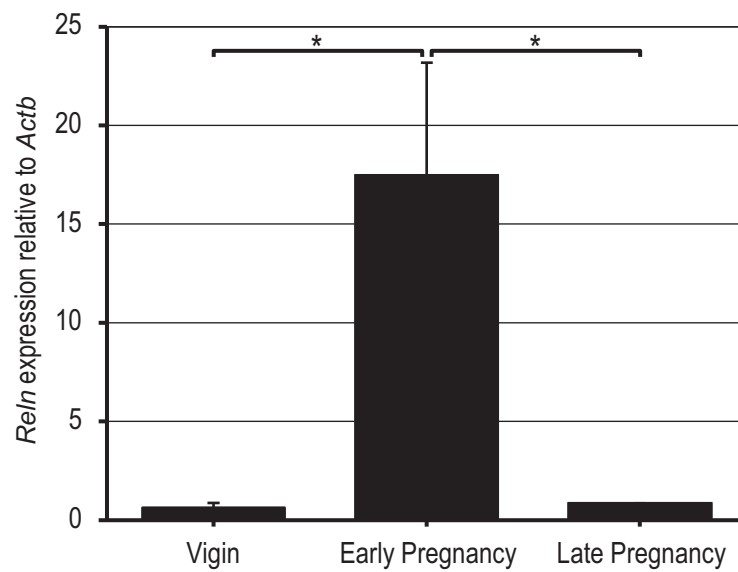


Figure 4.5 - *Reln* mRNA levels are increased at an early stage of pregnancy relative to virgin and late pregnant stages.

Real-time RT-PCR was used to determine the relative level of *Reln* gene expression in mammary glands from 9 week virgin compared with early (4.5 day) and late (16.5 day) pregnant wild-type female mice. Samples were pooled from at least two mice. Data shown represent the mean \pm standard error of the mean of three independent experiments. *P*-values were calculated using the two-tailed Student's *t*-test, **P*<0.05. RT-PCR - reverse transcription-polymerase chain reaction.

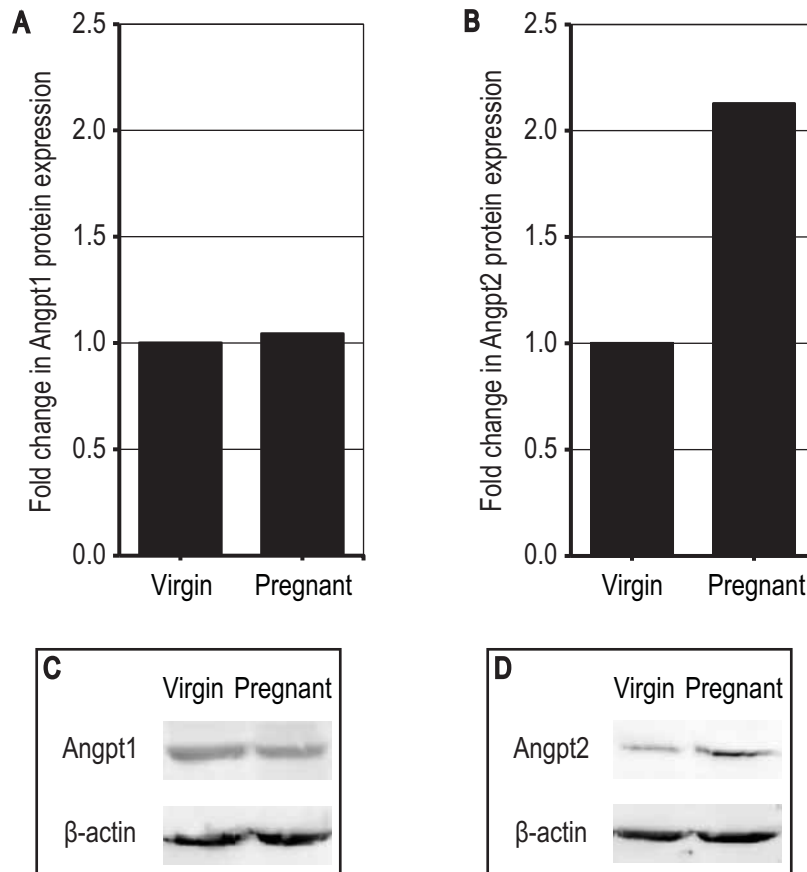


Figure 4.6 - Angpt2, but not Angpt1 protein, is increased in pregnant mouse mammary glands.

Fold change in Angpt1 (A) and Angpt2 (B) protein expression in 16.5 day pregnant mammary glands relative to 9 week virgin mammary glands, following normalisation to the loading control, β -actin. Samples were pooled from at least three mice. Data is representative of two independent experiments. Representative Western blots demonstrating Angpt1 (~70kDa, glycosylated form) (C), Angpt2 (~75kDa, glycosylated form) (D) and corresponding β -actin (42kDa) protein bands. kDa - kilodalton.

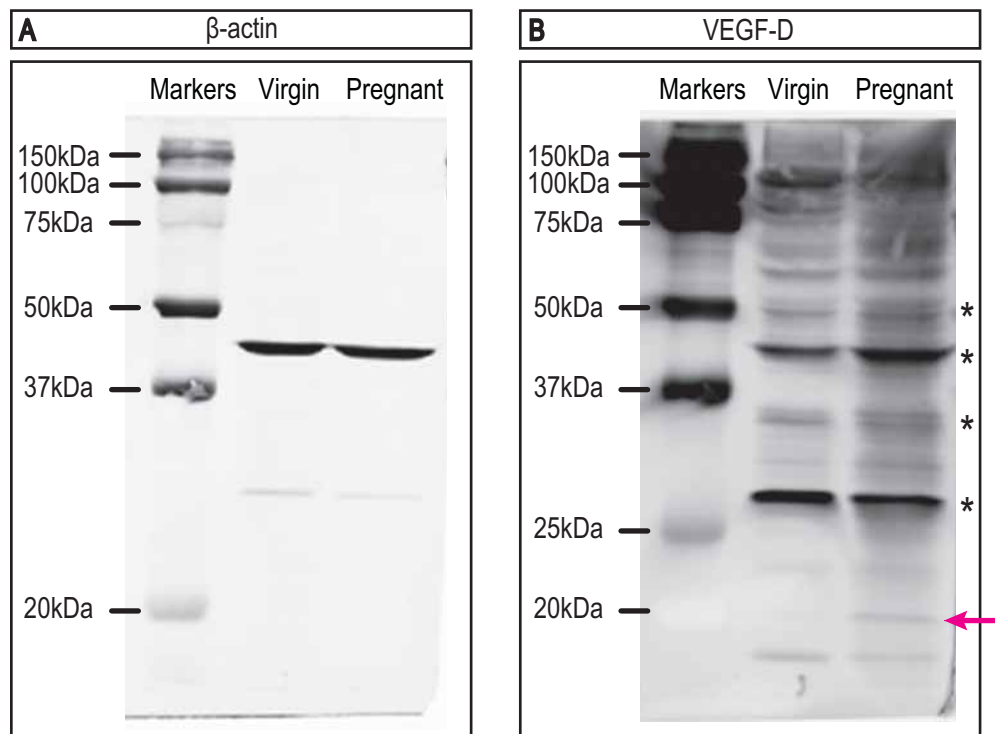


Figure 4.7 - Mature VEGF-D is present selectively in pregnant, but not virgin mouse mammary glands.

Western blots demonstrating the presence of a 21kDa band (arrow), corresponding to mature, fully-processed VEGF-D, in 16.5 day pregnant but not 9 week virgin mouse mammary glands (**B**) and matching β -actin (42kDa) protein loading controls (**A**). Samples were pooled from at least three mice. Data is representative of two independent experiments. kDa - kilodalton.

Unfortunately, a lack of good quality commercially-available antibodies designed to detect the mature, fully-processed, bioactive form of murine VEGF-C precluded extensive analysis of VEGF-C protein levels in the postnatal mouse mammary gland. VEGF-C antibodies available in our laboratory at the time of this study, including goat anti-VEGF-C (A-18) (Santa Cruz) and goat anti-VEGF-C (C-20) (Santa Cruz), only detect precursor forms of this protein and consequently results from these analyses were inconclusive (data not shown).

4.3.4 Myoepithelial cells are a rich source of pro-lymphangiogenic stimuli in the mouse mammary gland

Owing to our previous finding that lymphatic vessels share a close spatial association with mammary ducts (section 3.3.3), enriched populations of luminal and myoepithelial cells were isolated using fluorescence-activated cell sorting (FACS) (as detailed in section 5.2.1) from 9 week virgin and 16.5 day pregnant WT female mice, as a means of further delineating the cellular sources of lymphangiogenic stimuli in the mouse mammary gland. In retrospect, an earlier (4.5 day) stage of pregnancy might have represented a more appropriate morphogenetic stage to analyse lymphangiogenic growth factor expression in mouse mammary epithelial cells, as this time point corresponded to a peak in *Vegfc* and *Vegfd* expression in the mouse mammary gland (Figure 4.4A). Gene expression analyses using real-time RT-PCR revealed that established pro-lymphangiogenic growth factors are dynamically regulated between virgin and 16.5 day pregnant mammary epithelial cells. Moreover, the expression of pro-lymphangiogenic stimuli was found to be higher in myoepithelial compared to luminal epithelial cells in the mouse mammary gland (Figure 4.8). Due to the limiting cell numbers recovered post-FACS, this type of analysis was only able to be performed once using virgin mice, but was repeated twice from 16.5 day pregnant mice. Nevertheless, biological variation was minimised by pooling 8 x 9 week virgin mice and 4 x 16.5 day pregnant mice for cell sorting and isolation. Higher levels of expression of pro-lymphangiogenic growth factors in myoepithelial cells correlates with our previous observation that lymphatic vessels are intimately associated with epithelial ducts, which are a bi-layered structure encased by an outer layer of contractile myoepithelial cells, in the mouse mammary gland (Hennighausen and Robinson, 2005). Taken together, our data provides convincing evidence that the growth and patterning of mouse mammary gland lymphatic vessels is likely to be regulated by epithelial-derived lymphangiogenic growth factors.

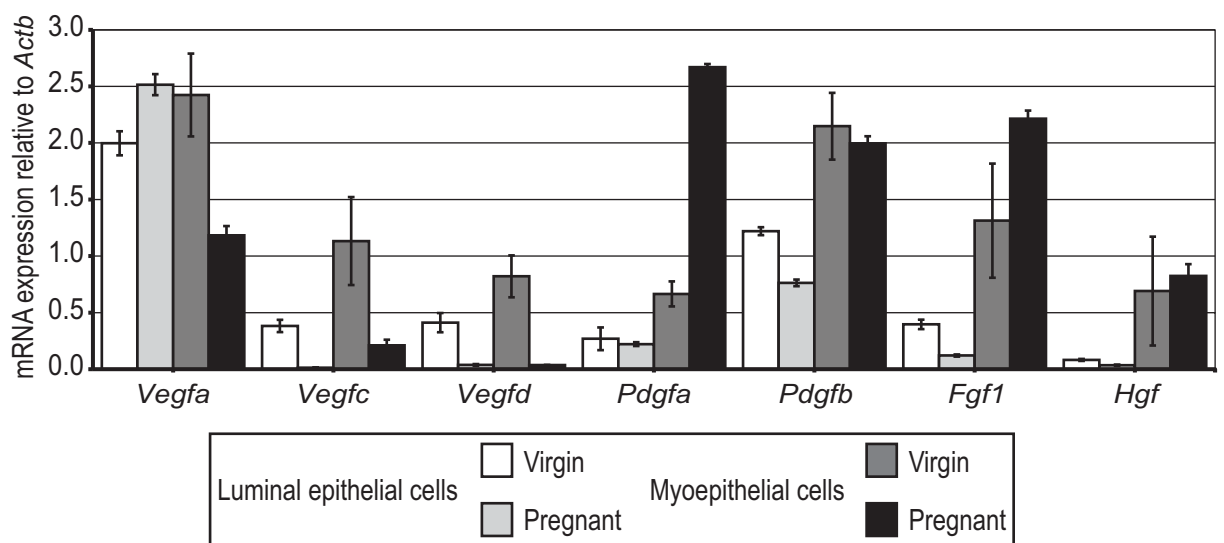


Figure 4.8 - The expression of pro-lymphangiogenic growth factors is elevated in myoepithelial cells.

Real-time RT-PCR analysis of isolated populations of 9 week virgin and 16.5 day pregnant epithelial cells reveals that expression of pro-lymphangiogenic stimuli is higher in myoepithelial compared to luminal epithelial cells in the mouse mammary gland. Data shown represent the mean \pm standard deviation of technical replicates from one experiment. RT-PCR - reverse transcription-polymerase chain reaction.

4.3.5 Lymphatic endothelial cell proliferation *ex vivo* is promoted by conditioned media harvested from mammary gland cell suspension cultures

In an effort to pinpoint potential factors responsible for lymphangiogenesis in the pregnant mouse mammary gland, primary LEC were isolated from the dermis of E16.5 mouse embryos (section 4.2.5.1) and cultured in the presence or absence of conditioned media (CM) harvested from 16.5 day pregnant mouse mammary gland cell suspension cultures (section 4.2.5.2). Cells isolated from 16.5 day pregnant mouse mammary glands were seeded in DMEM-10%FBS containing 50U/ml penicillin and 50µg/ml streptomycin (Gibco) and CM collected after 6 (CM1) and 72 (CM2) hours, at which point cells were approximately 90-95% confluent. At this time cells were passaged once and a final batch of CM was collected following a further 96 hours (CM3). These three time points were chosen in order to assess whether the cellular composition of mammary gland cell suspensions affected the growth factors secreted into the CM. Based on a previous report (Zeng et al., 2006), CM was added to LEC at a concentration of 30% (v/v) in EBM®-2 (Lonza), with corresponding controls consisting of 30% (v/v) base media that the CM was produced in (ie. DMEM-10%FBS containing 50U/ml penicillin and 50µg/ml streptomycin (Gibco)). LEC proliferation was measured 48 hours following the addition of CM using CellTiter 96® AQ_{ueous} One Solution Cell Proliferation Assay reagent (Promega). We observed a 1.76-fold increase in LEC proliferation with CM1 relative to control media following 48 hours in culture (Figure 4.9). Intriguingly, CM1 promoted LEC proliferation significantly more than CM2 and CM3 (Figure 4.9). Consistent results were obtained from three independent primary LEC isolations and three independent CM collections. These data illustrate that soluble, pro-lymphangiogenic growth factors are secreted by one or more cell types in the mouse mammary gland and act via paracrine signalling pathways to stimulate LEC proliferation.

In order to define the cell type(s) responsible for promoting LEC proliferation *ex vivo*, the identity of mammary gland cell suspensions in culture was investigated at each stage that CM was collected by immunofluorescent immunostaining. Strikingly, a distinct difference in the composition of cell populations was obvious at each passage. Based on morphology alone, it was evident that large sheets of flat, cuboidal, densely-packed epithelial cells predominated at passage 0 (arrows; Figure 4.10A); whereas at passage 1, cells primarily exhibited an elongated spindle-shape with numerous processes, characteristic of fibroblasts in culture (Figure 4.10B). This finding was corroborated by antibody staining of cell monolayers at passage 0 and 1. Staining with E-cadherin, which showed intense cell membrane staining, confirmed that indeed these flat, tightly-packed sheets of cells were epithelial in nature. At

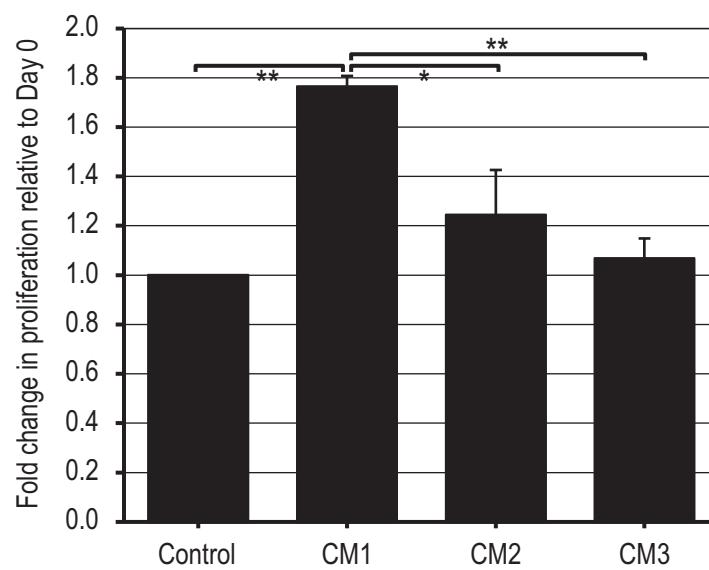
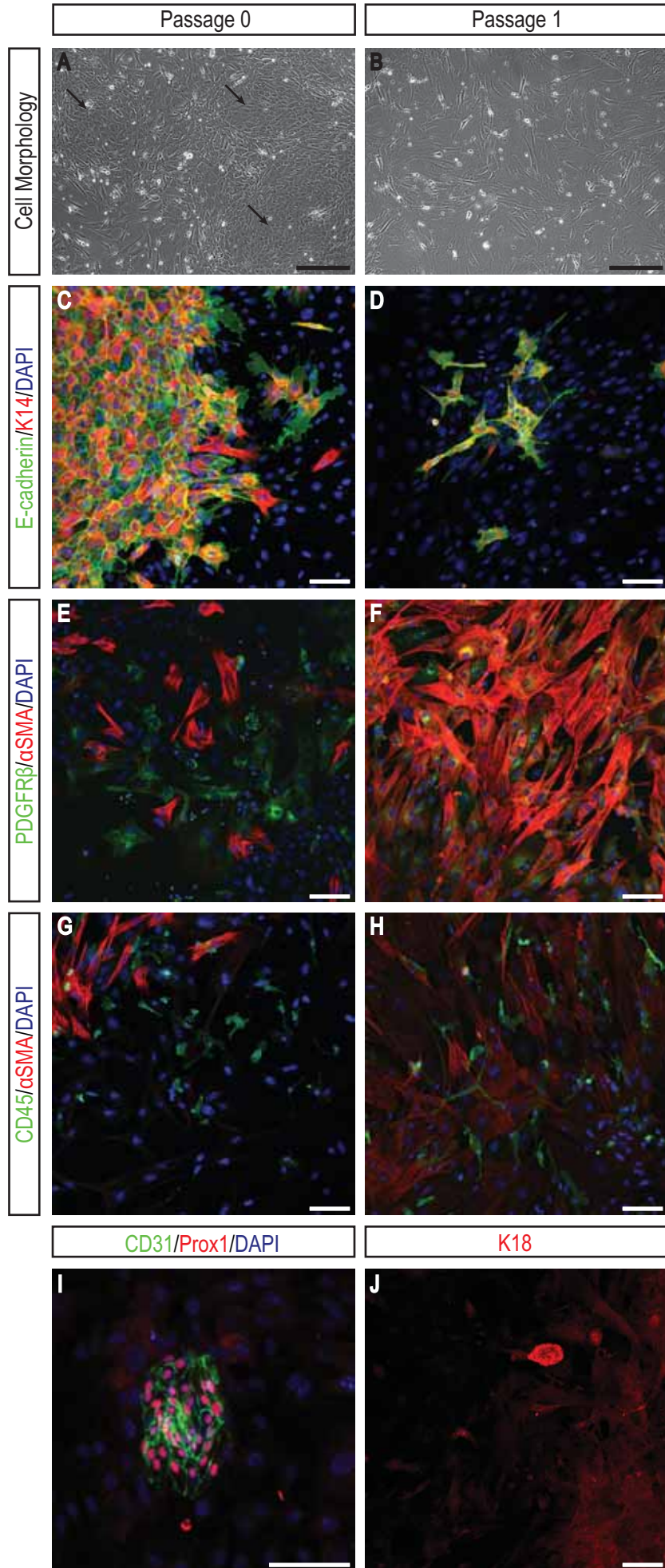


Figure 4.9 - Mammary gland conditioned media promotes lymphatic endothelial cell proliferation *ex vivo*.

Conditioned media (CM) harvested from 16.5 day pregnant mammary gland cell suspensions following 6 (CM1), 72 (CM2) and 168 hours (CM3) in culture results in increased proliferation of primary dermal lymphatic endothelial cells. Data shown represent the mean \pm standard error of the mean of three independent experiments. *P*-values were calculated using ANOVA with a Sidak adjustment for multiple comparisons, **P*<0.001, ***P*<0.0001.

Figure 4.10 - The cellular composition of mammary gland cell suspension cultures is different between passages 0 and 1.

Representative light microscopy images (**A,B**) and cell monolayer immunocytochemistry (**C-J**) of passage 0 (**A,C,E,G**) and passage 1 (**B,D,F,H**) mammary gland cell suspension cultures demonstrate that epithelial cells constitute the major cell type prior to passaging, whilst following passaging activated fibroblasts predominate. Small clusters of lymphatic endothelial cells (**I**) and luminal epithelial cells (**J**) are also present, but at a greatly reduced frequency. DAPI staining labels cell nuclei. α SMA - alpha smooth muscle actin, K14 - cytokeratin 14, K18 - cytokeratin 18, PDGFR β - platelet-derived growth factor receptor beta. Scale bars represent 250 μ m (**A,B**) and 100 μ m (**C-J**).



passage 0, corresponding to the collection of CM1 and CM2, large sheets of epithelial cells were apparent (Figure 4.10C); whilst at passage 1, corresponding to the collection of CM3, these large epithelial sheets were lost and rather only single and small groups of epithelial cells were observed (Figure 4.10D). Staining for platelet-derived growth factor receptor beta (PDGFR β) and α SMA confirmed that fibroblasts were present at both passages, however, at passage 1 they represented the major cell type and given the increase in α SMA expression, likely represented activated fibroblasts (Figure 4.10E-H) (Lewis and Norman, 1998). Numbers of CD45-positive haematopoietic cells, which include macrophages, appeared comparable between passages (Figure 4.10G,H). Occasionally, small clusters of LEC were also observed in these mammary gland cell cultures (Figure 4.10I). To further characterise the epithelial populations in culture, staining with antibodies detecting cytokeratins 14 (K14) and 18 (K18) was performed. K14 and K18 antibodies are specific for myoepithelial and luminal epithelial cells, respectively (Parmar and Cunha, 2004). Immunostaining revealed that the majority of epithelial cells present at both passages were K14-positive (Figure 4.10C,D), whilst almost no K18-positive cells were detected; any K18-positive cells that were observed likely represented small alveolar epithelial clusters (Figure 4.10J). Taken together, these data suggest that mammary epithelial cells and in particular myoepithelial cells, are likely the cellular source of soluble, pro-lymphangiogenic growth factors in the mammary gland CM.

4.3.6 Mammary gland conditioned media promotes lymphatic endothelial cell proliferation *ex vivo* via VEGFR-3 and FGFR-1

4.3.6.1 Selection of small molecule inhibitors

In order to identify the growth factor signalling pathways responsible for the promotion of LEC proliferation by mammary gland CM *ex vivo*, a panel of three tyrosine kinase small molecule inhibitors was employed. As we had determined that mRNAs encoding VEGF-C and VEGF-D were elevated early in pregnancy (Figure 4.4A), we predicted that these were the most likely candidates accounting for the increase in LEC proliferation. MAZ51 is an indolinone reported to selectively block VEGF-C and VEGF-D-induced phosphorylation of VEGFR-3 at low concentrations (ie. 5 μ M), whilst at high concentrations (ie. 50 μ M) it also partially blocks VEGFR-2 phosphorylation (Kirkin et al., 2001; Kirkin et al., 2004). Therefore, to ensure VEGFR-3-specificity, MAZ51 was used at 5 μ M in all cell proliferation assays. To investigate the respective contribution of signalling via VEGFR-2, SU5416, a potent and selective inhibitor of VEGFR-2, was also used (Fong et al., 1999). Recent work from our laboratory has

determined that FGF signalling through FGFR-1 plays an important role in LEC proliferation, migration and tube formation (Jan Kazenwadel, Genevieve Secker and Natasha L. Harvey, unpublished data) and therefore SU5402 was utilised to inhibit FGFR-1 tyrosine kinase activity (Mohammadi et al., 1997).

4.3.6.2 MAZ51 and SU5416 inhibit VEGF-C- and VEGF-D-induced lymphatic endothelial cell proliferation *ex vivo*

Before utilising the small molecule tyrosine kinase inhibitors to define the signalling pathways activated by mammary gland CM, we firstly ascertained their ability to effectively block VEGF-C- and VEGF-D-induced LEC proliferation *ex vivo*. To do this we cultured primary dermal LEC (section 4.2.5.1) for 48 hours in base media consisting of EBM@-2 (Lonza) supplemented with 0.5mg/ml ALBUMAX™ I (Gibco) in the presence and/or absence of the recombinant growth factors, VEGF-C (R&D Systems) and VEGF-D (R&D Systems), together with the tyrosine kinase inhibitors, MAZ51 (5µM) (Sigma) and SU5416 (5µM) (Sigma). 200ng/ml of VEGF-C was determined to be the optimal concentration to promote LEC proliferation, based on dose-response experiments performed in our laboratory (Jan Kazenwadel, Genevieve Secker and Natasha L. Harvey, unpublished data), whilst 200ng/ml and 1µg/ml of VEGF-D was chosen based on a previous report (Marconcini et al., 1999). LEC proliferation was measured 48 hours following the addition of media containing growth factors ± small molecule inhibitors using CellTiter 96® Aqueous One Solution Cell Proliferation Assay reagent (Promega) (section 4.2.5.3). We determined that VEGF-D used at a concentration of 200ng/ml was insufficient to stimulate primary dermal LEC proliferation above basal conditions (data not shown). Therefore, VEGF-D was used at 1µg/ml for all further *ex vivo* cell proliferation assays. MAZ51 inhibited VEGF-C- and VEGF-D-induced LEC proliferation, at least partially (Figure 4.11). More potent inhibition of VEGF-C-stimulated LEC proliferation was observed with SU5416 (Figure 4.11), reflecting the ability of VEGF-C to stimulate LEC proliferation induced by the formation of VEGFR-2/VEGFR-3 heterodimers (Dixelius et al., 2003). Given that mouse VEGF-D is not reported to bind to mouse VEGFR-2 (Baldwin et al., 2001a), VEGF-D was not cultured together with the VEGFR-2-specific tyrosine kinase inhibitor, SU5416 (Fong et al., 1999), in these assays. The ability of SU5402 (Calbiochem) to effectively inhibit FGF-2 (R&D Systems)-mediated LEC proliferation was determined in similar *ex vivo* LEC proliferation assays (Jan Kazenwadel, Genevieve Secker and Natasha L. Harvey, unpublished data). Collectively, these data demonstrate that the tyrosine kinase inhibitors MAZ51, SU5416 and SU5402 effectively block VEGFR and FGFR signalling pathways, respectively, in LEC *ex vivo*.

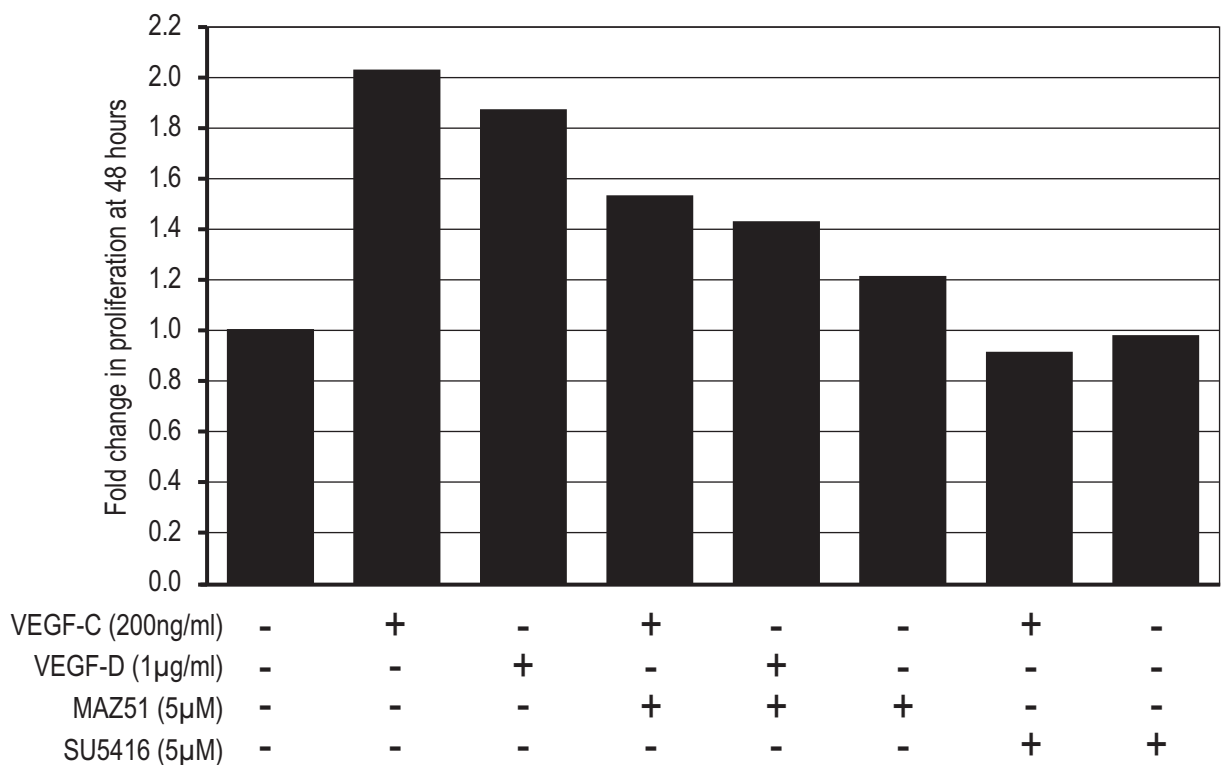


Figure 4.11 - MAZ51 and SU5416 inhibit VEGF-C- and VEGF-D-induced lymphatic endothelial cell proliferation *ex vivo*.

Primary dermal lymphatic endothelial cells were cultured for 48 hours in Endothelial Cell Basal Medium®-2 supplemented with 0.5mg/ml ALBUMAX™ I ± VEGF-C, VEGF-D and the tyrosine kinase inhibitors, MAZ51 or SU5416. VEGF-C- and VEGF-D-stimulated lymphatic endothelial cell proliferation was blocked by MAZ51 and SU5416. Data is representative of three independent experiments.

4.3.6.3 MAZ51 and SU5402 inhibit mammary gland conditioned media-induced lymphatic endothelial cell proliferation *ex vivo*

In order to determine the growth factors and signalling pathways responsible for the promotion of LEC proliferation by mammary gland CM *ex vivo*, the tyrosine kinase inhibitors MAZ51 (5 μ M) (Sigma), SU5416 (5 μ M) (Sigma) and SU5402 (10 μ M) (Calbiochem) were added to 30% CM1 (ie. the CM that exhibited the greatest increase in LEC proliferation - section 4.3.5) harvested from mammary gland cell suspension cultures after 6 hours. The effect of small molecule tyrosine kinase inhibitors on LEC proliferation was measured following 48 hours using CellTiter 96® Aqueous One Solution Cell Proliferation Assay reagent (Promega) (section 4.2.5.3). The data depicted in Figure 4.12 represents three independent experiments, encompassing three independent LEC isolations and three independent batches of mammary epithelial and stromal cell CM. The most potent inhibition of mammary gland CM-induced LEC proliferation was observed in the presence of MAZ51, which reduced LEC proliferation to levels comparable to unstimulated control cells (Figure 4.12). In addition, we also observed a more modest 0.72-fold reduction in CM-induced proliferation in the presence of SU5402 (Figure 4.12). However, negligible effects were observed with SU5416 (Figure 4.12). Surprisingly, MAZ51 also had an inhibitory effect on the proliferation of LEC grown in basal, control media, whilst SU5416 had a mild stimulatory effect (Figure 4.12). However, no effect on proliferation of unstimulated LEC was observed in the presence of SU5402 (Figure 4.12). Taken together, these data suggest that signalling via the receptors, VEGFR-3 and FGFR-1, but not VEGFR-2, are responsible for mammary gland CM-induced LEC proliferation *ex vivo*.

4.3.7 *Vegfd* is dispensable for lymphangiogenesis during postnatal mouse mammary gland morphogenesis

In order to definitively determine whether VEGF-D was required for postnatal mouse mammary gland lymphangiogenesis, we investigated lymphatic vascular patterning in virgin and pregnant *Vegfd*^{-/-} mammary glands. Lymphatic vascular patterning in inguinal mammary glands from two 13 week virgin *Vegfd*^{+/+} and *Vegfd*^{-/-} mice and two 14.5 day pregnant *Vegfd*^{-/-} mice was investigated using whole mount immunofluorescent staining (section 4.2.7). Pregnant *Vegfd*^{+/+} mammary glands were unavailable at the time of these studies and therefore comparison of *Vegfd*^{+/+} with *Vegfd*^{-/-} pregnant mouse mammary glands will be completed in future studies. These analyses revealed that lymphatic vessel (arrowheads) patterning was indistinguishable between *Vegfd*^{+/+} (Figure 4.13A-D) and *Vegfd*^{-/-} (Figure 4.13E-H) virgin

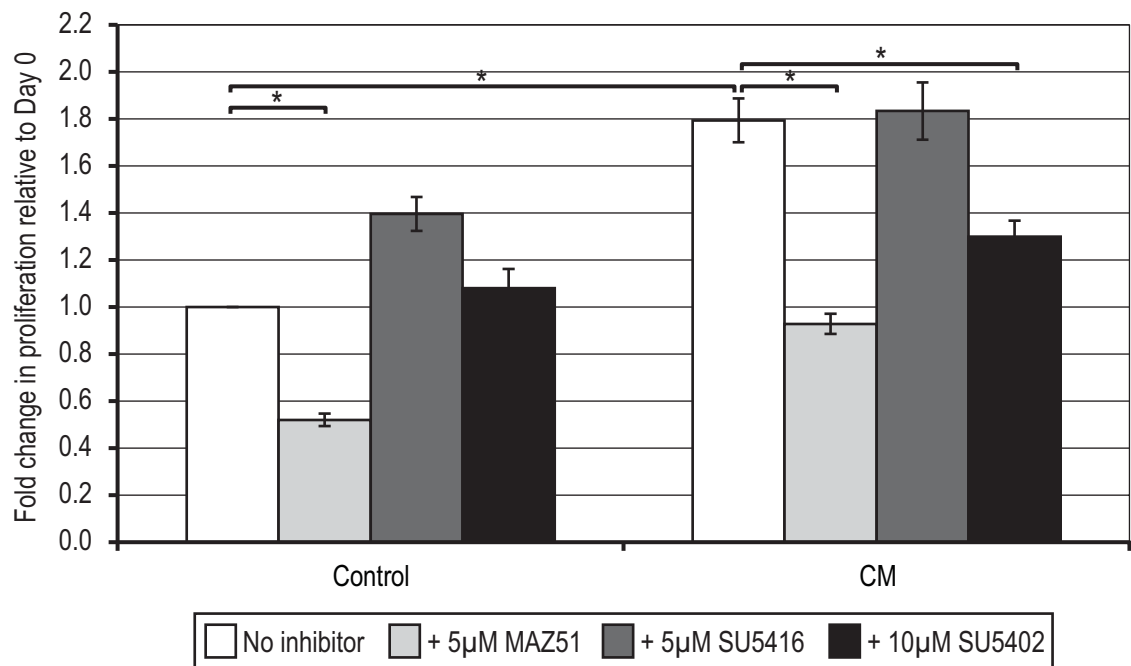


Figure 4.12 - Mammary gland conditioned media promotes lymphatic endothelial cell proliferation *ex vivo* via VEGFR-3 and FGFR-1.

Primary dermal lymphatic endothelial cells were cultured for 48 hours \pm mammary gland conditioned media (CM). Proliferation was blocked by the tyrosine kinase inhibitors, MAZ51 and SU5402, but not by SU5416. Data shown represent the mean \pm standard error of the mean of three independent experiments. *P*-values were calculated using ANOVA with a Sidak adjustment for multiple comparisons, **P*<0.0001.

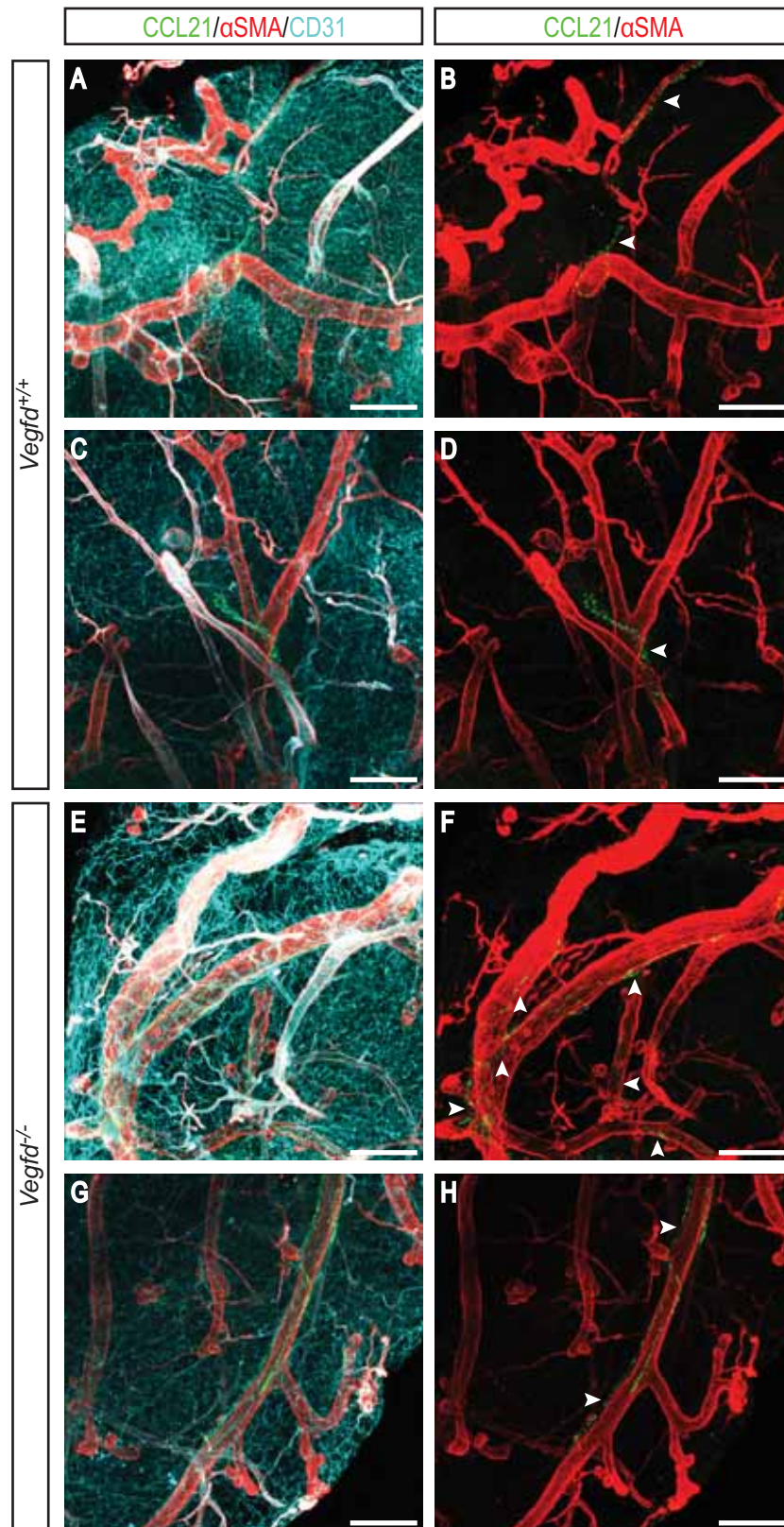


Figure 4.13 - Lymphatic vessel patterning is unaffected in virgin *Vegfd*^{-/-} mouse mammary glands.

Confocal z-stack images of 13 week virgin whole mount mammary glands demonstrate that lymphatic vessel (arrowheads) patterning is comparable between mammary glands from *Vegfd*^{+/+} (**A-D**) and *Vegfd*^{-/-} (**E-H**) mice. **B,D,F,H** represent dual-channel images of **A,C,E,G**, respectively. Images are representative of two mice. α SMA - alpha smooth muscle actin. Scale bars represent 150 μ m.

mice. Moreover, as previously documented in WT mice (section 3.3.3), lymphatic vessels (arrowheads) were observed in close spatial association with the mammary ducts in *Vegfd*^{-/-} virgin (Figure 4.13F,H) and pregnant (Figure 4.14B,D,F,H) mouse mammary glands. Whilst no overt differences in lymphatic vessel density were noted in virgin and pregnant *Vegfd*^{-/-} mammary glands using this whole mount immunofluorescent staining approach, subtle differences cannot be excluded. Taken together, these data suggest that *Vegfd* is dispensable for the growth and patterning of lymphatic vessels in the postnatal mouse mammary gland.

4.3.8 *Vegfd*-deficiency in the pregnant mouse mammary gland has no effect on epithelial architecture

Given that Northern blot analyses performed by Kirkin *et al.* on adult rat tissues demonstrated that *Vegfd* mRNA is most highly expressed in branched epithelial organs, including the mammary gland, kidney and lung (Kirkin *et al.*, 2001), we wanted to investigate whether *Vegfd*-deficiency had any effect on the epithelial architecture in the pregnant mouse mammary gland. To do this, we analysed carmine alum-stained (section 3.2.1) 14.5 day pregnant *Vegfd*^{+/+} and *Vegfd*^{-/-} whole mount mammary glands (performed by Sophie Paquet-Fifield, Tumour Angiogenesis Program, Peter MacCallum Cancer Centre, Melbourne, Australia) and found no overt differences in the epithelial architecture of *Vegfd*^{+/+} (Figure 4.15A,B) and *Vegfd*^{-/-} (Figure 4.15C,D) pregnant mouse mammary glands. This finding suggests that *Vegfd* is not required for epithelial branching morphogenesis in the pregnant mouse mammary gland.

4.4 DISCUSSION

In summary, data presented in this chapter illustrates that mammary epithelial cells, and in particular myoepithelial cells, are an important source of pro-lymphangiogenic growth factors in the postnatal mouse mammary gland. This is supported by three key findings. Firstly, ER α and PR were not detected in lymphatic vessels at any stage during postnatal mouse mammary gland morphogenesis, suggesting that lymphatic vessels in the mammary gland do not respond directly to estrogen and progesterone. Secondly, real-time RT-PCR analyses established that myoepithelial cells are a rich source of pro-lymphangiogenic stimuli in the mouse mammary gland and that mRNAs encoding VEGF-C and VEGF-D were elevated in expression early in pregnancy. Moreover, proteolytically-processed, active VEGF-D protein was present selectively in pregnant, but not virgin mouse mammary glands. Thirdly, LEC proliferation *ex vivo* was stimulated by CM harvested from mammary gland cell suspension cultures,

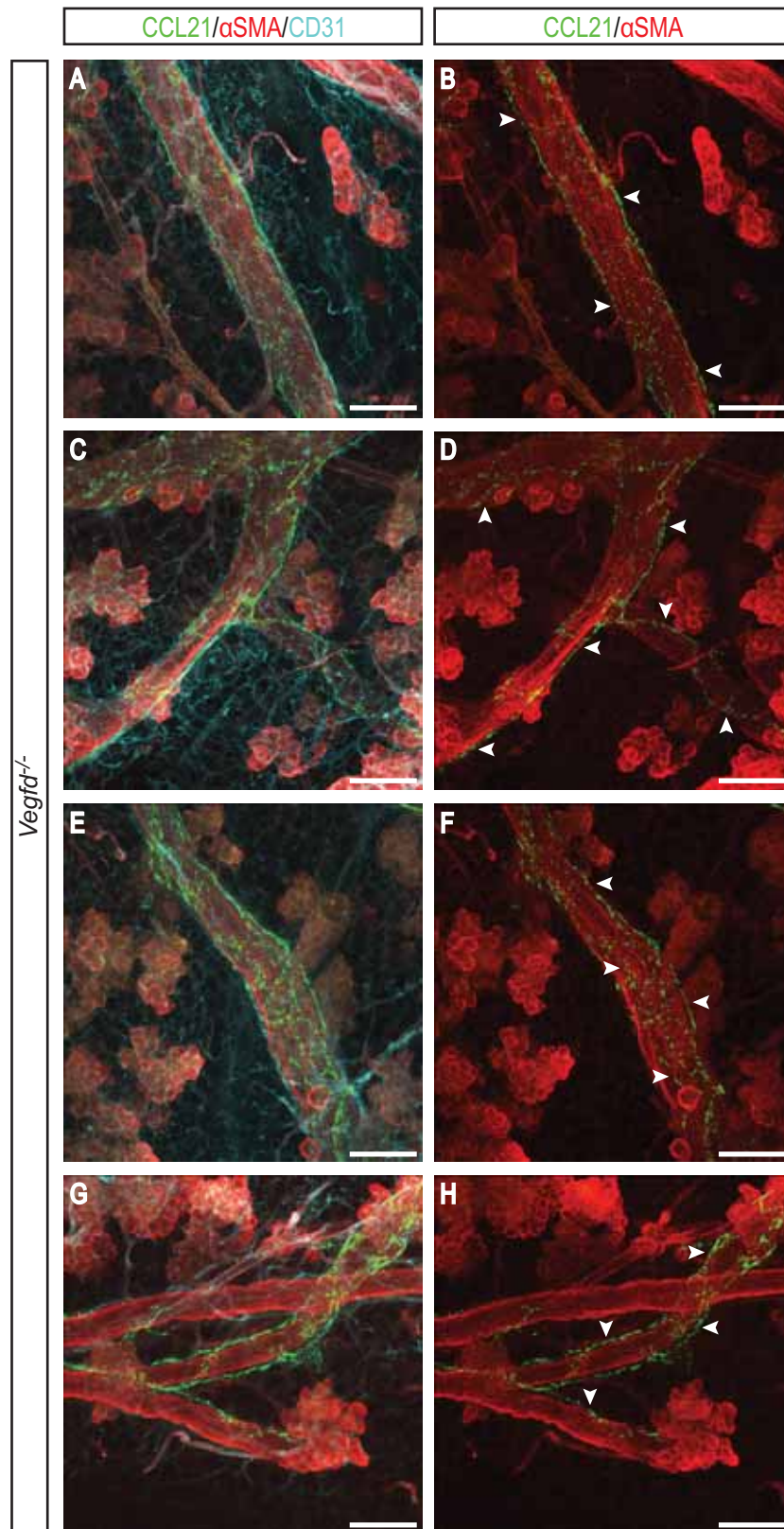


Figure 4.14 - Lymphatic vessel patterning is normal in pregnant *Vegfd*^{-/-} mouse mammary glands.

Confocal z-stack images of 14.5 day pregnant *Vegfd*^{-/-} whole mount mammary glands demonstrate that lymphatic vessels (arrowheads) are intimately associated with mammary ducts in *Vegfd*^{-/-} mammary glands (A-H). B,D,F,H represent dual-channel images of A,C,E,G, respectively. Images are representative of two mice. α SMA - alpha smooth muscle actin. Scale bars represent 150 μ m.

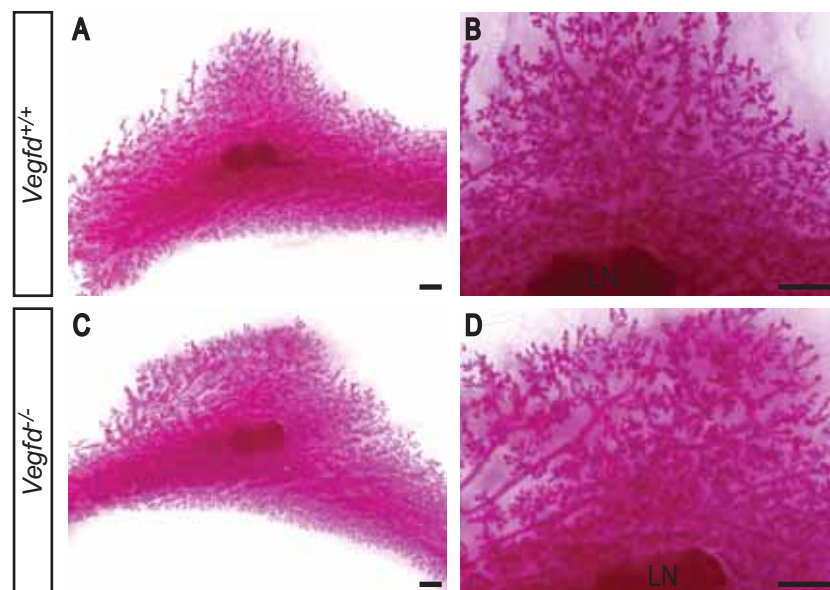


Figure 4.15 - The ductal architecture is normal in pregnant *Vegfd*^{-/-} mouse mammary glands.

Carmine alum-stained whole mount mammary glands reveal that gross ductal morphology is comparable between 14.5 day pregnant *Vegfd*^{+/+} (A,B) and *Vegfd*^{-/-} (C,D) mice. (A,B) are representative of one *Vegfd*^{+/+} mouse and (C,D) are representative of four *Vegfd*^{-/-} mice. LN - lymph node. Scale bars represent 1mm.

composed predominantly of myoepithelial cells, suggesting that myoepithelial cells represent the likely cellular source of soluble, pro-lymphangiogenic growth factors in mammary gland CM. Furthermore, a tyrosine kinase inhibitor specific for VEGFR-3 (Kirkin et al., 2001; Kirkin et al., 2004), the principal receptor for VEGF-C and VEGF-D, significantly blocked the proliferation of primary dermal LEC stimulated by mammary gland CM *ex vivo*, illustrating that VEGF-C and VEGF-D are the key pro-lymphangiogenic growth factors provided by myoepithelial cells in the postnatal mouse mammary gland.

Our observation that LEC in the mouse mammary gland lack detectable expression of ER α and PR at the protein level is not surprising given that limited reports exist documenting endothelial expression of these steroid hormone receptors. To date, cultured human coronary artery and human umbilical vein EC are the only vascular EC demonstrated to express estrogen receptors (Cid et al., 2002; Kim-Schulze et al., 1996). Furthermore, very little is known regarding the definitive effects of steroid hormones on angiogenesis in the normal human breast and even less is understood on their role in lymphangiogenesis. However, it has been proposed that the effects of estrogen in relation to the vascular endothelium involve its direct and indirect regulation of pro- and anti-angiogenic stimuli by the mammary epithelia (Dabrosin, 2005). Therefore, we would hypothesise that steroid hormones act indirectly on the mammary lymphatic endothelium by stimulating mammary epithelial and stromal cells, which express functional steroid hormone receptors (Brisken et al., 1998; Fendrick et al., 1998; Mueller et al., 2002), to produce lymphangiogenic stimuli, that can in turn act on nearby LEC in a paracrine mechanism. In accordance with this hypothesis, we observed expression of a number of lymphangiogenic growth factors in isolated luminal and myoepithelial cells of virgin and pregnant mouse mammary glands (Figure 4.8).

Our *in situ* hybridisation analyses of *Vegfa* expression in the postnatal mouse mammary gland correspond with previous expression studies in the rodent (Hovey et al., 2001; Islam et al., 2010; Pepper et al., 2000) and with our real-time RT-PCR data of isolated mammary epithelial populations demonstrating that *Vegfa* is expressed at a similar level in luminal and myoepithelial cells (Figure 4.8). In accordance with our *in situ* hybridisation data, Hovey *et al.* also reported a heterogeneity in the abundance of *Vegfa* mRNA within individual mammary epithelial cells during lactation and that *Vegfa* mRNA was localised to a distinct population of cells within the adipose tissue during puberty and pregnancy, which they attributed to adipocytes (Hovey et al., 2001). The latter observation is not surprising given the proposed functional relationship between developmental adipogenesis and angiogenesis and the upregulation of *Vegfa* isoforms by *in vitro* cultured preadipocytes (Cao, 2007; Hovey et al., 2001). However, given that VEGF-A has been shown to be expressed by tumour-

associated macrophages in a mouse model of breast cancer (Lin et al., 2006) and invasive breast carcinoma tissue samples (Lewis et al., 2000), it is possible that the stromal-distributed population of *Vegfa*-positive cells we detected by *in situ* hybridisation could represent macrophages. Immunostaining of *in situ* hybridisation-treated sections will be required to determine the exact identity of isolated *Vegfa*-positive cells in the mouse mammary gland and will form the basis of future investigations.

It has been reported that PDGF-A, and its receptor, platelet-derived growth factor receptor alpha (PDGFR α) are commonly expressed in separate, but adjacent cell layers (appositional) during mouse embryogenesis, generally epithelia and mesenchyme, respectively (Orr-Urtreger and Lonai, 1992). This appositional expression pattern indicates that PDGF-A/PDGFR α represents a signalling partnership involved in epithelial-mesenchymal interactions, where epithelial-derived PDGF-A acts in a paracrine manner to provide migratory, proliferative and other instructive signals to nearby developing PDGFR α -positive mesenchymal tissue during organogenesis (Andrae et al., 2008). The developing mammary gland is one such tissue demonstrating this reciprocal expression pattern, whereby *Pdgfa* is expressed by the epidermal mammary bud and *Pdgfra* by the surrounding dermal mesenchyme (Orr-Urtreger and Lonai, 1992). Our *in situ* hybridisation analysis of *Pdgfa* expression in the epithelia of the postnatal mouse mammary gland is in accordance with embryonic expression patterns of this ligand and our real-time RT-PCR data from isolated mammary epithelial populations demonstrating that *Pdgfa* is expressed most abundantly in the myoepithelial cell layer. Owing to embryonic lethality of *Pdgfa*-null mice (Boström et al., 1996), the precise role of PDGF-A in mammary gland morphogenesis has not been formally addressed. The possibility exists that *Pdgfa* expression in the mammary gland reflects a novel role for PDGF-A in mammary gland development, rather than a lymphangiogenic one, as currently PDGF-A has not been implicated in lymphangiogenesis. Definitive analysis of the role of PDGF-A in mammary gland morphogenesis will rely on the future generation of conditional knockout mice.

We demonstrated that *Vegfc* and *Vegfd* mRNA levels were significantly increased at an early stage of pregnancy relative to virgin and late pregnant stages (Figure 4.4A). In light of the fact that Baldwin *et al.* reported alternative RNA splicing of the mouse *Vegfd* gene, which generates two distinct *Vegfd* transcripts (Baldwin et al., 2001b), we compared the RNA splice donor site in exon 6 of the mouse *Vegfd* gene with our real-time RT-PCR primer sequences. Consequently, we established that our *Vegfd* mRNA levels reflect combined levels of both *Vegfd* transcripts. Nevertheless, it will be interesting to investigate the relative expression levels of both *Vegfd* transcripts and ultimately VEGF-D isoforms in the mouse mammary gland. Strikingly, Baldwin *et al.* found no difference in the relative levels of transcript expression during embryonic development and in range of adult mouse tissues, including the

lung, small intestine, stomach, heart, brain, thymus and pancreas, suggesting that both transcripts may be expressed accordingly in the mouse mammary gland (Baldwin et al., 2001b). Whilst it has been demonstrated that both VEGF-D isoforms display similar patterns of receptor binding (Baldwin et al., 2001b), an analysis of their individual functional roles have currently not been investigated.

Our finding that *Vegfc* and *Vegfd* mRNA levels are temporally regulated in the postnatal mouse mammary gland is in accordance with studies on the regulation of lymphangiogenesis in the ovary and endometrium. Work by Brown *et al.* demonstrated that *Vegfc* and *Vegfd* increase in a similar temporal manner in the ovary at time points that closely correspond to morphological ovarian lymphatic vascular development (Brown et al., 2010). Furthermore, *Vegfc* and *Vegfd* were shown to increase significantly in the presence of folliculogenic stimuli, follicle-stimulating hormone and estradiol, suggesting that ovarian lymphangiogenesis is hormonally-regulated. However, in these studies the expression of functional hormone receptors by ovarian LEC was not addressed (Brown et al., 2010). Interestingly, an estrogen response element which binds both ER α and ER β conferring hormone inducibility has been identified in the rat *Vegfa* gene, indicating that estrogen regulates *Vegfa* expression by direct transcriptional actions of the ER (Hyder et al., 2000). The possibility exists, given that we failed to detect expression of ER α and PR in lymphatic vessels in the mouse mammary gland, in combination with the apparent hormone-responsiveness of *Vegfc* and *Vegfd* in the mouse ovary (Brown et al., 2010), that a similar mechanism of hormone inducibility exists for the transcriptional control of the *Vegfc* and *Vegfd* genes. To date, however, no such studies have addressed this possibility.

Similarly, in the uterus, the mechanisms regulating endometrial lymphangiogenesis remain largely unknown. VEGF-C and VEGF-D have been localised via immunohistochemistry throughout human endometrial tissue with negligible difference in staining intensity across the various layers, despite the basalis region exhibiting an increased lymphatic vessel density compared to the functionalis layer (Donoghue et al., 2007; Rogers et al., 2008). Consequently, it has been postulated that the more biologically active 21kDa VEGF-C and VEGF-D peptides would be expressed in the basalis layer, where the necessary proteolytic enzymes required to process latent precursor proteins into their biologically active products would also be predominantly expressed. In the functionalis layer, where lymphatic vessels are three to five times less abundant, it is predicted that proteolytic cleavage of VEGF-C and VEGF-D would largely be restricted (Donoghue et al., 2007; Rogers et al., 2008). It is feasible that a similar mechanism might exist in the mouse mammary gland, whereby the proteolytic enzymes necessary to cleave VEGF-D to its active constituent are selectively expressed by the epithelial cells comprising the large mammary ducts and not the alveolar epithelium; accounting for the distinct lack of

lymphatic vessels associated with the alveoli during pregnancy and lactation. Investigation into the identity of VEGF-D processing enzymes, how they are temporally regulated and which cell types within the mammary gland express these enzymes, will undoubtedly provide important insight into the process of lymphangiogenesis in the postnatal mouse mammary gland. In fact, our microarray analyses (Chapter 5) revealed that the genes encoding for PC5 (*Pcsk5*) and PC7 (*Pcsk7*) were increased 3.5-fold ($P < 0.05$) in pregnant myoepithelial cells relative to pregnant luminal epithelial cells and 1.3-fold ($P = 0.47$) in pregnant compared to virgin myoepithelial cells, respectively. Whilst plasminogen (*Plg*), the inactive enzyme precursor to plasmin, was not differentially expressed in myoepithelial cells between virgin and pregnant stages, *Plau*, the gene encoding for urokinase-type plasminogen activator, was elevated 2.5-fold ($P = 0.32$) in pregnant haematopoietic cells compared to the same population in the virgin mammary gland. These data indicate candidate proteolytic enzymes are expressed in an appropriate spatial (ie. epithelial cells) and temporal (ie. during pregnancy) manner in the postnatal mouse mammary gland indicative of a potential role for these enzymes in the activation of VEGF-C and VEGF-D in mammary gland lymphangiogenesis. In order to definitively determine whether the candidate proteases, plasmin, furin, PC5 and PC7 (McColl et al., 2003; McColl et al., 2007), are responsible for mediating VEGF-D cleavage in the mouse mammary gland, the effect of CM from mammary gland cell cultures of protease knockout mice on LEC proliferation *ex vivo* could be determined similarly to assays performed in this study. Given that many of the PC knockout mice are embryonic lethal (Scamuffa et al., 2006), however, such studies may not be plausible. Alternatively, full-length VEGF-C and VEGF-D could be purified from the medium of transfected cells (Stacker et al., 1999) and subsequently incubated with mammary gland CM to determine whether proteolytic enzymes capable of processing full-length VEGF-C and VEGF-D are present in the CM. If cleavage of these proteins was observed, proteolysis by candidate enzymes, including plasmin and PCs, could be blocked using alpha 2-antiplasmin and decanoyl-Arg-Val-Lys-Arg-chloromethylketone, respectively, analogous to assays performed by McColl *et al.* (McColl et al., 2003; McColl et al., 2007). Such experiments would aid in the elucidation of the proteolytic enzymes required for cleavage of VEGF-C and VEGF-D in the postnatal mouse mammary gland and will form the basis of future investigative analyses.

The dynamic regulation of *Angpt1* and *Angpt2* at the level of mRNA and protein in the mouse mammary gland is no doubt a reflection of their well-documented roles in both angiogenesis and lymphangiogenesis (Dellinger et al., 2008; Gale et al., 2002; Maisonpierre et al., 1997; Morisada et al., 2005; Suri et al., 1996; Tammela et al., 2005). Based on studies by Tammela *et al.*, which demonstrated that *Angpt1* stimulated LEC proliferation, promoted vessel hyperplasia and lymphatic sprouting in the adult mouse ear (Tammela et al., 2005), the significant increase observed in *Angpt1* mRNA levels in

16.5 day pregnant mammary glands could contribute to the elevated lymphatic vessel density at this time. Furthermore, the observation that LEC express detectable levels of Tie2, which is known to bind Angpt1 (Morisada et al., 2005; Tammela et al., 2005), is in support of this proposition. Our investigation of Angpt1 and Angpt2 mRNA and protein levels in the mammary gland, however, indicate that levels of these two biomolecules do not necessarily correlate. *Angpt1* mRNA was increased in 16.5 day pregnant mammary glands compared to virgin glands (Figure 4.4B), whilst protein levels remained unchanged (Figure 4.6A,C). Conversely, *Angpt2* mRNA levels were downregulated in pregnant mammary glands (Figure 4.4B), whereas protein levels were increased approximately 2-fold compared to virgin mammary glands (Figure 4.6B,D). This is not surprising, given that the correlation between mRNA and relative protein abundances in the cell, contrary to dogma, has been reported to be extremely poor (Maier et al., 2009). Several biological factors have been identified which can influence the mRNA-protein correlation. These include RNA secondary structure which can affect translation efficiency; protein half-lives; the presence of small untranslated RNA species, such as microRNAs, which act as post-transcriptional regulators; as well as negative-feedback regulatory loops, which tightly control levels of gene transcription and translation (Maier et al., 2009). Any number of these factors could account for the discrepancy between mRNA and protein levels of Angpt1 and Angpt2 in the mouse mammary gland. In fact, Angpt2 protein has been shown to negatively regulate *Angpt2* mRNA levels in bovine mesenteric EC as well as human umbilical vein EC and thus a negative-feedback loop has been proposed to tightly regulate the expression of *Angpt2* (Daly et al., 2006; Mandriota and Pepper, 1998). It is therefore not unexpected that we observe a decrease in *Angpt2* mRNA levels with a concomitant increase in Angpt2 protein in the pregnant mouse mammary gland. Given that Angpt2 has been established as a critical regulator of postnatal blood and lymphatic vessel remodelling, by either acting as a Tie2 antagonist or agonist, respectively (Dellinger et al., 2008; Gale et al., 2002), we would predict that Angpt2 functions in the pregnant mouse mammary gland to ensure correct vascular patterning, maturation and function. Moreover, Angpt2 has been shown to be pro-lymphangiogenic (Gale et al., 2002) and thus increased Angpt2 protein correlates with peak lymphatic vessel density in the pregnant mouse mammary gland.

It is also important to bear in mind that measuring intracellular mRNA levels does not necessarily reflect the released and bioactive, extracellular levels of a protein (Dabrosin, 2005). It is therefore not unexpected that *Vegfa* mRNA levels were not markedly altered from a virgin to a pregnant state in the mouse mammary gland. This may simply reflect that VEGF-A undergoes some form of post-translational modification, such as proteolytic cleavage, secretion blockade by binding in a complex with additional proteins or sequestration of VEGF-A in the extracellular space by other molecules (Dabrosin, 2005), in order to temporally regulate bioactive VEGF-A levels necessary for angiogenesis in the mouse

mammary gland, without altering *Vegfa* transcription. Moreover, this phenomenon is particularly relevant to proteins such as VEGF-C and VEGF-D, which are secreted from the cell as full-length homodimers, which are then proteolytically-processed in a stepwise manner to generate bioactive forms (Joukov et al., 1997; Stacker et al., 1999). This could explain the discrepancy between VEGF-C and VEGF-D mRNA and protein levels in virgin and pregnant mammary glands. It is plausible that in late pregnancy, when levels of the mature form of VEGF-D are elevated (Figure 4.7), transcription of the *Vegfd* gene is correspondingly downregulated via a negative-feedback regulatory loop, therefore explaining the reduced levels of *Vegfd* mRNA at this time point. The molecular factors regulating *Vegfd* gene transcription, however, are not fully understood. Recently, it has been demonstrated that the interaction of hepatocyte nuclear factor 4 alpha, chicken ovalbumin upstream promoter transcription factor 1 and chicken ovalbumin upstream promoter transcription factor 2 (COUP-TFII) with a proximal, atypical direct repeat element in the human *Vegfd* gene promoter is indispensable for transcription (Schäfer et al., 2008). Factors controlling mouse *Vegfd* transcription are less well-understood. *In vitro*, at least, it is known that unlike *Vegfc*, *Vegfd* transcription is not stimulated by pro-inflammatory cytokines and growth factors, such as tumour necrosis factor alpha and interleukin 1 beta (Enholm et al., 1997; Orlandini and Oliviero, 2001; Ristimäki et al., 1998). Instead, *Vegfd* mRNA levels were found to be stimulated by a direct cell-cell contact-triggered mechanism involving cadherin-11 (Orlandini and Oliviero, 2001). In another report, it was shown that beta-catenin can downregulate *Vegfd* mRNA levels by influencing mRNA stability; a regulatory mechanism that is conserved between mouse and human *Vegfd* (Orlandini et al., 2003). Whether any of these regulatory mechanisms play a role in the transcriptional control of *Vegfd* in the postnatal mouse mammary gland remain to be elucidated. Future insights into such mechanisms have the potential to improve our understanding on the regulation of VEGF-D in lymphangiogenesis during development and disease.

Given our finding that mature, fully-processed VEGF-D is present selectively in pregnant, but not virgin adult female mammary glands, together with evidence from several *in vivo* studies which demonstrate that VEGF-D can also promote angiogenesis (Harris et al., 2011; Marconcini et al., 1999; Rissanen et al., 2003), it is possible that in the setting of the mammary gland, VEGF-D could promote both angiogenesis and lymphangiogenesis. This dual role would account for the concurrent and transient increase in both vascular beds during pregnancy (Djonov et al., 2001; Matsumoto et al., 1992; Pepper et al., 2000). Limited data, however, exists on the half-life of the VEGF-D protein. It is well-recognised that protein half-lives are highly variable and can range from a few seconds to several days (Maier et al., 2009). The cellular lifetime of a protein depends on several factors, including intrinsic protein stability, post-translational processing, such as phosphorylation and ubiquitination, and on the localisation of the

protein (Maier et al., 2009). A report by Veikkola *et al.* states that the half-life of recombinant VEGF-C and VEGF-D protein in the mouse circulation is less than 15 minutes (Veikkola et al., 2001). This suggests that VEGF-D is rapidly turned over and could explain why the mature form of VEGF-D is not detected in virgin mammary glands. Alternatively, increased expression and/or activity of the protease(s) responsible for VEGF-D cleavage events could explain the selective presence of this form of VEGF-D in pregnant mammary glands. In accordance with this premise is data derived from our microarrays (Chapter 5), demonstrating that genes encoding for the proteolytic enzymes, PC5 (*Pcsk5*) and PC7 (*Pcsk7*), are increased 3.5-fold ($P<0.05$) in pregnant myoepithelial cells relative to pregnant luminal epithelial cells and 1.3-fold ($P=0.47$) in pregnant compared to virgin myoepithelial cells, respectively. The caveat to the investigation of VEGF-D at the protein level is that much of the current literature analysing VEGF-D protein levels via Western blot are performed on protein lysates generated from *in vitro* cell lines transiently expressing recombinant VEGF-D protein; rather than native, endogenously expressed protein *in vivo* (Harris et al., 2011; McColl et al., 2003; McColl et al., 2007; Stacker et al., 1999). This may explain the presence of numerous currently unidentifiable bands on our Western blots following immunoblotting for VEGF-D in WT tissue (*; Figure 4.7), although the future preparation of tissue lysates from *Vegfd*^{-/-} mammary glands will hopefully aid in better characterisation of these bands. Furthermore, only a handful of commercially-available antibodies exist for the detection of VEGF-C and VEGF-D in mouse; whilst abundant antibodies are available for the detection these proteins in human tissues. Therefore, owing to the limited availability of reliable, commercial reagents for mouse, our analyses were mostly restricted to assessing mRNA rather than protein level and activity. We would hypothesise, however, that VEGF-D protein is largely expressed by mammary epithelial cells, given that in the uterus, another mammalian reproductive organ, VEGF-D immunostaining was significantly higher in the luminal and glandular epithelia of the endometrium in comparison to the surrounding stroma and myometrium (Girling et al., 2010). Our finding that *Vegfc* and *Vegfd* are more highly expressed in myoepithelial cells compared to luminal epithelial cells in the virgin and pregnant mouse mammary gland by both real-time RT-PCR (Figure 4.8) and microarray analysis (Chapter 5) provides further evidence in support of this hypothesis.

Reelin signalling is a critical pathway regulating several steps in neuronal cell migration and positioning throughout the central nervous system (Förster et al., 2010). Reelin, a large extracellular matrix glycoprotein, exerts its function by binding to two lipoprotein receptors, VLDLR and ApoER2, inducing the phosphorylation of the intracellular adaptor protein, disabled homolog 1 (Dab1) (Förster et al., 2010). Despite many neuronal path-finding molecules being shared by the vasculature (Larrivée et al., 2009), very little is known about the function of reelin signalling in non-neuronal tissues. Recently,

Khialeeva *et al.* demonstrated that reelin signalling pathway components are expressed throughout the embryonic and postnatal mouse mammary gland and are required for normal mammary gland morphogenesis; the first documentation of a role for reelin outside of the nervous system (Khialeeva *et al.*, 2011). In the postnatal mammary gland, *Dab1* was localised to the luminal epithelial cell layer, whereas reelin was expressed in a complimentary pattern in the surrounding periductal stroma and myoepithelia (Khialeeva *et al.*, 2011). The observation by Khialeeva *et al.* that reelin is expressed in the postnatal mouse mammary gland at the level of protein is consistent with our finding that *Reln* mRNA is significantly increased during early pregnancy compared to virgin and late pregnant stages (Figure 4.5). Taken together, these data indicate that reelin is spatially and temporally regulated during mouse mammary gland morphogenesis. Our *Reln* mRNA expression is likely attributed to periductal stromal and myoepithelial cell expression; however, additional cellular sources cannot be disregarded. Work from our laboratory indicates that *Reln* is highly expressed by primary dermal embryonic LEC. Even more intriguing, is that these primary dermal embryonic LEC also express *Vldlr* and *Apoer2* (Jan Kazenwadel and Natasha L. Harvey, unpublished data), suggesting that reelin signalling could also play a role in mammary gland lymphangiogenesis. It is therefore conceivable, given reelin's well-established role in neuronal migration (Förster *et al.*, 2010) and the expression of reelin by myoepithelial cells in the mouse mammary gland (Khialeeva *et al.*, 2011), that reelin signalling could impart key guidance cues to LEC via reciprocal endothelial-mesenchymal interactions; in a similar way that epithelial-mesenchymal cross-talk is obligatory in many aspects of mammary gland biology (Parmar and Cunha, 2004). Therefore, the reelin signalling axis could offer one potential mechanism explaining the spatial association of lymphatic vessels with mammary ducts in the mouse mammary gland. The molecular mechanisms by which reelin activates its receptors and controls cellular functions, however, currently remain largely unknown. It has been recently documented that ephrinB proteins bind to reelin and are essential for reelin signalling during neuronal migration (Sentürk *et al.*, 2011). This finding, combined with the previously reported functional requirement of ephrinB2 in the postnatal remodelling of the primary lymphatic capillary plexus (Mäkinen *et al.*, 2005) further strengthens a potential role for reelin signalling in the patterning of lymphatic vessels in the mouse mammary gland. Future studies aim to explore the role of reelin signalling in lymphangiogenesis.

Owing to the predominance of myoepithelial cells in mammary gland cell suspension cultures, together with the expression of pro-lymphangiogenic growth factors by myoepithelial cells, it is likely that pro-lymphangiogenic growth factors secreted by myoepithelial cells are responsible for the promotion of LEC proliferation by mammary gland CM *ex vivo*. Our microarray data (discussed further in Chapter 5) demonstrating that *Vegfc* and *Vegfd* were increased 3.7-fold ($P=0.07$) and 1.3-fold ($P=0.66$), respectively,

in pregnant myoepithelial cells compared to luminal epithelial cells, is in further support of this hypothesis. These findings do not exclude the possibility, however, that other and/or additional cellular sources of pro-lymphangiogenic growth factors in the mouse mammary gland are important. Given that the number of haematopoietic cells, encompassing macrophages, were comparable at both passage 0 and 1, it is unlikely that macrophages contributed to the increase in LEC proliferation, despite the fact they have been demonstrated to produce a vast array of lymphangiogenic growth factors, including VEGF-C and VEGF-D, in settings of inflammation and tumourigenesis (Baluk et al., 2005; Cursiefen et al., 2004; Jeon et al., 2008; Kataru et al., 2009; Maruyama et al., 2007; Schoppmann et al., 2002). Recent work from our laboratory illustrated that macrophages do not provide the principal source of pro-lymphangiogenic signals during embryonic dermal lymphatic vascular development, but act instead to restrain the calibre of dermal lymphatic vessels by regulating LEC proliferation (Gordon et al., 2010). Adipocytes, which are abundant in the mammary gland, have been reported to express and secrete an abundance of growth factors, including VEGF-A, VEGF-C, FGF-2, HGF, Angpt1 and Angpt2 (Saiki et al., 2006; Voros et al., 2005). Given that many of these growth factors have been implicated in lymphangiogenesis (see section 1.1.4.1), it is plausible that adipose tissue also represents a reservoir of lymphangiogenic growth factors in the mouse mammary gland. A recent review summarises mounting evidence that further supports a close relationship between lymphatic vessels and adipose tissue biology (Harvey, 2008). Therefore, adipocytes in mammary gland cell suspension cultures could potentially contribute to the selective promotion of LEC proliferation in the presence of CM1, compared to CM2 and CM3 (Figure 4.9). In order to substantiate this hypothesis, CM collected from mammary adipocyte cultures could be tested in a similar *ex vivo* LEC proliferation assay and compared to CM collected from whole mammary gland cell suspension cultures.

Given that MAZ51 is predominantly a VEGFR-3 inhibitor at the concentration used in our assays (Kirkin et al., 2001; Kirkin et al., 2004) and that the known activating ligands for this receptor are VEGF-C (Joukov et al., 1996) and VEGF-D (Achen et al., 1998), we predict that either of these two lymphangiogenic growth factors present in the CM are responsible for promoting LEC proliferation. However, owing to the fact that mouse VEGF-D is reported not to bind to mouse VEGFR-2, whilst VEGF-C does (Baldwin et al., 2001a) and that no significant reduction in LEC proliferation was observed in the presence of the VEGFR-2 inhibitor, SU5416 (Fong et al., 1999), it is more than likely that VEGF-D is the predominant soluble growth factor present in mammary gland epithelial and stromal cell CM responsible for the increase in LEC proliferation *ex vivo*. Our *ex vivo* data is consistent with *in vivo* data from Girling *et al.*, which demonstrated that in the uterus, VEGF-D-overexpression promoted the proliferation and enlargement of existing myometrial lymphatic vessels in a mouse model of endometrial

cancer (Girling et al., 2010). It will be interesting to compare VEGF-D protein levels at an earlier stage of pregnancy and assess the effect of CM collected from 4.5 day pregnant mammary gland cell suspension cultures on LEC proliferation. Whilst we see a significant increase in *Vegfd* at the mRNA level at this time point (Figure 4.4A), we currently do not know whether this corresponds to a peak in active VEGF-D protein, analogous to that observed in 16.5 day pregnant mammary glands. Furthermore, we observed a modest reduction in CM-induced LEC proliferation in the presence of SU5402, suggesting the presence of a small proportion of FGF-2 in mammary gland CM. This is consistent with current data from our laboratory demonstrating that FGF-2 promotes the proliferation, migration and tube formation of primary embryonic dermal LEC via FGFR-1, independent of VEGF receptors (Jan Kazenwadel, Genevieve Secker and Natasha L. Harvey, unpublished data). Surprisingly, we also observed a significant reduction in the proliferation of unstimulated control LEC in the presence of MAZ51. A similar phenomenon was reported by Kirkin *et al.*, whereby MAZ51 was observed to have an inhibitory effect on human dermal microvascular EC grown in serum-containing media. This inhibitory effect was attributed to a currently unidentified tyrosine kinase receptor, in addition to VEGFR-2 and VEGFR-3, that is expressed on EC and that is activated in response to growth factors present in serum (Kirkin et al., 2004). Alternatively, a cell-autonomous VEGF-C autocrine signalling mechanism important for LEC survival, just as autocrine VEGF-A signalling promotes BEC survival (Lee et al., 2007), may account for the observed reduction in proliferation of unstimulated control LEC with MAZ51. A study by Mäkinen *et al.* demonstrating that VEGF-C signalling via VEGFR-3 provides a survival signal for LEC (Mäkinen et al., 2001) is in further support of this hypothesis. In contrast, SU5416 promoted LEC proliferation when LEC were grown in the presence of serum (Figure 4.12). Whilst we are unable to definitively account for this phenomenon, it is possible that blockade of signalling via VEGFR-2 results in the upregulation of pro-lymphangiogenic growth factors that act independently of VEGF receptors. Fittingly, we have recently shown that FGF-2 promotes LEC proliferation, migration and tube formation via FGFR-1, independently of VEGFR-2 and VEGFR-3 (Jan Kazenwadel, Genevieve Secker and Natasha L. Harvey, unpublished data). Collectively, our *ex vivo* LEC proliferation data suggests that VEGF-D and FGF-2 are two key growth factors present in mammary gland CM. To further validate this finding we plan to assess whether CM derived from pregnant *Vegfd*^{-/-} mouse mammary glands promotes LEC proliferation *ex vivo* to the same extent as CM collected from WT mammary glands. In addition, we plan to quantify the levels of VEGF-C and VEGF-D contained in mammary gland CM using established enzyme-linked immunosorbent assay (ELISA) methodology (Harris et al., 2011). These experiments will form the basis of future work.

Northern blot analyses previously performed on adult rat tissues demonstrated that *Vegfd* mRNA is most highly expressed in the mammary gland, spleen, kidney, lung, tongue and ovary (Kirkin et al., 2001). Of these, the mammary gland, kidney and lung represent branched epithelial organs (Lu et al., 2006). Branching morphogenesis is a fundamental developmental process involved in invertebrate and vertebrate organogenesis; from the trachea and air sacs in *Drosophila*, to the mammalian lung and kidney, as well as many exocrine glands, including the mammary, prostate, pancreas and salivary gland (Lu et al., 2006; Lu and Werb, 2008). A common principle in the organogenesis of branched organs is coordinated branching morphogenesis of epithelial and blood vascular networks, culminating in their close spatial proximity (Lu and Werb, 2008). The concept of epithelial-mesenchymal cross-talk is well-known; however, there is emerging evidence for the existence of reciprocal epithelial-endothelial signalling during organ development. Two recent studies in the mouse embryo, using the pancreas (Pierreux et al., 2010) and lung (Lazarus et al., 2011) as models of branched organs, have assisted with this novel concept gaining momentum. The lung, just like the mammary gland, is a prime example of a branched organ in which there is co-alignment of blood vessels with all branching generations of the epithelial tree; from the primary bronchi to the alveoli (Lazarus et al., 2011). Lazarus *et al.* used different ablative strategies to eliminate the lung vasculature and eloquently demonstrated that proximity to the vasculature was indeed essential for correct patterning of airway branches (Lazarus et al., 2011). During branching morphogenesis in the pancreas, however, EC are preferentially located along the central (trunk) epithelial cells and remain at a distance from the branch tips where acinar differentiation of the epithelium occurs, correlating with prominent VEGF-A expression in the trunk epithelial cells of the pancreas (Pierreux et al., 2010). Similarly, in the pancreas, Pierreux *et al.* modulated levels of VEGF-A, a major regulator of blood vessel development, to show that epithelial production of VEGF-A determines the spatial organisation of EC which, in turn, limits acinar differentiation of the epithelium (Pierreux et al., 2010). Common to both of these studies was the obligatory requirement of the blood vascular network to ensure correct differentiation and architecture of the epithelia in these branched organs. Work by Rossiter *et al.* suggests that a similar mechanism of epithelial-endothelial cross-talk also exists in the mammary gland. In this study, *Vegfa* was inactivated in mammary epithelial cells, resulting in perturbed blood microvasculature architecture; not only were these vessels less abundant, less branched and less convoluted, they failed to retain their proximity to the alveoli and displayed signs of reduced permeability (Rossiter et al., 2007). Furthermore, inactivation of *Vegfa* in the mammary epithelium resulted in inadequate lobuloalveologenesis and epithelial differentiation during lactation, demonstrating that by regulating vascular density and function during lactation, *Vegfa* is crucial for proper mammary gland epithelial differentiation and milk production (Rossiter et al., 2007). Given that in the mammary gland, we established that lymphatic vessels are intimately associated with the ductal epithelium, the exciting

possibility exists that this complex interplay is also present between mammary epithelial cells and LEC and is likely mediated via epithelial expression of VEGF-C and/or VEGF-D. However, given that we observed no overt perturbations in epithelial architecture or lymphatic vessel patterning, and more importantly that lymphatic vessels remained intimately associated with mammary ducts in *Vegfd*^{-/-} virgin (Figure 4.13F,H) and pregnant (Figure 4.14B,D,F,H) mouse mammary glands, we would conclude that VEGF-D is not the sole regulator mediating epithelial-endothelial signalling in the postnatal mouse mammary gland. Our data demonstrating that *Vegfd* is dispensable for lymphangiogenesis in the postnatal mouse mammary gland is in accordance with previous work demonstrating a non-requisite role for endogenous *Vegfd* in settings of physiological lymphangiogenesis in mice during development (Baldwin et al., 2005; Haiko et al., 2008; Koch et al., 2009; Ny et al., 2008), postnatal life and adulthood (Koch et al., 2009). Alternatively, due to high structural homology (Achen et al., 1998) and functional redundancy (Haiko et al., 2008) between the lymphangiogenic growth factors, VEGF-C and VEGF-D, it is conceivable that endogenous levels of VEGF-C are adequate to completely compensate for the loss of *Vegfd* and sustain normal growth and patterning of lymphatic vessels in *Vegfd*^{-/-} postnatal mouse mammary glands. It will therefore be necessary to investigate levels of VEGF-C at the mRNA and protein level in *Vegfd*^{-/-} mouse mammary glands. In addition, we could analyse lymphatic vessel patterning in the mammary glands of mice which have epithelial cell-specific deletion of *Vegfc* or both *Vegfc* and *Vegfd*. Together, these studies will assist in clarifying whether VEGF-C and VEGF-D act in concert to orchestrate lymphatic vascular remodelling in the postnatal mouse mammary gland.

4.5 CONCLUSION

Data presented in this chapter provides convincing evidence that lymphatic vascular remodelling in the postnatal mouse mammary gland is under the regulatory control of lymphangiogenic signals produced by mammary myoepithelial cells in response to hormone signalling events; rather than via a direct mechanism mediated by estrogen and progesterone binding to cognate receptors expressed in LEC. This is evidenced by a lack of detectable expression of ER α and PR by lymphatic vessels in the mouse mammary gland, together with dynamic regulation of the expression of pro-lymphangiogenic growth factors by mammary epithelial cells. We also demonstrated that *Vegfc* and *Vegfd* mRNA levels were significantly increased at an early stage of pregnancy relative to virgin and late pregnant stages and that proteolytically-processed, active VEGF-D was expressed selectively in pregnant, but not virgin mouse mammary glands. Furthermore, we demonstrated that a tyrosine kinase inhibitor specific for VEGFR-3 (Kirkin et al., 2001; Kirkin et al., 2004), the principal receptor for mouse VEGF-D, but not VEGFR-2

(Fong et al., 1999), significantly blocked the proliferation of primary dermal LEC stimulated by mammary gland CM *ex vivo*. Collectively, these data suggest that VEGF-C and VEGF-D are likely to play key roles in the stimulation of lymphangiogenesis during pregnancy in the postnatal mouse mammary gland. Current work aims to further define the identity and source of additional lymphangiogenic signals that drive lymphatic vascular growth and remodelling during postnatal mouse mammary gland morphogenesis. This possibility is further addressed in Chapter 5.

CHAPTER 5

Microarray analysis of isolated mammary gland cell populations

5.1 INTRODUCTION

Whilst epithelial and blood vascular remodelling in the mouse mammary gland has been well documented, the growth and remodelling of lymphatic vessels has received little such attention. The identity and source of stimuli that drive lymphangiogenesis in the mouse mammary gland during development and disease is even more poorly understood. The data presented in Chapters 3 and 4 of this thesis provide compelling evidence that lymphatic vascular remodelling in the postnatal mouse mammary gland is likely to be regulated by lymphangiogenic signals produced by mammary epithelial cells in response to hormone signalling events, rather than by estrogen and progesterone binding directly to receptors expressed by LEC.

In order to gain further insight into the signals that regulate the dynamic growth and remodelling of the lymphatic vasculature during mammary gland morphogenesis, together with their respective cellular sources, we developed a complex fluorescence-activated cell sorting (FACS)-based protocol to isolate discrete populations of luminal epithelial, myoepithelial, endothelial and haematopoietic cells from the mammary fat pads of virgin and pregnant female mice. The aim of this chapter was to characterise the gene expression profiles of these isolated mammary gland cell populations via microarray analysis, in order to identify genes potentially involved in the regulation of lymphangiogenesis and/or angiogenesis in the postnatal mouse mammary gland.

5.2 METHODS

5.2.1 Mammary gland FACS

5.2.1.1 Cell labelling

Single-cell suspensions were isolated from the left and right inguinal mammary fat pads harvested from 10 x 8 week virgin and 2-4 x 16.5 day pregnant female mice (section 2.2.5.1). Cells were resuspended in 500 μ l HHF (HBSS containing 10mM HEPES and 5% (v/v) FBS) and Fc receptors were blocked on ice for 30 minutes with 50 μ g of mouse gamma globulin (Jackson ImmunoResearch Laboratories, Inc., West Grove, PA) per 10⁶ cells. Following blocking, cells were aliquoted into chilled polypropylene round-bottom tubes, using 2.5-5x10⁴ cells per control and the remaining cells (in the range of 1-5x10⁶) for sorting, with reaction volumes made up to 100 μ l using HHF. Controls consisted of unstained Fc-blocked

cells and single-stain controls for each fluorophore to enable compensation to be performed. Cells were labelled for 30 minutes in the dark on ice using phycoerythrin (PE)/Cy7 rat anti-mouse CD31 (BioLegend), PE/Cy5 rat anti-mouse CD24 (BioLegend), Alexa Fluor® 647 rat anti-mouse CD45 (BioLegend) and Alexa Fluor® 647 rat anti-mouse F4/80 (Invitrogen) all at a concentration of 0.25µg per 10⁶ cells, in combination with Alexa Fluor® 700 hamster anti-mouse/rat CD29 (BioLegend) at 0.5µg per 10⁶ cells. Unbound antibodies were removed via washing twice with 2ml HHF and pelleting cells at 300 x g for 5 minutes. Labelled cells were resuspended in HHF containing 3% (v/v) FBS at a concentration of 2x10⁶ cells per ml and stored temporarily on ice and in the dark, to avoid photo-bleaching, until sorting.

5.2.1.2 Flow cytometry

The sorting approach employed in this study was based on the use of similar cell-surface markers to those used in a previously established protocol by Shackleton *et al.* to isolate mammary epithelial and stem cells (Shackleton *et al.*, 2006). Labelled cells were sorted on a BD FACSAria flow cytometer (BD Biosciences, San Jose, CA). Subsequent data analysis was performed using BD FACSDiVa software (BD Biosciences). The complex four-way gating strategy employed to isolate enriched populations of cells from the mouse mammary gland is depicted in Table 5.1 and is described in more detail in section 5.3.1. Sorted cells were collected into microcentrifuge tubes containing PBS supplemented with 50% (v/v) FBS and stored on ice.

5.2.2 RNA isolation

Due to low numbers of cells isolated from virgin mammary glands, total RNA was isolated from each sorted population using RNAqueous®-Micro *Micro Scale RNA Isolation Kit* (Ambion) as per the manufacturer's instructions. Briefly, cells were pelleted in microcentrifuge tubes following FACS at 300 x g for 5 minutes, followed by complete removal of the supernatant and lysis via vigorous vortexing of the cell pellet in 100µl of Lysis Solution. The lysates were mixed with 50µl of 100% (v/v) ethanol, loaded onto a micro filter cartridge assembly and centrifuged at 16,000 x g for 30 seconds. The filter was then washed with 180µl Wash Solution 1, centrifuged at 16,000 x g for 30 seconds, washed twice with 180µl Wash Solution 2/3 and centrifuged at 16,000 x g for 30 seconds. The flow-through was discarded and samples centrifuged for 1 minute at 16,000 x g to remove any residual liquid. The filter was transferred to a micro elution tube and the bound RNA was eluted via the addition of 5-10µl of Elution Solution (pre-heated to 75°C) directly to the centre of the filter, incubated at RT for 1 minute, prior to centrifugation at

CELL POPULATION	CD45 / F4/80	CD31	CD24	CD29
<i>Haematopoietic cells</i>	+	/	/	/
<i>Endothelial cells</i>	-	+	/	/
<i>Luminal epithelial cells</i>	-	-	+	low
<i>Myoepithelial cells</i>	-	-	+	high

Table 5.1 - FACS gating strategy used to isolate enriched populations of cells from the mouse mammary gland.

16,000 x g for 30 seconds. This step was repeated using a second application of an equal volume of Elution Solution.

5.2.2.1 DNase inactivation

In order to remove trace amounts of contaminating genomic DNA before proceeding with RNA amplification, RNA samples were immediately treated with DNase I using the RNAqueous®-Micro *Micro Scale RNA Isolation Kit* (Ambion). 1/10th volume 10x DNase I Buffer and 1 µl (2U) of DNase I was added to the eluted RNA and incubated for 20 minutes at 37°C. Following incubation, 2 µl of DNase Inactivation Reagent was added, mixed well and the reaction stored at RT for 2 minutes, followed by pelleting the DNase Inactivation Reagent for 1.5 minutes at 16,000 x g. RNA was transferred to a clean microcentrifuge tube and stored at -70°C.

5.2.3 Determination of isolated cell population purity

Prior to microarray analysis, the purity of isolated mammary gland cell populations was verified using real-time RT-PCR (section 2.2.1.3-4). Total RNA used to synthesise first-strand cDNA for this analysis was isolated as per section 5.2.2, with the exclusion of the DNase inactivation step (section 5.2.2.1). The following genes, characteristic for each cell population isolated, were used as a measure of population purity; *Pecam1* (EC), *Ptprc* (haematopoietic cells), *Krt18* (luminal epithelial cells) and *Acta2* (myoepithelial cells). Primers used for these analyses are listed in Table 2.3.

5.2.4 Assessment of RNA quantity and quality

Following verification of the purity of isolated mammary gland cell populations, RNA concentration and quality was assessed on an Agilent 2100 Bioanalyser (Agilent Technologies, Inc., Santa Clara, CA) using a RNA 6000 Pico Chip (Agilent Technologies). Only samples that achieved a high RNA Integrity Number (RIN) score, on a scale of 1 to 10, with a RIN score of 10 indicating RNA of the highest quality, were used for subsequent amplification. Samples that met this requirement, achieving a RIN score between 7.6 and 9.9, were selected from three independent experiments for microarray profiling.

5.2.5 Generation of samples for microarray analysis

The subsequent procedures were performed following treatment of surfaces and equipment with RNase AWAY® (Invitrogen) and using ART® aerosol resistant filter tips (Molecular BioProducts). All thermal cycling was performed in an Eppendorf Mastercycler (Eppendorf).

5.2.5.1 RNA amplification

RNA amplification, to generate amplified cDNA, was performed using WT-Ovation™ Pico RNA Amplification System version 1.0 (NuGEN Technologies, Inc., San Carlos, CA), according to the manufacturer's specifications. 500pg of total RNA was used for first-strand cDNA synthesis. Briefly, 5µl (500pg) of input RNA was combined with 2µl First Strand Primer Mix and incubated at 65°C in a pre-warmed thermal cycler for 2 minutes and then cooled to 4°C. Samples were mixed with 3µl of first-strand master mix (5:1 mix of First Strand Buffer Mix and First Strand Enzyme Mix) and then incubated for 1 minute at 4°C, 10 minutes at 25°C, 10 minutes at 42°C, 15 minutes at 70°C and cooled to 4°C, prior to proceeding immediately with second-strand cDNA synthesis. 10µl of second-strand master mix (39:1 mix of Second Strand Buffer Mix and Second Strand Enzyme Mix) was added, mixed and then cycled for 1 minute at 4°C, 10 minutes at 25°C, 30 minutes at 50°C, 5 minutes at 70°C and cooled to 4°C, prior to continuing immediately with purification of the unamplified cDNA. 50ng of yeast tRNA (Ambion) was added as a carrier to each reaction before purification using Agencourt RNAClean® beads (Agencourt, Agencourt Bioscience Corporation, San Diego, CA). 32µl of bead suspension was added to each reaction, mixed via pipetting up and down 10 times and then incubated at RT for 10 minutes. Tubes were transferred to an Agencourt SPRIPlate® 96R-Ring Magnet Plate (Agencourt) for 5 minutes, where the magnetic beads formed a ring around the inner walls of the tubes. With the tubes remaining on the magnetic plate, 200µl of freshly prepared 80% (v/v) ethanol was added and allowed to settle before its removal. Washing with ethanol was repeated twice more. The samples were then left to air-dry for 15 minutes before proceeding with SPIA™ amplification. With the purified cDNA still bound to the dry beads, 160µl of the SPIA™ master mix (2:1:1 mix of SPIA™ Buffer Mix, SPIA™ Primer Mix and SPIA™ Enzyme Mix) was added to each sample, ensuring complete mixing to elute the cDNA from the beads. Samples were then split into 2 separate 0.2ml microcentrifuge tubes and incubated for 1 minute at 4°C, 1 hour at 47°C, 5 minutes at 95°C and cooled to 4°C before recombining the half-reactions. The samples were subsequently returned to the magnetic plate and left to stand for 5 minutes, prior to the removal of the cleared supernatant containing the eluted cDNA to a new 0.2ml microcentrifuge tube.

5.2.5.2 Purification of amplified cDNA

The resulting amplified cDNA was purified using Zymo Research DNA Clean & Concentrator-25™ (Zymo Research, Zymo Research Corporation, Irvine, CA), with modifications to the manufacturer's instructions. 320µl of DNA Binding Buffer was mixed with the resultant 160µl of amplified SPIA™ cDNA product in a new microcentrifuge tube. This mixture was loaded onto a Zymo-Spin™ Column and centrifuged at 16,000 x g for 30 seconds. Flow-through was discarded and columns were washed twice with 200µl 80% (v/v) ethanol and centrifuged at 16,000 x g for 30 seconds. Columns were placed in new microcentrifuge tubes and 30µl DEPC-treated MQ-H₂O was added directly to the centre of each column. Columns were incubated at RT for 1 minute, prior to elution of the purified amplified cDNA via centrifugation for 1 minute at 16,000 x g. Purified cDNA was stored at -20°C. The cDNA product yield and purity was determined using the single-stranded DNA setting on a NanoDrop™ 1000 spectrophotometer and version 3.7 software (NanoDrop Technologies).

5.2.5.3 Generation and purification of ST-cDNA

Sense transcript (ST)-cDNA, suitable for hybridisation to GeneChip® Mouse Gene 1.0 ST arrays (Affymetrix, Santa Clara, CA), was generated using WT-Ovation™ Exon Module version 1.0 (NuGEN Technologies) according to the manufacturer's instructions. Briefly, 3µg of purified cDNA (from section 5.2.5.2) was combined with 6µl Primer Mix and incubated for 5 minutes at 95°C and cooled to 4°C, prior to the addition of ST-cDNA master mix (38µl Buffer Mix and 6µl Enzyme Mix). Samples were thoroughly mixed via pipetting up and down 8-10 times and thermally cycled for 1 minute at 4°C, 10 minutes at 30°C, 1 hour at 42°C, 10 minutes at 75°C and cooled to 4°C. The resulting ST-cDNA was purified with a Zymo Research DNA Clean & Concentrator-25™ (Zymo Research), as previously described in section 5.2.5.2, using 200µl of DNA Binding Buffer mixed with the above 70µl ST-cDNA reaction. The ST-cDNA product yield and purity was subsequently determined using the single-stranded DNA setting on a NanoDrop™ 1000 spectrophotometer and version 3.7 software (NanoDrop Technologies).

5.2.5.4 Fragmentation and biotin-labelling of ST-cDNA

Fragmentation and subsequent biotin-labelling of single-stranded ST-cDNA to generate targets suitable for hybridisation to GeneChip® Mouse Gene 1.0 ST arrays (Affymetrix) was performed using FL-Ovation™ cDNA Biotin Module version 2.0 (NuGEN Technologies) according to the manufacturer's

instructions. In brief, 5µg per reaction of input ST-cDNA was combined with 7µl fragmentation master mix (5:2 mix of Fragmentation Buffer Mix and Fragmentation Enzyme Mix), mixed via pipetting and placed into a pre-warmed thermal cycler for 30 minutes at 37°C, 2 minutes at 95°C and cooled to 4°C, prior to proceeding immediately with labelling.

For biotin-labelling, 18µl of labelling master mix (10:1:1 mix of Labelling Buffer Mix, Labelling Reagent and Labelling Enzyme Mix) was added to each fragmented cDNA sample tube, mixed and placed into a pre-warmed thermal cycler for 1 hour at 37°C, 10 minutes at 70°C and cooled to 4°C. The fragmented and biotin-labelled cDNA was submitted to the Adelaide Microarray Centre (Adelaide, Australia) and stored at -20°C prior to array hybridisation.

5.2.6 Microarray data analysis

Samples were submitted to the Adelaide Microarray Centre (Adelaide, Australia) and hybridised to GeneChip® Mouse Gene 1.0 ST arrays (Affymetrix) for gene expression profiling. Microarray data analysis was performed using Partek Genomics Suite™ version 6.4 software (Partek Incorporated, St. Louis, MO). Differential gene expression was assessed by one-way ANOVA, with *P*-values adjusted for multiple testing using a step-up false discovery rate correction (Benjamini and Hochberg, 1995).

5.3 RESULTS

5.3.1 FACS gating strategy optimisation

Owing to the fact that the mammary gland comprises a heterogeneous mix of cell types, high levels of cellular autofluorescence were detected in the same emission range as that of the fluorophores, fluorescein isothiocyanate (FITC) (green) and PE (orange) (data not shown). In order to dramatically improve the signal-to-noise ratio and minimise autofluorescence, fluorophores for FACS isolation were selected with a longer emission wavelength in the far-red region of the electromagnetic spectrum, with as minimal spectral overlap as possible. The fluorophores chosen included: the tandem dye conjugates PE/Cy7 and PE/Cy5, Alexa Fluor® 647 and Alexa Fluor® 700, which were directly conjugated to the specific cell surface markers CD31, CD24, CD45 and F4/80 and CD29, respectively. Due to all four fluorophores emitting in a similar defined region of the electromagnetic spectrum, compensation was reasonably complicated, despite its automation (data not shown).

Labelled cells were fractionated from both 8 week virgin (Figure 5.1) and 16.5 day pregnant (Figure 5.2) mammary fat pads in an identical manner. Data analysis was performed on the live cell gate from freshly isolated mammary gland cell suspensions (Figure 5.1A; Figure 5.2A). The substantial haematopoietic cell fraction, including macrophages, was isolated on the basis of positive expression for the macrophage marker, F4/80, and/or the haematopoietic marker, CD45 (Figure 5.1D; Figure 5.2D). EC, encompassing both LEC and BEC, were selected on the basis of positive CD31 expression (Figure 5.1B; Figure 5.2B), followed by gating to exclude CD45-positive haematopoietic cells and F4/80-positive macrophages (Figure 5.1C; Figure 5.2C). Epithelial cells were gated to exclude any residual cells expressing CD31 (Figure 5.1E; Figure 5.2E), CD45 or F4/80 (Figure 5.1F; Figure 5.2F), followed by positive selection using CD24 and differential expression of CD29; luminal epithelial cells are CD24-positive/CD29^{low}, whilst mature myoepithelial cells are CD24-positive/CD29^{high} (Figure 5.1G; Figure 5.2G) (Shackleton et al., 2006). Typical cell yields from these isolations are represented in Table 5.2.

5.3.2 Assessment of the purity of isolated mammary gland cell populations

To ascertain purity of the isolated mammary gland cell populations prior to the selection of samples for microarray analysis, real-time RT-PCR was performed on two independent biological samples of each cell population from both virgin and pregnant stages. The result from one such analysis is represented in Figure 5.3. One gene characteristic of each cell population isolated was chosen for analysis and real-time RT-PCR primers were designed accordingly (section 2.2.1.4 and Table 2.3). EC identity was investigated using *Pecam1* (encoding CD31), a commonly used pan-EC marker. *Ptprc*, encoding CD45, was used to determine haematopoietic cell identity. Luminal epithelial cells express high levels of cytokeratin 18 (K18) (Parmar and Cunha, 2004) and thus were assessed by measuring *Krt18* mRNA expression, whilst myoepithelial cells strongly express alpha smooth muscle actin (α SMA) encoded by *Acta2* (Parmar and Cunha, 2004). As expected, *Pecam1* was most highly expressed in the EC populations (Figure 5.3A,B), *Ptprc* in the haematopoietic fractions (Figure 5.3C,D), *Krt18* in the luminal epithelial cell samples (Figure 5.3E,F) and *Acta2* in myoepithelial cells (Figure 5.3G,H) isolated from both virgin and pregnant mammary glands. Despite the extremely complex FACS isolation strategy employed for this study, these data indicate that the isolated populations were highly enriched for the particular cells of interest, with minimal contamination from other cell types.

Figure 5.1 - FACS gating strategy used for the isolation of 8 week virgin mammary gland cell populations.

All live cells were gated as indicated in (A). EC (encompassing both lymphatic and blood EC) were selected on the basis of positive CD31 expression (B) and negativity for both the haematopoietic and macrophage markers, CD45 and F4/80, respectively (C). The haematopoietic population, including macrophages, was isolated simply on the basis of positive expression for F4/80 and/or CD45 (D). The remaining epithelial cells were gated firstly to exclude any residual cells expressing CD31 (E), followed by CD45 and F4/80 (F) and ultimately separated on the basis of their differential CD24 and CD29 expression patterns (G). All gated population percentages reflect the proportion of the preceding parent population. EC - endothelial cells, FACS - fluorescence-activated cell sorting, PE - phycoerythrin.

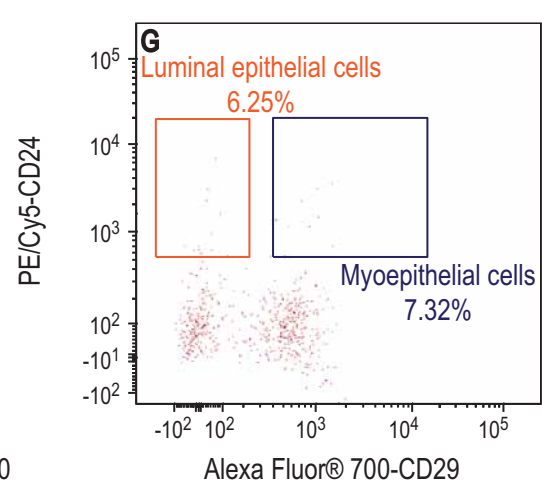
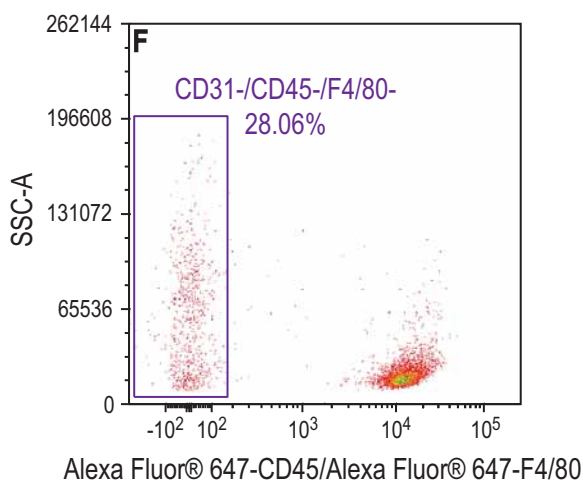
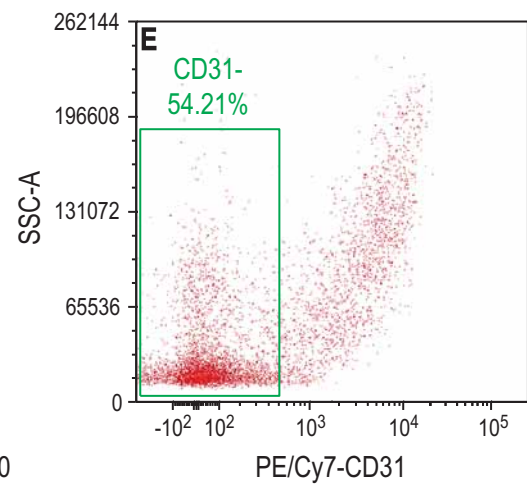
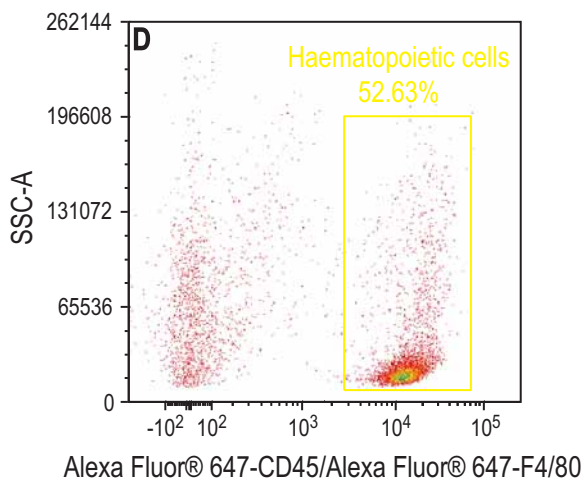
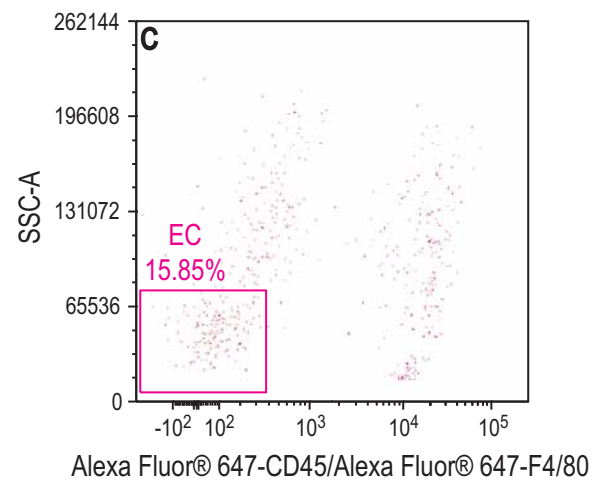
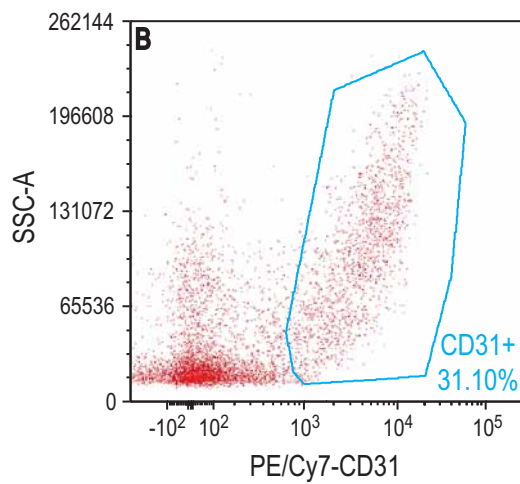
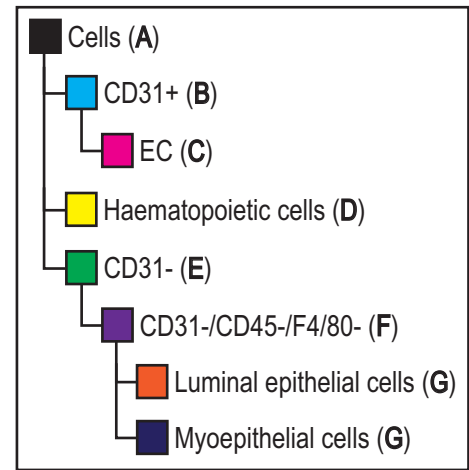
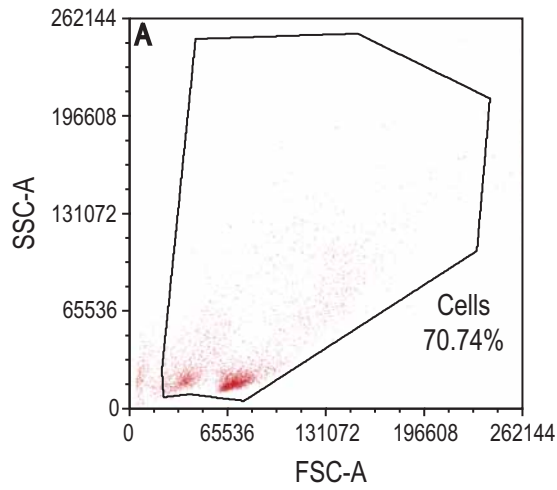
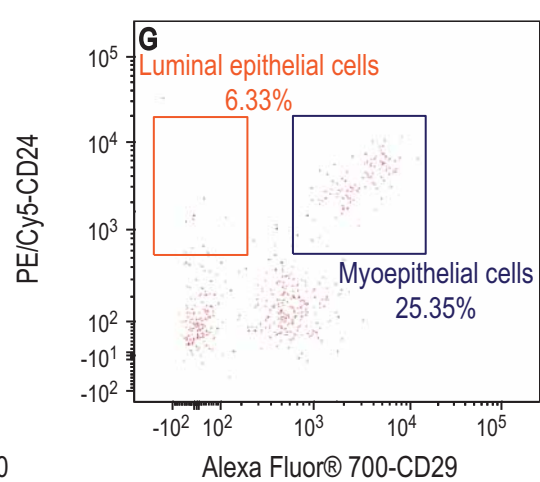
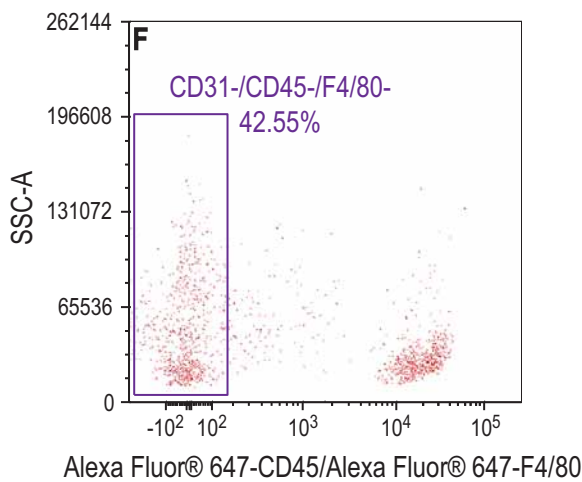
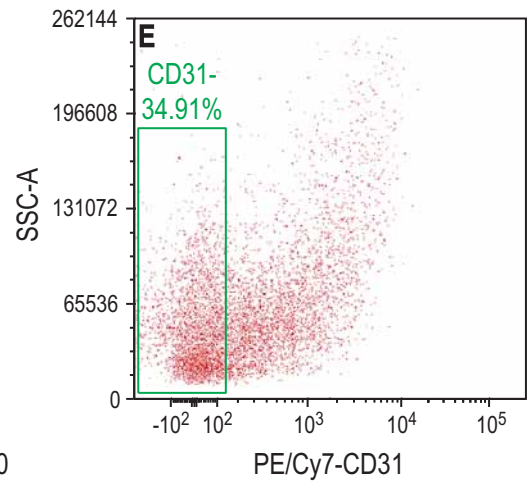
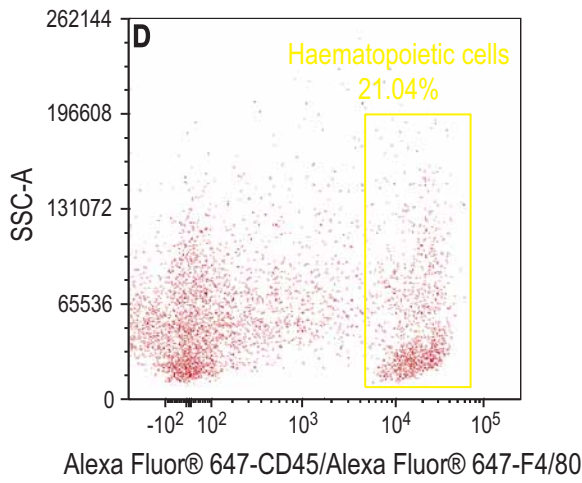
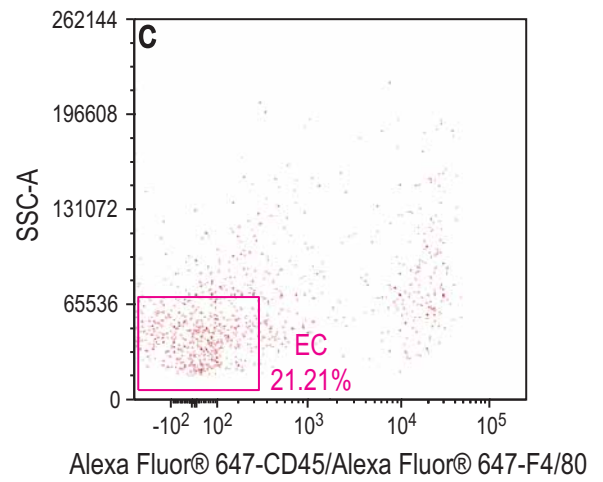
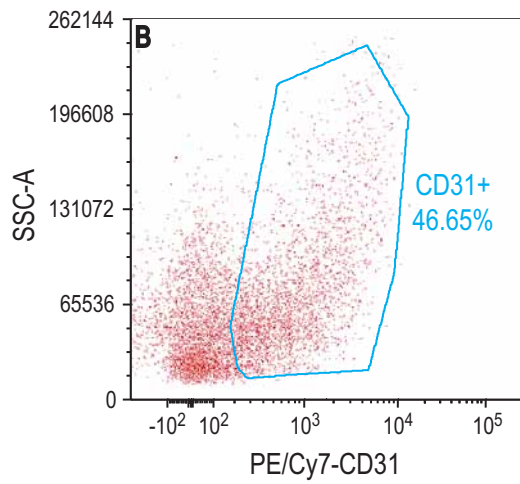
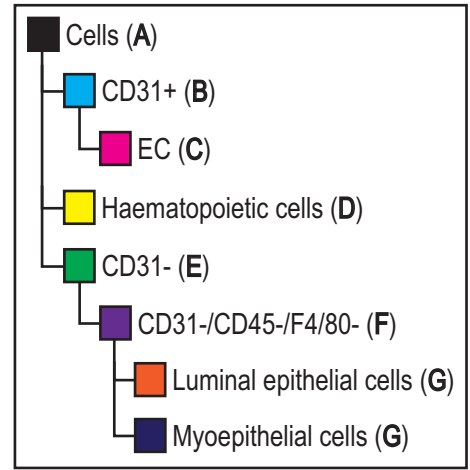
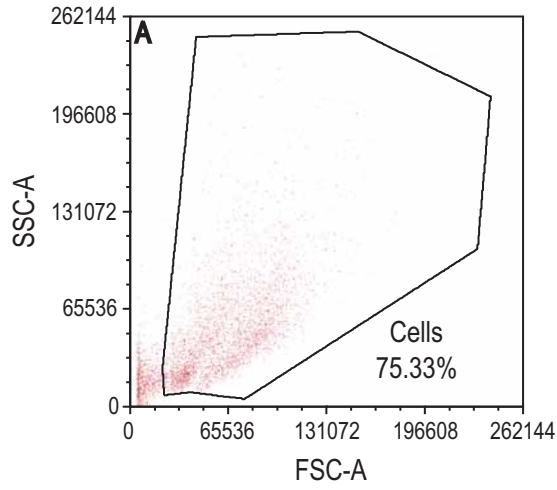


Figure 5.2 - FACS gating strategy used for the isolation of 16.5 day pregnant mammary gland cell populations.

All live cells were gated as indicated in **(A)**. EC (encompassing both lymphatic and blood EC) were selected on the basis of positive CD31 expression **(B)** and negativity for both the haematopoietic and macrophage markers, CD45 and F4/80, respectively **(C)**. The haematopoietic population, including macrophages, was isolated simply on the basis of positive expression for F4/80 and/or CD45 **(D)**. The remaining epithelial cells were gated firstly to exclude any residual cells expressing CD31 **(E)**, followed by CD45 and F4/80 **(F)** and ultimately separated on the basis of their differential CD24 and CD29 expression patterns **(G)**. All gated population percentages reflect the proportion of the preceding parent population. EC - endothelial cells, FACS - fluorescence-activated cell sorting, PE - phycoerythrin.



	8 WEEK VIRGIN	16.5 DAY PREGNANT
<i>Number of mice</i>	10	2-4
<i>Number of inguinal fat pads</i>	20	4-8
<i>Starting cell suspension</i>	1.5-2.5x10 ⁶ cells	3.5-5.5x10 ⁶ cells
<i>Haematopoietic cells</i>	>5x10 ⁵	>5x10 ⁵
<i>Endothelial cells</i>	5x10 ⁴ -1x10 ⁵	1.5x10 ⁵ -2.5x10 ⁵
<i>Myoepithelial cells</i>	1x10 ⁴ -2x10 ⁴	2x10 ⁵ -4x10 ⁵
<i>Luminal epithelial cells</i>	5x10 ³ -1.5x10 ⁴	1x10 ⁵ -2.5x10 ⁵

Table 5.2 - A comparison of cell yields following FACS of virgin and pregnant mouse mammary glands.

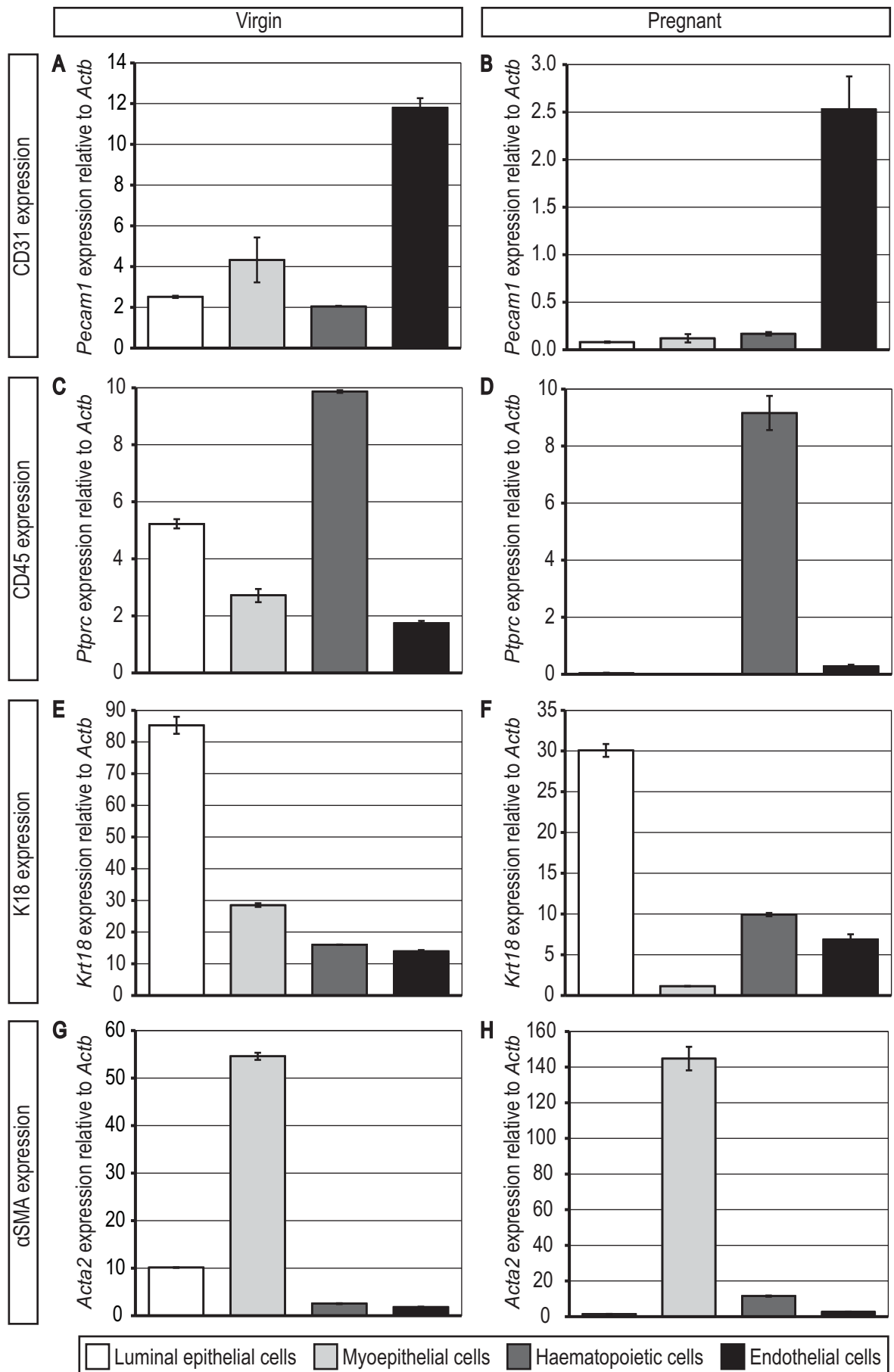


Figure 5.3 - Assessment of isolated mammary gland cell population purity.

Real-time RT-PCR was used to assess the purity of isolated mammary gland cell populations from virgin (A,C,E,G) and pregnant (B,D,F,H) female mice. Error bars represent the mean \pm standard deviation of technical replicates. Data is normalised to the house-keeping gene, *Actb*, and is representative of two independent experiments. α SMA - alpha smooth muscle actin, K18 - cytokeratin 18, RT-PCR - reverse transcription-polymerase chain reaction.

5.3.3 Microarray analyses

With the ultimate aim of identifying novel genes involved in mammary gland lymphangiogenesis and angiogenesis, we performed gene expression profiling using GeneChip® Mouse Gene 1.0 ST arrays (Affymetrix), comparing enriched populations of endothelial, haematopoietic, luminal epithelial and myoepithelial cells in 8 week virgin and 16.5 day pregnant mammary glands. Due to limiting cell yields following FACS in isolated virgin epithelial populations, generating a meagre 1-3ng of total cellular RNA, a method for the robust amplification of total cellular RNA was necessary to circumvent the minimal requirement of 100ng of total cellular RNA for array hybridisation. The WT-Ovation™ Pico RNA Amplification System version 1.0 (NuGEN Technologies), enabling microgram quantities of cDNA to be amplified from as little as 500pg of total cellular RNA, was employed and combined with WT-Ovation™ Exon Module version 1.0 (NuGEN Technologies) and FL-Ovation™ cDNA Biotin Module version 2.0 (NuGEN Technologies) to generate sufficient quantities of fragmented and biotin-labelled cDNA for hybridisation to GeneChip® Mouse Gene 1.0 ST arrays (Affymetrix). Without such RNA amplification measures, the microarray analyses described herein would not have been feasible. To ensure that the RNA was of a high quality, with little or no evidence of degradation and free of contaminants, RNA quality was assessed prior to RNA amplification using an Agilent 2100 Bioanalyser (Agilent Technologies) (section 5.2.4) and only samples that achieved a high RIN score (ie. ≥ 7.6) were used for microarray profiling analyses.

Principal component analysis (PCA) was used to demonstrate the degree of relatedness among the three biological replicates for each cell fraction, at each developmental stage (Figure 5.4). The majority of data sets displayed tight clustering, however, the data sets denoted 'LV1' (virgin luminal epithelial cells) (Figure 5.4C) and 'MV1' (virgin myoepithelial cells) (Figure 5.4D) appeared as potential outliers, based on the failure of these samples to cluster with the remaining two biological replicates. These samples were therefore excluded from further data analyses. Microarray data analysis was performed at the Adelaide Microarray Centre (Adelaide, Australia) (section 5.2.6). The top 40 most significantly and differentially expressed genes between virgin and pregnant cell populations are listed in Table 5.3 (EC), Table 5.4 (haematopoietic cells), Table 5.5 (luminal epithelial cells) and Table 5.6 (myoepithelial cells).

Based on our finding that lymphatic vessel density is increased in pregnancy, together with the observation that lymphatic vessels are intimately associated with epithelial ducts in the mouse mammary gland, we also compared gene expression profiles between pregnant luminal and myoepithelial cell populations, in an attempt to uncover lymphangiogenic and/or angiogenic growth

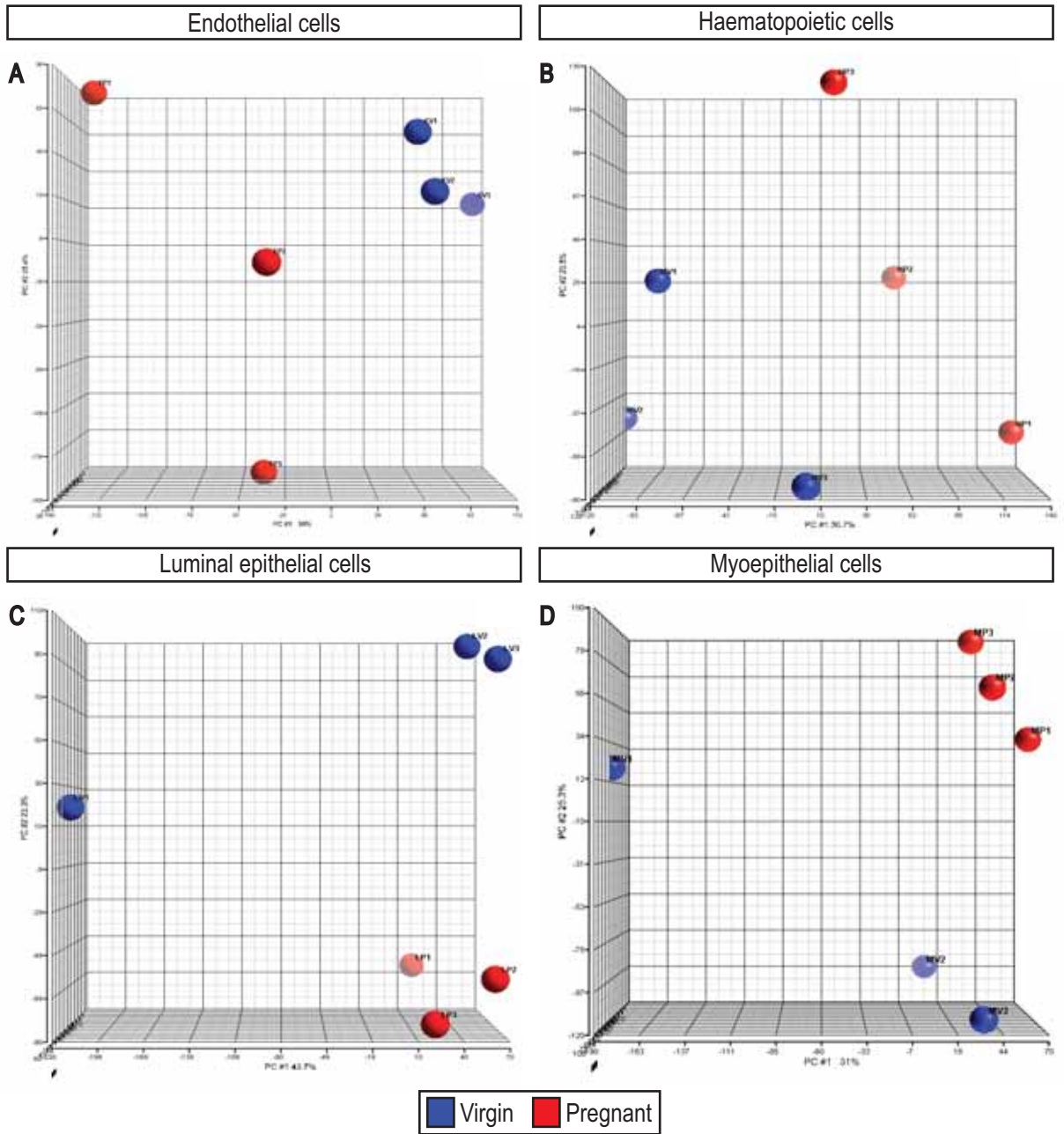


Figure 5.4 - Principal component analysis plots.

Principal component analysis plots demonstrating the clustering of data sets used for microarray analysis; endothelial cells (A), haematopoietic cells (B), luminal epithelial cells (C) and myoepithelial cells (D).

NO.	GENE SYMBOL	STEP-UP P-VALUE	FOLD CHANGE (PREGNANT RELATIVE TO VIRGIN)
1	<i>ENSMUSG00000075582</i>	0.006	2.4 ↑
2	<i>Cited1</i>	0.006	7.0 ↓
3	<i>Rasgrf1</i>	0.006	5.0 ↓
4	<i>Pigr</i>	0.006	7.2 ↑
5	<i>Cyp3a57</i>	0.006	30.5 ↓
6	<i>Fgb</i>	0.016	49.2 ↓
7	<i>Cldn10</i>	0.017	10.5 ↓
8	<i>Bfk</i>	0.017	37.8 ↑
9	<i>Olah</i>	0.017	28.7 ↑
10	<i>Anxa1</i>	0.017	2.4 ↓
11	<i>Thrsp</i>	0.017	3.6 ↑
12	<i>Gfpt2</i>	0.019	10.0 ↓
13	<i>Gjb2</i>	0.019	12.2 ↑
14	<i>Lao1</i>	0.019	7.8 ↑
15	<i>5430419D17Rik</i>	0.019	1.4 ↓
16	<i>Fasn</i>	0.021	2.8 ↑
17	<i>Expi</i>	0.021	2.4 ↑
18	<i>BC029169</i>	0.021	9.0 ↑
19	<i>Indo</i>	0.029	13.6 ↓
20	<i>Cd79b</i>	0.030	1.5 ↓
21	<i>Wap</i>	0.032	22.3 ↑
22	-	0.033	1.5 ↑
23	<i>Elf5</i>	0.033	11.9 ↑
24	<i>Slc28a3</i>	0.033	9.0 ↑
25	<i>Slc7a2</i>	0.033	8.1 ↓
26	<i>Impa2</i>	0.033	1.7 ↑
27	<i>Mtmr7</i>	0.033	6.5 ↓
28	<i>Cxcl15</i>	0.033	43.2 ↓
29	<i>Adam10</i>	0.033	2.6 ↓
30	<i>Atp13a3</i>	0.033	2.2 ↓
31	<i>Chpt1</i>	0.033	2.9 ↑
32	<i>Kif5c</i>	0.033	2.3 ↓
33	<i>Grina</i>	0.036	1.9 ↓
34	<i>Atp6v1c2</i>	0.036	6.5 ↑
35	<i>Gcnt2</i>	0.036	3.5 ↓
36	<i>Tnc</i>	0.036	1.7 ↑
37	<i>Rbm35a</i>	0.036	2.2 ↑
38	<i>Slc12a2</i>	0.038	4.1 ↓
39	<i>Tmed3</i>	0.038	2.6 ↓
40	<i>ENSMUSG00000074421</i>	0.038	2.9 ↓

Table 5.3 - Top 40 differentially expressed genes between endothelial cells in virgin and pregnant mouse mammary glands.

NO.	GENE SYMBOL	STEP-UP P-VALUE	FOLD CHANGE (PREGNANT RELATIVE TO VIRGIN)
1	<i>Csn2</i>	0.001	115.7 ↑
2	<i>Csn1s2a</i>	0.027	108.4 ↑
3	<i>Csn1s1</i>	0.042	196.0 ↑
4	<i>Cadm1</i>	0.054	2.9 ↑
5	<i>Mcoln1</i>	0.054	1.5 ↓
6	<i>Aff1</i>	0.059	1.4 ↓
7	<i>H2Ob</i>	0.076	5.5 ↓
8	<i>Aff4</i>	0.099	1.4 ↓
9	<i>2310007B03Rik</i>	0.116	1.2 ↑
10	<i>Cmah</i>	0.116	5.1 ↓
11	<i>EG434094</i>	0.175	1.2 ↓
12	<i>Rspo1</i>	0.175	2.9 ↑
13	<i>Serbp1</i>	0.175	1.1 ↑
14	<i>Clip4</i>	0.178	3.0 ↓
15	<i>Vldlr</i>	0.180	3.9 ↑
16	<i>Pecam1</i>	0.192	4.0 ↓
17	<i>A530032D15Rik</i>	0.200	1.6 ↓
18	<i>Igh6</i>	0.201	1.5 ↓
19	<i>Hebp1</i>	0.201	3.4 ↑
20	<i>Lama1</i>	0.201	2.8 ↑
21	<i>EG633457</i>	0.201	2.8 ↓
22	<i>Cenpe</i>	0.201	2.8 ↑
23	<i>Itgb5</i>	0.201	2.8 ↑
24	<i>Hells</i>	0.201	2.5 ↑
25	<i>Dmx11</i>	0.201	1.9 ↓
26	<i>Tacc3</i>	0.201	2.0 ↑
27	<i>Ptn</i>	0.201	10.1 ↓
28	<i>LOC100043385</i>	0.201	1.7 ↑
29	<i>Lpcat2</i>	0.201	4.1 ↑
30	-	0.201	1.2 ↓
31	<i>Cldn3</i>	0.201	2.6 ↑
32	<i>Krt23</i>	0.201	7.8 ↑
33	<i>Mki67</i>	0.201	2.2 ↑
34	<i>Kif20b</i>	0.201	2.5 ↑
35	<i>Mc1r</i>	0.201	1.3 ↓
36	<i>Gm484</i>	0.201	1.2 ↓
37	<i>Fcer2a</i>	0.201	10.3 ↓
38	<i>Galnt4</i>	0.201	2.8 ↑
39	<i>Slc39a12</i>	0.201	1.3 ↓
40	<i>4933407H18Rik</i>	0.201	1.4 ↓

Table 5.4 - Top 40 differentially expressed genes between haematopoietic cells in virgin and pregnant mouse mammary glands.

NO.	GENE SYMBOL	STEP-UP P-VALUE	FOLD CHANGE (PREGNANT RELATIVE TO VIRGIN)
1	<i>Acs1</i>	0.048	10.6 ↑
2	<i>Csn1s1</i>	0.048	313.4 ↑
3	<i>Csn1s2a</i>	0.048	154.4 ↑
4	<i>Crabp2</i>	0.060	3.5 ↑
5	<i>Cnn3</i>	0.060	2.6 ↓
6	<i>Mpp7</i>	0.060	1.7 ↓
7	<i>Xbp1</i>	0.084	2.8 ↑
8	<i>Fabp3</i>	0.084	55.9 ↑
9	<i>Csn2</i>	0.084	113.5 ↑
10	<i>St5</i>	0.084	3.7 ↑
11	<i>Frmd6</i>	0.084	1.7 ↑
12	<i>Bank1</i>	0.084	10.1 ↓
13	<i>Ubd</i>	0.084	9.8 ↑
14	<i>Acaca</i>	0.084	10.4 ↑
15	<i>Cd3d</i>	0.086	8.7 ↓
16	<i>Tln2</i>	0.086	2.5 ↑
17	<i>Trf</i>	0.088	3.6 ↑
18	<i>Sox5</i>	0.088	2.0 ↑
19	<i>Atp1b2</i>	0.090	1.8 ↓
20	<i>Gjb6</i>	0.090	5.5 ↑
21	<i>Cxcl15</i>	0.090	39.7 ↓
22	<i>DOH4S114</i>	0.090	9.0 ↑
23	<i>Fabp3</i>	0.093	51.7 ↑
24	<i>Pigr</i>	0.093	15.9 ↑
25	<i>Mapkbp1</i>	0.094	1.6 ↑
26	<i>4632419K20Rik</i>	0.094	2.9 ↑
27	<i>Tlr1</i>	0.094	3.0 ↓
28	<i>5730522E02Rik</i>	0.094	1.1 ↑
29	<i>Acs16</i>	0.094	1.2 ↑
30	<i>Abca9</i>	0.094	4.5 ↓
31	<i>Lepr</i>	0.094	2.3 ↓
32	<i>Hmcn1</i>	0.094	5.4 ↓
33	-	0.094	1.8 ↑
34	<i>Glb1l</i>	0.094	1.6 ↓
35	<i>Btla</i>	0.094	2.9 ↓
36	<i>Slc28a3</i>	0.094	23.4 ↑
37	<i>Hif</i>	0.094	3.6 ↑
38	<i>9530008L14Rik</i>	0.094	5.1 ↓
39	<i>Lao1</i>	0.094	47.7 ↑
40	<i>Ii4i1</i>	0.094	1.6 ↓

Table 5.5 - Top 40 differentially expressed genes between luminal epithelial cells in virgin and pregnant mouse mammary glands.

NO.	GENE SYMBOL	STEP-UP P-VALUE	FOLD CHANGE (PREGNANT RELATIVE TO VIRGIN)
1	<i>Lrrc32</i>	0.106	1.8 ↓
2	<i>Gm628</i>	0.106	1.4 ↑
3	<i>Psg20</i>	0.106	1.4 ↑
4	<i>H2afz</i>	0.106	1.3 ↓
5	<i>Ccdc110</i>	0.106	1.4 ↑
6	<i>D14Ert668e</i>	0.115	5.8 ↓
7	<i>Mageb4</i>	0.115	1.1 ↑
8	<i>Gimap5</i>	0.115	3.2 ↓
9	<i>Ankrd1</i>	0.115	3.7 ↓
10	<i>1110018J18Rik</i>	0.115	1.4 ↓
11	<i>Nts</i>	0.115	2.4 ↓
12	<i>Deaf1</i>	0.146	1.7 ↑
13	<i>Scarb1</i>	0.146	3.0 ↓
14	<i>Col22a1</i>	0.146	1.2 ↑
15	<i>Papss2</i>	0.146	3.8 ↓
16	<i>Selp</i>	0.146	10.1 ↓
17	<i>Klf4</i>	0.146	2.0 ↓
18	-	0.146	3.9 ↓
19	<i>Chst3</i>	0.147	1.3 ↑
20	<i>Pdzd7</i>	0.147	2.0 ↑
21	<i>Efhd1</i>	0.184	5.7 ↓
22	<i>D8Ert738e</i>	0.187	1.6 ↓
23	<i>Zmym4</i>	0.198	1.2 ↑
24	<i>Nes</i>	0.198	1.6 ↓
25	<i>Rcan1</i>	0.198	4.2 ↓
26	<i>Mageb18</i>	0.198	1.1 ↓
27	<i>Flna</i>	0.198	1.8 ↑
28	<i>Adnp</i>	0.198	1.3 ↑
29	<i>Olf70</i>	0.198	1.1 ↑
30	<i>Ggt6</i>	0.198	1.3 ↑
31	<i>Art3</i>	0.198	4.9 ↓
32	<i>Ebf1</i>	0.198	14.9 ↓
33	<i>Ptprb</i>	0.198	10.0 ↓
34	<i>Sft2d3</i>	0.198	1.4 ↑
35	<i>5730403B10Rik</i>	0.198	1.4 ↑
36	<i>BC034902</i>	0.198	1.1 ↑
37	<i>Gm6322</i>	0.198	1.3 ↓
38	<i>Ldb2</i>	0.198	7.2 ↓
39	<i>Gm10648</i>	0.198	1.3 ↑
40	<i>Trim30</i>	0.198	7.5 ↓

Table 5.6 - Top 40 differentially expressed genes between myoepithelial cells in virgin and pregnant mouse mammary glands.

factors that are differentially expressed between these epithelial subtypes. The top 40 most significantly and differentially expressed genes from this analysis are listed in Table 5.7.

5.3.4 Validation of microarray data sets

As a means of validating the approach used to isolate discrete cell populations from the mouse mammary gland, we examined our microarray data sets for genes that have an established role in each of the cell types isolated. The restricted expression of genes characteristic of each cell population not only validates the FACS method used for cell isolation, but further strengthens the likelihood that candidate genes are highly enriched specifically in the cell populations of interest.

5.3.4.1 Luminal epithelial cell array

Milk protein genes, the expression of which defines a mature and differentiated luminal epithelial cell (Hennighausen and Robinson, 2005), were found to be massively upregulated in pregnant compared to virgin luminal epithelial cells. Such genes are indicative of the mammary gland's preparation for parturition and the requirement for milk synthesis and secretion to support suckling young. Genes involved in milk production that were increased in expression in luminal epithelial cells isolated from pregnant mice included *Wap* (91.3-fold, $P=0.09$) encoding whey acidic protein and casein genes; *Csn1s1* (313.4-fold, $P<0.05$), *Csn1s2a* (154.4-fold, $P<0.05$) and *Csn2* (113.5-fold, $P=0.08$) (Table 5.5); representing 3 of the top 9 most differentially expressed genes in the luminal epithelial microarray data set. In addition, *Elf5* was increased 12.8-fold ($P=0.13$) in pregnant luminal epithelial cells compared with the same population in the virgin state, consistent with a role for *Elf5* in the specification of secretory alveolar epithelial cell fate (Oakes et al., 2008). The luminal epithelial cell microarray data set therefore accurately reflects luminal epithelial cell-expressed genes.

5.3.4.2 Myoepithelial cell array

The expression levels of VEGF family members in the myoepithelial cell array were consistent with our real-time RT-PCR analyses (Figure 4.4A). *Vegfa* levels were not markedly altered between pregnant and virgin samples (1.1-fold, $P=0.75$), whilst *Vegfc* (1.5-fold, $P=0.48$) and *Vegfd* (4.2-fold, $P=0.44$) were downregulated in pregnant compared to virgin myoepithelial cells. Analysis of gene expression profiles comparing myoepithelial cells isolated from pregnant and virgin mouse mammary glands revealed a handful of differentially expressed genes that have established roles in myoepithelial cells. Nestin, an

NO.	GENE SYMBOL	STEP-UP P-VALUE	FOLD CHANGE (MYOEPIHELUM RELATIVE TO LUMINAL EPITHELIUM)
1	<i>Cacna1g</i>	0.003	2.7 ↑
2	<i>Ehd2</i>	0.006	3.8 ↑
3	<i>Htra1</i>	0.007	14.2 ↑
4	<i>Hmcn1</i>	0.009	30.5 ↑
5	<i>H2-Q8</i>	0.009	4.0 ↓
6	<i>Robo1</i>	0.009	8.7 ↑
7	<i>Hmcn1</i>	0.010	13.9 ↑
8	<i>Dock2</i>	0.010	2.2 ↓
9	<i>Tgfb1i1</i>	0.010	13.1 ↑
10	<i>Muc1</i>	0.010	13.0 ↓
11	<i>D630013G24Rik</i>	0.010	9.3 ↓
12	<i>Mansc1</i>	0.010	4.9 ↓
13	<i>Cnn3</i>	0.010	5.9 ↑
14	<i>Gucy1b3</i>	0.010	5.8 ↑
15	-	0.010	8.4 ↑
16	<i>Inhbb</i>	0.010	3.1 ↓
17	<i>Npr1</i>	0.010	4.5 ↑
18	<i>Hmcn1</i>	0.010	3.5 ↑
19	<i>Jag2</i>	0.010	5.6 ↑
20	<i>Col14a1</i>	0.010	13.0 ↑
21	<i>Sdk1</i>	0.010	3.9 ↑
22	<i>Col11a1</i>	0.010	4.5 ↑
23	<i>App</i>	0.010	2.5 ↑
24	<i>Lama3</i>	0.010	13.6 ↑
25	<i>Chst15</i>	0.010	10.0 ↑
26	<i>Gm13547</i>	0.010	1.3 ↓
27	<i>Sdhaf1</i>	0.010	3.4 ↓
28	<i>Gm3002</i>	0.010	8.3 ↑
29	<i>Gm2897</i>	0.010	8.3 ↑
30	<i>Tead1</i>	0.010	8.5 ↑
31	<i>Bdnf</i>	0.010	3.5 ↑
32	<i>Hhipl2</i>	0.010	7.3 ↓
33	<i>Moxd1</i>	0.010	17.5 ↑
34	<i>Ceacam1</i>	0.010	13.0 ↓
35	<i>Cnn3</i>	0.010	5.7 ↑
36	<i>Csmd1</i>	0.010	2.2 ↑
37	<i>Adamts18</i>	0.010	14.5 ↑
38	<i>Lamb1-1</i>	0.010	9.4 ↑
39	<i>1500015O10Rik</i>	0.010	16.0 ↑
40	<i>Gucy1a3</i>	0.010	10.2 ↑

Table 5.7 - Top 40 differentially expressed genes between myoepithelial and luminal epithelial cells in pregnant mouse mammary glands.

intermediate filament protein, has been documented to be expressed in the myoepithelial cell layer of the human breast (Li et al., 2007); *Nes* mRNA levels were found to be reduced 1.6-fold ($P=0.20$) in pregnant compared with virgin myoepithelial cells (Table 5.6). Reelin signalling has been recently implicated in the directed migration of mammary epithelial cells, driving ductal elongation into the mammary fat pad. Reelin expression has been documented in the myoepithelium and periductal stroma of the adult mouse mammary gland (Khialeeva et al., 2011). In accordance with reelin's reported role in mammary gland morphogenesis, *Reln* mRNA was found to be increased approximately 2.8-fold ($P=0.26$) in pregnant relative to virgin myoepithelial cells. In the same array data set, *Slit2* was decreased 5.4-fold ($P=0.20$) in pregnant compared to virgin myoepithelial cells. This is consistent with studies by Strickland et al., which demonstrate broad expression of *Slit2* by the epithelial layers during ductal elongation in the developing mouse mammary gland (Strickland et al., 2006). In addition, the genes *Eya2*, *Runx2*, *Trp63* and *Etv5*, all of which have been previously documented to be expressed in the myoepithelial cell lineage via transcriptome analysis of mammary epithelial cell populations (Kendrick et al., 2008), were represented in this array data set. Combined with our purity assessment (section 5.3.2), these data indicate that our myoepithelial cell microarray data set accurately reflects myoepithelial cell gene expression.

5.3.4.3 Haematopoietic cell array

Analysis of genes differentially expressed in haematopoietic cells isolated from virgin and pregnant mouse mammary glands revealed many genes characteristically expressed by haematopoietic cells, including macrophages. These included *Vldlr*, increased 3.9-fold ($P=0.18$) in pregnant haematopoietic cells (Table 5.4) and documented to be expressed by macrophages in atherosclerotic lesions (Eck et al., 2005; Mulhaupt et al., 1996); *Pecam1*, decreased 4.0-fold ($P=0.19$) in pregnant compared to virgin haematopoietic cells (Table 5.4), consistent with the expression of *Pecam1* by mature haematopoietic cells, including neutrophils, monocytes and T cell subsets (Watt et al., 1995); and the increased expression of a number of matrix metalloproteinases (MMP) by pregnant haematopoietic cells. These included *Mmp2* (5.6-fold, $P=0.29$), *Mmp13* (5.0-fold, $P=0.27$) and *Mmp14* (3.1-fold, $P=0.29$), consistent with an active role for MMPs in tissue remodelling and mammary gland branching morphogenesis (Fata et al., 2004; Goetzl et al., 1996; Green and Lund, 2005; Page-McCaw et al., 2007). In addition, *Plau*, the gene encoding for urokinase-type plasminogen activator, expressed predominantly by macrophages in atherosclerotic lesions (Falkenberg et al., 1998), was elevated 2.5-fold ($P=0.32$) in pregnant haematopoietic cells compared to the same population in the virgin mammary gland. This finding is consistent with a well-known role for *Plau* in activation of the serine protease, plasmin, which degrades

extracellular matrix proteins involved in mouse mammary gland morphogenesis (Green and Lund, 2005). Of note, the top 3 most differentially expressed genes in the microarray data set comparing pregnant and virgin haematopoietic cells were casein genes; *Csn2* (115.7-fold, $P < 0.05$), *Csn1s2a* (108.4-fold, $P < 0.05$) and *Csn1s1* (196.0-fold, $P < 0.05$) (Table 5.4). The expression of milk protein genes is characteristic of mature and differentiated luminal epithelial cells (Hennighausen and Robinson, 2005), suggesting that increased expression of casein milk protein genes in the haematopoietic array data set might reflect a degree of luminal epithelial cell contamination. The fact that genes involved in milk production are increased by such a large magnitude during pregnancy (section 5.3.4.1), means that only a few contaminating cells could account for the appearance of these genes in the haematopoietic cell list. Taken together, these data suggest that whilst the isolated haematopoietic cell fractions may contain a small proportion of contaminating luminal epithelial cells, the haematopoietic gene expression profiles still largely reflect haematopoietic cell-specific genes.

5.3.4.4 Endothelial cell array

Genes characteristic of sprouting angiogenesis, lymphangiogenesis and vascular remodelling, such as components of the VEGF (Olsson et al., 2006; Tammela et al., 2008) and Notch (Hellström et al., 2007; Phng and Gerhardt, 2009; Suchting et al., 2007; Zheng et al., 2011) signalling pathways, semaphorins/neuropilins (Neufeld et al., 2002; Xu et al., 2010), ephrins/Eph tyrosine kinase receptors (Kuijpera et al., 2007; Mäkinen et al., 2005) and angiopoietins/Tie receptors (Dumont et al., 1994; Gale et al., 2002; Maisonpierre et al., 1997; Morisada et al., 2005; Suri et al., 1996; Tammela et al., 2005), were not represented in our EC microarray data set. This was surprising given that pregnancy corresponds to a time of peak blood (Figure 1.7F) (Djonov et al., 2001; Matsumoto et al., 1992; Pepper et al., 2000) and lymphatic (Figure 3.2C) vessel density in the postnatal mouse mammary gland. The absence of established angiogenic/lymphangiogenic genes does not necessarily reflect a lack of expression by mammary gland EC, nor does it underscore the validity of this microarray data set, it may simply indicate a lack of differential expression of these genes between the stages chosen for microarray analysis. In retrospect, the critical peak in angiogenic and lymphangiogenic gene expression was potentially underestimated in the EC microarray comparisons between virgin and 16.5 day pregnant mammary glands (Table 5.3). This is evidenced by downregulation of the key VEGF EC mitogens, *Vegfa* (1.1-fold, $P = 0.75$), *Vegfc* (1.5-fold, $P = 0.48$) and *Vegfd* (4.2-fold, $P = 0.44$), in our microarray data set comparing 16.5 day pregnant to virgin myoepithelial cells, combined with our real-time RT-PCR expression analyses demonstrating that *Vegfc* and *Vegfd* are significantly increased at the mRNA level

at a much earlier (4.5 day) stage of pregnancy (Figure 4.4A) than the stage at which our arrays were performed (16.5 days).

5.3.4.5 Pregnant epithelial cell array

Further validation to support purity of the isolated mammary gland cell populations used in our microarray studies was provided on analysis of the microarray data set comparing the gene expression profiles of pregnant epithelial subtypes (Table 5.7). In this data set, the genes encoding for the luminal epithelial-specific cytokeratins 8 and 18 (Parmar and Cunha, 2004), *Krt8* (1.7-fold, $P=0.15$) and *Krt18* (6.8-fold, $P<0.05$), were decreased accordingly in pregnant myoepithelial cells compared to luminal epithelial cells. In accordance, genes indicative of a myoepithelial cell phenotype, *Krt5* (4.6-fold, $P=0.37$) and *Krt14* (4.0-fold, $P=0.27$), together with *Acta2* (4.9-fold, $P<0.05$) (Parmar and Cunha, 2004), were all increased in pregnant myoepithelial cells relative to luminal epithelial cells. In addition, *Muc1*, a marker of differentiated luminal epithelial cells (Stingl et al., 1998) was decreased 13.0-fold ($P<0.05$) (Table 5.7), and *Robo1*, expression of which has been demonstrated to be restricted to myoepithelial cells, where it functions to control branch formation in the mouse mammary gland (Macias et al., 2011; Strickland et al., 2006), was increased 8.7-fold ($P<0.05$) (Table 5.7) in pregnant myoepithelial cells compared to luminal epithelial cells. Furthermore, the extracellular matrix-modifying enzyme, *Lox12*, has recently been shown to be highly expressed in cells of the myoepithelial lineage in the mouse mammary gland (Barker et al., 2011) and accordingly *Lox12* was increased 2.5-fold ($P=0.11$) in pregnant myoepithelial cells relative to luminal epithelial cells. *Elf5*, a key transcription factor essential for normal alveolar development (Oakes et al., 2008) was decreased 17.2-fold ($P<0.05$) in pregnant myoepithelial cells compared to luminal epithelial cells at the same stage. Furthermore, *ErbB3*, a member of the epidermal growth factor receptor family has been documented to be expressed exclusively in luminal epithelial cells in the mouse mammary gland (Kendrick et al., 2008) and was aptly decreased in expression 15.8-fold ($P<0.05$) in pregnant myoepithelial cells relative to pregnant luminal epithelial cells. Collectively, these data indicate distinct separation of luminal and myoepithelial cell subtypes from one another by FACS and pave the way for novel genes involved in mammary gland morphogenesis to be identified in our microarrays.

5.3.5 Candidate genes identified from microarray analyses likely involved in vascular remodelling in the postnatal mouse mammary gland

Chemokine (CXC motif) ligand 15 (*Cxcl15*) is a relatively uncharacterised member of the ELR⁺ CXC chemokine family, shown to be potent stimulators of angiogenesis *in vivo* (Frederick and Clayman, 2001; Strieter et al., 2006; Strieter et al., 1995). *Cxcl15* was downregulated 43.2 ($P<0.05$), 39.7 ($P=0.09$) and 25.0-fold ($P=0.28$) in our arrays in pregnant endothelial (Table 5.3), luminal (Table 5.5) and haematopoietic cells, compared with these populations in the virgin state, respectively. Owing to the fact that *Cxcl15* was found to be differentially expressed in a similar direction across the majority of our microarray data sets, we performed real-time RT-PCR on three independently-derived biological samples using RNA isolated from whole 9 week virgin, 4.5 day and 16.5 day pregnant mammary glands (section 4.2.3), as opposed to population-specific RNA which was used for the initial microarray analyses, to validate this finding. Real-time RT-PCR analyses revealed that *Cxcl15* mRNA levels were significantly downregulated 96.5-fold at late (16.5 day) pregnant stages compared to virgin mammary glands (Figure 5.5). Interestingly, *Cxcl15* mRNA levels were transiently increased 2.4-fold and a staggering 236.0-fold at an early (4.5 day) stage of pregnancy relative to both virgin and late pregnant stages, respectively (Figure 5.5). Taken together, these data suggest that *Cxcl15* expression is temporally-regulated in the postnatal mouse mammary gland, with peak mRNA levels corresponding to peak vascular density (Figure 1.7F; Figure 3.2C). The significance of changes in *Cxcl15* expression remains to be determined.

In addition to *Cxcl15*, we identified a number of differentially expressed genes in our microarray data sets, as discussed below, that have previously been ascribed putative roles in angiogenesis in diverse biological settings. These include *Adam10*, *Anxa1*, *Tnc* and *Bdnf*. Given their expression levels in the mouse mammary gland, together with published literature, we predict that these genes may play a role in vascular remodelling during postnatal mouse mammary gland morphogenesis.

A disintegrin and metalloproteinase 10 (ADAM10) has recently been established as the primary protease required for the activation of Notch signalling, a key pathway involved in angiogenesis and lymphangiogenesis (Phng and Gerhardt, 2009; Zheng et al., 2011), during development and disease (Zhang et al., 2010). *Adam10* was reduced 2.6-fold ($P<0.05$) in pregnant compared to virgin EC (Table 5.3) in the mouse mammary gland, suggesting a suppression of active Notch signalling and concomitant

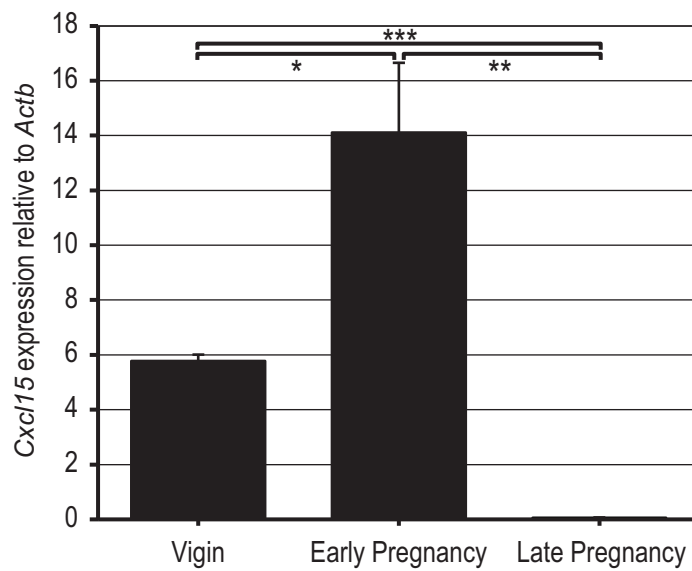


Figure 5.5 - *Cxcl15* mRNA levels are elevated at an early stage of pregnancy relative to virgin and late pregnant stages.

Real-time RT-PCR was used to determine the relative level of *Cxcl15* gene expression in mammary glands from 9 week virgin compared with early (4.5 day) and late (16.5 day) pregnant wild-type female mice. Samples were pooled from at least two mice. Data shown represent the mean \pm standard error of the mean of three (9 week virgin, 16.5 day pregnant) or four (4.5 day pregnant) independent experiments. *P*-values were calculated using the two-tailed Student's *t*-test, **P*<0.05, ***P*<0.01, ****P*<0.00001. RT-PCR - reverse transcription-polymerase chain reaction.

increase in angiogenic (Hellström et al., 2007; Suchting et al., 2007) and lymphangiogenic (Zheng et al., 2011) sprouting during pregnancy.

Annexin A1 (AnxA1) has recently been established as having a pro-angiogenic role in vascular EC sprouting, wound healing, tumour growth and metastasis (Yi and Schnitzer, 2009). In the mouse mammary gland, *Anxa1* was decreased 2.4-fold ($P < 0.05$) in pregnant EC compared to virgin EC (Table 5.3). We would predict a role for AnxA1 in sprouting angiogenesis in the pregnant mouse mammary gland. Given that sprouting angiogenesis is the predominate mechanism driving expansion of the microvasculature early on in pregnancy, downregulation of *Anxa1* is not unexpected at 16.5 days of pregnancy, when sprouting angiogenesis is dampened and a switch to intussusception occurs (Djonov et al., 2001; Matsumoto et al., 1992).

Tenascin C (Tnc) has been demonstrated to promote numerous key steps involved in angiogenesis, such as EC adhesion, sprouting and migration (Ballard et al., 2006; Canfield and Schor, 1995; Castellon et al., 2002; Sriramarao et al., 1993; Zagzag et al., 2002) and has been associated with vascular development (Ando et al., 2011). Furthermore, Tnc expression has been linked with angiogenesis in a number of pathological settings (Castellon et al., 2002; Zagzag et al., 1996; Zagzag et al., 1995). In accordance, we observed a 1.7-fold ($P < 0.05$) increase in *Tnc* expression in pregnant mammary EC compared to virgin mammary EC (Table 5.3).

Recent work has implicated brain-derived neurotrophic factor (BDNF) as a novel, potent stimulator of angiogenesis, promoting EC proliferation, migration, invasion and survival in several mouse models (Lam et al., 2011; Liu et al., 2010). Our microarray analyses revealed a 3.5-fold ($P < 0.05$) increase in *Bdnf* in pregnant myoepithelial cells compared to luminal epithelial cells (Table 5.7), suggesting that BDNF might contribute to the promotion of angiogenesis in the postnatal mouse mammary gland.

Mmp2, recently implicated in lymphangiogenesis (Bruyère et al., 2008) was increased 5.6-fold ($P = 0.29$) in pregnant haematopoietic cells compared to virgin haematopoietic cells. Consistent with this finding, a second MMP, *Mmp14*, which has been reported to activate pro-MMP-2 (Strongin et al., 1995), was elevated 3.1-fold ($P = 0.29$) in the same microarray data set. In addition, the gene encoding tissue inhibitor of metalloproteinase (TIMP) 2, *Timp2*, which has been shown to activate MMP-2 by acting as a co-factor in a complex with MMP-14 and pro-MMP-2 at the cell surface (Wang et al., 2000), was increased 2.0-fold ($P = 0.18$) in pregnant myoepithelial cells compared to luminal epithelial cells. The increased expression of *Mmp2*, *Mmp14* and *Timp2* in the pregnant mouse mammary gland corresponds

with a time of peak lymphatic vessel density (Figure 3.2C), and together with MMP-2's pro-lymphangiogenic activity (Bruyère et al., 2008), is supportive of a role for these proteases in lymphangiogenesis during postnatal mouse mammary gland morphogenesis.

5.3.6 *Bfk* is increased during pregnancy in the mouse mammary gland

B-cell lymphoma 2 (Bcl2) family kin (*Bfk*), a member of the mammalian Bcl2 family of proteins, has been previously demonstrated to be expressed at both the mRNA and protein level in the postnatal mouse mammary gland (Coultas et al., 2003; Pujianto et al., 2007); however, the functional role of *Bfk* in the mouse mammary gland remains uncharacterised. In our microarray analyses, *Bfk* was found to be increased 37.8-fold ($P < 0.05$), 53.8-fold ($P = 0.09$) and 36.7-fold ($P = 0.21$) in pregnant endothelial (Table 5.3), luminal and haematopoietic cells compared to virgin populations, respectively. Owing to the fact that *Bfk* was found to be differentially expressed in a similar direction in 3 out of 4 of our microarray data sets, we performed real-time RT-PCR on three independently-derived biological samples using RNA isolated from whole 9 week virgin, 4.5 day and 16.5 day pregnant mouse mammary glands (section 4.2.3), analogous to *Cxcl15* analyses described above, in order to substantiate this finding. Real-time RT-PCR data verified that *Bfk* mRNA levels were indeed upregulated in pregnant mouse mammary glands, yielding a 50.3-fold induction in early (4.5 day) and a corresponding 62.1-fold increase in late (16.5 day) pregnant mammary glands compared to 9 week virgin glands (Figure 5.6). These data indicate that *Bfk* is temporally-regulated in the postnatal mouse mammary gland.

5.4 DISCUSSION

Collectively, this chapter describes the development and optimisation of a sophisticated approach to isolate enriched populations of luminal epithelial, myoepithelial, EC and haematopoietic cells from the virgin and pregnant mouse mammary gland for microarray profiling studies, with the ultimate aim of identifying candidate genes, together with their cellular sources, involved in lymphangiogenesis and/or angiogenesis during postnatal mouse mammary gland morphogenesis. The amplification of limited quantities of RNA in the isolated cell fractions by WT-Ovation™ Pico RNA Amplification System version 1.0 (NuGEN Technologies) was an essential step, without which the wide-scale gene expression profiling in the mouse mammary gland would not have been possible. Whilst we have since determined that genes important in regulating peak angiogenesis and/or lymphangiogenesis during mammary gland morphogenesis may have been better represented on comparison of virgin with early (4.5 day) pregnant

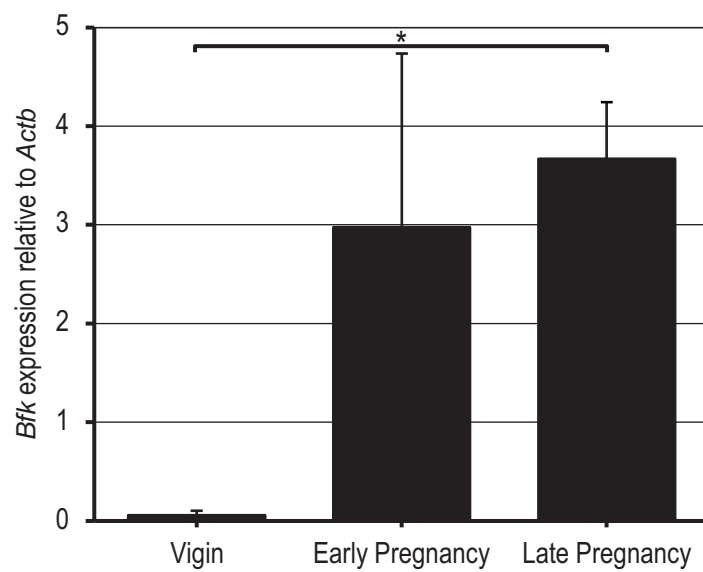


Figure 5.6 - *Bfk* mRNA levels are increased in pregnant mouse mammary glands.

Real-time RT-PCR was used to determine the relative level of *Bfk* gene expression in mammary glands from 9 week virgin compared with early (4.5 day) and late (16.5 day) pregnant wild-type female mice. Samples were pooled from at least two mice. Data shown represent the mean \pm standard error of the mean of three (9 week virgin, 16.5 day pregnant) or four (4.5 day pregnant) independent experiments. *P*-values were calculated using the two-tailed Student's *t*-test, **P*<0.01. RT-PCR - reverse transcription-polymerase chain reaction.

mouse mammary glands, as opposed to late (16.5 day) pregnancy, we did, however, identify a number of candidate genes, including *Cxcl15*, *Adam10*, *Anxa1*, *Tnc*, *Mmp2* and *Bdnf*, likely to be involved in orchestrating remodelling of the blood and lymphatic vascular beds in the postnatal mouse mammary gland. The microarray data sets generated contain a wealth of information and whilst beyond the scope of this study, hold the substantial potential as an important repository for the elucidation of novel, cell-specific regulators of postnatal mouse mammary gland morphogenesis, not restricted to angiogenesis and lymphangiogenesis.

Gene expression profiling using microarray technology is a powerful method to investigate the phenotype of complex biological systems. However, one of the critical limitations of current microarray technologies is the relatively large amount of input RNA required, typically in the order of microgram quantities; an amount which isn't readily achievable from minute biological samples generated via flow cytometry or laser capture microdissection. Today, this problem is largely overcome by RNA amplification methods, but not without its own set of shortcomings. In our study, a much more realistic quantity of 100ng of total cellular RNA was the minimal recommended starting amount for hybridisation to our chosen GeneChip® Mouse Gene 1.0 ST arrays (Affymetrix). Unfortunately, limiting RNA yields (ie. less than 100ng) from a number of isolated cell fractions, particularly from virgin mammary gland epithelial populations, which contained a meagre 1-3ng of total RNA, still meant that gene expression analysis of this calibre was not feasible. Only a handful of robust commercially-available methodologies exist which are effective at amplifying picogram quantities of input RNA; the WT-Ovation™ Pico RNA Amplification System version 1.0 (NuGEN Technologies) is one such technology enabling microgram quantities of cDNA to be amplified from as little as 500pg of total cellular RNA. This system is based on a novel three-step linear isothermal amplification process of double-stranded cDNA that encompasses a unique DNA/RNA heteroduplex and activity of an RNA-dependent DNA polymerase, compared with the routinely used linear amplification method of *in vitro* transcription which utilises T7 RNA polymerase (Clément-Ziza et al., 2009; Kurn et al., 2005). Our decision to use the WT-Ovation™ Pico RNA Amplification System has been independently validated in a recent report by Clément-Ziza *et al.*, whereby four commercial products for the amplification of picogram amounts of input RNA were experimentally evaluated and compared. In this study, NuGEN's technology was deemed most suitable for RNA amplification of this scale and subsequent gene expression analysis owing to the rapid nature, ease to perform, high sensitivity and reproducibility, ability to maintain relative transcript abundance and sequence fidelity between technical replicates, lack of requirement for several rounds of amplification or exponential PCR cycles and most importantly, permitted the identification of differentially regulated genes (Clément-Ziza et al., 2009; Kurn et al., 2005). Therefore, whilst RNA amplification of any degree

is not favourable due to the potential for the introduction of transcript bias, it was albeit necessary in our case to enable gene expression analysis of the populations of cells that we were interested in.

Based on our real-time RT-PCR data, cell populations isolated from pregnant mammary glands were of a higher purity compared to those isolated from virgin mammary glands. This is not surprising given the fact that the cell yields from virgin mammary glands were at least 10-fold less than the corresponding population isolated from pregnant mammary glands. This is simply a reflection of the degree of cellularity of the glands at these developmental time points. In an 8 week virgin mammary gland, despite the presence of a regularly-spaced arborised network of primary and secondary ducts, adipose tissue constitutes a large portion of the gland, whereas during pregnancy the epithelial to adipocyte ratio increases due to the extensive proliferation of ductal branches and the formation of alveoli (Richert et al., 2000). A small number of contaminating cells would therefore have a greater impact on real-time RT-PCR gene expression profiles and hence indication of population purity in the virgin samples. Due to limiting cell numbers and the relative sparseness of lymphatic vessels in the postnatal mouse mammary gland when compared with blood vessels, we had to reassess our initial FACS strategy to independently isolate LEC from BEC. Instead, a compromise was made to collect all EC as a single population to improve cell yield. This ultimately may have been a key factor contributing to the under-representation of lymphangiogenic-specific genes in our EC microarray data set.

It is not unexpected that low levels of genes characteristic of one particular cell type are expressed in another unrelated cell type and is not necessarily a reflection of contamination per se. For example, *Pecam1* expression is not restricted to EC and is also expressed on a variety of mature haematopoietic cells, including neutrophils, monocytes and T cell subsets, therefore low levels of *Pecam1* in the haematopoietic fractions is not unexpected (Watt et al., 1995). Furthermore, vascular smooth muscle cells, or pericytes, express *Acta2* and thus any blood vascular EC which are not completely dissociated from these contractile cells may artefactually increase *Acta2* in the EC fractions (Nehls and Drenckhahn, 1991; Skalli et al., 1989). In contrast, the relatively high levels of *Krt18* mRNA levels in the haematopoietic cell fractions isolated from virgin and pregnant (Figure 5.3E,F) mammary glands, may reflect luminal epithelial cell contamination. This concern is further corroborated by the expression of casein genes, *Csn2*, *Csn1s2a* and *Csn1s1*; representing the top three most differentially expressed genes between virgin and pregnant haematopoietic cells (Table 5.4). The expression of milk protein genes is known to define a mature and differentiated luminal epithelial cell (Hennighausen and Robinson, 2005). Given that these genes are so highly upregulated during pregnancy, compared to the virgin state, only small numbers of contaminating luminal epithelial cells would be required to account

for the observed expression levels. Potential contamination is an important reason to validate the expression of candidate genes *in vivo*. Nevertheless, despite the highly complex nature of the FACS approach employed in these investigative studies, many genes characteristic of discrete cell populations and with established roles in the mouse mammary gland were expressed in the relevant microarray data sets, reinforcing that the resultant mammary gland cell populations were highly enriched.

Mammary gland stromal cells, encompassing fibroblasts and adipocytes, were not selected for in our FACS approach due to technical limitations. Mammary stromal cells, however, represent additional cell types that have the potential to be a rich source of instructive patterning signals in the mouse mammary gland, given the relative abundance of fibroblasts in the human breast, combined with the importance of stromal-epithelial crosstalk in many aspects of mouse mammary gland biology, including development of the embryonic mammary gland and branching morphogenesis (Parmar and Cunha, 2004).

In retrospect, the critical peak in angiogenic/lymphangiogenic growth factor expression was potentially underestimated in our current microarray comparisons between virgin and 16.5 day pregnant mammary glands. This is based on the downregulation of the VEGF family members, *Vegfa* (1.1-fold, $P=0.75$), *Vegfc* (1.5-fold, $P=0.48$) and *Vegfd* (4.2-fold, $P=0.44$), in our microarray data set comparing pregnant with virgin myoepithelial cells, combined with our real-time RT-PCR expression analyses demonstrating that *Vegfc* and *Vegfd* are significantly increased at the mRNA level at an earlier (4.5 day) stage of pregnancy and then decreased by 16.5 days of pregnancy (Figure 4.4A); the stage at which our arrays were performed. *Reln* and *Cxcl15* demonstrated a similar transient peak in expression at 4.5 days of pregnancy (Figure 4.5; Figure 5.5). It therefore seems likely that genes important in orchestrating peak angiogenesis and lymphangiogenesis during pregnancy may have been better represented on comparison of virgin with early (4.5 day) pregnant mouse mammary glands. This analysis could form the basis of future investigations.

5.4.1 Novel genes likely involved in vascular remodelling in the postnatal mouse mammary gland

From our microarray analyses we have identified a handful of differentially expressed genes which have previously been ascribed putative roles in angiogenesis in diverse biological settings. However, a definitive role for these genes in blood vascular remodelling in the postnatal mouse mammary gland has not been described to date and their role in lymphangiogenesis has not been investigated. Establishing

the precise spatial and temporal expression patterns of these angiogenic genes in the postnatal mouse mammary gland, either via commercially-available antibodies or by *in situ* hybridisation, in combination with the generation of conditional knockout mice, will be essential in elucidating the roles of these genes in mouse mammary gland biology. Such analyses will form the basis of future work.

5.4.1.1 *Cxcl15*

Murine CXCL15, better known as lungkine or weird chemokine (WECHE) was first described as a protein secreted into the airway spaces of the lung by bronchoepithelial cells, where it functions to recruit neutrophils during pulmonary inflammation (Rossi et al., 1999). CXCL15 is a novel member of the ELR⁺ CXC chemokine family, whose members share a non-conserved amino acid between the first two cysteine residues (CXC), in addition to another conserved three amino acid sequence; glutamic acid-leucine-arginine, denoted the ELR motif (ELR⁺) (Frederick and Clayman, 2001). Chemokines belonging to this family have been shown to play a pivotal role in neutrophil chemotaxis and all are potent stimulators of angiogenesis *in vivo* compared with members that lack the ELR motif; mediating their angiogenic activity via binding to the CXCR2 receptor on vascular endothelium (Frederick and Clayman, 2001; Rossi et al., 1999; Strieter et al., 2006; Strieter et al., 1995). The receptor and human homologue of murine CXCL15, however, remains to be determined. In addition to its abundant expression in the adult lung, CXCL15 mRNA and protein has since been documented to be expressed, albeit at a greatly reduced level, in other murine mucosal and endocrine organs including the pseudostratified epithelial cells of the trachea, colonic goblet cells, endometrial cells of the uterus, gastric prezymogenic cells and the adrenal gland. Predominant localisation of CXCL15 to epithelial cells is suggestive of a role for this protein at epithelial surfaces in sensing external infection and initiating immune responses (Schmitz et al., 2007). However, the exact biological function of CXCL15 at many of these anatomical sites remains to be elucidated. In addition, studies by Ohneda *et al.* demonstrated that CXCL15 acts as a chemoattractant for bone marrow progenitor cells and also has a more divergent role in the regulation of haematopoietic differentiation, where it inhibits the formation of the erythroid lineage (Ohneda et al., 2000). Unlike Bfk, CXCL15 has not been previously documented to be expressed in the mouse mammary gland.

Our finding that *Cxcl15* is differentially expressed in mammary haematopoietic cells is in agreement with a reported role in haematopoietic differentiation (Ohneda et al., 2000). Furthermore, the differential expression of *Cxcl15* in both our endothelial and luminal epithelial cell microarray data sets is consistent with presumptive roles for this novel protein in the regulation of angiogenesis (Strieter et al., 2006;

Strieter et al., 1995) and in mediating the recruitment of immune cells to epithelial surfaces (Schmitz et al., 2007), respectively. Our observation that *Cxcl15* mRNA levels peak at an early stage of pregnancy (Figure 5.5) aligns accordingly with a phase of mammary gland development that involves rapid expansion of the mammary blood vasculature via sprouting angiogenesis (Djonov et al., 2001; Matsumoto et al., 1992). It will be interesting to explore whether CXCL15 does in fact regulate angiogenesis in the mouse mammary gland and whether, in addition, this protein has any notable effect on lymphangiogenesis.

5.4.1.2 *Adam10*

ADAM10 belongs to a large family of transmembrane and secreted proteins with diverse functions in cell adhesion and proteolytic processing of membrane-bound protein ectodomains (Edwards et al., 2008). ADAM10 was initially identified as an α -secretase and a key proteinase in the processing of the amyloid precursor protein; the precursor of the principal proteinaceous component found in amyloid plaques in the brains of Alzheimer's patients (Lammich et al., 1999). Whilst the biological functions of ADAM10 are diverse, for the purpose of this study the role of ADAM10 in the context of the cardiovascular system will be addressed. *Adam10*^{-/-} mice display classic Notch loss-of-function phenotypes and die at E9.5 with multiple defects in the developing central nervous system, somites and cardiovascular system (Hartmann et al., 2002). This observation, along with the finding that ADAM10 is required for cleavage of Notch (van Tetering et al., 2009), led to the more recent discovery that *Adam10* in the endothelium is the primary protease essential for activation of Notch signalling during embryonic cardiac and vascular development (Zhang et al., 2010). In addition, studies by Schulz *et al.* have identified a critical role for ADAM10 in the regulation of vascular permeability and demonstrated that ADAM10-mediated proteolysis of vascular endothelial-cadherin (VE-cadherin), the major component of endothelial adherens junctions, is an important mechanism regulating endothelial adhesion (Schulz et al., 2008). More recently, Donners *et al.* identified ADAM10 as a novel binding partner of VEGFR-2 that is responsible for the ectodomain shedding of VEGFR-2. Furthermore, ADAM10 was demonstrated as a novel mediator of VEGF-induced EC function, including vascular permeability and EC migration (Donners et al., 2010). Interestingly, Donners *et al.* also observed that ADAM10 was highly expressed in plaque microvessel EC of human atherosclerotic lesions and that ADAM10 expression in these lesions was associated with plaque progression and neovascularisation. Even more recently, work by Glomski *et al.* demonstrated that deletion of *Adam10* specifically in EC resulted in a variety of vascular abnormalities and enhanced pathological neovascularisation, implicating *Adam10* as a crucial regulator of EC fate decisions (Glomski et al., 2011). These more recent studies indicate that ADAM10 not only

functions in the development of the cardiovascular system, but also has key roles in EC biology and angiogenesis.

Consistent with the reported roles of ADAM10 in EC, as discussed above, *Adam10* expression was downregulated in pregnant compared to virgin EC (Table 5.3) in the mouse mammary gland. Whilst the exact biological relevance of ADAM10 in mammary EC is currently unknown, we can speculate as to its function. Given that ADAM10 has been demonstrated to increase vascular permeability via proteolysis of VE-cadherin (Donners et al., 2010; Schulz et al., 2008), we would predict that a reduction in *Adam10* in pregnant EC would result in reduced proteolysis of VE-cadherin and subsequently reduced EC permeability. However, this hypothesis contradicts peak EC permeability during the reproductive cycle in the mouse mammary gland. During pregnancy, not only does the extent of the microvasculature increase, but there is a marked increase in permeability due to decreased cell-cell contacts, thereby enabling the highly efficient transport of nutrients and fluids required during lactation (Matsumoto et al., 1992). It is conceivable that a reduction in *Adam10* at the level of mRNA reflects a negative-feedback regulatory loop, and does not necessarily correlate to protein levels of ADAM10, which could be increased during pregnancy. Alternatively, the downregulation of *Adam10* in 16.5 day pregnant EC compared to virgin EC could reflect that we may have missed peak expression levels of this gene, which may have been increased in expression earlier during pregnancy. In light of this, it seems more likely that ADAM10 functions independently of vascular permeability in mammary gland EC.

Given the well-established role for Notch signalling in blood vascular EC tip versus stalk cell formation and angiogenesis (Phng and Gerhardt, 2009), it is possible that ADAM10 could function as an important mediator of Notch signalling in mammary gland EC. A critical step involved in the activation of the Notch pathway is proteolytic cleavage of the Notch receptor upon ligand binding, which releases the Notch intracellular domain into the cytoplasm, where it can translocate to the nucleus and drive expression of downstream target genes (Bray, 2006). Three consecutive cleavage events of Notch have been defined; with ADAM10 likely the key protease responsible for the second cleavage event (van Tetering et al., 2009; Zhang et al., 2010). Suppression of Notch signalling in the mouse leads to excessive sprouting of blood vascular EC as a result of increased tip cell formation (Hellström et al., 2007; Suchting et al., 2007). Consistent with the negative regulatory role of Notch in angiogenesis, current work by Zheng *et al.* has demonstrated that suppression of Notch signalling, in synergy with VEGF-A, induces lymphangiogenesis both *in vitro* and *in vivo* (Zheng et al., 2011). Taken together, it is plausible that in the pregnant mouse mammary gland, a time corresponding to a peak in both blood (Figure 1.7F) (Djonov et al., 2001; Matsumoto et al., 1992; Pepper et al., 2000) and lymphatic (Figure 3.2C) vessel

density, EC levels of *Adam10* are dampened in order to reduce Notch activation, leading to increased angiogenesis and lymphangiogenesis. Given that blood and lymphatic sprouting following Notch inhibition have been shown to be dependent, at least in part in lymphatic vessels, by VEGFR-2 (Suchting et al., 2007; Zheng et al., 2011) and that ADAM10 is responsible for the ectodomain shedding of VEGFR-2 (Donners et al., 2010); ADAM10 could further augment this process by maintaining adequate levels of membrane-bound VEGFR-2 on the endothelium to promote sprouting angiogenesis. The precise role of ADAM10 in EC in the mouse mammary gland remains to be validated experimentally; nevertheless ADAM10 represents an exciting and novel avenue to pursue in the future.

5.4.1.3 *Anxa1*

AnxA1 is an endogenous anti-inflammatory protein belonging to the annexin superfamily of calcium-dependent phospholipid binding proteins. Although the exact function of AnxA1 is unknown, it is speculated to play a role in many diverse cellular functions, including membrane aggregation, inflammation, phagocytosis, proliferation and apoptosis (Lim and Pervaiz, 2007). Intriguingly, AnxA1 was recently found by subtractive proteomic mapping to be selectively expressed *in vivo* on the outer luminal surface of tumour, but not normal vascular EC (Oh et al., 2004). In accordance with this observation, studies by Yi and Schnitzer have established a novel pro-angiogenic function for AnxA1 in vascular EC sprouting, wound healing, tumour growth and metastasis (Yi and Schnitzer, 2009). *Ex vivo* aortic rings from *Anxa1*-null mice showed significantly fewer vascular sprouts than aortic rings from WT mice, a defect which could be rescued by the re-expression of *Anxa1* in EC; tumours in *Anxa1*-null mice developed fewer blood vessels, grew more slowly and failed to metastasise, all of which likely contributed to increased survival; and incisional wounds on *Anxa1*-null mice healed far slower than similar wounds on WT mice. Taken together, these data suggest that AnxA1 may serve a unique function in EC sprouting (Yi and Schnitzer, 2009). However, given that *Anxa1*-null mice lack any obvious vascular defects during development (Hannon et al., 2003), it would suggest an apparently distinct role for AnxA1 in pathological, rather than physiological angiogenesis.

In our EC array data set, *Anxa1* expression was decreased 2.4-fold ($P < 0.05$) in pregnant EC compared to virgin EC (Table 5.3) in the mouse mammary gland. This finding is not unexpected given that the vascular endothelium in the postnatal mouse mammary gland is actively remodelled and represents an activated, rather than a quiescent endothelium (Djonov et al., 2001; Matsumoto et al., 1992). Based on recent studies (Yi and Schnitzer, 2009), we would predict that AnxA1 has a functional role in sprouting angiogenesis during mouse mammary gland morphogenesis. During the early stage of pregnancy in the

mouse mammary gland, sprouting angiogenesis predominates as evidenced by an abundance of capillary sprouts on the microvasculature, however, during the late phase of pregnancy there is a switch from sprouting angiogenesis to intussusception (Djonov et al., 2001; Matsumoto et al., 1992). Therefore, a decrease in EC *Anxa1* expression in late pregnancy is further support for a role of *Anxa1* in EC sprouting and it is likely that *Anxa1* expression in the postnatal mouse mammary gland, like *Vegfc*, *Vegfd*, *Reln* and *Cxcl15*, peaks earlier on in pregnancy corresponding with a time of peak angiogenic sprouting.

5.4.1.4 *Tnc*

Tnc is a large multimeric extracellular matrix glycoprotein, expression of which is limited in adult tissues. However, *Tnc* is strongly expressed in settings of tissue repair and in pathological states, including cancer and chronic inflammation (Ando et al., 2011). Numerous studies have demonstrated that *Tnc* promotes EC adhesion, sprouting and migration (Canfield and Schor, 1995; Castellon et al., 2002; Sriramarao et al., 1993; Zagzag et al., 2002); all critical steps in angiogenesis. The involvement of *Tnc* in angiogenesis has further been suggested based on its expression in pathological settings of angiogenesis, such as cerebral neoplastic disease (Zagzag et al., 1996; Zagzag et al., 1995) and diabetic retinopathy (Castellon et al., 2002). Interestingly, it has been demonstrated that in human astrocytomas, *Tnc* expression correlates with angiogenesis, whereby *Tnc* mRNA is expressed at increased levels in hyperplastic vessels at the invasive edge of astrocytomas, but not in vessels of normal brain tissue (Zagzag et al., 1996; Zagzag et al., 1995). In accordance, human brain microvessel EC have been shown to synthesise and secrete *Tnc in vitro* (Zagzag et al., 1996), whilst *Tnc* expression has been detected in migrating vascular EC in cerebral microvascular ring *in vitro* assays (Zagzag et al., 2002). Furthermore, studies by Ballard *et al.* have demonstrated *Tnc* as a mediator of postnatal cardiac angiogenesis (Ballard et al., 2006). Very recently, studies in avian embryonic hearts have suggested a possible role for *Tnc* in vascular development, specifically in the recruitment of vascular smooth muscle cells (Ando et al., 2011). Taken together, the expression of *Tnc* by EC within adult tissues undergoing active vascular remodelling and the promotion of EC migration by *Tnc* unequivocally support a role for *Tnc* in angiogenesis.

In accordance with the above studies, *Tnc* was found to be elevated 1.7-fold ($P < 0.05$) in pregnant EC compared to virgin EC (Table 5.3) in the mouse mammary gland. Based on studies by Zagzag *et al.* and Canfield and Schor, which demonstrated the preferential expression of *Tnc* in hyperplastic angiogenic vessels (Zagzag et al., 1996; Zagzag et al., 1995) and sprouting EC (Canfield and Schor, 1995),

respectively; the upregulation of *Tnc* in pregnant EC in the mouse mammary gland is likely indicative of an activated vascular endothelium, rather than a quiescent state. Given that late in pregnancy, sprouting angiogenesis is markedly reduced (Djonov et al., 2001; Matsumoto et al., 1992), yet *Tnc* expression persists in pregnant EC, in the setting of the mammary gland it is plausible that *Tnc* has additional functions in EC. These could include vessel stabilisation, based on the putative role for *Tnc* in the recruitment of vascular smooth muscle cells (Ando et al., 2011) and the promotion of capillary-tube stability by *Tnc* in cultured retinal EC (Castellon et al., 2002); or one of pro-survival, based on findings that *Tnc* decreased apoptosis of retinal EC *in vitro* in pro-apoptotic culture settings (Castellon et al., 2002). Whilst a role for *Tnc* in vascular remodelling during mammary gland morphogenesis is only hypothetical at this stage, further investigative analyses will no doubt aid in unravelling a novel role for *Tnc* in this dynamic process.

5.4.1.5 *Mmp2*

MMPs comprise a large and diverse family of zinc-dependent proteolytic enzymes, known as endopeptidases. Collectively, MMPs are capable of degrading all kinds of extracellular matrix proteins, and can also process a number of bioactive molecules which regulate various cell behaviours. MMPs are synthesized as latent zymogens and are only activated upon proteolytic cleavage, involving processing of the cysteine-rich N-terminal propeptide (Egeblad and Werb, 2002). In fact, pro-MMP-2 is activated at the cell surface through a unique multistep pathway that involves a second interacting membrane-bound MMP, MMP-14 (Strongin et al., 1995). MMP activity is also tightly controlled by endogenous inhibitors, such as thrombospondin 1 (TSP1) and thrombospondin 2 (TSP2), which form a complex with MMPs and facilitate scavenger receptor-mediated endocytosis leading to irreversible clearance, and TIMPs, which reversibly inhibit MMPs in a stoichiometric manner (Egeblad and Werb, 2002). TSP1 binds pro-MMP-2 and directly inhibits MMP-2 activation (Bein and Simons, 2000), whilst TSP2 forms a complex with MMP-2 and facilitates scavenger receptor-mediated endocytosis and clearance (Yang et al., 2001) as a means of regulating extracellular MMP-2 levels. Although TIMPs are typically inhibitors of MMP activity, paradoxically, studies using *Timp2*-deficient mice established that TIMP-2 can in fact activate MMP-2 by acting as a co-factor in a complex with MMP-14 and pro-MMP-2 at the cell surface (Wang et al., 2000). Intriguingly, Bruyère *et al.* recently identified MMP-2 as a pro-lymphangiogenic growth factor in a lymphatic ring assay (Bruyère et al., 2008). In addition, *Mmp2* expression was demonstrated to closely correlate with the onset of lymphangiogenesis in a mouse model of adult skin regeneration (Rutkowski et al., 2006). Taken together, these data highlight a potential role for MMP-2, and its associated regulators, in lymphangiogenesis.

In accordance, our microarray studies revealed increased levels of *Mmp2* (5.6-fold, $P=0.29$), *Mmp14* (3.1-fold, $P=0.29$) and *Timp2* (2.0-fold, $P=0.18$), in haematopoietic and myoepithelial cells of the pregnant mouse mammary gland, respectively. Given that MMP-14 (Strongin et al., 1995) and TIMP-2 (Wang et al., 2000) have been shown to activate pro-MMP-2, the increase in *Mmp14* and *Timp2* illustrates a likely mechanism by which the processing and activity of MMP-2 is further enhanced in the pregnant mouse mammary gland. Consistent with increased expression of the initiators of MMP-2 activity, we found levels of the gene coding for TSP1, *Thsd1*, an established inhibitor of MMP-2 (Bein and Simons, 2000), were unchanged in pregnant compared to virgin myoepithelial cells. The upregulation of *Mmp2*, *Mmp14* and *Timp2* in pregnancy corresponds with a time of peak lymphatic vessel density (Figure 3.2C) in the mouse mammary gland. The recent documentation that MMP-2 is pro-lymphangiogenic (Bruyère et al., 2008) suggests a role for MMP-2 and positive mediators of MMP-2 activity, MMP-14 and TIMP-2, in the regulation of lymphangiogenesis during postnatal mouse mammary gland morphogenesis. Further investigation of MMP-2 protein levels and its role *in vivo* in the mouse mammary gland is required and could be an interesting possibility to pursue in the future.

5.4.1.6 *Bdnf*

BDNF is a member of the neurotrophin family of soluble peptide growth factors, which are best known for their role in the nervous system (Skaper, 2008). BDNF is required for the maintenance of cardiac vessel wall stability during embryonic development through direct angiogenic actions on EC expressing the tropomyosin-related kinase B (TrkB) receptor (Donovan et al., 2000). In addition, adenoviral delivery of BDNF has been shown to induce neovascularisation in ischemic and non-ischemic adult mouse tissues, as evidenced by increased vascular density, by acting either directly on EC through the interaction with the TrkB receptor, or via the recruitment of bone marrow-derived precursors (Kermani et al., 2005). Similarly, overexpression of BDNF in the mid-gestational mouse heart results in an increase in capillary density (Donovan et al., 2000). More recently, work by Liu *et al.* suggested that retinal neuronal tissue releases neurotrophic factors that regulate new vessel growth in pathological retinal neovascularisation, characteristic of diabetic retinopathy (Liu et al., 2010) and a recent publication by Lam *et al.* showed that the overexpression of BDNF promoted EC proliferation, migration, invasion and survival. Lam *et al.* demonstrated that BDNF is a potent angiogenic factor facilitating tumour growth by promoting angiogenesis in a mouse tumour xenograft model and that BEC exhibited strong BDNF immunoreactivity in human hepatocellular carcinoma tissue samples (Lam et al., 2011). Taken together, these data indicate that BDNF is a novel, relatively uncharacterised but potent stimulator of angiogenesis.

Interestingly, *Bdnf* was found to be increased 3.5-fold ($P < 0.05$) in pregnant myoepithelial cells compared to luminal epithelial cells (Table 5.7) in the mouse mammary gland. We can speculate that this increase in *Bdnf* may be responsible, at least in part, for the increased capillary density observed in the postnatal mouse mammary gland at this time (Figure 1.7F) (Pepper et al., 2000), whereby BDNF secreted from ductal epithelial cells, most likely the myoepithelium, can interact with the TrkB receptor on the surface of EC in a paracrine mechanism to induce vessel growth. Whether EC in the mouse mammary gland actually express the TrkB receptor necessary to respond to BDNF remains to be determined and forms the basis of future investigative analyses.

5.4.2 *Bfk* is an interesting gene likely involved in postnatal mouse mammary gland morphogenesis

Bfk, also known as BCL2-like 15, is a relatively new and uncharacterised member of the mammalian Bcl2 family; a family of intracellular proteins which orchestrate the evolutionary conserved process of programmed cell death, known as apoptosis. This family of proteins all share at least one conserved Bcl2 homology (BH) domain and can be further subdivided on the basis of their function, as either anti- or pro-apoptotic (Cory and Adams, 2002). *Bfk* is considered a rather unusual member of the Bcl2 family in the sense that it contains a BH2 and BH3 domain, but not a BH4 or defined BH1 region, it weakly induces apoptosis and fails to interact with any other Bcl2 family member and thus *Bfk* is structurally most closely related to Bcl-G_L (Coultas et al., 2003); another weakly pro-apoptotic protein which contains both a BH2 and BH3 domain, whilst lacking a clearly identifiable BH1 domain (Guo et al., 2001). *Bfk* also lacks a C-terminal hydrophobic membrane anchor, however, unlike Bcl-G_L which associates with organelles, *Bfk* is localised primarily in the cytosol (Coultas et al., 2003; Guo et al., 2001). Low amounts of *Bfk* protein has been documented to be expressed in the stomach, bone marrow, spleen, ovary, uterus and testes, while of interest to this study, high levels are present in the mammary gland (Coultas et al., 2003; Pujianto et al., 2007). Interestingly, two independent research groups documented that *Bfk* is temporally regulated at both the mRNA and protein level in the postnatal mouse mammary gland; being below the level of detection in adult virgin females, dramatically increasing during mid-late pregnancy, prior to a peak in expression on the first day of lactation, followed by a subsequent decline in levels at the onset of involution (Coultas et al., 2003; Pujianto et al., 2007). This unique expression pattern suggests that *Bfk* may potentially be regulated by female steroid hormones. A more recent study by Pujianto *et al.* demonstrated expression of the *Bfk* transcript in the mouse epididymis at a level comparable to that previously demonstrated in the mammary gland. In the

epididymis, however, Bfk was found to localise predominantly to the nucleus of epididymal principal cells and was shown to be regulated by androgens and other testicular growth factors (Pujianto et al., 2007). Given the correlation of Bfk expression in the epididymis and mammary gland with stages when these tissues are undergoing an increase in cell number and the appearance of different cell types, Pujianto *et al.* concluded that in the epididymis, at least, Bfk may be involved in the proliferation and differentiation of epithelial cells (Pujianto et al., 2007). Despite these initial investigations being some years ago now, no additional studies have shed any further light on this novel protein and therefore a definitive role for Bfk in these tissues remains to be experimentally validated.

The increase in *Bfk* transcript levels in the pregnant mouse mammary gland is intriguing and is no doubt indicative of a role for *Bfk* in mouse mammary gland morphogenesis. Although our microarray and real-time RT-PCR data is in accordance with studies from both Coultas *et al.* and Pujianto *et al.*, such an expression profile is inconsistent with its reported role as weakly pro-apoptotic protein (Coultas et al., 2003; Pujianto et al., 2007). A pro-apoptotic protein, such as Bfk, would be expected to be elevated during involution; a period when apoptosis occurs in a rampant manner (Richert et al., 2000). It is conceivable that in the setting of the mammary gland, *Bfk* functions as a pro-survival signal rather than a pro-apoptotic one in a similar fashion to *Bcl-x*; another member of the Bcl2 family. *Bcl-x* is the most abundant cell survival factor expressed in the mammary epithelia. Although mRNA levels are low in virgin mammary tissue, levels markedly increase during pregnancy (Walton et al., 2001), mirroring our and others' expression patterns of *Bfk* (Coultas et al., 2003; Pujianto et al., 2007). Furthermore, it has been suggested that the weak pro-apoptotic activity of full-length Bfk could represent a latent form and only upon cleavage via an intracellular protease that Bfk switches to a highly potent apoptotic BH3-only protein (Coultas et al., 2003). As the precise role of Bfk in the mammary gland currently remains a mystery, ascertaining the precise spatial and temporal expression patterns of Bfk in the mammary gland will be critical to further understanding the functional role of Bfk *in vivo* in postnatal mouse mammary gland morphogenesis. The generation of knockout mice will further prove advantageous in determining the exact biological function of this novel protein in the whole animal setting.

5.5 CONCLUSION

The work described in this chapter documents the development and optimisation of techniques designed to isolate enriched populations of cells from virgin and pregnant mouse mammary glands for subsequent microarray analyses. Essential to the success of this wide-scale gene expression profiling

study was the acquisition of sufficient quantities of high quality RNA. Due to limiting cell yields following FACS in isolated virgin epithelial populations, a method for the robust amplification of total cellular RNA was successfully employed. In retrospect, the optimal morphogenetic time point corresponding with peak angiogenesis and lymphangiogenesis in the postnatal mouse mammary gland may have been earlier in pregnancy than the time point used for our microarrays and consequently genes important for mammary gland angiogenesis and lymphangiogenesis may have been inadvertently overlooked. Nonetheless, *Cxcl15*, *Adam10*, *Anxa1* and *Tnc* were identified as highly differentially expressed genes between virgin and pregnant mammary gland EC and *Bdnf* was differentially expressed between pregnant luminal and myoepithelial cells. All of these genes have previously been ascribed putative angiogenic roles in various biological settings. Moreover, *Mmp2* was identified as a likely pro-lymphangiogenic growth factor elevated in expression in the pregnant mouse mammary gland. Together, these genes undoubtedly have the potential to be novel key players in the regulation of vascular remodelling during postnatal mouse mammary gland morphogenesis and will form the basis of future studies.

CHAPTER 6

Investigating the role of *Patched 1* in mammary gland lymphatic vessels

6.1 INTRODUCTION

While studies to investigate lymphatic vessel patterning and remodelling via the analysis of mammary gland tissue sections were in progress, a study was published suggesting that the Hedgehog (Hh) transmembrane receptor, Patched 1 (*Ptch1*), and the Hh target gene, glioma-associated 1 (*Gli1*), were expressed in the lymphatic vessels of mouse mammary glands and other adult tissues (Hatsell and Cowin, 2006). The Hh signalling axis has demonstrated roles in the formation of many vertebrate epidermal appendages; these include exocrine glands, hair, whiskers, feathers, scales, teeth and nails (Chuong et al., 2000). *Ptch1*, a key component of the Hh pathway, represses Hh signalling in the absence of Hh ligand. Upon binding to Hh, however, *Ptch1* repression of Smoothed (Smo), a second transmembrane receptor, is relieved and downstream Hh target genes are activated (Hooper and Scott, 2005; Ingham and McMahon, 2001). Studies by Hatsell and Cowin, utilising a variety of mouse models, demonstrated that unlike other epidermal appendages, positive Hh signalling was absent or repressed throughout embryonic mammary gland development, with the exception of *Ptch1-lacZ* and *Gli1-lacZ* expression in the lymphatic vasculature of the adult mammary gland. Moreover, their work demonstrated that repression of Hh signalling was required for normal mammary gland development (Hatsell and Cowin, 2006). These expression studies were performed using *Ptch1^{lacZ/+}* and *Gli1^{lacZ/+}* mice, in which the *lacZ* reporter gene was knocked in to the endogenous *Ptch1* and *Gli1* loci, respectively.

On the basis of Hatsell and Cowin's claim that *Ptch1* and *Gli1* were expressed in mammary gland lymphatic vessels (Hatsell and Cowin, 2006), we reasoned that *Ptch1^{lacZ/+}* mice (Goodrich et al., 1997) would provide a suitable model system in which to assess lymphatic vascular patterning in three-dimensions in whole mouse mammary glands, using X-gal staining to detect *lacZ* reporter gene activity. In addition, we postulated that *Ptch1^{lacZ/+}* mice would prove a useful tool in which to investigate the role of Hh signalling in lymphatic vascular development.

6.1.1 An overview of the Hedgehog signalling pathway

The Hh intracellular signalling pathway is one of the key evolutionarily conserved pathways governing a wide variety of processes fundamental to both embryonic development and the adult organism (Hooper and Scott, 2005; Jiang and Hui, 2008). Hh, the pathway's namesake, was first identified in the early 1990's in genetic screens of *Drosophila melanogaster*, as a segment-polarity gene (Nüsslein-Volhard

and Wieschaus, 1980). Since this time, homologues of many components of the *Drosophila* Hh family have been identified in vertebrates. In contrast to the single *Hh* gene found in *Drosophila*, three Hh homologues have been identified in mammals; Sonic hedgehog (Shh), Desert hedgehog and Indian hedgehog, of which Shh is the most commonly expressed and best characterised (Ingham and McMahon, 2001). The activities of these genes are equally important during vertebrate embryogenesis as they are in the insect. Hh signalling is active in a variety of cell types and organs and controls events such as cell fate determination, proliferation, patterning and morphogenesis (Ingham and McMahon, 2001; Jiang and Hui, 2008). The three *Hh* genes are expressed in different tissues and at different stages of development and potentially have distinct biological roles. Furthermore, these morphogens can act in a short- or long-range fashion and in a direct or indirect mechanism (Ingham and McMahon, 2001). Aberrant activation and dysfunction of this key developmental pathway is associated with numerous forms of human cancer, including basal cell carcinoma and medulloblastoma (Evangelista et al., 2006; Jiang and Hui, 2008). Furthermore, the Hh signalling axis is becoming increasingly linked with breast cancer initiation, progression and metastasis (Kasper et al., 2009).

Hh signal transduction is triggered by binding of the secreted Hh ligand, which undergoes auto-processing and lipid modification, to the 12-pass transmembrane receptor, Ptch1. In the absence of the Hh protein, Ptch1 represses signal transduction by preventing localisation of the seven-transmembrane protein, Smo, a positive regulator of Hh signalling, at the cell surface (Figure 6.1A). Three homologues of the *Drosophila* segment-polarity gene, *cubitus interruptus*, exist and are known as the glioma-associated (Gli) family of zinc-finger transcription factors, designated Gli1, Gli2 and Gli3. In mammalian cells, Gli1 and Gli2 predominantly serve as activators of downstream Hh target genes, whilst Gli3 acts mostly as a transcriptional repressor (Hooper and Scott, 2005; Ingham and McMahon, 2001). Thus, in the 'inactive' state, the transcriptional activators, Gli1 and Gli2, are prevented from entering the nucleus and as a result, the transcription of Hh target genes is repressed (Figure 6.1A). Upon Hh binding, however, the inhibitory function of Ptch1 on Smo is relieved, resulting in cell surface accumulation and activation of Smo (Figure 6.1B). Once activated, Smo modulates the activities of the Gli transcription factors leading to transcription of Hh target genes (Evangelista et al., 2006; Ingham and McMahon, 2001; Ingham and Placzek, 2006; Jiang and Hui, 2008). The Gli effectors also control the expression of *Ptch1* and *Gli1* themselves, providing negative and positive feedback regulation of Hh signalling, respectively (Ingham and McMahon, 2001). In addition to these core constituents, other members of the mammalian Hh signalling axis have been identified and their respective roles determined, but for simplicity purposes, will not be discussed here.

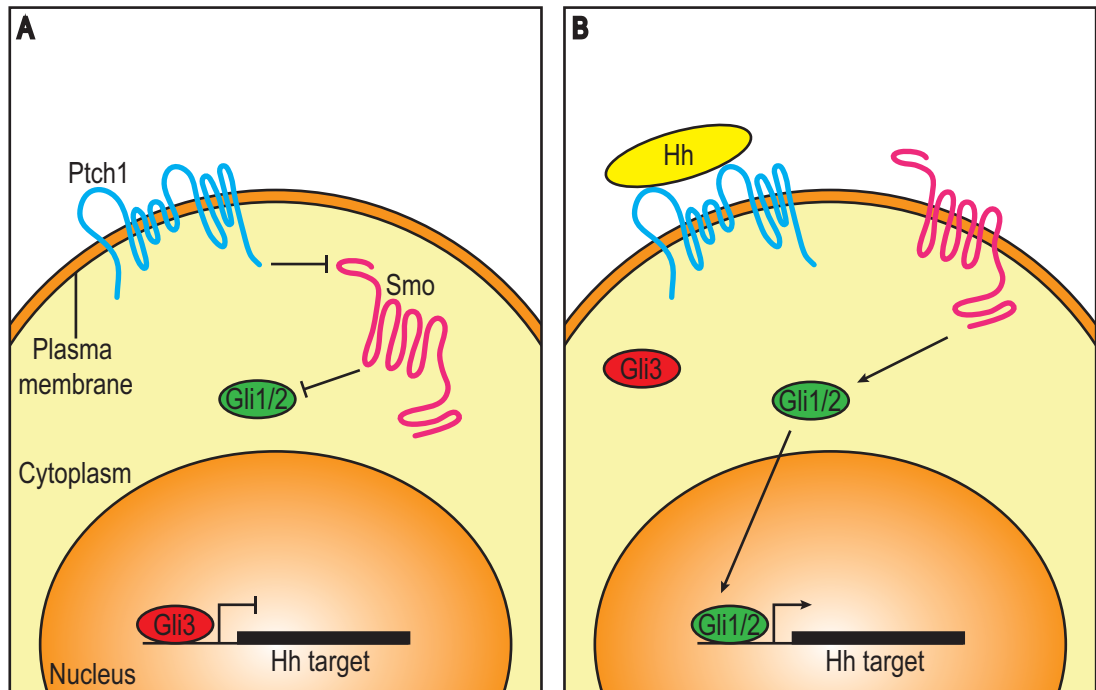


Figure 6.1 - A simplified model of Hedgehog signalling in mammalian cells.

(A) In the absence of Hedgehog (Hh) protein ligand, the transmembrane receptor, Patched 1 (Ptch1), suppresses signal transduction by inhibiting the cell surface localisation of a second transmembrane receptor, Smoothed (Smo). Therefore, the transcriptional activators, Glioma-associated (Gli)1 and Gli2 are prevented from entering the nucleus and as a result downstream Hh target genes are not transcribed. (B) Upon Hh binding, the inhibitory function of Ptch1 on Smo is relieved, resulting in cell surface accumulation and activation of Smo. Smo is now able to activate the Gli transcription factors, leading to transcription of Hh target genes. Figure adapted from Hooper and Scott, 2005; Ingham and Placzek, 2006.

6.1.2 Patched 1

Despite an understanding of the primary function of the multipass transmembrane *Ptch1* receptor as the chief negative regulator of the Hh signalling cascade (section 6.1.1); many aspects of *Ptch1* signalling still remain uncertain. What is recognised, however, is that *Ptch1* is important in a number of human disorders and is generally accepted as having a tumour suppressive role (Hahn et al., 1996b; Hahn et al., 1999).

Mutations in the *PTCH1* gene, the human homologue of the *Drosophila* segment-polarity *patched* gene, have been identified in Gorlin syndrome, also known as basal cell nevus syndrome (Hahn et al., 1996b; Johnson et al., 1996). This rare autosomal dominant disorder is characterised by skeletal defects; such as syndactyly (the fusion of two or more digits), polydactyly (extra digits), closure defects of the spinal cord, rib and vertebrae anomalies, a large body size, characteristic broad facial features and an increased propensity to develop medulloblastoma, a highly malignant primary childhood brain tumour that originates in the cerebellum, and skin basal cell carcinomas (Kimonis et al., 1997). The anatomical location of these defects correlates with the major sites of murine embryonic *Ptch1* expression, which includes the developing somites, neural tube, branchial arches, limb buds and spinal cord (Goodrich et al., 1996; Hahn et al., 1996a). Other regions of *Ptch1* expression during mouse embryogenesis include the gut, palate, tongue, tooth buds, genital eminence, hair and whisker (vibrissae) follicles (Goodrich et al., 1996; Hahn et al., 1996a). Inactivating mutations in the *PTCH1* gene have also been detected in a large cohort of patients with sporadic basal cell carcinomas (Gailani et al., 1996; Hahn et al., 1996b) and at least a subset of sporadic cases of medulloblastoma (Raffel et al., 1997); further reiterating that *Ptch1* plays important roles as a tumour suppressor gene.

6.1.2.1 Generation of *Ptch1^{lacZ/+}* mice

The generation of *Ptch1^{lacZ/+}* mice has been previously reported (Goodrich et al., 1997). These mice were produced on a C57BL/6 background by homologous recombination; part of *Ptch1* exon 1 and all of exon 2 were replaced with the reporter gene encoding beta-galactosidase (β -gal), *lacZ*, and a neomycin resistance gene. This modification results in the *lacZ* reporter gene being expressed selectively in cells in which *Ptch1* is normally expressed. At the same time, the insertion of *lacZ* into the *Ptch1* locus results in *Ptch1* gene expression being interrupted, leading to a loss of function of *Ptch1* and early embryonic lethality of homozygous *Ptch1* mice (*Ptch1^{lacZ/lacZ}*) (Goodrich et al., 1997; Hahn et al., 1998). Mice

containing a single copy of the *lacZ* gene are therefore heterozygous for *Ptch1* (*Ptch1^{lacZ/+}*) and are viable (Goodrich et al., 1997; Hahn et al., 1998).

6.1.2.2 *Patched 1* mouse models

As detailed above, activation of the Hh pathway is initiated by binding of the Hh ligand to Ptch1. Since Ptch1 acts as a negative regulator of the Hh signaling axis, loss of Ptch1 function in a mouse model results in Hh pathway activation and constitutive stimulation of downstream target genes, even in the absence of Hh signal (Hahn et al., 1999). As such, loss of function of *Ptch1* in a mouse model faithfully recapitulates many symptoms of the human Gorlin syndrome phenotype. Heterozygous *Ptch1* knockout mice display the characteristic features of Gorlin syndrome including skeletal abnormalities; such as hindlimb defects, extra and fused digits, a failure of the neural tube to close, a generalised overgrowth, and a predisposition to medulloblastoma and rhabdomyosarcoma tumours. Thus far, no basal cell carcinomas have been reported in *Ptch1* heterozygous mice (Goodrich et al., 1997; Hahn et al., 1999; Hahn et al., 1998). Interestingly, the phenotype of *Ptch1* heterozygous mice has been noted to be dependent on the genetic background of the mice, with more *Ptch1* heterozygous embryos dying prenatally on an inbred, compared to an outbred background (Hahn et al., 1998). On the other hand, homozygous *Ptch1* mutants die in utero during early embryogenesis between E9.0-10.5. A failure in the closure of the neural tube was observed in all these mice; however, aberrant development of the foetal heart is speculated to be the likely cause of the embryonic lethality (Goodrich et al., 1997; Hahn et al., 1998).

Ptch1^{lacZ/+} mice were recently the subject of a study by Hatsell and Cowin investigating the role of Hh signalling in embryonic and postnatal mouse mammary gland development. Whilst the key results generated from their study have little bearing on our project, Hatsell and Cowin claimed that although expression of the Hh target genes, *Gli1* and *Ptch1*, were not detected in the adult mammary gland parenchyma, both *Gli1* and *Ptch1*, by virtue of *lacZ* reporter expression, were expressed in mammary lymphatic vessels (Hatsell and Cowin, 2006). *LacZ* reporter gene expression was also detected in lymphatic vessels of other adult tissues, including the surface of the heart and omentum, a region of the peritoneal membrane (Hatsell and Cowin, 2006).

Despite the fact that this lymphatic vessel-restricted expression profile was a minor finding in Hatsell and Cowin's published work (Hatsell and Cowin, 2006), it had the potential to have a profound impact on this project for two reasons:

1. A lymphatic vessel-restricted *lacZ* expression profile would provide a useful tool for the three-dimensional imaging of lymphatic vascular growth and remodelling in whole mouse mammary glands.
2. The expression of *Ptch1* specifically in lymphatic vessels would suggest a role for Hh signalling in lymphatic vessel development and/or function; a possibility not previously explored in the field.

To this end, we embarked on an extensive analysis of *Ptch1* expression with respect to the lymphatic vasculature in *Ptch1^{lacZ/+}* mice.

6.2 METHODS

6.2.1 Genotyping of *Ptch1^{lacZ/+}* mice

6.2.1.1 Genomic DNA extraction from mouse tails

In order to maintain the *Ptch1^{lacZ/+}* mice on a C57BL/6 background, C57BL/6 mice were crossed with *Ptch1^{lacZ/+}* mice to generate litters that were a mix of *Ptch1^{lacZ/+}* mice and *Ptch1^{+/+}* control littermates. The distal one third of tails were removed from 10 day old suckling pups for maintenance of the breeding colony or from mouse embryos prior to experimentation. The tails were digested overnight in 700µl (pup tails) or 500µl (embryonic tails) of digestion buffer containing 20mM Tris-Cl (pH 8.0), 5mM EDTA (pH 8.0), 400mM NaCl, 1% (w/v) SDS and 0.5mg/ml proteinase K (Roche) at 55°C in an Eppendorf Thermomixer (Eppendorf) at 800 revolutions per minute. Genomic DNA was extracted via the addition of 600µl of a 1:1 mix of phenol and chloroform, mixing and then centrifugation for 10 minutes at 9,500 x g. Following centrifugation the aqueous phase, containing the genomic DNA, was carefully removed avoiding the interface and transferred to a new tube. An equal volume of isopropanol was added to the aqueous phase to precipitate the genomic DNA, followed by centrifugation for 15 minutes at 16,000 x g. The resulting DNA pellet was washed with 500µl of ice-cold 70% (v/v) ethanol and centrifuged for a further 5 minutes at 16,000 x g, prior to drying the pellet at 37°C for 10-15 minutes. Once dry, the DNA pellet was resuspended in 100µl (pup tails) or 40µl (embryonic tails) sterile MQ-H₂O, vortexed briefly and incubated at 37°C overnight. Genomic DNA was stored at 4°C.

6.2.1.2 Genotyping PCR primers

Genotyping primer sequences were kindly provided by Trudy Oliver from Duke University (Durham, NC). Two primers sets were utilised; one to detect WT mice using 5'-CTGCGGCAAGTTTTTGGTTG-3' and 5'-AGGGCTTCTCGTTGGCTACAAG-3' primers and a second set to detect insertion of the *lacZ* and neomycin resistance genes using 5'-TGGGGTGGGATTAGATAAATGCC-3' and 5'-TGTCTGTGTGCTCCTGAATCAC-3' primers, generating a 217bp and 501bp PCR product, respectively. Because *Ptch1^{lacZ/lacZ}* embryos die prior to the embryonic stages collected for our studies, *Ptch1^{+/+}* and *Ptch1^{lacZ/+}* mice were easily distinguished by the presence of a 217bp band or both a 217bp and 501bp band, respectively, when analysed via DNA gel electrophoresis (section 2.2.2.2).

6.2.1.3 Genotyping PCR

Genomic DNA concentration was determined on a NanoDrop™ 1000 spectrophotometer (NanoDrop Technologies) (section 2.2.2.11) and diluted to 150ng/μl. Genotyping PCRs were performed in a 20μl total reaction volume containing 1x ThermoPol buffer (New England BioLabs), 150ng of genomic DNA template, 0.2mM dNTPs, 1U *Taq* DNA polymerase (New England BioLabs) and 10pmol of both forward and reverse primers. Amplification was performed in an Eppendorf Mastercycler (Eppendorf) with the following parameters: an initial denaturation step of 94°C for 5 minutes, followed by 35 cycles of denaturation at 94°C for 30 seconds, primer annealing at 56°C for 1 minute and extension at 72°C for 1 minute, followed by a final extension at 72°C for 5 minutes and cooling to 4°C. Reactions were stored at 4°C until visualisation using DNA AGE (section 2.2.2.2).

6.2.2 Mammary gland whole mount X-gal staining

Mammary glands were dissected as per section 2.2.4.1 and fixed in 4% PFA on ice for 1 hour. Following fixation, glands were incubated on ice for 3 x 1 hour in 'rinse buffer' consisting of PBS with 2mM MgCl₂, 0.1% (w/v) sodium deoxycholate and 0.2% (v/v) Igepal CA-630 (Sigma-Aldrich). Glands were then stained overnight at 30°C in the dark in 'rinse buffer' containing 1mg/ml 5-bromo-4-chloro-3-indolyl-β-D-galactopyranoside (X-gal), 5mM potassium ferricyanide and 5mM potassium ferrocyanide. Glands were subsequently washed 3 x 10 minutes in PBS on ice and post-fixed in 4% PFA for 1 hour at RT (for whole mount processing) or overnight at 4°C (for cryopreservation), followed by 3 x 10 minute washes in PBS on ice. Mammary glands processed for cryosectioning were prepared as previously described in section 2.2.4.3.1, followed by 3,3'-diaminobenzidine (DAB) immunostaining (section 6.2.3). Alternatively,

mammary glands that were processed for whole mount staining were rinsed in MQ-H₂O, dehydrated through a graded ethanol series (70%, 90% and 100% (v/v), diluted using MQ-H₂O) for 15 minutes each step, cleared in xylene for 2 x 15 minutes and then mounted using DePeX mounting medium (BDH) and a 24mm x 50mm glass coverslip. Any gaps that appeared on drying were filled with fresh DePeX mounting medium the following day and left to set completely. Image acquisition was as detailed previously in section 3.2.1.

6.2.3 Mammary gland section DAB immunostaining

DAB immunohistochemistry was performed following X-gal staining (section 6.2.2). All incubations were performed at RT unless otherwise indicated. Selected slides were removed from -70°C storage, framed with an ImmEdge™ Pen (Vector Laboratories) and air-dried for 5 minutes. Slides were washed for 15 minutes in TBS-0.1%TW20, followed by 2 x 5 minute washes in PBS and quenching of endogenous peroxidase activity with 0.33% (v/v) hydrogen peroxide in PBS for 30 minutes. Slides were then washed 2 x 5 minutes in PBS, blocked for 30 minutes using 20% (v/v) newborn bovine serum (SAFC Biosciences), 60% (v/v) maleate buffer (pH 7.5) and 2% (w/v) Blocking Reagent (Roche) in a humidified chamber, followed by the addition of primary antibodies (Table 2.1) diluted in blocking solution and incubated overnight. Sections were washed 2 x 5 minutes in PBS, followed by incubation with biotin-conjugated secondary antibodies (Vector Laboratories) (Table 2.2), also diluted in blocking solution, for 1 hour in a humidified chamber, prior to 2 x 5 minute washes in PBS. Sections were then incubated for 30 minutes with VECTASTAIN® *Elite* ABC Kit (Vector Laboratories) reagent, prepared in advance as described in the kit instructions, followed by 2 x 5 minute washes in PBS. Next the slides were incubated with DAB Peroxidase Substrate Kit (Vector Laboratories) until optimal colour development, followed by 2 x 5 minutes in PBS. Sections were subsequently air-dried and mounted using VectaMount™ AQ Aqueous Mounting Medium (Vector Laboratories). Images were acquired as detailed previously in section 4.2.1.

6.2.4 Embryonic and adult mouse tissue collection, processing and immunostaining

6.2.4.1 Embryonic and adult tissue collection and fixation

Embryos were harvested from pregnant female mice at the desired embryonic day and adult tissues were dissected as required with the aid of an Olympus SZX7 stereo microscope (Olympus). Post-dissection, all tissues were washed 3 x 10 minutes in PBS on ice. Depending on subsequent experiments, tissues were subjected to differential fixation in 4% PFA. Embryos and adult tissues that were subsequently whole mount X-gal stained, cryopreserved, sectioned and DAB immunostained (section 6.2.4.2-4) were fixed for 1 hour in 4% PFA on ice. Alternatively, E16.5 embryos used for dermal skin immunofluorescence (section 6.2.4.5) were fixed overnight at 4°C in 4% PFA with gentle agitation, followed by 3 x 10 minute washes in PBS on ice and storage at 4°C in PBS containing 0.01% (w/v) thimerosal.

6.2.4.2 Embryonic and adult tissue whole mount X-gal staining

Following appropriate fixation, embryos and tissues were rinsed twice on ice for 10 minutes each in PBS, prior to permeabilisation for 15 minutes on ice using MQ-H₂O containing 2mM MgCl₂, 0.01% (w/v) sodium deoxycholate and 0.02% (v/v) Igepal CA-630 (Sigma-Aldrich). A second permeabilisation step was performed in the same solution, but incubated at RT for a further 15 minutes. Tissues were stained overnight at 30°C in the dark in PBS containing 1mg/ml X-gal, 5mM potassium ferricyanide, 5mM potassium ferrocyanide, 2mM MgCl₂ and 0.2% (v/v) Igepal CA-630 (Sigma-Aldrich), then washed 3 x 10 minutes on ice in PBS. At this point in time, images were obtained as previously detailed in section 3.2.1. Following imaging, a selection of adult tissues were post-fixed overnight at 4°C in 4% PFA, washed 3 x 10 minutes in PBS on ice and stored at 4°C for subsequent whole mount DAB immunostaining (section 6.2.4.4.2). Alternatively, embryos and remaining adult tissues for cryopreservation were post-fixed for 6 hours at 4°C in 4% PFA, rinsed 3 x 10 minutes in PBS on ice and transferred to PBS containing 30% (w/v) sucrose.

6.2.4.3 Embryonic and adult tissue cryopreservation and sectioning

Embryonic and adult tissues were cryopreserved and embedded into Tissue-Tek® O.C.T Compound (Sakura) as previously described in section 2.2.4.3.1. 10µm transverse cryosections were collected onto Polysine® slides (Menzel-Gläser) and air-dried at RT for 2 hours. Slides were stored at -70°C.

6.2.4.4 Embryonic and adult tissue DAB immunostaining

6.2.4.4.1 Embryonic and adult tissue section DAB immunostaining

DAB immunostaining was performed on X-gal-stained embryonic and adult tissue cryosections as previously detailed in section 6.2.3.

6.2.4.4.2 Adult tissue whole mount DAB immunostaining

X-gal-stained adult tissues (from section 6.2.4.2) were blocked for 6 hours on ice in a 24 well flat-bottomed tissue culture plate with PBS-0.3%TX100 containing 5% (w/v) normal goat serum (Jackson ImmunoResearch Laboratories) and 0.2% (w/v) BSA. Samples were incubated overnight at 4°C with primary antibodies (Table 2.1) diluted in the same solution used for blocking. Tissues were washed on ice for 6 x 1 hour in PBS-0.1%TX100, followed by the addition of biotin-conjugated secondary antibodies (Vector Laboratories) (Table 2.2) diluted in PBS-0.1%TX100 and incubation overnight at 4°C with gentle agitation. Samples were then washed on ice in PBS-0.1%TX100 for 6 x 1 hour and incubated overnight at 4°C with VECTASTAIN® *Elite* ABC Kit (Vector Laboratories) reagent, prepared in advance as described in the kit instructions. Tissues were extensively washed on ice for 6 x 1 hour in PBS-0.1%TX100, incubated with DAB Peroxidase Substrate Kit (Vector Laboratories) for approximately 2 minutes or until optimal colour development, followed by a brief rinse in PBS. Images were captured as per section 3.2.1. Samples were stored at 4°C in PBS containing 0.01% (w/v) thimerosal.

6.2.4.5 Whole mount embryonic dermal skin immunofluorescent immunostaining

Immunofluorescent immunostaining on E16.5 dermal skin was performed as described previously (Gordon et al., 2008). Following the appropriate fixative procedures (section 6.2.4.1), dermal skin was dissected from the body of the embryo, ensuring that each piece of skin contained a region spanning the mid-line to the flank, to provide a global representation of embryonic skin vasculature. In brief, skin pieces were blocked for 6 hours to overnight at 4°C in a 24 well flat-bottomed tissue culture plate with PBS-0.3%TX100 containing 0.2% (w/v) BSA and 5% (w/v) normal goat serum (Jackson

ImmunoResearch Laboratories), although goat serum was omitted if any of the primary antibodies used were raised in goat. Following blocking, dermal skin samples were incubated with one or more primary antibodies (Table 2.1) diluted in blocking solution overnight at 4°C with gentle agitation, before washing extensively for 6 x 1 hour on ice using PBS-0.1%TX100. Skin samples were subsequently incubated with the respective Alexa Fluor®-conjugated secondary antibodies (Invitrogen) (Table 2.2) overnight at 4°C with gentle agitation, followed by 6 x 1 hour washes on ice in PBS-0.1%TX100. From this point onwards, samples were maintained in the dark to avoid photo-bleaching. Skin samples were mounted in ProLong® Gold antifade reagent (Invitrogen), sealed with nail polish and stored at 4°C. Image acquisition was performed as previously described in section 3.2.2.

6.3 RESULTS

6.3.1 *Ptch1* is not expressed in mammary gland lymphatic vessels

Whole mount X-gal staining of 8 week virgin (Figure 6.2A,B) and 16.5 day pregnant (Figure 6.2C,D) *Ptch1^{lacZ/+}* inguinal mammary glands revealed positive nuclear *lacZ* reporter gene expression in what appeared to be a vascular network, analogous to the reported literature (Hatsell and Cowin, 2006). In order to confirm the identity of these structures as lymphatic vessels, immunostaining with EC antibodies was performed. Our data revealed that the pan-EC marker CD31 was not co-expressed with *lacZ* reporter gene expression (Figure 6.2E,F), suggesting that the β -gal-positive structures were neither blood nor lymphatic vessels. Despite a lack of direct co-localisation of CD31 with *lacZ*, it was interesting to note that CD31-positive vessels, likely blood capillaries, were intimately associated with and, often observed traversing alongside and wrapping around, these structures (Figure 6.2E,F). In contrast, strong immunoreactivity was evident in the structures bounded by β -gal-positive cells upon staining with a rabbit anti-class III β -tubulin antibody (Covance, Princeton, NJ) (Figure 6.2G,H), a routinely used neuronal marker (Katsetos et al., 2003). This data demonstrates that the 'vessel-like' structures present in the mammary gland were in fact neuronal in nature, and in combination with their morphology, represent peripheral nerve fibres. β -gal-positive cells were not β -tubulin-positive, but ensheathed β -tubulin-positive nerve fibres. Immunostaining with LYVE1, a frequently used marker of lymphatic vessels, confirmed that β -gal-positive cells in the mammary gland were not lymphatic vessels. Interestingly, a population of LYVE1-positive macrophages (Gordon et al., 2010) was observed in close association with the nerve fibres (arrowheads; Figure 6.2I). Taken together, these findings unequivocally demonstrate that *Ptch1* is not expressed in lymphatic vessels of the mouse mammary gland, as

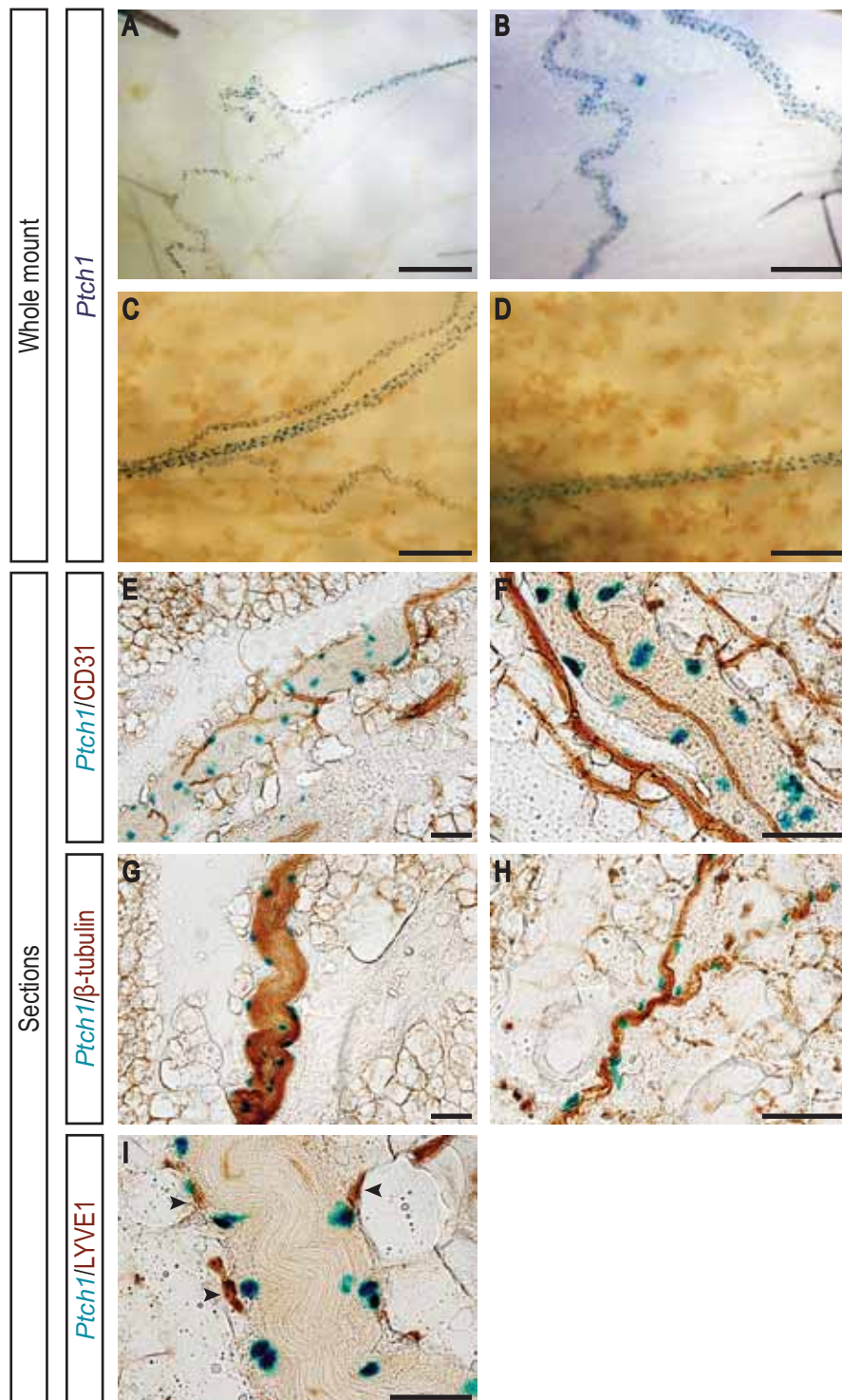


Figure 6.2 - *Ptch1* is expressed in a subset of cells associated with peripheral nerve fibres in the mouse mammary gland.

Whole mount X-gal staining of 8 week virgin (**A,B**) and 16.5 day pregnant (**C,D**) *Ptch1^{lacZ/+}* inguinal mammary glands. DAB immunostaining on 8 week virgin *Ptch1^{lacZ/+}* mammary gland sections reveals that *lacZ* reporter gene expression does not co-localise with CD31 staining (**E,F**), but is rather expressed by a subpopulation of cells associated with β -tubulin-positive peripheral nerve fibres (**G,H**). LYVE1-positive macrophages (arrowheads) are closely associated with these nerve fibres (**I**). Scale bars represent 500 μ m (**A-D**) and 50 μ m (**E-I**).

previously reported (Hatsell and Cowin, 2006), but rather by a subpopulation of cells closely associated with peripheral nerve fibres. We predict that β -gal-positive cells in the mouse mammary gland are perineurial cells, owing to their location, together with previous studies documenting robust *Ptch1* expression in a restricted population of cells encasing developing nerve bundles mid-gestation and in the perineurium of postnatal nerve fibres (Mirsky et al., 1999; Parmantier et al., 1999).

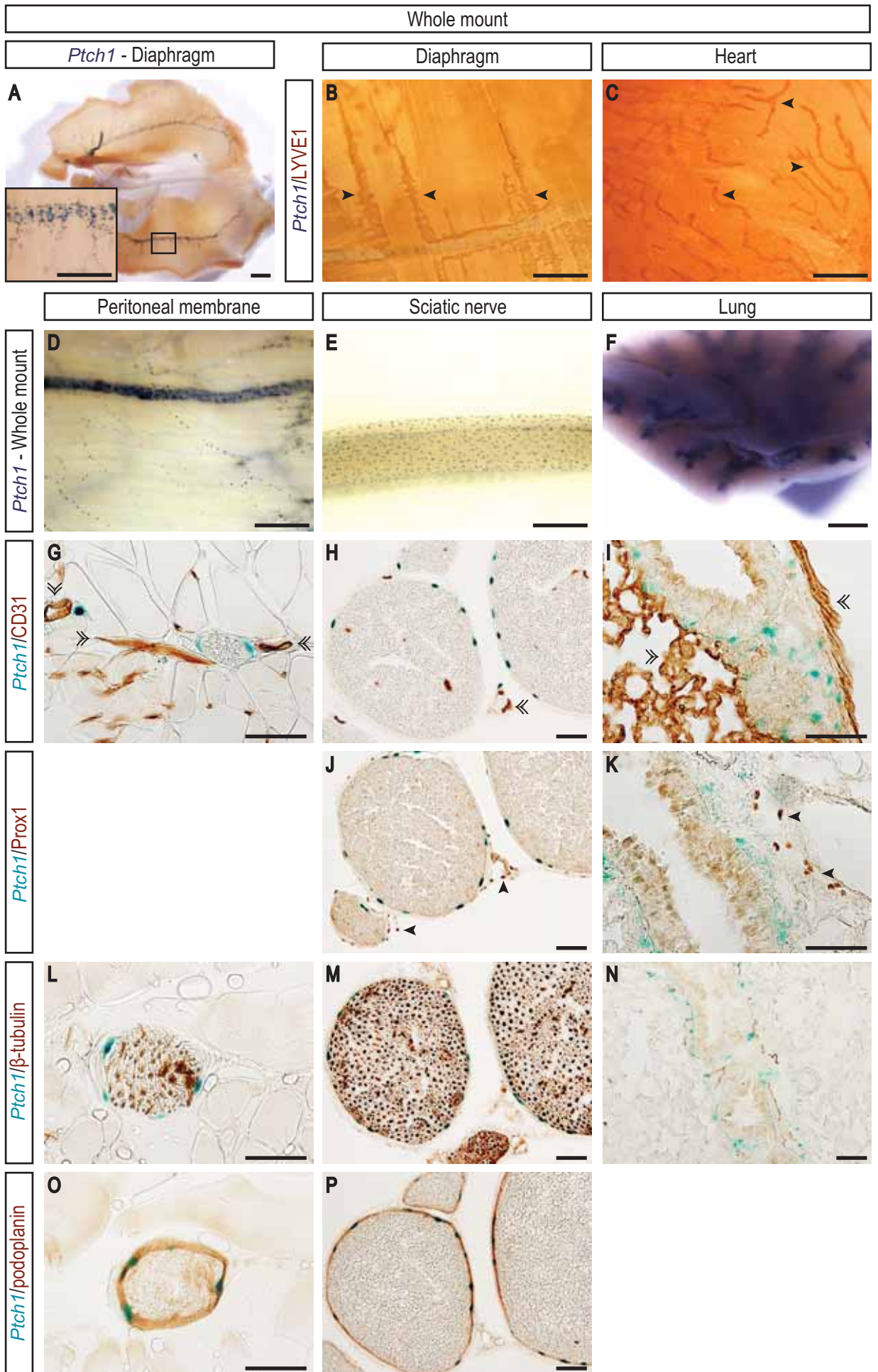
6.3.2 *Ptch1* is not expressed in the lymphatic vasculature of other adult tissues

Due to the lack of detectable *lacZ* reporter gene expression in lymphatic vessels of the mammary gland, additional adult tissues from *Ptch1^{lacZ/+}* mice were analysed for transgene expression. Following whole mount X-gal staining, the diaphragm (Figure 6.3A) and peritoneal membrane (Figure 6.3D) demonstrated robust *lacZ* expression in an elaborate 'vascular-like' network akin to that seen previously in the mammary gland (Figure 6.2A-D). Subsequent whole mount immunostaining using a rabbit anti-mouse LYVE-1 antibody (AngioBio) to detect lymphatic vessels revealed no co-expression with β -gal in adult tissues, including the diaphragm (Figure 6.3B) and heart (Figure 6.3C). This data revealed that, like the mammary gland, *Ptch1* is not expressed in lymphatic vessels of other adult tissues. Based on our demonstration that *Ptch1* is expressed by a subset of cells associated with peripheral nerve fibres in the mouse mammary gland, the sciatic nerve, one of the single largest nerve fibres, was dissected and X-gal-stained, revealing a similar staining pattern on the surface of the nerve (Figure 6.3E) to that seen previously in the mammary gland (Figure 6.2A-D), diaphragm (Figure 6.3A) and peritoneal membrane (Figure 6.3D). This observation verified that the β -gal-positive cells were indeed neural in identity. Interestingly, the lung demonstrated a distinct pattern of intense *lacZ* reporter gene expression in the bronchiolar tree (Figure 6.3F), correlating with an established role for *Ptch1* in lung morphogenesis (Bellusci et al., 1997; Chuang et al., 2003; Pepicelli et al., 1998).

To further investigate the identity and localisation of β -gal-positive cells in adult tissues, X-gal-stained tissues were cryopreserved, sectioned and subjected to DAB immunostaining with a panel of markers. There was no observed co-expression of CD31 (Figure 6.3G,H,I) or Prox1 (Figure 6.3J,K) with *lacZ*, indicating that *Ptch1* is not expressed in blood (double arrowheads) or lymphatic vessels (arrowheads), respectively, in any tissue analysed. Staining with β -tubulin, however, confirmed the neuronal identity of these structures both in the peritoneal membrane (Figure 6.3L), and in transverse sections of the sciatic nerve (Figure 6.3M). Although β -tubulin highlighted small nerve fibres in the lung parenchyma, it did not co-localise with *lacZ* reporter gene expression, which appeared to be expressed by a distinct, non-neuronal population of cells, commonly found scattered at the basal side of the respiratory epithelial

Figure 6.3 - *Ptch1* is not expressed in lymphatic vessels of adult mouse tissues.

Whole mount X-gal staining (**A-F**), followed by subsequent DAB immunostaining on *Ptch1*^{lacZ/+} sections (**G-P**) reveals that *Ptch1* is not expressed in blood (double arrowheads) or lymphatic (arrowheads) vessels in the diaphragm (**A,B**), heart (**C**), peritoneal membrane (**D,G,L,O**) or sciatic nerve (**E,H,J,M,P**), but rather expression is restricted to neuronal structures and a distinct population of cells in the lung (**F,I,K,N**). Inset represents a magnified view of the boxed area in (**A**). Scale bars represent 1mm (**A,F**), 500µm (**inset,B-E**) and 50µm (**G-P**).



layer (Figure 6.3N). Intriguingly, podoplanin staining of both the peritoneal membrane (Figure 6.3O) and sciatic nerve (Figure 6.3P) yielded a positive correlation between the concentric ring of *Ptch1*-expressing cells and a podoplanin-positive sheath surrounding these nerve fibres. Despite podoplanin being an established marker of the lymphatic endothelium, it is also documented to be highly expressed by cells comprising the perineurium (Jokinen et al., 2008; Schacht et al., 2005). Collectively, these results further substantiate the fact that *Ptch1* is expressed in perineurial cells, but not in blood or lymphatic vascular EC, in all adult tissues analysed.

6.3.3 *Ptch1* is not expressed in lymphatic vessels during embryonic development

In order to investigate the expression pattern of *Ptch1* with respect to the lymphatic vasculature during mouse embryogenesis, we performed whole mount X-gal staining on E12.5, E14.5 and E16.5 *Ptch1^{lacZ/+}* and *Ptch1^{+/+}* embryos. At E12.5, prominent *Ptch1* expression was observed in the developing neural tube, somites, limb buds and vibrissae (Figure 6.4A,D,G). A similar pattern of *Ptch1* expression was evident at E14.5 (Figure 6.4B,E,H). By E16.5, however, robust X-gal staining was present in the hair follicles of the skin, vibrissae and digits of the fore and hindlimbs (Figure 6.4C,F,I). As expected, no β -gal staining was detected in WT *Ptch1^{+/+}* littermate controls (insets; Figure 6.4A,B,C). Moreover, no *lacZ* transgene expression was observed in a pattern corresponding to the dermal lymphatic vasculature at these embryonic stages (Figure 6.4).

To further analyse the expression of *Ptch1* at the cellular level we performed DAB immunostaining on transverse sections of X-gal-stained *Ptch1^{lacZ/+}* embryos. At E12.5, *lacZ* reporter gene expression was localised in areas of condensing bone (Figure 6.5A); the ventricular zone of the neural tube and cells comprising, and adjacent to, the notochord (Figure 6.5G). Reporter gene expression was also observed in broad areas of mesenchyme throughout the embryo (Figure 6.5D) and in an area in close proximity to developing tooth buds (Figure 6.5J). *LacZ* expression was not detected in developing Prox1-positive lymphatic vessels (arrowheads; Figure 6.5M), nor was it expressed by the blood vasculature, as visualised with CD31 (Figure 6.5A,D), at this stage of embryonic development. *Ptch1* was expressed in a similar panel of tissues at E14.5, including areas of condensing bone (Figure 6.5B), the developing tongue and tooth primordia (Figure 6.5E), the neural tube ventricular zone (Figure 6.5H) and the gut (Figure 6.5K); but was not present in the liver (Figure 6.5K), or in and around the LEC comprising the jugular lymph sac (Figure 6.5N). By E16.5, the most prominent sites of *Ptch1* expression included areas of condensing bone in the limbs (Figure 6.5C) and tail (Figure 6.5O), hair follicles (Figure 6.5F,I), the tongue and vibrissae (Figure 6.5L) and a discrete population of cells that surround developing nerve

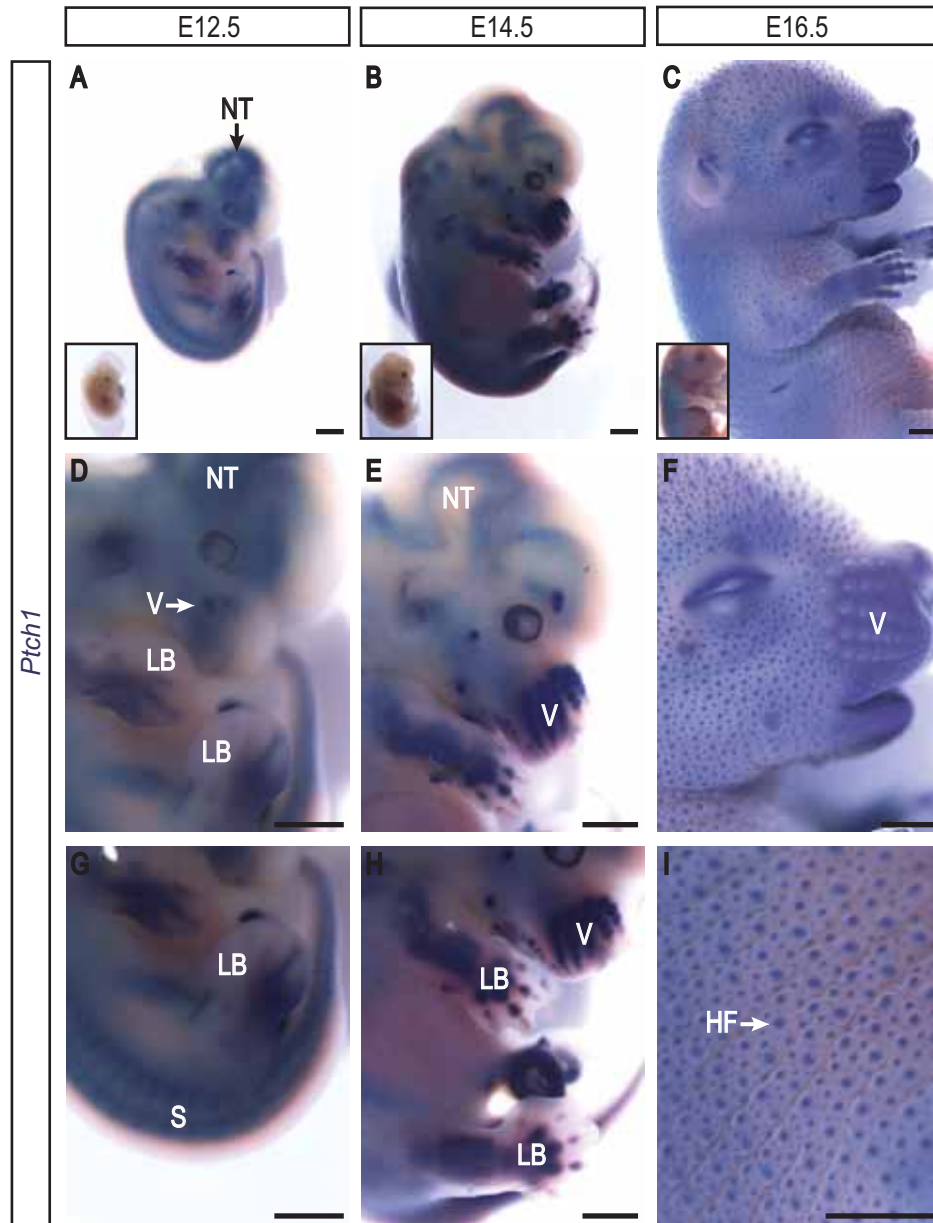
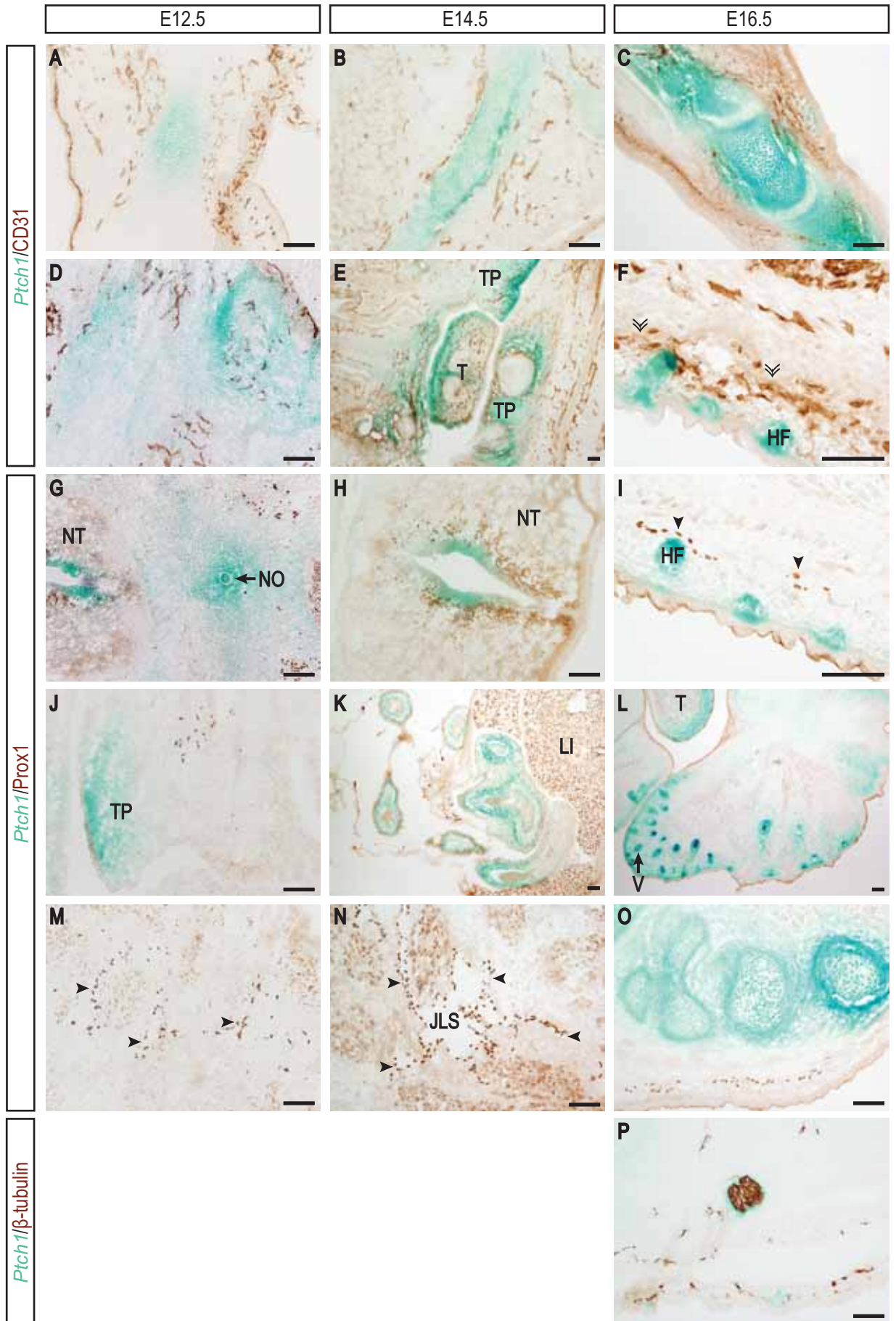


Figure 6.4 - Expression of *Ptch1* during murine embryogenesis.

Whole mount X-gal staining of E12.5 (**A,D,G**), E14.5 (**B,E,H**) and E16.5 (**C,F,I**) *Ptch1^{lacZ/+}* embryos. Insets represent *Ptch1^{+/+}* littermate control embryos. HF - hair follicle, LB - limb bud, NT - neural tube, S - somites, V - vibrissae. Scale bars represent 1mm.

Figure 6.5 - Detailed expression analysis of *Ptch1* during murine embryogenesis.

DAB immunostaining on transverse sections of E12.5 (**A,D,G,J,M**), E14.5 (**B,E,H,K,N**) and E16.5 (**C,F,I,L,O,P**) X-gal-stained *Ptch1^{lacZ/+}* embryos. *Ptch1* expression was detected in several anatomical sites of condensing bone (**A,B,C,O**), mesenchyme (**D**), the developing tongue and tooth primordia (**E,J**), hair follicles (**F,I**) and vibrissae (**L**), the gut (**K**), the neural tube ventricular zone and notochord (**G,H**) and surrounding developing nerve bundles (**P**). *Ptch1* was absent from deep (**M,N**) and superficial dermal (l) lymphatic (arrowheads) and blood vessels (double arrowheads; **F**). HF - hair follicle, JLS - jugular lymph sac, LI - liver, NO - notochord, NT - neural tube, T - tongue, TP - tooth primordia, V - vibrissae. Scale bars represent 100µm.



bundles (Figure 6.5P). Whilst at all three developmental stages analysed *Ptch1* was absent from deeper lymphatic vessels, it was also lacking from the superficial dermal lymphatic (arrowheads; Figure 6.5I) and blood (arrowheads; Figure 6.5F) vascular plexuses. Thus, no evidence of *Ptch1* expression was detected in the developing embryonic lymphatic vasculature, despite robust expression in the nervous system and many other tissues.

6.3.4 *Ptch1* haploinsufficiency does not affect lymphatic vessel patterning in embryonic skin

In order to determine whether *Ptch1* has any functional role in the regulation of lymphatic vessels, we investigated dermal lymphatic vascular development and patterning in heterozygous *Ptch1^{lacZ/+}* and WT *Ptch1^{+/+}* E16.5 embryonic skin via whole mount immunofluorescent immunostaining (section 6.2.4.5). Owing to the early embryonic lethality of homozygous *Ptch1^{lacZ/lacZ}* mice (Goodrich et al., 1997; Hahn et al., 1998) the vascular phenotype of these mice was unable to be assessed. No striking alterations in lymphatic vessel calibre or patterning were observed in *Ptch1^{lacZ/+}* embryos (Figure 6.6C,G) relative to their WT littermates (Figure 6.6A,E). This was particularly evident on comparison of Prox1-positive and Nrp2-positive lymphatic vessels in *Ptch1^{lacZ/+}* (Figure 6.6D,H) and WT controls (Figure 6.6B,F), clearly demonstrating that the dermal lymphatic network is indistinguishable across genotypes. Nrp2-positive hair follicles appeared slightly more pronounced in *Ptch1^{lacZ/+}* skin (Figure 6.6H). The calibre and patterning of the blood vasculature; including arteries, veins and capillaries, as visualised with CD31 and α SMA, in embryonic *Ptch1^{lacZ/+}* skin (Figure 6.6C,G) was comparable to that observed in WT counterparts (Figure 6.6A,E). The same was true for the patterning of dermal nerves as detected with β -tubulin (Figure 6.6E,G). Therefore, *Ptch1* haploinsufficiency has no discernable effect, at least at the morphological level, on the development, calibre and patterning of the embryonic dermal lymphatic vasculature, at the stage analysed.

6.4 DISCUSSION

The results presented in this chapter reveal, in contrast to published data (Hatsell and Cowin, 2006), that *Ptch1* is not expressed in the lymphatic vasculature. The discrepancy between the reported literature and our results clearly demonstrate why it is of the utmost importance to use multiple markers of blood and lymphatic vascular EC identity in combination with one another, in order to ascertain vascular identity. The expression of many lymphatic markers, like LYVE1, is not restricted solely to

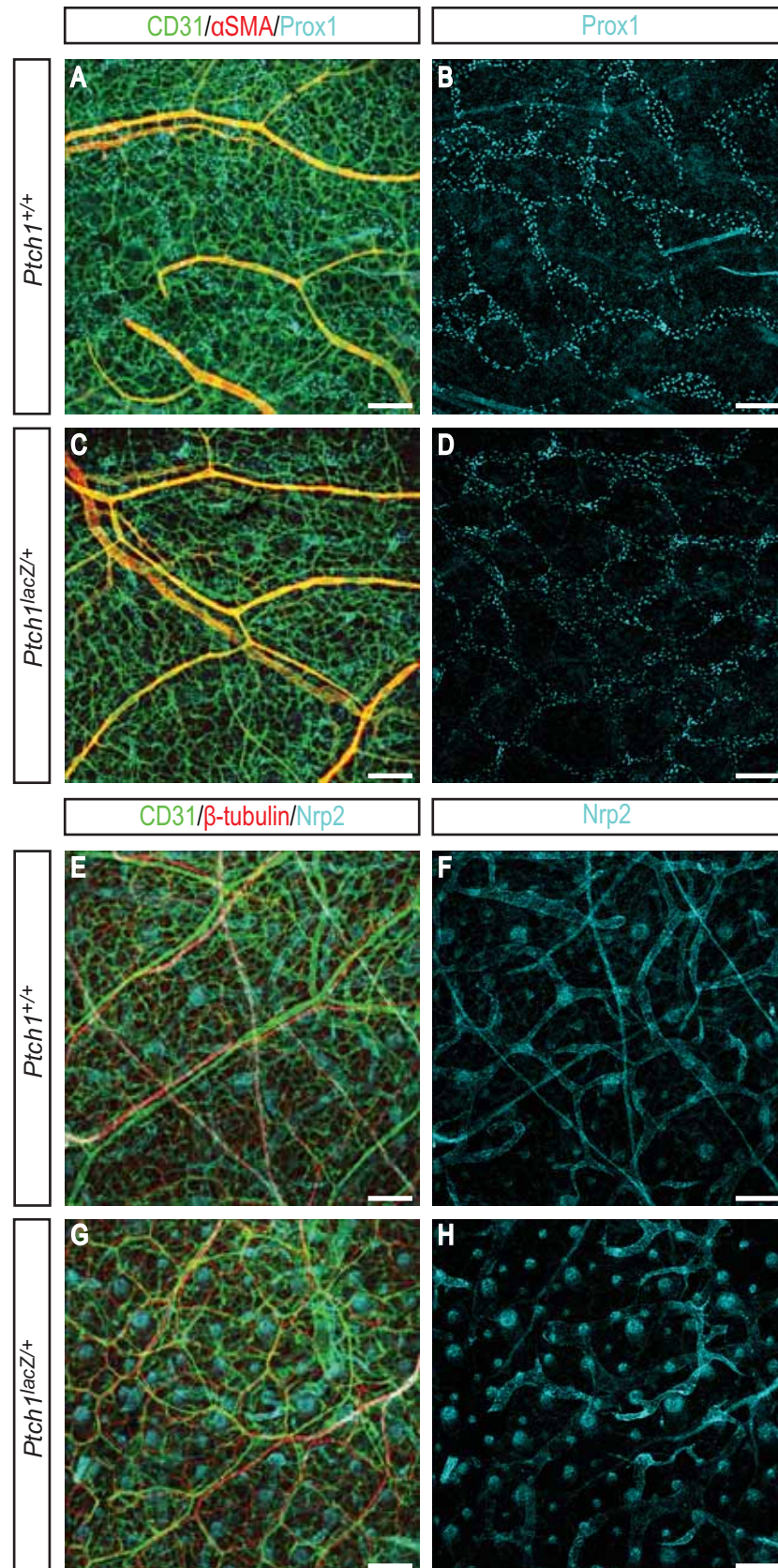


Figure 6.6 - Dermal lymphatic vessels are patterned normally in *Ptch1*^{lacZ/+} mice.

Whole mount immunofluorescent immunostaining of E16.5 dermal skin from *Ptch1*^{+/+} (**A,E**) and *Ptch1*^{lacZ/+} (**C,G**) embryos stained with CD31, α SMA and Prox1 (**A,C**) and CD31, β -tubulin and Nrp2 (**E,G**). Single-channel images showing Prox1-positive (**B,D**) and Nrp2-positive (**F,H**) lymphatic vessels are indistinguishable from that of wild-type littermates. α SMA - alpha smooth muscle actin. Scale bars represent 150 μ m.

lymphatic vessels in either embryonic or adult settings (Banerji et al., 1999; Gordon et al., 2008; Gordon et al., 2010; Lee et al., 2011; Mouta Carreira et al., 2001; Prevo et al., 2001; Schledzewski et al., 2006). Of particular interest here is why Hatsell and Cowin omitted showing images for the co-expression of LYVE1 with the β -gal-positive 'vessel-like' structures in their report (Hatsell and Cowin, 2006), when it is well-established that macrophages also express LYVE1 (Gordon et al., 2010; Schledzewski et al., 2006). It seems that greater emphasis was placed on the morphology of these structures, being described as vessels of large diameter, lacking red blood cells and extending from the periphery of the fat pad towards the lymph node (Hatsell and Cowin, 2006), rather than their expression of cell-specific markers. Additional studies undertaken as part of this project have demonstrated that LYVE1-positive macrophages are extremely abundant in the mammary gland milieu (double arrowheads; Figure 6.7A,B). Furthermore, it was observed that these LYVE1-positive macrophages arranged themselves in linear trajectories throughout the mammary gland, somewhat resembling vessels (double arrowheads; Figure 6.7A,B). These observations, in combination with the aforementioned finding that LYVE1-positive macrophages were found in close association with the subpopulation of peripherally-located β -gal-positive cells of nerve fibres in the mouse mammary gland (arrowheads; Figure 6.2I); potentially contributed to the incorrect identification of these structures as lymphatic vessels by Hatsell and Cowin (Hatsell and Cowin, 2006).

In addition to the lack of *Ptch1-lacZ* transgene expression in mammary gland lymphatic vessels, we also failed to detect *lacZ* reporter gene expression in lymphatic vessels on the surface of the heart and omentum, a region of the peritoneal membrane (Hatsell and Cowin, 2006). Whilst we did observe β -gal-positive structures in the peritoneal membrane, we can now unequivocally refer to these as neuronal in identity. No comparable staining was detected on the surface of the heart, in contrast to what was previously described by Hatsell and Cowin (Hatsell and Cowin, 2006). Our work, together with the work of others (Mirsky et al., 1999; Parmantier et al., 1999), provides strong evidence to demonstrate that *Ptch1* is expressed in perineurial cells. This conclusion is drawn firstly from the co-localisation of *Ptch1*-positive cells with the podoplanin-positive perineurium of the sciatic nerve (Figure 6.3P) and equivalent structures in the peritoneal membrane (Figure 6.3O); and secondly, from published literature which elucidated a role for Hh signalling in the development of peripheral nerve sheaths (Mirsky et al., 1999; Parmantier et al., 1999). In these studies, *Ptch1* was localised via *in situ* hybridisation to a restricted population of cells, hypothesised to be perineurial precursors, that form a concentric ring around the outer margins of developing nerve bundles at E15 (Mirsky et al., 1999; Parmantier et al., 1999); a similar finding to our studies (Figure 6.5P). In addition, *Ptch1* was demonstrated to be expressed in the perineurium of postnatal nerve fibres and in embryonic, newborn and adult peripheral nerves, albeit at a

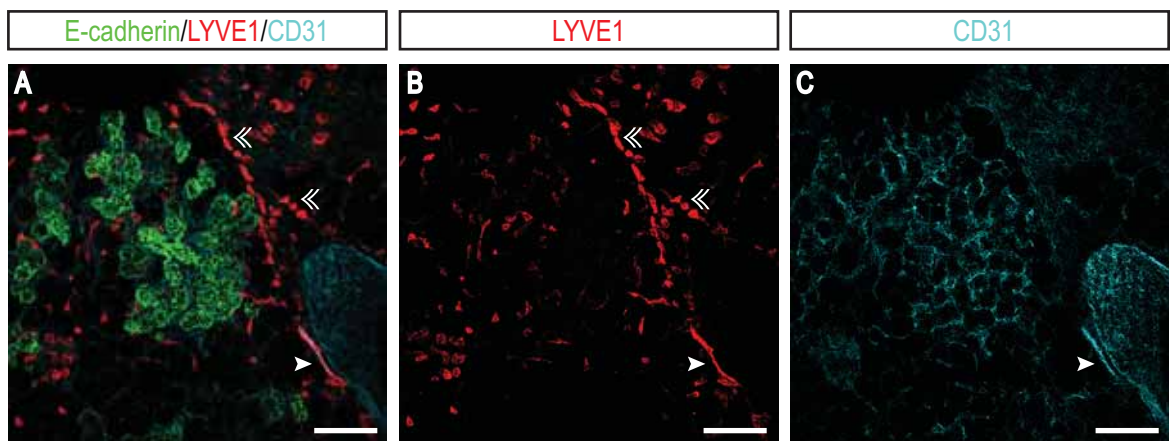


Figure 6.7 - LYVE1-positive macrophages in the mouse mammary gland.

A confocal z-stack image demonstrating the relative abundance, and distinct spatial distribution, of LYVE1-positive macrophages (double arrowheads; **A**), distinct from a lymphatic vessel (arrowheads) co-expressing LYVE1 (**B**) and CD31 (**C**) in a 14.5 day pregnant mouse mammary gland. Scale bars represent 100µm.

much reduced level (Mirsky et al., 1999; Parmantier et al., 1999). Perineurial cells constitute the outer layer of peripheral nerves, known as the perineurium, which functions to modulate external stretching forces and forms the blood-nerve barrier (Piña-Oviedo and Ortiz-Hidalgo, 2008). Furthermore, our observation of the restricted expression pattern of *Ptch1* in the lung of *Ptch1^{lacZ/+}* mice, as distinct from the neuronal expression profile, is consistent with an ascribed role for Hh signalling in mammalian lung development and a previous report documenting high levels of *Ptch1* expression in the mesenchyme surrounding the distal epithelium of the embryonic lung (Bellusci et al., 1997; Chuang et al., 2003; Pepicelli et al., 1998). The precise identity of this population of cells in the lung, however, still remains elusive.

Our expression analysis of *Ptch1* during murine embryogenesis faithfully recapitulates previous documented embryonic expression patterns (Goodrich et al., 1996; Hahn et al., 1996a; Hatsell and Cowin, 2006). The only striking anomaly found was a lack of detectable transgene expression upon X-gal staining in the hair follicles of the skin in E14.5 *Ptch1^{lacZ/+}* embryos, compared with Hatsell and Cowin who documented expression in such structures by E13.5 (Hatsell and Cowin, 2006). However, both studies do correspond in the noted absence of *Ptch1* expression in the developing mammary placodes of mid-gestation embryos. The robust expression of *Ptch1* in hair follicles is consistent with an established obligatory role for the Hh signalling axis in hair follicle morphogenesis (Chiang et al., 1999). Furthermore, fitting with a lack of reported oedema and haemorrhage in heterozygous *Ptch1^{lacZ/+}* embryos (Goodrich et al., 1997; Hahn et al., 1996a), no overt defect in the patterning of dermal blood, or lymphatic vessels, was observed in the embryonic skin of *Ptch1^{lacZ/+}* mice. In combination with a lack of *Ptch1* expression in the developing lymphatic vasculature, this is further evidence in support of a non-requisite role for *Ptch1* in embryonic lymphatic vessels.

6.5 CONCLUSION

Taken together, the data presented in this chapter reveal that the *Ptch1-lacZ* reporter gene is not expressed in the lymphatic vasculature of embryonic or adult tissues, but instead is expressed selectively in perineurial cells in *Ptch1^{lacZ/+}* mice. Whilst the documentation of *Ptch1* expression in this particular neuronal cell lineage is not novel (Mirsky et al., 1999; Parmantier et al., 1999), our finding that *Ptch1* is not expressed in mammary gland lymphatic vessels, contrary to published literature (Hatsell and Cowin, 2006), is an important result and renders this mouse model unsuitable as a tool to study the lymphatic vasculature. In addition, haploinsufficiency of *Ptch1* was found to have a negligible effect on

the patterning of dermal blood and lymphatic vessels in embryonic skin. In conclusion, it is highly probable that *Ptch1* has no substantial role in embryonic or postnatal lymphangiogenesis.

CHAPTER 7

Discussion

7.1 DISCUSSION

To date there have been relatively few detailed studies analysing lymphatic vessels in the disease-free human breast, despite the well-accepted link between lymphatic vessels and breast cancer. In fact, lymphatic vessels can be considered of fundamental importance in breast cancer in at least two ways. Firstly, lymphatic vessels can facilitate metastasis, a leading cause of mortality in breast cancer patients, by providing an accessible route for the dissemination of tumour cells (Ran et al., 2010). Metastasis to the lymph nodes represents the single most important prognostic indicator in breast cancer patients (Fisher et al., 1983). Recent evidence from breast cancer tissue samples has shown a strong predilection toward lymphatic vessel invasion over blood vessel invasion (Mohammed et al., 2007a). However, it is unclear what mechanisms underlie the ability of breast cancer cells to metastasise preferentially via the lymphatic vessels. Secondly, secondary lymphoedema is a frequent complication for up to 40% of breast cancer patients following surgical resection of axillary lymph nodes (Armer et al., 2009) and is a debilitating condition for which there is currently very little effective treatment. Clinical evidence such as this supports the necessity to understand the genes and molecular mechanisms that regulate lymphangiogenesis in the normal human breast, before we can begin to appreciate how these mechanisms are deregulated to facilitate tumour metastasis in breast cancer and how these pathways might be modulated to repair lymphatic vessels and provide new therapeutic options for secondary lymphoedema.

Collectively, work presented in this study has been aimed toward understanding how the growth and remodelling of lymphatic vessels is regulated in the postnatal mouse mammary gland. This study has provided the first evidence demonstrating that the lymphatic vasculature is dynamically remodelled along with the mammary epithelial tree and blood vasculature during postnatal mouse mammary gland morphogenesis. In addition, lymphatic vessels were observed to share an intimate spatial association with epithelial ducts and to a lesser extent, large blood vessels, in the mouse mammary gland. We hypothesised that the signals that regulate lymphangiogenesis in the mammary gland could either be direct, involving the interaction of steroid hormones, such as estrogen and progesterone, that tightly regulate the remodelling of the mammary epithelium, or indirect, encompassing signals arising from nearby mammary epithelial, blood vascular or stromal tissue components, in response to these hormone signalling events. Data from our study provides compelling evidence to illustrate that the growth and remodelling of the lymphatic vasculature in the mouse mammary gland is under the influence of mammary epithelial-derived lymphangiogenic stimuli, rather than direct steroid hormone

control. We determined that LEC in the mouse mammary gland lack detectable expression of ER α and PR and revealed that mammary gland myoepithelial cells are a source of pro-lymphangiogenic growth factors. We also established that *Vegfc* and *Vegfd* mRNA levels in the postnatal mouse mammary gland are significantly increased at an early stage of pregnancy and that proteolytically-processed, active VEGF-D is expressed selectively in pregnant, but not virgin mouse mammary glands, corresponding with peak lymphatic vessel density. In accordance with these findings, we demonstrated that a tyrosine kinase inhibitor specific for VEGFR-3 (Kirkin et al., 2001; Kirkin et al., 2004), the principal receptor for mouse VEGF-C and VEGF-D, inhibits the proliferation of primary dermal LEC stimulated by mammary gland conditioned media (CM) *ex vivo*. These data suggest that VEGF-C and VEGF-D, two of the best characterised lymphangiogenic stimuli to date, are likely to play a key role in the regulation of lymphangiogenesis in the pregnant mouse mammary gland. Elucidation of the molecular mechanisms controlling lymphatic vessel growth and remodelling in the mouse mammary gland has the potential to reveal important targets for the future generation of therapeutics to modulate lymphangiogenesis in settings of disease, including breast cancer.

It is generally accepted that blood vessels are often aligned with nerves and display similar branching patterns in many adult peripheral tissues (Carmeliet and Tessier-Lavigne, 2005; Larrivée et al., 2009). Whilst the factors controlling blood vascular patterning are not understood in their entirety, there is now clear evidence that many axon guidance molecules, including ephrins, semaphorins, slits, netrins and their respective receptors, also play a key role in blood vessel guidance (Carmeliet and Tessier-Lavigne, 2005; Larrivée et al., 2009). However, the molecular mechanisms governing lymphatic vessel patterning remain poorly understood in comparison. Pioneering studies by Bussmann *et al.* in zebrafish, have revealed that intersegmental lymphatic vessels have a striking tendency to align with arterial, rather than venous, intersegmental vessels in the zebrafish trunk, suggesting that arteries provide essential guidance cues for LEC migration and patterning (Bussmann et al., 2010). Owing to this observation, Bussmann *et al.* hypothesised that arterial EC likely secrete particular lymphangiogenic growth factors, such as VEGF-C, or deposit extracellular matrix components that provide an essential substrate for directed LEC migration (Bussmann et al., 2010). A similar preference for an arterial association has been documented in the endometrial layer of the human uterus, whereby lymphatic vessels were observed encircling spiral arteries, forming intimate contact with the vascular smooth muscle cells surrounding these arteries (Donoghue et al., 2007; Volchek et al., 2010). Whilst our data in Chapter 3 demonstrates that a small proportion of lymphatic vessels in the mouse mammary gland follow the path of large blood vessels, most likely arteries, the majority of lymphatic vessels, however, were closely associated with mammary ducts; often observed to track alongside, or alternatively, coil themselves

around the mammary ducts. To the best of our knowledge, this represents the first illustration of an intimate association of lymphatic vessels with epithelial ducts, a finding which has important implications for the spatial organisation of lymphatic vessels and the signals that regulate lymphangiogenesis in other branched epithelial tissues, including the lung, kidney, pancreas and prostate, which at present remain poorly characterised. Precisely what factor(s) are responsible for the distinct patterning of lymphatic vessels in the mouse mammary gland and other epithelial tissues remain to be elucidated. Our work suggests that VEGF-C and VEGF-D are likely to be key lymphangiogenic signals produced by epithelial cells in the mouse mammary gland.

During branching morphogenesis in the pancreas, blood vessels are preferentially located along central trunk epithelial cells and lack a close association with branch tips, where acinar differentiation of the epithelium occurs (Pierreux et al., 2010). Blood vascular patterning in the pancreas appears analogous to our observations of lymphatic vessel patterning in the postnatal mouse mammary gland (Chapter 3), whereby lymphatic vessels have a spatial predilection for ductal, but not alveolar epithelial cells. In the pancreas, VEGF-A production selectively by the trunk epithelial cells regulates endothelial patterning, strengthening our hypothesis that pro-angiogenic/lymphangiogenic gene expression might be differentially regulated between ductal and alveolar epithelial cells. As mentioned previously, our most likely candidate to explain the lack of lymphatic vessels associated with the alveoli is soluble VEGFR-2 (sVEGFR-2); a native and specific inhibitor of lymphangiogenesis (Albuquerque et al., 2009). We would predict that sVEGFR-2 is expressed specifically by alveolar epithelial cells in the mouse mammary gland, where it could function to sequester endogenously-available VEGF-C. The finding by Albuquerque *et al.* that native sVEGFR-2 exists as a monomer, which unlike membrane-bound VEGFR-2, has a poor avidity for VEGF-A (Albuquerque et al., 2009), would explain the selective presence of blood vascular 'capillary baskets', but not lymphatic vessels, in close association with the alveoli. The caveat to this hypothesis is that sVEGFR-2 appears not to trap endogenous mouse VEGF-D (Albuquerque et al., 2009), consistent with an earlier report by Baldwin *et al.* demonstrating that mouse VEGF-D is specific for VEGFR-3 and does not bind mouse VEGFR-2 (Baldwin et al., 2001a). Consequently, for this hypothesis to be biologically relevant, it would rely on VEGF-C being the key growth factor driving lymphangiogenesis in the mouse mammary gland. Our data (Chapter 4) demonstrate that *Vegfc* and *Vegfd* mRNA levels are significantly increased at an early stage of pregnancy relative to virgin and late pregnant stages, that proteolytically-processed, active VEGF-D is expressed selectively in pregnant, but not virgin mouse mammary glands, and that a tyrosine kinase inhibitor specific for VEGFR-3 (Kirkin et al., 2001; Kirkin et al., 2004), the principal receptor for VEGF-C and VEGF-D, can block the proliferation of primary dermal LEC stimulated by mammary gland CM ex

vivo. Taken together, these data strongly advocate a key role for VEGF-C and VEGF-D in mediating pregnancy-induced lymphangiogenesis in the mouse mammary gland. This poses the intriguing question as to whether VEGF-C and VEGF-D act in concert to orchestrate lymphatic vascular remodelling in the mouse mammary gland. Defining the relative contribution of each of these growth factors in mammary gland lymphangiogenesis will form the basis of future work. Expression of VEGF-C and VEGF-D has been associated with increased lymphangiogenesis, elevated lymphatic vascular invasion (LVI), increased frequency of lymph node metastasis and poor patient prognosis in several studies of human breast cancer patients (Choi et al., 2005; Gu et al., 2008; Mohammed et al., 2007b; Nakamura et al., 2005; Nakamura et al., 2003). Consistent with human tumour samples, VEGF-D has also been shown to induce pathological lymphangiogenesis and metastasis in mouse tumour models (Koch et al., 2009; Stacker et al., 2001).

Our data furthermore suggests that proteolytic processing of VEGF-D is important for the regulation of lymphangiogenesis in the mouse mammary gland. However, we do not know the exact identity of these enzymes, how they are in turn regulated and which cell types in the mouse mammary gland they are expressed in. These are all important questions that will provide valuable insight into the molecular regulation of lymphatic vascular remodelling in the postnatal mouse mammary gland. Recent work from Harris *et al.* demonstrated that proteolytic processing of VEGF-D is necessary to promote tumour growth and metastasis in a mouse tumour xenograft model (Harris et al., 2011). It therefore remains an intriguing possibility that proteolytic enzymes with the ability to process VEGF-D could prove to be relevant future therapeutic targets, particularly in the breast. As such, the overexpression of proprotein convertases (PC), a family of serine proteases that have been shown to promote cleavage of VEGF-C (Siegfried et al., 2003) and VEGF-D (McColl et al., 2007), in multiple human tumours has been reported to correlate with a more aggressive phenotype and fittingly have been coined 'master switches' in the regulation of tumour growth and progression (Bassi et al., 2005). Consistent with a role for PCs in tumourigenesis, studies in several mouse models have demonstrated that PC inhibition results in a reduction in tumour incidence, tumour multiplicity, tumour vascularisation and metastasis (Bassi et al., 2010; Khatib et al., 2001), suggesting that PC inhibition is a potential therapeutic approach for solid tumours, like breast cancer.

In addition to VEGF-C and VEGF-D, we also demonstrated that a number of other key pro-lymphangiogenic growth factors, including Angpt1 and Angpt2, were dynamically regulated at the mRNA and protein level during mammary gland morphogenesis, suggesting that they may also play a role in regulating lymphangiogenesis in the postnatal mouse mammary gland (Chapter 4). Angpt1 and Angpt2

have been implicated in the pathogenesis of breast cancer owing firstly, to their elevated levels in the plasma of breast cancer patients (Caine et al., 2003), and secondly, Angpt2 expression has been shown to correlate with lymph node invasion and reduced survival in breast cancer patients (Sfiligoi et al., 2003). These studies pose the question as to whether increased expression of pro-lymphangiogenic factors, such as VEGF-C, VEGF-D, Angpt1 and Angpt2, in the normal mammary gland accounts for the increased propensity for breast cancer cells to metastasise via a lymphogenous, rather than a haematogenous route.

Our key finding that lymphatic vessels have a strong spatial predilection for epithelial ducts in the mouse mammary gland (Chapter 3) has important implications for breast cancer, and other epithelial cancers which have a predilection to spread via lymphatic vessels, such as prostate cancer (Jennbacken et al., 2005). Breast cancer is a histologically heterogeneous disease, with ductal and lobular carcinomas representing the most common histological types of invasive breast cancer. Invasive ductal carcinomas (IDC) and invasive lobular carcinomas (ILC) account for 70-85% and 5-20% of all invasive breast carcinomas, respectively (Toikkanen et al., 1997). This nomenclature, however, is a misnomer, since both types of tumours essentially originate from the same anatomical structure, the terminal ductal lobular unit (TDLU), and either develop within the TDLU itself or from the terminal ducts that enter the lobular units, rather than in the collecting epithelial ducts as implied by the term 'ductal' (Cardiff et al., 2000). Whilst these terminologies provoke a misleading concept about the cellular origin of the tumour they do, however, delineate two morphological, pathologically and clinically distinct types of tumours (Wasif et al., 2010). LVI, a significant predictor of poor patient prognosis and disease outcome due to its strong association with axillary nodal metastasis in breast cancer (Marinho et al., 2008; Mohammed et al., 2007a; Schoppmann et al., 2004; Woo et al., 2002), is detected less frequently in ILC (7-13%) compared with IDC (26-30%) (Laser et al., 2008). However, great conjecture currently exists as to whether the prognoses of IDC and ILC differ (Wasif et al., 2010). Given that in the mouse mammary gland we observed a striking tendency for lymphatic vessels to align with the mammary ducts and not the alveoli, the increased incidence of LVI in IDC compared to ILC could potentially be attributed to the spatial location of the lymphatic vessels, a key route of metastatic spread in breast cancer (Fisher et al., 1983; Schoppmann et al., 2004). We would predict that if the lymphatic vessels are in closer proximity to the site of the primary tumour (ie. the terminal ducts), it would provide tumour cells ready access to the lymphatic vasculature, therefore resulting in an increased propensity for LVI. Furthermore, data in Chapter 4 of our study indicate that mammary epithelial cells are a source of several pro-lymphangiogenic factors, and thus deregulated growth of abnormal epithelial cells has the potential to result in increased production of these growth factors, which would in turn drive the growth of new

lymphatic vessels at the site of the primary tumour and ultimately facilitate tumour cell dissemination. Whilst the precise location of lymphatic vessels in relation to the epithelial tree in the human breast still remains to be experimentally validated, we can use our findings in the mouse mammary gland to predict patterns in the human breast, in order to provide an explanation of why breast cancers readily metastasise via a lymphogenous route. These data have the potential to aid in the future development of novel anti-lymphangiogenic therapeutics.

Whilst it is well-established that the endothelium lining blood vessels in settings of pathological angiogenesis, particularly tumourigenesis, is molecularly and functionally distinct from the endothelium in vessels of tissues undergoing normal physiological processes, such as corpus luteum formation in the ovary, wound healing and endometrial regeneration during the menstrual cycle, it is becoming increasingly evident that many of the genes differentially expressed in tumour endothelium are also expressed in EC during settings of physiological angiogenesis (Seaman et al., 2007; St. Croix et al., 2000). Microarray data presented in Chapter 5 of this study comparing differentially expressed genes between virgin and pregnant EC in the mouse mammary gland, which undergoes repeated cycles of physiological angiogenic expansion and regression during adulthood (Djonov et al., 2001; Matsumoto et al., 1992), supports this concept of a shared gene expression profile between EC of normal and tumourigenic tissue. Many of the top genes differentially expressed between virgin and pregnant mammary gland EC, including *Adam10*, *Anxa1* and *Tnc* (as addressed in Chapter 5), have all been previously implicated in settings of pathological angiogenesis, such as human atherosclerotic lesions (Donners et al., 2010), tumour growth and metastasis (Oh et al., 2004; Yi and Schnitzer, 2009), cerebral neoplastic disease (Zagzag et al., 1996; Zagzag et al., 1995) and diabetic retinopathy (Castellon et al., 2002). The expression of such genes is indicative of an activated endothelium, compared to a quiescent endothelial layer, which raises the question as to whether this activated state renders the blood vasculature in the mammary gland more receptive to growth factors produced by tumour cells and therefore more easily co-opted by tumours to develop aberrant neovascularisation. This question will no doubt form the basis of future investigations in the search for specific targets for the prevention of neovascularisation, with minimal detrimental effects on the normal blood vascular endothelium. Comparative profiling of normal and tumour-associated LEC has also revealed a novel gene expression profile in lymphatic vessels associated with tumour growth and nodal metastasis (Clasper et al., 2008). However, owing to the fact that in adults, similarly to blood vessels, lymphatic vessels remain relatively quiescent, except in settings of tissue and organ repair, wound healing and inflammation (Tammela and Alitalo, 2010), it will be important to perform comprehensive screening of normal adult tissues that

undergo physiological lymphangiogenesis, such as the mammary gland as identified in this study, in order to identify robust new tumour-specific lymphatic markers for both prognosis and therapy.

Essential to the success of this study was the ability to visualise lymphatic vessels in a three-dimensional setting, as distinct from tissue sections, in the mouse mammary gland. During the search for such an approach, we made the important observation that *Patched 1 (Ptch1)-lacZ* is not expressed specifically in the lymphatic vasculature of the postnatal mouse mammary gland (Chapter 6), contrary to published literature (Hatsell and Cowin, 2006). Rather we demonstrated that *Ptch1* was expressed selectively in a population of cells that ensheath peripheral nerve fibres, most likely perineurial cells, in *Ptch1^{lacZ/+}* mice. Whilst the documentation of *Ptch1* in this particular neuronal cell lineage is not novel, the observation that *Ptch1* is not expressed in mammary lymphatic vessels as previously reported (Hatsell and Cowin, 2006) is an important finding nonetheless and one that needs to be carefully addressed in future studies utilising this transgenic mouse line. Unfortunately, owing to the fact that *Ptch1-lacZ* was not expressed in lymphatic vessels of the postnatal mouse mammary gland, the *Ptch1^{lacZ/+}* mouse was not suitable for the visualisation of lymphatic vessels and as a result was not used for any further analyses in the mammary gland. Additionally, we found no evidence for the expression of *Ptch1-lacZ* in the developing embryonic and adult lymphatic vasculature in other tissues and haploinsufficiency of *Ptch1* did not alter patterning of the dermal lymphatic vasculature in embryonic skin. These data indicate that *Ptch1* and Hedgehog (Hh) signalling are unlikely to play a major role in embryonic lymphangiogenesis. Whilst it is well-established that the Hh signalling pathway governs a wide variety of processes during embryonic development and adult tissue homeostasis, including angiogenesis (Hooper and Scott, 2005; Jiang and Hui, 2008; Nagase et al., 2008) and that aberrant activation and dysfunction of this key developmental pathway is linked with many types of human cancer (Evangelista et al., 2006; Kasper et al., 2009), the precise role of the Hh signalling axis in lymphangiogenesis remains to be formally addressed.

7.2 FUTURE DIRECTIONS

Collectively, this study has immensely aided our understanding of lymphatic vascular growth and remodelling in the postnatal mouse mammary gland, however, it has also highlighted the need for further investigative analyses; some of which are outlined below.

The models used to define the signals that regulate the growth and remodelling of the lymphatic vasculature in the postnatal mouse mammary gland in this study were unable to definitively dissect out the relative contribution of lymphangiogenic signals derived from the mammary blood vasculature compared to those derived from epithelial cells. One way of addressing this problem would be to perform 'fat pad clearing' experiments. In a 3 week old mouse the ductal network is still confined to the most proximal part of the fat pad near the nipple. As a result, this small area can be surgically removed to essentially leave a 'cleared' fat pad, devoid of an epithelial tree, but with the majority of the blood vasculature intact (Hennighausen and Robinson, 2005). Whilst this technique is routinely used in mammary epithelial transplant studies to assess the function of gene deletion during mammary gland development, it could nonetheless be modified for our intended purpose. At the desired time point during the reproductive cycle, the cleared mammary fat pads could be analysed for lymphatic vessel density and compared to the contralateral inguinal mammary gland that was not cleared. Based on our data suggesting that the majority of lymphangiogenic stimuli in the mouse mammary gland are epithelial-derived, we would predict that lymphatic vessel density would be severely reduced in glands lacking an epithelial tree.

From our microarray analyses we identified *Cxcl15*, *Adam10*, *Anxa1*, *Tnc*, *Mmp2* and *Bdnf*, all of which have previously been linked with angiogenesis or lymphangiogenesis, as candidate genes potentially involved in vascular remodelling in the mouse mammary gland. To the best of our knowledge, none of these genes have been ascribed a role in vascular remodelling in the postnatal mouse mammary gland to date. Given that LEC and BEC represent functionally and molecularly distinct endothelial populations (Johnson et al., 2008; Oliver and Srinivasan, 2010), isolating independent populations of LEC and BEC from the mouse mammary gland will enable more specific interrogation of these distinct populations at the molecular level using real-time RT-PCR. Such analyses will require further optimisation of our FACS approach to enable isolation of sufficient numbers of these cells. In contrast, *Bfk*, also identified as a key gene differentially expressed between virgin and pregnant mammary glands, however, has previously been documented to be expressed in the mouse mammary gland (Coultas et al., 2003; Pujianto et al., 2007), yet its biological function currently remains enigmatic. Further confirmatory experiments are necessary to establish the precise spatial and temporal expression patterns of *Cxcl15*, *Adam10*, *Anxa1*, *Tnc*, *Mmp2*, *Bdnf* and *Bfk* using immunohistochemistry, where suitable antibodies are available, or *in situ* hybridisation. Studies to assess gene function in EC *ex vivo* could be performed using primary LEC and BEC isolated from embryonic mouse dermis, as previously reported (Kazenwadel et al., 2010). Candidate genes could be ectopically expressed in primary LEC and BEC and potential angiogenic/lymphangiogenic growth factors purchased, or produced recombinantly, and cultured with

EC. The effect of ectopic gene expression and candidate growth factors on EC cellular functions including proliferation, migration and tube formation can further be assessed according to established protocols in our laboratory (Jan Kazenwadel, Genevieve Secker and Natasha L. Harvey, unpublished data). In a complimentary set of experiments, the effect of ablating endogenous gene expression, using small interfering RNA to knock down gene expression, on the cell functions listed above could also be assessed. Taken together, these experiments will provide valuable information regarding the function, and relative importance, of candidate genes in multiple angiogenic and lymphangiogenic processes. However, definitive analysis of the *in vivo* role of such genes in mammary gland vascular remodelling and morphogenesis will rely on the generation of conditional knockout mice. We are currently generating a *Vegfc* conditional knockout mouse line in collaboration with Dr Nick Gale (Regeneron, Tarrytown, NY), which will be utilised to inactivate *Vegfc* in particular cell populations of interest in the mouse mammary gland, including myoepithelial cells and macrophages. These analyses will define the role of VEGF-C in mammary gland lymphangiogenesis in a tissue-specific and temporal manner. Such analyses, combined with more extensive interrogation of our microarray data sets, will form the basis of future work.

Given the strong evidence presented in Chapter 4 in support of VEGF-D as one of the key growth factors responsible for the stimulation of lymphangiogenesis during pregnancy in the postnatal mouse mammary gland, further investigation into the precise cellular localisation and proteolytic processing of VEGF-D, along with further analysis of *Vegfd*-deficient mammary glands is warranted. Together, these analyses will determine the precise role of VEGF-D in lymphangiogenesis in the postnatal mouse mammary gland.

One of the interesting and outstanding questions not addressed in the present study is, how do the lymphatic vessels first grow into the mouse mammary gland? We would predict that large collecting lymphatic vessels first enter the mammary fat pad following the path of large blood vessels and progressively expand to become intimately associated with the ductal epithelium as it grows into the fat pad. The lymphatic-specific, fluorescent *Prox1*-green fluorescent protein (GFP) mouse (Choi et al., 2011) provides an ideal tool to address this question using real-time imaging and will be the focus of future studies.

7.3 CONCLUSION

The current study, the first specific analysis of lymphangiogenesis in the postnatal mouse mammary gland, demonstrates that the mammary gland lymphatic vasculature is dynamically remodelled concurrently with the mammary epithelial tree and blood vasculature during postnatal mouse mammary gland morphogenesis. Furthermore, it represents the first illustration of an intimate association of lymphatic vessels with epithelial ducts. Data from our study provides compelling evidence that the growth and remodelling of the lymphatic vasculature in the postnatal mouse mammary gland is under the influence of mammary epithelial-derived lymphangiogenic stimuli, rather than direct steroid hormone control. Whilst our understanding of the precise identity of pro-lymphangiogenic signals that regulate lymphatic vascular growth and remodelling during mammary gland morphogenesis currently remains incomplete; VEGF-C and VEGF-D represent the most likely candidates to date. Future work aims to further define the identity and source of additional lymphangiogenic growth factors that drive lymphangiogenesis in the mouse mammary gland, in the hope that the identification of such genes may contribute valuable new targets for the design of therapeutic agents able to ablate, or stimulate, mammary gland lymphangiogenesis in settings of disease.

REFERENCES

-
- Abràmoff, M. D., Magalhães, P. J. and Ram, S. J.** (2004). Image processing with ImageJ. *Biophotonics International* **11**, 36-42.
- Abtahian, F., Guerriero, A., Sebzda, E., Lu, M.-M., Zhou, R., Mocsai, A., Myers, E. E., Huang, B., Jackson, D. G., Ferrari, V. A. et al.** (2003). Regulation of blood and lymphatic vascular separation by signaling proteins SLP-76 and Syk. *Science* **299**, 247-251.
- Achen, M. G., Jeltsch, M., Kukk, E., Mäkinen, T., Vitali, A., Wilks, A. F., Alitalo, K. and Stacker, S. A.** (1998). Vascular endothelial growth factor D (VEGF-D) is a ligand for the tyrosine kinases VEGF receptor 2 (Flk1) and VEGF receptor 3 (Flt4). *Proceedings of the National Academy of Sciences of the United States of America* **95**, 548-553.
- Albuquerque, R. J. C., Hayashi, T., Cho, W. G., Kleinman, M. E., Dridi, S., Takeda, A., Baffi, J. Z., Yamada, K., Kaneko, H., Green, M. G. et al.** (2009). Alternatively spliced vascular endothelial growth factor receptor-2 is an essential endogenous inhibitor of lymphatic vessel growth. *Nature Medicine* **15**, 1023-1030.
- Alders, M., Hogan, B. M., Gjini, E., Salehi, F., Al-Gazali, L., Hennekam, E. A., Holmberg, E. E., Mannens, M. M. A. M., Mulder, M. F., Offerhaus, G. J. A. et al.** (2009). Mutations in *CCBE1* cause generalized lymph vessel dysplasia in humans. *Nature Genetics* **41**, 1272-1274.
- Alitalo, K., Tammela, T. and Petrova, T.** (2005). Lymphangiogenesis in development and human disease. *Nature* **438**, 946-953.
- Ambati, B. K., Nozaki, M., Singh, N., Takeda, A., Jani, P. D., Suthar, T., Albuquerque, R. J. C., Richter, E., Sakurai, E., Newcomb, M. T. et al.** (2006). Corneal avascularity is due to soluble VEGF receptor-1. *Nature* **443**, 993-997.
- Ando, K., Takahashi, M., Yamagishi, T., Miyagawa-Tomita, S., Imanaka-Yoshida, K., Yoshida, T. and Nakajima, Y.** (2011). Tenascin C may regulate the recruitment of smooth muscle cells during coronary artery development. *Differentiation* **81**, 299-306.
- Andrae, J., Gallini, R. and Betsholtz, C.** (2008). Role of platelet-derived growth factors in physiology and medicine. *Genes & Development* **22**, 1276-1312.
- Andreasen, P. A., Egelund, R. and Petersen, H. H.** (2000). The plasminogen activation system in tumor growth, invasion, and metastasis. *Cellular and Molecular Life Sciences* **57**, 25-40.
- Andres, A.-C. and Djonov, V.** (2010). The mammary gland vasculature revisited. *Journal of Mammary Gland Biology and Neoplasia* **15**, 319-328.
- Andres, A.-C. and Strange, R.** (1999). Apoptosis in the estrous and menstrual cycles. *Journal of Mammary Gland Biology and Neoplasia* **4**, 221-228.
- Armer, J. M., Stewart, B. R. and Shook, R. P.** (2009). 30-month post-breast cancer treatment lymphoedema. *Journal of Lymphoedema* **4**, 14-18.
- Asellius, G.** (1627). *De lactibus sive lacteis venis*. Milan: J.B. Bidellium, Mediolani.
- Asselin-Labat, M.-L., Sutherland, K. D., Barker, H., Thomas, R., Shackleton, M., Forrest, N. C., Hartley, L., Robb, L., Grosveld, F. G., van der Wees, J. et al.** (2007). Gata-3 is an essential regulator of mammary-gland morphogenesis and luminal-cell differentiation. *Nature Cell Biology* **9**, 201-209.
-

-
- Auguste, P., Javerzat, S. and Bikfalvi, A.** (2003). Regulation of vascular development by fibroblast growth factors. *Cell and Tissue Research* **314**, 157-166.
- Aupperlee, M. D., Smith, K. T., Kariagina, A. and Haslam, S. Z.** (2005). Progesterone receptor isoforms A and B: temporal and spatial differences in expression during murine mammary gland development. *Endocrinology* **146**, 3577-3588.
- Australian Institute of Health and Welfare & National Breast and Ovarian Cancer Centre.** (2009). Breast cancer in Australia: an overview, 2009. Canberra: Australian Institute of Health and Welfare.
- Bäckhed, F., Crawford, P. A., O'Donnell, D. and Gordon, J. I.** (2007). Postnatal lymphatic partitioning from the blood vasculature in the small intestine requires fasting-induced adipose factor. *Proceedings of the National Academy of Sciences of the United States of America* **104**, 606-611.
- Baldocchi, R. A., Tan, L., King, D. S. and Nicoll, C. S.** (1993). Mass spectrometric analysis of the fragments produced by cleavage and reduction of rat prolactin: evidence that the cleaving enzyme is cathepsin D. *Endocrinology* **133**, 935-938.
- Baldwin, M. E., Catimel, B., Nice, E. C., Roufail, S., Hall, N. E., Stenvers, K. L., Karkkainen, M. J., Alitalo, K., Stacker, S. A. and Achen, M. G.** (2001a). The specificity of receptor binding by vascular endothelial growth factor-D is different in mouse and man. *The Journal of Biological Chemistry* **276**, 19166-19171.
- Baldwin, M. E., Halford, M. M., Roufail, S., Williams, R. A., Hibbs, M. L., Grail, D., Kubo, H., Stacker, S. A. and Achen, M. G.** (2005). Vascular endothelial growth factor D is dispensable for development of the lymphatic system. *Molecular and Cellular Biology* **25**, 2441-2449.
- Baldwin, M. E., Roufail, S., Halford, M. M., Alitalo, K., Stacker, S. A. and Achen, M. G.** (2001b). Multiple forms of mouse vascular endothelial growth factor-D are generated by RNA splicing and proteolysis. *The Journal of Biological Chemistry* **267**, 44307-44314.
- Ballard, V. L. T., Sharma, A., Duignan, I., Holm, J. M., Chin, A., Choi, R., Hajjar, K. A., Wong, S.-C. and Edelberg, J. M.** (2006). Vascular tenascin-C regulates cardiac endothelial phenotype and neovascularization. *The FASEB Journal* **20**, 717-719.
- Baluk, P., Fuxe, J., Hashizume, H., Romano, T., Lashnits, E., Butz, S., Vestweber, D., Corada, M., Molendini, C., Dejana, E. et al.** (2007). Functionally specialized junctions between endothelial cells of lymphatic vessels. *The Journal of Experimental Medicine* **204**, 2349-2362.
- Baluk, P., Tammela, T., Ator, E., Lyubynska, N., Achen, M. G., Hicklin, D. J., Jeltsch, M., Petrova, T. V., Pytowski, B., Stacker, S. A. et al.** (2005). Pathogenesis of persistent lymphatic vessel hyperplasia in chronic airway inflammation. *The Journal of Clinical Investigation* **115**, 247-257.
- Banerji, S., Ni, J., Wang, S.-X., Clasper, S., Su, J., Tammi, R., Jones, M. and Jackson, D. G.** (1999). LYVE-1, a new homologue of the CD44 glycoprotein, is a lymph-specific receptor for hyaluronan. *The Journal of Cell Biology* **144**, 789-801.
- Barker, H. E., Chang, J., Cox, T. R., Lang, G., Bird, D., Nicolau, M., Evans, H. R., Gartland, A. and Erler, J. T.** (2011). LOXL2-mediated matrix remodeling in metastasis and mammary gland involution. *Cancer Research* **71**, 1561-1572.
-

-
- Barresi, V., Reggiani-Bonetti, L., Di Gregorio, C., De Leon, M. P. and Barresi, G.** (2011). Lymphatic vessel density and its prognostic value in stage I colorectal carcinoma. *Journal of Clinical Pathology* **64**, 6-12.
- Bassi, D. E., Fu, J., Lopez de Cicco, R. and Klein-Szanto, A. J. P.** (2005). Proprotein convertases: "master switches" in the regulation of tumor growth and progression. *Molecular Carcinogenesis* **44**, 151-161.
- Bassi, D. E., Zhang, J., Cenna, J., Litwin, S., Cukierman, E. and Klein-Szanto, A. J. P.** (2010). Proprotein convertase inhibition results in decreased skin cell proliferation, tumorigenesis, and metastasis. *Neoplasia* **12**, 512-526.
- Bazigou, E., Xie, S., Chen, C., Weston, A., Miura, N., Sorokin, L., Adams, R., Muro, A. F., Sheppard, D. and Mäkinen, T.** (2009). Integrin- α 9 is required for fibronectin matrix assembly during lymphatic valve morphogenesis. *Developmental Cell* **17**, 175-186.
- Becker, C., Assouad, J., Riquet, M. and Hidden, G.** (2006). Postmastectomy lymphedema: long-term results following microsurgical lymph node transplantation. *Annals of Surgery* **243**, 313-315.
- Bein, K. and Simons, M.** (2000). Thrombospondin type 1 repeats interact with matrix metalloproteinase 2. Regulation of metalloproteinase activity. *The Journal of Biological Chemistry* **275**, 32167-32173.
- Bellusci, S., Furuta, Y., Rush, M. G., Henderson, R., Winnier, G. and Hogan, B. L. M.** (1997). Involvement of Sonic hedgehog (*Shh*) in mouse embryonic lung growth and morphogenesis. *Development* **124**, 53-63.
- Benaud, C., Dickson, R. B. and Thompson, E. W.** (1998). Roles of the matrix metalloproteinases in mammary gland development and cancer. *Breast Cancer Research and Treatment* **50**, 97-116.
- Benjamini, Y. and Hochberg, Y.** (1995). Controlling the false discovery rate: a practical and powerful approach to multiple testing. *Journal of the Royal Statistical Society Series B Methodological* **57**, 289-300.
- Bertozzi, C. C., Schmaier, A. A., Mericko, P., Hess, P. R., Zou, Z., Chen, M., Chen, C.-Y., Xu, B., Lu, M.-m., Zhou, D. et al.** (2010). Platelets regulate lymphatic vascular development through CLEC-2-SLP-76 signaling. *Blood* **116**, 661-670.
- Birnboim, H. C. and Doly, J.** (1979). A rapid alkaline extraction procedure for screening recombinant plasmid DNA. *Nucleic Acids Research* **7**, 1513-1523.
- Björndahl, M., Cao, R., Nissen, L. J., Clasper, S., Johnson, L. A., Xue, Y., Zhou, Z., Jackson, D., Hansen, A. J. and Cao, Y.** (2005). Insulin-like growth factors 1 and 2 induce lymphangiogenesis *in vivo*. *Proceedings of the National Academy of Sciences of the United States of America* **102**, 15593-15598.
- Bocchinfuso, W. P., Lindzey, J. K., Hewitt, S. C., Clark, J. A., Myers, P. H., Cooper, R. and Korach, K. S.** (2000). Induction of mammary gland development in estrogen receptor- α knockout mice. *Endocrinology* **141**, 2982-2994.
- Boström, H., Willetts, K., Pekny, M., Levéen, P., Lindahl, P., Hedstrand, H., Pekna, M., Hellström, M., Gebre-Medhin, S., Schalling, M. et al.** (1996). PDGF-A signaling is a critical event in lung alveolar myofibroblast development and alveogenesis. *Cell* **85**, 863-873.
-

-
- Bray, S. J.** (2006). Notch signalling: a simple pathway becomes complex. *Nature Reviews Molecular Cell Biology* **7**, 678-689.
- Breiteneder-Geleff, S., Matsui, K., Soleiman, A., Meraner, P., Poczewski, H., Kalt, R., Schaffner, G. and Kerjaschki, D.** (1997). Podoplanin, novel 43-kd membrane protein of glomerular epithelial cells, is down-regulated in puromycin nephrosis. *The American Journal of Pathology* **151**, 1141-1152.
- Brice, G., Mansour, S., Bell, R., Collin, J. R. O., Child, A. H., Brady, A. F., Sarfarazi, M., Burnand, K. G., Jeffery, S., Mortimer, P. et al.** (2002). Analysis of the phenotypic abnormalities in lymphoedema-distichiasis syndrome in 74 patients with *FOXC2* mutations or linkage to 16q24. *Journal of Medical Genetics* **39**, 478-483.
- Brisken, C., Park, S., Vass, T., Lydon, J. P., O'Malley, B. W. and Weinberg, R. A.** (1998). A paracrine role for the epithelial progesterone receptor in mammary gland development. *Proceedings of the National Academy of Sciences of the United States of America* **95**, 5076-5081.
- Brown, H. M., Robker, R. L. and Russell, D. L.** (2010). Development and hormonal regulation of the ovarian lymphatic vasculature. *Endocrinology* **151**, 5446-5455.
- Bruyère, F., Melen-Lamalle, L., Blacher, S., Roland, G., Thiry, M., Moons, L., Frankenne, F., Carmeliet, P., Alitalo, K., Libert, C. et al.** (2008). Modeling lymphangiogenesis in a three-dimensional culture system. *Nature Methods* **5**, 431-437.
- Bundred, N. J., Morgan, D. A. L. and Dixon, J. M.** (1994). ABC of breast diseases: management of regional nodes in breast cancer. *BMJ* **309**, 1222-1225.
- Burton, J. B., Priceman, S. J., Sung, J. L., Brakenhielm, E., An, D. S., Pytowski, B., Alitalo, K. and Wu, L.** (2008). Suppression of prostate cancer nodal and systemic metastasis by blockade of the lymphangiogenic axis. *Cancer Research* **68**, 7828-7837.
- Bussmann, J., Bos, F. L., Urasaki, A., Kawakami, K., Duckers, H. J. and Schulte-Merker, S.** (2010). Arteries provide essential guidance cues for lymphatic endothelial cells in the zebrafish trunk. *Development* **137**, 2653-2657.
- Buttler, K., Ezaki, T. and Wilting, J.** (2008). Proliferating mesodermal cells in murine embryos exhibiting macrophage and lymphendothelial characteristics. *BMC Developmental Biology* **8**, 43-55.
- Buttler, K., Kreysing, A., von Kaisenberg, C. S., Schweigerer, L., Gale, N., Papoutsis, M. and Wilting, J.** (2006). Mesenchymal cells with leukocyte and lymphendothelial characteristics in murine embryos. *Developmental Dynamics* **235**, 1554-1562.
- Caine, G. J., Blann, A. D., Stonelake, P. S., Ryan, P. and Lip, G. Y. H.** (2003). Plasma angiopoietin-1, angiopoietin-2 and Tie-2 in breast and prostate cancer: a comparison with VEGF and Flt-1. *European Journal of Clinical Investigation* **33**, 883-890.
- Canfield, A. E. and Schor, A. M.** (1995). Evidence that tenascin and thrombospondin-1 modulate sprouting of endothelial cells. *Journal of Cell Science* **108**, 797-809.
- Cao, R., Björndahl, M. A., Gallego, M. I., Chen, S., Religa, P., Hansen, A. J. and Cao, Y.** (2006). Hepatocyte growth factor is a lymphangiogenic factor with an indirect mechanism of action. *Blood* **107**, 3531-3536.
-

- Cao, R., Björndahl, M. A., Religa, P., Clasper, S., Garvin, S., Galter, D., Meister, B., Ikomi, F., Tritsarlis, K., Dissing, S. et al. (2004). PDGF-BB induces intratumoral lymphangiogenesis and promotes lymphatic metastasis. *Cancer Cell* **6**, 333-345.
- Cao, Y. (2007). Angiogenesis modulates adipogenesis and obesity. *The Journal of Clinical Investigation* **117**, 2362-2368.
- Cardiff, R. D. (1998). Are the TDLU of the human the same as the LA of mice? *Journal of Mammary Gland Biology and Neoplasia* **3**, 3-5.
- Cardiff, R. D., Anver, M. R., Gusterson, B. A., Hennighausen, L., Jensen, R. A., Merino, M. J., Rehm, S., Russo, J., Tavassoli, F. A., Wakefield, L. M. et al. (2000). The mammary pathology of genetically engineered mice: the consensus report and recommendations from the Annapolis meeting. *Oncogene* **19**, 968-988.
- Cardiff, R. D. and Muller, W. J. (1993). Transgenic mouse models of mammary tumorigenesis. *Cancer Surveys* **16**, 97-113.
- Carmeliet, P. and Tessier-Lavigne, M. (2005). Common mechanisms of nerve and blood vessel wiring. *Nature* **436**, 193-200.
- Castellon, R., Caballero, S., Hamdi, H. K., Atilano, S. R., Aoki, A. M., Tarnuzzer, R. W., Kenney, M. C., Grant, M. B. and Ljubimov, A. V. (2002). Effects of tenascin-C on normal and diabetic retinal endothelial cells in culture. *Investigative Ophthalmology & Visual Science* **43**, 2758-2766.
- Caunt, M., Mak, J., Liang, W.-C., Stawicki, S., Pan, Q., Tong, R. K., Kowalski, J., Ho, C., Reslan, H. B., Ross, J. et al. (2008). Blocking neuropilin-2 function inhibits tumor cell metastasis. *Cancer Cell* **13**, 331-342.
- Chang, L. K., Garcia-Cardena, G., Farnebo, F., Fannon, M., Chen, E. J., Butterfield, C., Moses, M. A., Mulligan, R. C., Folkman, J. and Kaipainen, A. (2004). Dose-dependent response of FGF-2 for lymphangiogenesis. *Proceedings of the National Academy of Sciences of the United States of America* **101**, 11658-11663.
- Chiang, C., Swan, R. Z., Grachtchouk, M., Bolinger, M., Litingtung, Y., Robertson, E. K., Cooper, M. K., Gaffield, W., Westphal, H., Beachy, P. A. et al. (1999). Essential role for *Sonic hedgehog* during hair follicle morphogenesis. *Developmental Biology* **205**, 1-9.
- Choi, I., Chung, H. K., Ramu, S., Lee, H. N., Kim, K. E., Lee, S., Yoo, J., Choi, D., Lee, Y. S., Aguilar, B. et al. (2011). Visualization of lymphatic vessels by *Prox1*-promoter directed GFP reporter in a bacterial artificial chromosome-based transgenic mouse. *Blood* **117**, 362-365.
- Choi, W. W. L., Lewis, M. M., Lawson, D., Yin-Goen, Q., Birdsong, G. G., Cotsonis, G. A., Cohen, C. and Young, A. N. (2005). Angiogenic and lymphangiogenic microvessel density in breast carcinoma: correlation with clinicopathologic parameters and VEGF-family gene expression. *Modern Pathology* **18**, 143-152.
- Chuang, P.-T., Kawcak, T. and McMahon, A. P. (2003). Feedback control of mammalian Hedgehog signaling by the Hedgehog-binding protein, Hip1, modulates Fgf signaling during branching morphogenesis of the lung. *Genes & Development* **17**, 342-347.

-
- Chuong, C.-M., Patel, N., Lin, J., Jung, H.-S. and Widelitz, R. B.** (2000). Sonic hedgehog signaling pathway in vertebrate epithelial appendage morphogenesis: perspectives in development and evolution. *Cellular and Molecular Life Sciences* **57**, 1672-1681.
- Cid, M. C., Schnaper, H. W. and Kleinman, H. K.** (2002). Estrogens and the vascular endothelium. *Annals of the New York Academy of Sciences* **966**, 143-157.
- Cirulli, V. and Yebra, M.** (2007). Netrins: beyond the brain. *Nature Reviews Molecular Cell Biology* **8**, 296-306.
- Clapp, C., Thebault, S. and Martínez de la Escalera, G.** (2008). Role of prolactin and vasoinhibins in the regulation of vascular function in mammary gland. *Journal of Mammary Gland Biology and Neoplasia* **13**, 55-67.
- Clasper, S., Royston, D., Baban, D., Cao, Y., Ewers, S., Butz, S., Vestweber, D. and Jackson, D. G.** (2008). A novel gene expression profile in lymphatics associated with tumor growth and nodal metastasis. *Cancer Research* **68**, 7293-7303.
- Clément-Ziza, M., Gentien, D., Lyonnet, S., Thiery, J.-P., Besmond, C. and Decraene, C.** (2009). Evaluation of methods for amplification of picogram amounts of total RNA for whole genome expression profiling. *BMC Genomics* **10**, 246-260.
- Conneely, O. M., Mulac-Jericevic, B. and Lydon, J. P.** (2003). Progesterone-dependent regulation of female reproductive activity by two distinct progesterone receptor isoforms. *Steroids* **68**, 771-778.
- Connell, F., Kalidas, K., Ostergaard, P., Brice, G., Homfray, T., Roberts, L., Bunyan, D. J., Mitton, S., Mansour, S., Mortimer, P. et al.** (2010). Linkage and sequence analysis indicate that *CCBE1* is mutated in recessively inherited generalised lymphatic dysplasia. *Human Genetics* **127**, 231-241.
- Cory, S. and Adams, J. M.** (2002). The Bcl2 family: regulators of the cellular life-or-death switch. *Nature Reviews Cancer* **2**, 647-656.
- Coultas, L., Pellegrini, M., Visvader, J. E., Lindeman, G. J., Chen, L., Adams, J. M., Huang, D. C. S. and Strasser, A.** (2003). Bfk: a novel weakly proapoptotic member of the Bcl-2 protein family with a BH3 and a BH2 region. *Cell Death and Differentiation* **10**, 185-192.
- Cueni, L. N. and Detmar, M.** (2008). The lymphatic system in health and disease. *Lymphatic Research and Biology* **6**, 109-122.
- Cursiefen, C., Chen, L., Borges, L. P., Jackson, D., Cao, J., Radziejewski, C., D'Amore, P. A., Dana, M. R., Wiegand, S. J. and Streilein, J. W.** (2004). VEGF-A stimulates lymphangiogenesis and hemangiogenesis in inflammatory neovascularization via macrophage recruitment. *The Journal of Clinical Investigation* **113**, 1040-1050.
- D'Amico, G., Korhonen, E. A., Waltari, M., Saharinen, P., Laakkonen, P. and Alitalo, K.** (2010). Loss of endothelial Tie1 receptor impairs lymphatic vessel development. *Arteriosclerosis, Thrombosis, and Vascular Biology* **30**, 207-209.
- Dabrosin, C.** (2003). Variability of vascular endothelial growth factor in normal human breast tissue *in vivo* during the menstrual cycle. *The Journal of Clinical Endocrinology & Metabolism* **88**, 2695-2698.
- Dabrosin, C.** (2005). Sex steroid regulation of angiogenesis in breast tissue. *Angiogenesis* **8**, 127-136.
-

-
- Dadras, S. S., Paul, T., Bertoncini, J., Brown, L. F., Muzikansky, A., Jackson, D. G., Ellwanger, U., Garbe, C., Mihm, M. C. and Detmar, M.** (2003). Tumor lymphangiogenesis: a novel prognostic indicator for cutaneous melanoma metastasis and survival. *The American Journal of Pathology* **162**, 1951-1960.
- Dagenais, S. L., Hartsough, R. L., Erickson, R. P., Witte, M. H., Butler, M. G. and Glover, T. W.** (2004). Foxc2 is expressed in developing lymphatic vessels and other tissues associated with lymphedema-distichiasis syndrome. *Gene Expression Patterns* **4**, 611-619.
- Daly, C., Pasnikowski, E., Burova, E., Wong, V., Aldrich, T. H., Griffiths, J., Ioffe, E., Daly, T. J., Fandl, J. P., Papadopoulos, N. et al.** (2006). Angiopoietin-2 functions as an autocrine protective factor in stressed endothelial cells. *Proceedings of the National Academy of Sciences of the United States of America* **103**, 15491-15496.
- de Jong, E. K., Vinet, J., Stanulovic, V. S., Meijer, M., Wesseling, E., Sjollem, K., Boddeke, H. W. G. M. and Biber, K.** (2008). Expression, transport, and axonal sorting of neuronal CCL21 in large dense-core vesicles. *The FASEB Journal* **22**, 4136-4145.
- dela Paz, N. G. and D'Amore, P. A.** (2009). Arterial versus venous endothelial cells. *Cell and Tissue Research* **335**, 5-16.
- Dellinger, M., Hunter, R., Bernas, M., Gale, N., Yancopoulos, G., Erickson, R. and Witte, M.** (2008). Defective remodeling and maturation of the lymphatic vasculature in Angiopoietin-2 deficient mice. *Developmental Biology* **319**, 309-320.
- Dixelius, J., Mäkinen, T., Wirzenius, M., Karkkainen, M. J., Wernstedt, C., Alitalo, K. and Claesson-Welsh, L.** (2003). Ligand-induced vascular endothelial growth factor receptor-3 (VEGFR-3) heterodimerization with VEGFR-2 in primary lymphatic endothelial cells regulates tyrosine phosphorylation sites. *The Journal of Biological Chemistry* **278**, 40973-40979.
- Djonov, V., Andres, A.-C. and Ziemiecki, A.** (2001). Vascular remodelling during the normal and malignant life cycle of the mammary gland. *Microscopy Research and Technique* **52**, 182-189.
- Doe, C. Q., Chu-LaGraff, Q., Wright, D. M. and Scott, M. P.** (1991). The *prospero* gene specifies cell fates in the Drosophila central nervous system. *Cell* **65**, 451-464.
- Donners, M. M. P. C., Wolfs, I. M. J., Olieslagers, S., Mohammadi-Motahhari, Z., Tchaikovski, V., Heeneman, S., van Buul, J. D., Caolo, V., Molin, D. G. M., Post, M. J. et al.** (2010). A disintegrin and metalloprotease 10 is a novel mediator of vascular endothelial growth factor-induced endothelial cell function in angiogenesis and is associated with atherosclerosis. *Arteriosclerosis, Thrombosis, and Vascular Biology* **30**, 2188-2195.
- Donoghue, J. F., Lederman, F. L., Susil, B. J. and Rogers, P. A. W.** (2007). Lymphangiogenesis of normal endometrium and endometrial adenocarcinoma. *Human Reproduction* **22**, 1705-1713.
- Donovan, M. J., Lin, M. I., Wiegand, P., Ringstedt, T., Kraemer, R., Hahn, R., Wang, S., Ibañez, C. F., Rafii, S. and Hempstead, B. L.** (2000). Brain derived neurotrophic factor is an endothelial cell survival factor required for intramyocardial vessel stabilization. *Development* **127**, 4531-4540.
- Dumont, D. J., Gradwohl, G., Fong, G.-H., Puri, M. C., Gertsenshtein, M., Auerbach, A. and Breitman, M. L.** (1994). Dominant-negative and targeted null mutations in the endothelial receptor
-

tyrosine kinase, *tek*, reveal a critical role in vasculogenesis of the embryo. *Genes & Development* **8**, 1897-1909.

Dumont, D. J., Gradwohl, G. J., Fong, G.-H., Auerbach, R. and Breitman, M. L. (1993). The endothelial-specific receptor tyrosine kinase, *tek*, is a member of a new subfamily of receptors. *Oncogene* **8**, 1293-1301.

Dumont, D. J., Jussila, L., Taipale, J., Lymboussaki, A., Mustonen, T., Pajusola, K., Breitman, M. and Alitalo, K. (1998). Cardiovascular failure in mouse embryos deficient in VEGF receptor-3. *Science* **282**, 946-949.

Dyer, M. A., Livesey, F. J., Cepko, C. L. and Oliver, G. (2003). Prox1 function controls progenitor cell proliferation and horizontal cell genesis in the mammalian retina. *Nature Genetics* **34**, 53-58.

Eccles, S. A. and Welch, D. R. (2007). Metastasis: recent discoveries and novel treatment strategies. *Lancet* **369**, 1742-1757.

Eck, M. V., Oost, J., Goudriaan, J. R., Hoekstra, M., Hildebrand, R. B., Bosa, I. S. T., van Dijk, K. W. and Van Berkel, T. J. C. (2005). Role of the macrophage very-low-density lipoprotein receptor in atherosclerotic lesion development. *Atherosclerosis* **183**, 230-237.

Edwards, D. R., Handsley, M. M. and Pennington, C. J. (2008). The ADAM metalloproteinases. *Molecular Aspects of Medicine* **29**, 258-289.

Egeblad, M. and Werb, Z. (2002). New functions for the matrix metalloproteinases in cancer progression. *Nature Reviews Cancer* **2**, 161-174.

Enholm, B., Paavonen, K., Ristimäki, A., Kumar, V., Gunji, Y., Klefstrom, J., Kivinen, L., Laiho, M., Olofsson, B., Joukov, V. et al. (1997). Comparison of VEGF, VEGF-B, VEGF-C and Ang-1 mRNA regulation by serum, growth factors, oncoproteins and hypoxia. *Oncogene* **14**, 2475-2483.

Erdmann, S., Ricken, A., Merkwitz, C., Struman, I., Castino, R., Hummitzsch, K., Gaunitz, F., Isidoro, C., Martial, J. and Spanel-Borowski, K. (2007). The expression of prolactin and its cathepsin D-mediated cleavage in the bovine corpus luteum vary with the estrous cycle. *American Journal of Physiology, Endocrinology and Metabolism* **293**, E1365-E1377.

Evangelista, M., Tian, H. and de Sauvage, F. J. (2006). The hedgehog signaling pathway in cancer. *Clinical Cancer Research* **12**, 5924-5928.

Falkenberg, M., Björnheden, T., Lindnér, P. and Risberg, B. (1998). Co-localization of fibrinolytic activators and inhibitors with macrophages in atherosclerotic vessels. *Cardiovascular Pathology* **7**, 223-231.

Fang, J., Dagenais, S. L., Erickson, R. P., Arlt, M. F., Glynn, M. W., Gorski, J. L., Seaver, L. H. and Glover, T. W. (2000). Mutations in *FOXC2* (*MFH-1*), a forkhead family transcription factor, are responsible for the hereditary lymphedema-distichiasis syndrome. *The American Journal of Human Genetics* **67**, 1382-1388.

Fata, J. E., Chaudhary, V. and Khokha, R. (2001). Cellular turnover in the mammary gland is correlated with systemic levels of progesterone and not 17 β -estradiol during the estrous cycle. *Biology of Reproduction* **65**, 680-688.

-
- Fata, J. E., Werb, Z. and Bissell, M. J.** (2004). Regulation of mammary gland branching morphogenesis by the extracellular matrix and its remodeling enzymes. *Breast Cancer Research* **6**, 1-11.
- Fendrick, J. L., Raafat, A. M. and Haslam, S. Z.** (1998). Mammary gland growth and development from the postnatal period to postmenopause: ovarian steroid receptor ontogeny and regulation in the mouse. *Journal of Mammary Gland Biology and Neoplasia* **3**, 7-22.
- Ferrara, N. and Davis-Smyth, T.** (1997). The biology of vascular endothelial growth factor. *Endocrine Reviews* **18**, 4-25.
- Finegold, D. N., Kimak, M. A., Lawrence, E. C., Levinson, K. L., Cherniske, E. M., Pober, B. R., Dunlap, J. W. and Ferrell, R. E.** (2001). Truncating mutations in *FOXC2* cause multiple lymphedema syndromes. *Human Molecular Genetics* **10**, 1185-1189.
- Fisher, B., Bauer, M., Wickerham, D. L., Redmond, C. K., Fisher, E. R., Cruz, A. B., Foster, R., Gardner, B., Lerner, H., Margolese, R. et al.** (1983). Relation of number of positive axillary nodes to the prognosis of patients with primary breast cancer. An NSABP update. *Cancer* **52**, 1551-1557.
- Flanagan, J. G. and Vanderhaeghen, P.** (1998). The ephrins and Eph receptors in neural development. *Annual Review of Neuroscience* **21**, 309-345.
- Fong, T. A. T., Shawver, L. K., Sun, L., Tang, C., App, H., Powell, T. J., Kim, Y. H., Schreck, R., Wang, X., Risau, W. et al.** (1999). SU5416 is a potent and selective inhibitor of the vascular endothelial growth factor receptor (Flk-1/KDR) that inhibits tyrosine kinase catalysis, tumor vascularization, and growth of multiple tumor types. *Cancer Research* **59**, 99-106.
- Förster, C., Mäkela, S., Wärrri, A., Kietz, S., Becker, D., Hultenby, K., Warner, M. and Gustafsson, J.-Å.** (2002). Involvement of estrogen receptor β in terminal differentiation of mammary gland epithelium. *Proceedings of the National Academy of Sciences of the United States of America* **99**, 15578-15583.
- Förster, E., Bock, H. H., Herz, J., Chai, X., Frotscher, M. and Zhao, S.** (2010). Emerging topics in Reelin function. *European Journal of Neuroscience* **31**, 1511-1518.
- François, M., Caprini, A., Hosking, B., Orsenigo, F., Wilhelm, D., Browne, C., Paavonen, K., Karnezis, T., Shayan, R., Downes, M. et al.** (2008). Sox18 induces development of the lymphatic vasculature in mice. *Nature* **456**, 643-647.
- Frederick, M. J. and Clayman, G. L.** (2001). Chemokines in cancer. *Expert Reviews in Molecular Medicine* **3**, 1-18.
- Fritz-Six, K. L., Dunworth, W. P., Li, M. and Caron, K. M.** (2008). Adrenomedullin signaling is necessary for murine lymphatic vascular development. *The Journal of Clinical Investigation* **118**, 40-50.
- Gailani, M. R., Stähle-Bäckdahl, M., Leffell, D. J., Glynn, M., Zaphiropoulos, P. G., Pressman, C., Undén, A. B., Dean, M., Brash, D. E., Bale, A. E. et al.** (1996). The role of the human homologue of *Drosophila patched* in sporadic basal cell carcinomas. *Nature Genetics* **14**, 78-81.
- Gale, N. W., Prevo, R., Espinosa, J., Ferguson, D. J., Dominguez, M. G., Yancopoulos, G. D., Thurston, G. and Jackson, D. G.** (2007). Normal lymphatic development and function in mice deficient for the lymphatic hyaluronan receptor LYVE-1. *Molecular and Cellular Biology* **27**, 595-604.
-

-
- Gale, N. W., Thurston, G., Hackett, S. F., Renard, R., Wang, Q., McClain, J., Martin, C., Witte, C., Witte, M. H., Jackson, D. et al.** (2002). Angiopoietin-2 is required for postnatal angiogenesis and lymphatic patterning, and only the latter role is rescued by angiopoietin-1. *Developmental Cell* **3**, 411-423.
- Girling, J. E., Donoghue, J. F., Lederman, F. L., Cann, L. M., Achen, M. G., Stacker, S. A. and Rogers, P. A. W.** (2010). Vascular endothelial growth factor-D over-expressing tumor cells induce differential effects on uterine vasculature in a mouse model of endometrial cancer. *Reproductive Biology and Endocrinology* **8**, 84-97.
- Glomski, K., Monette, S., Manova, K., De Strooper, B., Saftig, P. and Blobel, C. P.** (2011). Deletion of Adam10 in endothelial cells leads to defects in organ-specific vascular structures. *Blood* **118**, 1163-1174.
- Goetzl, E. J., Bando, M. J. and Leppert, D.** (1996). Matrix metalloproteinases in immunity. *Journal of Immunology* **156**, 1-4.
- Goodrich, L. V., Johnson, R. L., Milenković, L., McMahon, J. A. and Scott, M. P.** (1996). Conservation of the *hedgehog/patched* signaling pathway from flies to mice: induction of a mouse *patched* gene by Hedgehog. *Genes & Development* **10**, 301-312.
- Goodrich, L. V., Milenković, L., Higgins, K. M. and Scott, M. P.** (1997). Altered neural cell fates and medulloblastoma in mouse *patched* mutants. *Science* **277**, 1109-1113.
- Gordon, E. J., Gale, N. W. and Harvey, N. L.** (2008). Expression of the hyaluronan receptor LYVE-1 is not restricted to the lymphatic vasculature; LYVE-1 is also expressed on embryonic blood vessels. *Developmental Dynamics* **237**, 1901-1909.
- Gordon, E. J., Rao, S., Pollard, J. W., Nutt, S. L., Lang, R. A. and Harvey, N. L.** (2010). Macrophages define dermal lymphatic vessel calibre during development by regulating lymphatic endothelial cell proliferation. *Development* **137**, 3899-3910.
- Green, K. A. and Lund, L. R.** (2005). ECM degrading proteases and tissue remodelling in the mammary gland. *BioEssays* **27**, 894-903.
- Gu, Y., Qi, X. and Guo, S.** (2008). Lymphangiogenesis induced by VEGF-C and VEGF-D promotes metastasis and a poor outcome in breast carcinoma: a retrospective study of 61 cases. *Clinical & Experimental Metastasis* **25**, 717-725.
- Gunn, M. D., Kyuwa, S., Tam, C., Kakiuchi, T., Matsuzawa, A., Williams, L. T. and Nakano, H.** (1999). Mice lacking expression of secondary lymphoid organ chemokine have defects in lymphocyte homing and dendritic cell localization. *The Journal of Experimental Medicine* **189**, 451-460.
- Gunn, M. D., Tangemann, K., Tam, C., Cyster, J. G., Rosen, S. D. and Williams, L. T.** (1998). A chemokine expressed in lymphoid high endothelial venules promotes the adhesion and chemotaxis of naive T lymphocytes. *Proceedings of the National Academy of Sciences of the United States of America* **95**, 258-263.
- Guo, B., Godzik, A. and Reed, J. C.** (2001). Bcl-G, a novel pro-apoptotic member of the Bcl-2 family. *The Journal of Biological Chemistry* **276**, 2780-2785.
- Gupta, G. P. and Massagué, J.** (2006). Cancer metastasis: building a framework. *Cell* **127**, 679-695.
-

- Guy, C. T., Cardiff, R. D. and Muller, W. J.** (1992). Induction of mammary tumors by expression of polyomavirus middle T oncogene: a transgenic mouse model for metastatic disease. *Molecular and Cellular Biology* **12**, 954-961.
- Hahn, H., Christiansen, J., Wicking, C., Zaphiropoulos, P. G., Chidambaram, A., Gerrardi, B., Vorechovsky, I., Bale, A. E., Toftgård, R., Dean, M. et al.** (1996a). A mammalian *patched* homolog is expressed in target tissues of *sonic hedgehog* and maps to a region associated with developmental abnormalities. *The Journal of Biological Chemistry* **271**, 12125-12128.
- Hahn, H., Wicking, C., Zaphiropoulos, P. G., Gailani, M. R., Shanley, S., Chidambaram, A., Vorechovsky, I., Holmberg, E., Undén, A. B., Gillies, S. et al.** (1996b). Mutations of the human homolog of *Drosophila patched* in the nevoid basal cell carcinoma syndrome. *Cell* **85**, 841-851.
- Hahn, H., Wojnowski, L., Miller, G. and Zimmer, A.** (1999). The *patched* signaling pathway in tumorigenesis and development: lessons from animal models. *Journal of Molecular Medicine* **77**, 459-468.
- Hahn, H., Wojnowski, L., Zimmer, A. M., Hall, J., Miller, G. and Zimmer, A.** (1998). Rhabdomyosarcomas and radiation hypersensitivity in a mouse model of Gorlin syndrome. *Nature Medicine* **4**, 619-622.
- Haiko, P., Mäkinen, T., Keskitalo, S., Taipale, J., Karkkainen, M. J., Baldwin, M. E., Stacker, S. A., Achen, M. G. and Alitalo, K.** (2008). Deletion of vascular endothelial growth factor C (VEGF-C) and VEGF-D is not equivalent to VEGF receptor 3 deletion in mouse embryos. *Molecular and Cellular Biology* **28**, 4843-4850.
- Haldimann, M., Custer, D., Munarini, N., Stirnimann, C., Zürcher, G., Rohrbach, V., Djonov, V., Ziemiecki, A. and Andres, A.-C.** (2009). Deregulated ephrin-B2 expression in the mammary gland interferes with the development of both the glandular epithelium and vasculature and promotes metastasis formation. *International Journal of Oncology* **35**, 525-536.
- Hannon, R., Croxtall, J. D., Getting, S. J., Roviezzo, F., Yona, S., Paul-Clark, M. J., Gavins, F. N. E., Perretti, M., Morris, J. F., Buckingham, J. C. et al.** (2003). Aberrant inflammation and resistance to glucocorticoids in annexin 1^{-/-} mouse. *The FASEB Journal* **17**, 253-255.
- Harada, M., Hato, T. and Horio, H.** (2011). Intratumoral lymphatic vessel involvement is an invasive indicator of completely resected pathologic stage I non-small cell lung cancer. *Journal of Thoracic Oncology* **6**, 48-54.
- Harris, N. C., Paavonen, K., Davydova, N., Roufail, S., Sato, T., Zhang, Y.-F., Karnezis, T., Stacker, S. A. and Achen, M. G.** (2011). Proteolytic processing of vascular endothelial growth factor-D is essential for its capacity to promote the growth and spread of cancer. *The FASEB Journal* **25**, 2615-2625.
- Hartmann, D., de Strooper, B., Serneels, L., Craessaerts, K., Herreman, A., Annaert, W., Umans, L., Lübke, T., Lena Illert, A., von Figura, K. et al.** (2002). The disintegrin/metalloprotease ADAM 10 is essential for Notch signalling but not for α -secretase activity in fibroblasts. *Human Molecular Genetics* **11**, 2615-2624.
- Harvey, N. L.** (2008). The link between lymphatic function and adipose biology. *Annals of the New York Academy of Sciences* **1131**, 82-88.

-
- Harvey, N. L., Srinivasan, R. S., Dillard, M. E., Johnson, N. C., Witte, M. H., Boyd, K., Sleeman, M. W. and Oliver, G. (2005). Lymphatic vascular defects promoted by Prox1 haploinsufficiency cause adult-onset obesity. *Nature Genetics* **37**, 1072-1081.
- Hatsell, S. J. and Cowin, P. (2006). Gli3-mediated repression of Hedgehog targets is required for normal mammary development. *Development* **133**, 3661-3670.
- He, Y., Kozaki, K.-i., Karpanen, T., Koshikawa, K., Ylä-Herttuala, S., Takahashi, T. and Alitalo, K. (2002). Suppression of tumor lymphangiogenesis and lymph node metastasis by blocking vascular endothelial growth factor receptor 3 signaling. *Journal of the National Cancer Institute* **94**, 819-825.
- Hellström, M., Kalén, M., Lindahl, P., Abramsson, A. and Betsholtz, C. (1999). Role of PDGF-B and PDGFR- β in recruitment of vascular smooth muscle cells and pericytes during embryonic blood vessel formation in the mouse. *Development* **126**, 3047-3055.
- Hellström, M., Phng, L.-K., Hofmann, J. J., Wallgard, E., Coultas, L., Lindblom, P., Alva, J., Nilsson, A.-K., Karlsson, L., Gaiano, N. et al. (2007). Dll4 signalling through Notch1 regulates formation of tip cells during angiogenesis. *Nature* **445**, 776-780.
- Hennighausen, L. and Robinson, G. W. (1998). Think globally, act locally: the making of a mouse mammary gland. *Genes & Development* **12**, 449-455.
- Hennighausen, L. and Robinson, G. W. (2005). Information networks in the mammary gland. *Nature Reviews Molecular Cell Biology* **6**, 715-725.
- Hirakawa, S., Hong, Y.-K., Harvey, N., Schacht, V., Matsuda, K., Libermann, T. and Detmar, M. (2003). Identification of vascular lineage-specific genes by transcriptional profiling of isolated blood vascular and lymphatic endothelial cells. *The American Journal of Pathology* **162**, 575-586.
- Hoch, R. V. and Soriano, P. (2003). Roles of PDGF in animal development. *Development* **130**, 4769-4784.
- Hogan, B. M., Bos, F. L., Bussmann, J., Witte, M., Chi, N. C., Duckers, H. J. and Schulte-Merker, S. (2009a). *ccbe1* is required for embryonic lymphangiogenesis and venous sprouting. *Nature Genetics* **41**, 396-398.
- Hogan, B. M., Herpers, R., Witte, M., Heloterä, H., Alitalo, K., Duckers, H. J. and Schulte-Merker, S. (2009b). *Vegfc/Flt4* signalling is suppressed by Dll4 in developing zebrafish intersegmental arteries. *Development* **136**, 4001-4009.
- Holopainen, T., Huang, H., Chen, C., Kim, K. E., Zhang, L., Zhou, F., Han, W., Li, C., Yu, J., Wu, J. et al. (2009). Angiopoietin-1 overexpression modulates vascular endothelium to facilitate tumor cell dissemination and metastasis establishment. *Cancer Research* **69**, 4656-4664.
- Hong, Y.-K., Harvey, N., Noh, Y.-H., Schacht, V., Hirakawa, S., Detmar, M. and Oliver, G. (2002). Prox1 is a master control gene in the program specifying lymphatic endothelial cell fate. *Developmental Dynamics* **225**, 351-357.
- Hooper, J. E. and Scott, M. P. (2005). Communicating with Hedgehogs. *Nature Reviews Molecular Cell Biology* **6**, 306-317.
-

-
- Hope, K. J., Celot, S., Ting, S. B., MacRae, T., Mayotte, N., Iscove, N. N. and Sauvageau, G.** (2010). An RNAi screen identifies *Msi2* and *Prox1* as having opposite roles in the regulation of hematopoietic stem cell activity. *Cell Stem Cell* **7**, 101-113.
- Hovey, R. C., Goldhar, A. S., Baffi, J. and Vonderhaar, B. K.** (2001). Transcriptional regulation of vascular endothelial growth factor expression in epithelial and stromal cells during mouse mammary gland development. *Molecular Endocrinology* **15**, 819-831.
- Howlin, J., McBryan, J. and Martin, F.** (2006). Pubertal mammary gland development: insights from mouse models. *Journal of Mammary Gland Biology and Neoplasia* **11**, 283-297.
- Huang, S. S., Liu, I. H., Smith, T., Shah, M. R., Johnson, F. E. and Huang, J. S.** (2006). CRISP-1/LYVE-1-null mice exhibit identifiable morphological and functional alterations of lymphatic capillary vessels. *FEBS Letters* **580**, 6259-6268.
- Huang, X. Z., Wu, J. F., Ferrando, R., Lee, J. H., Wang, Y. L., Farese, R. V. and Sheppard, D.** (2000). Fatal bilateral chylothorax in mice lacking the integrin $\alpha_5\beta_1$. *Molecular and Cellular Biology* **20**, 5208-5215.
- Huntington, G. S. and McClure, C. F.** (1910). The anatomy and development of the jugular lymph sacs in the domestic cat (*Felis domestica*). *American Journal of Anatomy* **10**, 177-312.
- Hyder, S. M., Nawaz, Z., Chiappetta, C. and Stancel, G. M.** (2000). Identification of functional estrogen response elements in the gene coding for the potent angiogenic factor vascular endothelial growth factor. *Cancer Research* **60**, 3183-3190.
- Ikomi, F., Yokoyama, Y., Ogiwara, N., Sasaki, K., Mizuno, R. and Ohhashi, T.** (2006). Recanalization of the collecting lymphatics in rabbit hind leg. *Microcirculation* **13**, 365-376.
- Imanishi, Y., Hu, B., Jarzynka, M. J., Guo, P., Elishaev, E., Bar-Joseph, I. and Cheng, S.-Y.** (2007). Angiopoietin-2 stimulates breast cancer metastasis through the $\alpha_5\beta_1$ integrin-mediated pathway. *Cancer Research* **67**, 4254-4263.
- Inderdeo, D. S., Edwards, D. R., Han, V. K. M. and Khokha, R.** (1996). Temporal and spatial expression of tissue inhibitors of metalloproteinases during the natural ovulatory cycle of the mouse. *Biology of Reproduction* **55**, 498-508.
- Ingham, P. W. and McMahon, A. P.** (2001). Hedgehog signaling in animal development: paradigms and principles. *Genes & Development* **15**, 3059-3087.
- Ingham, P. W. and Placzek, M.** (2006). Orchestrating ontogenesis: variations on a theme by sonic hedgehog. *Nature Reviews Genetics* **7**, 841-850.
- Irrthum, A., Devriendt, K., Chitayat, D., Matthijs, G., Glade, C., Steijlen, P. M., Fryns, J.-P., Van Steensel, M. A. M. and Vikkula, M.** (2003). Mutations in the transcription factor gene *SOX18* underlie recessive and dominant forms of hypotrichosis-lymphedema-telangiectasia. *The American Journal of Human Genetics* **72**, 1470-1480.
- Islam, M. S., Matsumoto, M., Ishida, R., Oka, T. and Kanouchi, H.** (2010). Change in VEGF expression in mouse mammary gland during reproductive cycle. *The Journal of Veterinary Medical Science* **72**, 1159-1163.
-

- Jeltsch, M., Kaipainen, A., Joukov, V., Meng, X., Lakso, M., Rauvala, H., Swartz, M., Fukumura, D., Jain, R. K. and Alitalo, K.** (1997). Hyperplasia of lymphatic vessels in VEGF-C transgenic mice. *Science* **276**, 1423-1425.
- Jennbacken, K., Vallbo, C., Wang, W. and Damber, J.-E.** (2005). Expression of vascular endothelial growth factor C (VEGF-C) and VEGF receptor-3 in human prostate cancer is associated with regional lymph node metastasis. *The Prostate* **65**, 110-116.
- Jeon, B.-H., Jang, C., Han, J., Kataru, R. P., Piao, L., Jung, K., Cha, H. J., Schwendener, R. A., Jang, K. Y., Kim, K.-S. et al.** (2008). Profound but dysfunctional lymphangiogenesis via vascular endothelial growth factor ligands from CD11b⁺ macrophages in advanced ovarian cancer. *Cancer Research* **68**, 1100-1109.
- Jiang, J. and Hui, C.-c.** (2008). Hedgehog signaling in development and cancer. *Developmental Cell* **15**, 801-812.
- Johnson, N. C., Dillard, M. E., Baluk, P., McDonald, D. M., Harvey, N. L., Frase, S. L. and Oliver, G.** (2008). Lymphatic endothelial cell identity is reversible and its maintenance requires Prox1 activity. *Genes & Development* **22**, 3282-3291.
- Johnson, R. L., Rothman, A. L., Xie, J., Goodrich, L. V., Bare, J. W., Bonifas, J. M., Quinn, A. G., Myers, R. M., Cox, D. R., Epstein, E. H. et al.** (1996). Human homolog of patched, a candidate gene for the basal cell nevus syndrome. *Science* **272**, 1668-1671.
- Jokinen, C. H., Dadras, S. S., Goldblum, J. R., van de Rijn, M., West, R. B. and Rubin, B. P.** (2008). Diagnostic implications of podoplanin expression in peripheral nerve sheath neoplasms. *American Journal of Clinical Pathology* **129**, 886-893.
- Joory, K. D., Levick, J. R., Mortimer, P. S. and Bates, D. O.** (2006). Vascular endothelial growth factor-C (VEGF-C) expression in normal human tissues. *Lymphatic Research and Biology* **4**, 73-82.
- Joukov, V., Pajusola, K., Kaipainen, A., Chilov, D., Lahtinen, I., Kukk, E., Saksela, O., Kalkkinen, N. and Alitalo, K.** (1996). A novel vascular endothelial growth factor, VEGF-C, is a ligand for the Flt4 (VEGFR-3) and KDR (VEGFR-2) receptor tyrosine kinases. *The EMBO Journal* **15**, 290-298.
- Joukov, V., Sorsa, T., Kumar, V., Jeltsch, M., Claesson-Welsh, L., Cao, Y., Saksela, O., Kalkkinen, N. and Alitalo, K.** (1997). Proteolytic processing regulates receptor specificity and activity of VEGF-C. *The EMBO Journal* **16**, 3898-3911.
- Kaipainen, A., Korhonen, J., Mustonen, T., van Hinsbergh, V. W. M., Fang, G.-H., Dumont, D., Breitman, M. and Alitalo, K.** (1995). Expression of the fms-like tyrosine kinase 4 gene becomes restricted to lymphatic endothelium during development. *Proceedings of the National Academy of Sciences of the United States of America* **92**, 3566-3570.
- Kajii, T., Ferrier, A., Niikawa, N., Takahara, H., Ohama, K. and Avirachan, S.** (1980). Anatomic and chromosomal anomalies in 639 spontaneous abortuses. *Human Genetics* **55**, 87-98.
- Kajiya, K., Hirakawa, S., Ma, B., Drinnenberg, I. and Detmar, M.** (2005). Hepatocyte growth factor promotes lymphatic vessel formation and function. *The EMBO Journal* **24**, 2885-2895.
- Kampmeier, O. F. and Birch, C. L. F.** (1927). The origin and development of the venous valves, with particular reference to the saphenous district. *American Journal of Anatomy* **38**, 451-499.

-
- Karkkainen, M. J., Ferrell, R. E., Lawrence, E. C., Kimak, M. A., Levinson, K. L., McTigue, M. A., Alitalo, K. and Finegold, D. N. (2000). Missense mutations interfere with VEGFR-3 signalling in primary lymphoedema. *Nature Genetics* **25**, 153-159.
- Karkkainen, M. J., Haiko, P., Sainio, K., Partanen, J., Taipale, J., Petrova, T. V., Jeltsch, M., Jackson, D. G., Talikka, M., Rauvala, H. et al. (2004). Vascular endothelial growth factor C is required for sprouting of the first lymphatic vessels from embryonic veins. *Nature Immunology* **5**, 74-80.
- Karkkainen, M. J., Saaristo, A., Jussila, L., Karila, K. A., Lawrence, E. C., Pajusola, K., Bueler, H., Eichmann, A., Kauppinen, R., Kettunen, M. I. et al. (2001). A model for gene therapy of human hereditary lymphedema. *Proceedings of the National Academy of Sciences of the United States of America* **98**, 12677-12682.
- Karpanen, T., Egeblad, M., Karkkainen, M. J., Kubo, H., Ylä-Herttuala, S., Jäättelä, M. and Alitalo, K. (2001). Vascular endothelial growth factor C promotes tumor lymphangiogenesis and intralymphatic tumor growth. *Cancer Research* **61**, 1786-1790.
- Karpanen, T., Heckman, C. A., Keskitalo, S., Jeltsch, M., Ollila, H., Neufeld, G., Tamagnone, L. and Alitalo, K. (2006). Functional interaction of VEGF-C and VEGF-D with neuropilin receptors. *The FASEB Journal* **20**, 1462-1472.
- Kasper, M., Jaks, V., Fiaschi, M. and Toftgård, R. (2009). Hedgehog signalling in breast cancer. *Carcinogenesis* **30**, 903-911.
- Kataru, R. P., Jung, K., Jang, C., Yang, H., Schwendener, R. A., Baik, J. E., Han, S. H., Alitalo, K. and Koh, G. Y. (2009). Critical role of CD11b⁺ macrophages and VEGF in inflammatory lymphangiogenesis, antigen clearance, and inflammation resolution. *Blood* **113**, 5650-5659.
- Katsetos, C. D., Herman, M. M. and Mörk, S. J. (2003). Class III β -tubulin in human development and cancer. *Cell Motility and the Cytoskeleton* **55**, 77-96.
- Kazenwadel, J., Michael, M. Z. and Harvey, N. L. (2010). *Prox1* expression is negatively regulated by *miR-181* in endothelial cells. *Blood* **116**, 2395-2401.
- Kendrick, H., Regan, J. L., Magnay, F.-A., Grigoriadis, A., Mitsopoulos, C., Zvelebil, M. and Smalley, M. J. (2008). Transcriptome analysis of mammary epithelial subpopulations identifies novel determinants of lineage commitment and cell fate. *BMC Genomics* **9**, 591-618.
- Kerjaschki, D., Huttary, N., Raab, I., Regele, H., Bojarski-Nagy, K., Bartel, G., Kröber, S. M., Greinix, H., Rosenmaier, A., Karlhofer, F. et al. (2006). Lymphatic endothelial progenitor cells contribute to de novo lymphangiogenesis in human renal transplants. *Nature Medicine* **12**, 230-234.
- Kerjaschki, D., Regele, H. M., Moosberger, I., Nagy-Bojarski, K., Watschinger, B., Soleiman, A., Birner, P., Krieger, S., Hovorka, A., Silberhumer, G. et al. (2004). Lymphatic neoangiogenesis in human kidney transplants is associated with immunologically active lymphocytic infiltrates. *Journal of the American Society of Nephrology* **15**, 603-612.
- Kermani, P., Rafii, D., Jin, D. K., Whitlock, P., Schaffer, W., Chiang, A., Vincent, L., Friedrich, M., Shido, K., Hackett, N. R. et al. (2005). Neurotrophins promote revascularization by local recruitment of TrkB⁺ endothelial cells and systemic mobilization of hematopoietic progenitors. *The Journal of Clinical Investigation* **115**, 653-663.
-

- Khatib, A.-M., Siegfried, G., Prat, A., Luis, J., Chrétien, M., Metrakos, P. and Seidah, N. G.** (2001). Inhibition of proprotein convertases is associated with loss of growth and tumorigenicity of HT-29 human colon carcinoma cells: importance of insulin-like growth factor-1 (IGF-1) receptor processing in IGF-1-mediated functions. *The Journal of Biological Chemistry* **276**, 30686-30693.
- Khialeeva, E., Lane, T. F. and Carpenter, E. M.** (2011). Disruption of reelin signaling alters mammary gland morphogenesis. *Development* **138**, 767-776.
- Kim-Schulze, S., McGowan, K. A., Hubchak, S. C., Cid, M. C., Martin, M. B., Kleinman, H. K., Greene, G. L. and Schnaper, H. W.** (1996). Expression of an estrogen receptor by human coronary artery and umbilical vein endothelial cells. *Circulation* **94**, 1402-1407.
- Kimonis, V. E., Goldstein, A. M., Pastakia, B., Yang, M. L., Kase, R., DiGiovanna, J. J., Bale, A. E. and Bale, S. J.** (1997). Clinical manifestations in 105 persons with nevoid basal cell carcinoma syndrome. *American Journal of Medical Genetics* **69**, 299-308.
- Kirkin, V., Mazitschek, R., Krishnan, J., Steffen, A., Waltenberger, J., Pepper, M. S., Giannis, A. and Sleeman, J. P.** (2001). Characterization of indolinones which preferentially inhibit VEGF-C- and VEGF-D-induced activation of VEGFR-3 rather than VEGFR-2. *European Journal of Biochemistry* **268**, 5530-5540.
- Kirkin, V., Thiele, W., Baumann, P., Mazitschek, R., Rohde, K., Fellbrich, G., Weich, H., Waltenberger, J., Giannis, A. and Sleeman, J. P.** (2004). MAZ51, an indolinone that inhibits endothelial cell and tumor cell growth *in vitro*, suppresses tumor growth *in vivo*. *International Journal of Cancer* **112**, 986-993.
- Koch, M., Dettori, D., Van Nuffelen, A., Souffreau, J., Marconcini, L., Wallays, G., Moons, L., Bruyère, F., Oliviero, S., Noel, A. et al.** (2009). VEGF-D deficiency in mice does not affect embryonic or postnatal lymphangiogenesis but reduces lymphatic metastasis. *The Journal of Pathology* **219**, 356-364.
- Koukourakis, M. I., Giatromanolaki, A., Sivridis, E., Simopoulos, C., Gatter, K. C., Harris, A. L. and Jackson, D. G.** (2005). LYVE-1 immunohistochemical assessment of lymphangiogenesis in endometrial and lung cancer. *Journal of Clinical Pathology* **58**, 202-206.
- Kriehuber, E., Breiteneder-Geleff, S., Groeger, M., Soleiman, A., Schoppmann, S. F., Stingl, G., Kerjaschki, D. and Maurer, D.** (2001). Isolation and characterization of dermal lymphatic and blood endothelial cells reveal stable and functionally specialized cell lineages. *The Journal of Experimental Medicine* **194**, 797-808.
- Kubo, H., Cao, R., Bräkenhielm, E., Mäkinen, T., Cao, Y. and Alitalo, K.** (2002). Blockade of vascular endothelial growth factor receptor-3 signaling inhibits fibroblast growth factor-2-induced lymphangiogenesis in mouse cornea. *Proceedings of the National Academy of Sciences of the United States of America* **99**, 8868-8873.
- Kubo, H., Fujiwara, T., Jussila, L., Hashi, H., Ogawa, M., Shimizu, K., Awane, M., Sakai, Y., Takabayashi, A., Alitalo, K. et al.** (2000). Involvement of vascular endothelial growth factor receptor-3 in maintenance of integrity of endothelial cell lining during tumor angiogenesis. *Blood* **96**, 546-553.
- Kuijpera, S., Turnera, C. J. and Adams, R. H.** (2007). Regulation of angiogenesis by Eph-ephrin interactions. *Trends in Cardiovascular Medicine* **17**, 141-151.

-
- Kukk, E., Lymboussaki, A., Taira, S., Kaipainen, A., Jeltsch, M., Joukov, V. and Alitalo, K.** (1996). VEGF-C receptor binding and pattern of expression with VEGFR-3 suggests a role in lymphatic vascular development. *Development* **122**, 3829-3837.
- Kunstfeld, R., Hirakawa, S., Hong, Y.-K., Schacht, V., Lange-Asschenfeldt, B., Velasco, P., Lin, C., Fiebiger, E., Wei, X., Wu, Y. et al.** (2004). Induction of cutaneous delayed-type hypersensitivity reactions in VEGF-A transgenic mice results in chronic skin inflammation associated with persistent lymphatic hyperplasia. *Blood* **104**, 1048-1057.
- Kurn, N., Chen, P., Heath, J. D., Kopf-Sill, A., Stephens, K. M. and Wang, S.** (2005). Novel isothermal, linear nucleic acid amplification systems for highly multiplexed applications. *Clinical Chemistry* **51**, 1973-1981.
- Kyzas, P. A., Geleff, S., Batistatou, A., Agnantis, N. J. and Stefanou, D.** (2005). Evidence for lymphangiogenesis and its prognostic implications in head and neck squamous cell carcinoma. *The Journal of Pathology* **206**, 170-177.
- Lacovara, J. E. and Yoder, L. H.** (2006). Secondary lymphedema in the cancer patient. *MedSurg Nursing* **15**, 302-306.
- Lam, C.-T., Yang, Z.-F., Lau, C.-K., Tam, K.-H., Fan, S.-T. and Poon, R. T. P.** (2011). Brain-derived neurotrophic factor promotes tumorigenesis via induction of neovascularization: implication in hepatocellular carcinoma. *Clinical Cancer Research* **17**, 3123-3133.
- Lammich, S., Kojro, E., Postina, R., Gilbert, S., Pfeiffer, R., Jasionowski, M., Haass, C. and Fahrenholz, F.** (1999). Constitutive and regulated α -secretase cleavage of Alzheimer's amyloid precursor protein by a disintegrin metalloprotease. *Proceedings of the National Academy of Sciences of the United States of America* **96**, 3922-3927.
- Larri e, B., Freitas, C., Suchting, S., Brunet, I. and Eichmann, A.** (2009). Guidance of vascular development: lessons from the nervous system. *Circulation Research* **104**, 428-441.
- Laser, J., Cangiarella, J., Singh, B., Melamed, J., Chiriboga, L., Yee, H. and Darvishian, F.** (2008). Invasive lobular carcinoma of the breast: role of endothelial lymphatic marker D2-40. *Annals of Clinical & Laboratory Science* **38**, 99-104.
- Laurent, T. C. and Fraser, J. R. E.** (1992). Hyaluronan. *The FASEB Journal* **6**, 2397-2404.
- Lauria, R., Perrone, F., Carlomagno, C., De Laurentiis, M., Morabito, A., Gallo, C., Varriale, E., Pettinato, G., Panico, L., Petrella, G. et al.** (1995). The prognostic value of lymphatic and blood vessel invasion in operable breast cancer. *Cancer* **76**, 1772-1778.
- Lavado, A., Lagutin, O. V., Chow, L. M. L., Baker, S. J. and Oliver, G.** (2010). Prox1 is required for granule cell maturation and intermediate progenitor maintenance during brain neurogenesis. *PLoS Biology* **8**, e1000460.
- Lavado, A. and Oliver, G.** (2007). *Prox1* expression patterns in the developing and adult murine brain. *Developmental Dynamics* **236**, 518-524.
-

- Lazarus, A., Del-Moral, P. M., Ilovich, O., Mishani, E., Warburton, D. and Keshet, E.** (2011). A perfusion-independent role of blood vessels in determining branching stereotypy of lung airways. *Development* **138**, 2359-2368.
- Lee, H.-W., Qin, Y.-X., Kim, Y.-M., Park, E.-Y., Hwang, J.-S., Huo, G.-H., Yang, C.-W., Kim, W.-Y. and Kim, J.** (2011). Expression of lymphatic endothelium-specific hyaluronan receptor LYVE-1 in the developing mouse kidney. *Cell and Tissue Research* **343**, 429-444.
- Lee, S., Chen, T. T., Barber, C. L., Jordan, M. C., Murdock, J., Desai, S., Ferrara, N., Nagy, A., Roos, K. P. and Iruela-Arispe, M. L.** (2007). Autocrine VEGF signaling is required for vascular homeostasis. *Cell* **130**, 691-703.
- Lewis, J. S., Landers, R. J., Underwood, J. C., Harris, A. L. and Lewis, C. E.** (2000). Expression of vascular endothelial growth factor by macrophages is up-regulated in poorly vascularized areas of breast carcinomas. *The Journal of Pathology* **192**, 150-158.
- Lewis, M. P. and Norman, J. T.** (1998). Differential response of activated versus non-activated renal fibroblasts to tubular epithelial cells: a model of initiation and progression of fibrosis? *Experimental Nephrology* **6**, 132-143.
- Li, H., Cherukuri, P., Li, N., Cowling, V., Spinella, M., Cole, M., Godwin, A. K., Wells, W. and DiRenzo, J.** (2007). Nestin is expressed in the basal/myoepithelial layer of the mammary gland and is a selective marker of basal epithelial breast tumors. *Cancer Research* **67**, 501-510.
- Lim, L. H. K. and Pervaiz, S.** (2007). Annexin 1: the new face of an old molecule. *The FASEB Journal* **21**, 968-975.
- Lin, E. Y., Jones, J. G., Li, P., Zhu, L., Whitney, K. D., Muller, W. J. and Pollard, J. W.** (2003). Progression to malignancy in the polyoma middle T oncoprotein mouse breast cancer model provides a reliable model for human diseases. *The American Journal of Pathology* **163**, 2113-2126.
- Lin, E. Y., Li, J.-F., Gnatovskiy, L., Deng, Y., Zhu, L., Grzesik, D. A., Qian, H., Xue, X.-n. and Pollard, J. W.** (2006). Macrophages regulate the angiogenic switch in a mouse model of breast cancer. *Cancer Research* **66**, 11238-11246.
- Lin, F.-J., Chen, X., Qin, J., Hong, Y.-K., Tsai, M.-J. and Tsai, S. Y.** (2010). Direct transcriptional regulation of neuropilin-2 by COUP-TFII modulates multiple steps in murine lymphatic vessel development. *The Journal of Clinical Investigation* **120**, 1694-1707.
- Liu, X., Li, Y., Liu, Y., Luo, Y., Wang, D., Annex, B. H. and Goldschmidt-Clermont, P. J.** (2010). Endothelial progenitor cells (EPCs) mobilized and activated by neurotrophic factors may contribute to pathologic neovascularization in diabetic retinopathy. *The American Journal of Pathology* **176**, 504-515.
- Livak, K. J. and Schmittgen, T. D.** (2001). Analysis of relative gene expression data using real-time quantitative PCR and the $2^{-\Delta\Delta C(T)}$ method. *Methods* **25**, 402-408.
- Loudon, L. and Petrek, J.** (2000). Lymphedema in women treated for breast cancer. *Cancer Practice* **8**, 65-71.
- Lu, P., Sternlicht, M. D. and Werb, Z.** (2006). Comparative mechanisms of branching morphogenesis in diverse systems. *Journal of Mammary Gland Biology and Neoplasia* **11**, 213-228.

- Lu, P. and Werb, Z.** (2008). Patterning mechanisms of branched organs. *Science* **322**, 1506-1509.
- Ma, G.-C., Liu, C.-S., Chang, S.-P., Yeh, K.-T., Ke, Y.-Y., Chen, T.-H., Wang, B. B.-T., Kuo, S.-J., Shih, J.-C. and Chen, M.** (2008). A recurrent *ITGA9* missense mutation in human fetuses with severe chylothorax: possible correlation with poor response to fetal therapy. *Prenatal Diagnosis* **28**, 1057-1063.
- Macias, H., Moran, A., Samara, Y., Moreno, M., Compton, J. E., Harburg, G., Strickland, P. and Hinck, L.** (2011). SLIT/ROBO1 signaling suppresses mammary branching morphogenesis by limiting basal cell number. *Developmental Cell* **20**, 827-840.
- Macotela, Y., Aguilar, M. B., Guzmán-Morales, J., Rivera, J. C., Zermeño, C., López-Barrera, F., Nava, G., Lavalle, C., Martínez de la Escalera, G. and Clapp, C.** (2006). Matrix metalloproteases from chondrocytes generate an antiangiogenic 16 kDa prolactin. *Journal of Cell Science* **119**, 1790-1800.
- Maier, T., Güell, M. and Serrano, L.** (2009). Correlation of mRNA and protein in complex biological samples. *FEBS Letters* **583**, 3966-3973.
- Mailleux, A. A., Spencer-Dene, B., Dillon, C., Ndiaye, D., Savona-Baron, C., Itoh, N., Kato, S., Dickson, C., Thiery, J. P. and Bellusci, S.** (2002). Role of FGF10/FGFR2b signaling during mammary gland development in the mouse embryo. *Development* **129**, 53-60.
- Maisonpierre, P. C., Suri, C., Jones, P. F., Bartunkova, S., Wiegand, S. J., Radziejewski, C., Compton, D., McClain, J., Aldrich, T. H., Papadopoulos, N. et al.** (1997). Angiopoietin-2, a natural antagonist for Tie2 that disrupts in vivo angiogenesis. *Science* **277**, 55-60.
- Mäkinen, T., Adams, R. H., Bailey, J., Lu, Q., Ziemiecki, A., Alitalo, K., Klein, R. and Wilkinson, G. A.** (2005). PDZ interaction site in ephrinB2 is required for the remodeling of lymphatic vasculature. *Genes & Development* **19**, 397-410.
- Mäkinen, T., Norrmén, C. and Petrova, T. V.** (2007). Molecular mechanisms of lymphatic vascular development. *Cellular and Molecular Life Sciences* **64**, 1915-1929.
- Mäkinen, T., Veikkola, T., Mustjoki, S., Karpanen, T., Catimel, B., Nice, E. C., Wise, L., Mercer, A., Kowalski, H., Kerjaschki, D. et al.** (2001). Isolated lymphatic endothelial cells transduce growth, survival and migratory signals via the VEGF-C/D receptor VEGFR-3. *The EMBO Journal* **20**, 4762-4773.
- Maller, O., Martinson, H. and Schedin, P.** (2010). Extracellular matrix composition reveals complex and dynamic stromal-epithelial interactions in the mammary gland. *Journal of Mammary Gland Biology and Neoplasia* **15**, 301-318.
- Mandriota, S. J. and Pepper, M. S.** (1998). Regulation of angiopoietin-2 mRNA levels in bovine microvascular endothelial cells by cytokines and hypoxia. *Circulation Research* **83**, 852-859.
- Marconcini, L., Marchio, S., Morbidelli, L., Cartocci, E., Albin, A., Ziche, M., Bussolino, F. and Oliviero, S.** (1999). *c-fos*-induced growth factor/vascular endothelial growth factor D induces angiogenesis *in vivo* and *in vitro*. *Proceedings of the National Academy of Sciences of the United States of America* **96**, 9671-9676.
- Marinho, V. F. Z., Metze, K., Sanches, F. S. F., Rocha, G. F. S. and Gobbi, H.** (2008). Lymph vascular invasion in invasive mammary carcinomas identified by the endothelial lymphatic marker D2-40 is associated with other indicators of poor prognosis. *BMC Cancer* **8**, 64-72.

- Maruyama, K., Asai, J., Ii, M., Thorne, T., Losordo, D. W. and D'Amore, P. A.** (2007). Decreased macrophage number and activation lead to reduced lymphatic vessel formation and contribute to impaired diabetic wound healing. *The American Journal of Pathology* **170**, 1178-1191.
- Maruyama, K., Ii, M., Cursiefen, C., Jackson, D. G., Keino, H., Tomita, M., Van Rooijen, N., Takenaka, H., D'Amore, P. A., Stein-Streilein, J. et al.** (2005). Inflammation-induced lymphangiogenesis in the cornea arises from CD11b-positive macrophages. *The Journal of Clinical Investigation* **115**, 2363-2372.
- Matsumoto, M., Nishinakagawa, H., Kurohmaru, M., Hayashi, Y. and Otsuka, J.** (1992). Pregnancy and lactation affect the microvasculature of the mammary gland in mice. *The Journal of Veterinary Medical Science* **54**, 937-943.
- Mattila, M. M.-T., Ruohola, J. K., Karpanen, T., Jackson, D. G., Alitalo, K. and Härkönen, P. L.** (2002). VEGF-C induced lymphangiogenesis is associated with lymph node metastasis in orthotopic MCF-7 tumours. *International Journal of Cancer* **98**, 946-951.
- McColl, B. K., Baldwin, M. E., Roufail, S., Freeman, C., Moritz, R. L., Simpson, R. J., Alitalo, K., Stacker, S. A. and Achen, M. G.** (2003). Plasmin activates the lymphangiogenic growth factors VEGF-C and VEGF-D. *The Journal of Experimental Medicine* **198**, 863-868.
- McColl, B. K., Paavonen, K., Karnezis, T., Harris, N. C., Davydova, N., Rothacker, J., Nice, E. C., Harder, K. W., Roufail, S., Hibbs, M. L. et al.** (2007). Proprotein convertases promote processing of VEGF-D, a critical step for binding the angiogenic receptor VEGFR-2. *The FASEB Journal* **21**, 1088-1098.
- Mellor, R. H., Brice, G., Stanton, A. W. B., French, J., Smith, A., Jeffery, S., Levick, J. R., Burnand, K. G. and Mortimer, P. S.** (2007). Mutations in *FOXC2* are strongly associated with primary valve failure in veins of the lower limb. *Circulation* **115**, 1912-1920.
- Mirsky, R., Parmantier, E., McMahon, A. P. and Jessen, K. R.** (1999). Schwann cell-derived desert hedgehog signals nerve sheath formation. *Annals of the New York Academy of Sciences* **883**, 196-202.
- Mohammadi, M., McMahon, G., Sun, L., Tang, C., Hirth, P., Yeh, B. K., Hubbard, S. R. and Schlessinger, J.** (1997). Structures of the tyrosine kinase domain of fibroblast growth factor receptor in complex with inhibitors. *Science* **276**, 955-960.
- Mohammed, R. A., Martin, S. G., Gill, M. S., Green, A. R., Paish, E. C. and Ellis, I. O.** (2007a). Improved methods of detection of lymphovascular invasion demonstrate that it is the predominant method of vascular invasion in breast cancer and has important clinical consequences. *The American Journal of Surgical Pathology* **31**, 1825-1833.
- Mohammed, R. A. A., Green, A., El-Shikh, S., Paish, E. C., Ellis, I. O. and Martin, S. G.** (2007b). Prognostic significance of vascular endothelial cell growth factors -A, -C and -D in breast cancer and their relationship with angio- and lymphangiogenesis. *British Journal of Cancer* **96**, 1092-1100.
- Morisada, T., Oike, Y., Yamada, Y., Urano, T., Akao, M., Kubota, Y., Maekawa, H., Kimura, Y., Ohmura, M., Miyamoto, T. et al.** (2005). Angiopoietin-1 promotes LYVE-1-positive lymphatic vessel formation. *Blood* **105**, 4649-4656.

- Mouta Carreira, C., Nasser, S. M., di Tomaso, E., Padera, T. P., Boucher, Y., Tomarev, S. I. and Jain, R. K. (2001). LYVE-1 is not restricted to the lymph vessels: expression in normal liver blood sinusoids and down-regulation in human liver cancer and cirrhosis. *Cancer Research* **61**, 8079-8084.
- Mueller, S. O., Clark, J. A., Myers, P. H. and Korach, K. S. (2002). Mammary gland development in adult mice requires epithelial and stromal estrogen receptor α . *Endocrinology* **143**, 2357-2365.
- Multhaupt, H. A. B., Gåfvvels, M. E., Kariko, K., Jin, H., Arenas-Elliott, C., Goldman, B. I., Strauss, J. F., Angelin, B., Warhol, M. J. and McCrae, K. R. (1996). Expression of very low density lipoprotein receptor in the vascular wall. *Analysis of human tissues by in situ hybridization and immunohistochemistry. The American Journal of Pathology* **148**, 1985-1997.
- Nagase, T., Nagase, M., Machida, M. and Fujita, T. (2008). Hedgehog signalling in vascular development. *Angiogenesis* **11**, 71-77.
- Nakamura, Y., Yasuoka, H., Tsujimoto, M., Imabun, S., Nakahara, M., Nakao, K., Nakamura, M., Mori, I. and Kakudo, K. (2005). Lymph vessel density correlates with nodal status, VEGF-C expression, and prognosis in breast cancer. *Breast Cancer Research and Treatment* **91**, 125-132.
- Nakamura, Y., Yasuoka, H., Tsujimoto, M., Yang, Q., Imabun, S., Nakahara, M., Nakao, K., Nakamura, M., Mori, I. and Kakudo, K. (2003). Flt-4-positive vessel density correlates with vascular endothelial growth factor-D expression, nodal status, and prognosis in breast cancer. *Clinical Cancer Research* **9**, 5313-5317.
- Nehls, V. and Drenckhahn, D. (1991). Heterogeneity of microvascular pericytes for smooth muscle type alpha-actin. *The Journal of Cell Biology* **113**, 147-154.
- Neufeld, G., Cohen, T., Shraga, N., Lange, T., Kessler, O. and Herzog, Y. (2002). The neuropilins: multifunctional semaphorin and VEGF receptors that modulate axon guidance and angiogenesis. *Trends in Cardiovascular Medicine* **12**, 13-19.
- Norrmén, C., Ivanov, K. I., Cheng, J., Zangger, N., Delorenzi, M., Jaquet, M., Miura, N., Puolakkainen, P., Horsley, V., Hu, J. et al. (2009). FOXC2 controls formation and maturation of lymphatic collecting vessels through cooperation with NFATc1. *The Journal of Cell Biology* **185**, 439-457.
- Nüsslein-Volhard, C. and Wieschaus, E. (1980). Mutations affecting segment number and polarity in *Drosophila*. *Nature* **287**, 795-801.
- Ny, A., Koch, M., Schneider, M., Neven, E., Tong, R. T., Maity, S., Fischer, C., Plaisance, S., Lambrechts, D., Héligon, C. et al. (2005). A genetic *Xenopus laevis* model to study lymphangiogenesis. *Nature Medicine* **11**, 998-1004.
- Ny, A., Koch, M., Vandeveld, W., Schneider, M., Fischer, C., Diez-Juan, A., Neven, E., Geudens, I., Maity, S., Moons, L. et al. (2008). Role of VEGF-D and VEGFR-3 in developmental lymphangiogenesis, a chemicogenetic study in *Xenopus* tadpoles. *Blood* **112**, 1740-1749.
- Oakes, S. R., Naylor, M. J., Asselin-Labat, M.-L., Blazek, K. D., Gardiner-Garden, M., Hilton, H. N., Kazlauskas, M., Pritchard, M. A., Chodosh, L. A., Pfeffer, P. L. et al. (2008). The Ets transcription factor Elf5 specifies mammary alveolar cell fate. *Genes & Development* **22**, 581-586.

-
- Ochoa, A., Montes de Oca, P., Rivera, J. C., Dueñas, Z., Nava, G., Martínez de la Escalera, G. and Clapp, C. (2001). Expression of prolactin gene and secretion of prolactin by rat retinal capillary endothelial cells. *Investigative Ophthalmology & Visual Science* **42**, 1639-1645.
- Oh, P., Li, Y., Yu, J., Durr, E., Krasinska, K. M., Carver, L. A., Testa, J. E. and Schnitzer, J. E. (2004). Subtractive proteomic mapping of the endothelial surface in lung and solid tumours for tissue-specific therapy. *Nature* **429**, 629-635.
- Ohneda, O., Ohneda, K., Nomiya, H., Zheng, Z., Gold, S. A., Arai, F., Miyamoto, T., Taillon, B. E., McIndoe, R. A., Shimkets, R. A. et al. (2000). WECH: a novel hematopoietic regulatory factor. *Immunity* **12**, 141-150.
- Ohtani, O., Shao, X.-J., Saitoh, M. and Ohtani, Y. (1998). Lymphatics of the rat mammary gland during virgin, pregnant, lactating and post-weaning periods. *Italian Journal of Anatomy and Embryology* **103**, 335-342.
- Oliver, G. (2004). Lymphatic vasculature development. *Nature Reviews Immunology* **4**, 34-45.
- Oliver, G. and Detmar, M. (2002). The rediscovery of the lymphatic system: old and new insights into the development and biological function of the lymphatic vasculature. *Genes & Development* **16**, 773-783.
- Oliver, G. and Harvey, N. (2002). A stepwise model of the development of lymphatic vasculature. *Annals of the New York Academy of Sciences* **979**, 159-165.
- Oliver, G., Sosa-Pineda, B., Geisendorf, S., Spana, E. P., Doe, C. Q. and Gruss, P. (1993). Prox 1, a prospero-related homeobox gene expressed during mouse development. *Mechanisms of Development* **44**, 3-16.
- Oliver, G. and Srinivasan, R. S. (2010). Endothelial cell plasticity: how to become and remain a lymphatic endothelial cell. *Development* **137**, 363-372.
- Olsson, A.-K., Dimberg, A., Kreuger, J. and Claesson-Welsh, L. (2006). VEGF receptor signalling - in control of vascular function. *Nature Reviews Molecular Cell Biology* **7**, 359-371.
- Orlandini, M. and Oliviero, S. (2001). In fibroblasts *Vegf-D* expression is induced by cell-cell contact mediated by cadherin-11. *The Journal of Biological Chemistry* **276**, 6576-6581.
- Orlandini, M., Semboloni, S. and Oliviero, S. (2003). β -catenin inversely regulates vascular endothelial growth factor-D mRNA stability. *The Journal of Biological Chemistry* **278**, 44650-44656.
- Orr-Urtreger, A. and Lonai, P. (1992). Platelet-derived growth factor-A and its receptor are expressed in separate, but adjacent cell layers of the mouse embryo. *Development* **115**, 1045-1058.
- Östman, A., Thyberg, J., Westermark, B. and Heldin, C.-H. (1992). PDGF-AA and PDGF-BB biosynthesis: proprotein processing in the Golgi complex and lysosomal degradation of PDGF-BB retained intracellularly. *The Journal of Cell Biology* **118**, 509-519.
- Paavonen, K., Mandelin, J., Partanen, T., Jussila, L., Li, T. F., Ristimäki, A., Alitalo, K. and Konttinen, Y. T. (2002). Vascular endothelial growth factors C and D and their VEGFR-2 and 3 receptors in blood and lymphatic vessels in healthy and arthritic synovium. *The Journal of Rheumatology* **29**, 39-45.

-
- Padera, T. P., Kadambi, A., di Tomaso, E., Mouta Carreira, C., Brown, E. B., Boucher, Y., Choi, N. C., Mathisen, D., Wain, J., Mark, E. J. et al.** (2002). Lymphatic metastasis in the absence of functional intratumor lymphatics. *Science* **296**, 1883-1886.
- Page-McCaw, A., Ewald, A. J. and Werb, Z.** (2007). Matrix metalloproteinases and the regulation of tissue remodelling. *Nature Reviews Molecular Cell Biology* **8**, 221-233.
- Parmantier, E., Lynn, B., Lawson, D., Turmaine, M., Namini, S. S., Chakrabarti, L., McMahon, A. P., Jessen, K. R. and Mirsky, R.** (1999). Schwann cell-derived Desert hedgehog controls the development of peripheral nerve sheaths. *Neuron* **23**, 713-724.
- Parmar, H. and Cunha, G. R.** (2004). Epithelial-stromal interactions in the mouse and human mammary gland *in vivo*. *Endocrine-Related Cancer* **11**, 437-458.
- Partanen, T. A., Alitalo, K. and Miettinen, M.** (1999). Lack of lymphatic vascular specificity of vascular endothelial growth factor receptor 3 in 185 vascular tumors. *Cancer* **86**, 2406-2412.
- Pepicelli, C. V., Lewis, P. M. and McMahon, A. P.** (1998). Sonic hedgehog regulates branching morphogenesis in the mammalian lung. *Current Biology* **8**, 1083-1086.
- Pepper, M. S., Baetens, D., Mandriota, S. J., Di Sanza, C., Oikemus, S., Lane, T. F., Soriano, J. V., Montesano, R. and Iruela-Arispe, M. L.** (2000). Regulation of VEGF and VEGF receptor expression in the rodent mammary gland during pregnancy, lactation, and involution. *Developmental Dynamics* **218**, 507-524.
- Petrova, T. V., Karpanen, T., Normén, C., Mellor, R., Tamakoshi, T., Finegold, D., Ferrell, R., Kerjaschki, D., Mortimer, P., Ylä-Herttuala, S. et al.** (2004). Defective valves and abnormal mural cell recruitment underlie lymphatic vascular failure in lymphedema distichiasis. *Nature Medicine* **10**, 974-981.
- Petrova, T. V., Mäkinen, T., Mäkelä, T. P., Saarela, J., Virtanen, I., Ferrell, R. E., Finegold, D. N., Kerjaschki, D., Ylä-Herttuala, S. and Alitalo, K.** (2002). Lymphatic endothelial reprogramming of vascular endothelial cells by the Prox-1 homeobox transcription factor. *The EMBO Journal* **21**, 4593-4599.
- Pfarr, K. M., Debrah, A. Y., Specht, S. and Hoerauf, A.** (2009). Filariasis and lymphoedema. *Parasite Immunology* **31**, 664-672.
- Phng, L.-K. and Gerhardt, H.** (2009). Angiogenesis: a team effort coordinated by Notch. *Developmental Cell* **16**, 196-208.
- Pierreux, C. E., Cordi, S., Hick, A.-C., Achouri, Y., Ruiz de Almodovar, C., Prévot, P.-P., Courtoy, P. J., Carmeliet, P. and Lemaigre, F. P.** (2010). Epithelial:endothelial cross-talk regulates exocrine differentiation in developing pancreas. *Developmental Biology* **347**, 216-227.
- Piña-Oviedo, S. and Ortiz-Hidalgo, C.** (2008). The normal and neoplastic perineurium: a review. *Advances in Anatomic Pathology* **15**, 147-164.
- Prevo, R., Banerji, S., Ferguson, D. J., Clasper, S. and Jackson, D. G.** (2001). Mouse LYVE-1 is an endocytic receptor for hyaluronan in lymphatic endothelium. *The Journal of Biological Chemistry* **276**, 19420-19430.
-

- Pujianto, D. A., Damdimopoulos, A. E., Sipilä, P., Jalkanen, J., Huhtaniemi, I. and Poutanen, M.** (2007). *Bfk*, a novel member of the *Bcl2* gene family, is highly expressed in principal cells of the mouse epididymis and demonstrates a predominant nuclear localization. *Endocrinology* **148**, 3196-3204.
- Puri, M. C., Rossant, J., Alitalo, K., Bernstein, A. and Partanen, J.** (1995). The receptor tyrosine kinase TIE is required for integrity and survival of vascular endothelial cells. *The EMBO Journal* **14**, 5884-5891.
- Qu, X., Tompkins, K., Batts, L. E., Puri, M. and Baldwin, S.** (2010). Abnormal embryonic lymphatic vessel development in *Tie1* hypomorphic mice. *Development* **137**, 1285-1295.
- Raffel, C., Jenkins, R. B., Frederick, L., Hebrink, D., Alderete, B., Fults, D. W. and James, C. D.** (1997). Sporadic medulloblastomas contain *PTCH* mutations. *Cancer Research* **57**, 842-845.
- Ran, S., Volk, L., Hall, K. and Flister, M. J.** (2010). Lymphangiogenesis and lymphatic metastasis in breast cancer. *Pathophysiology* **17**, 229-251.
- Red-Horse, K., Rivera, J., Schanz, A., Zhou, Y., Winn, V., Kapidzic, M., Maltepe, E., Okazaki, K., Kochman, R., Vo, K. C. et al.** (2006). Cytotrophoblast induction of arterial apoptosis and lymphangiogenesis in an in vivo model of human placentation. *The Journal of Clinical Investigation* **116**, 2643-2652.
- Religa, P., Cao, R., Bjorndahl, M., Zhou, Z., Zhu, Z. and Cao, Y.** (2005). Presence of bone marrow-derived circulating progenitor endothelial cells in the newly formed lymphatic vessels. *Blood* **106**, 4184-4190.
- Ribatti, D., Nico, B., Spinazzi, R., Vacca, A. and Nussdorfer, G. G.** (2005). The role of adrenomedullin in angiogenesis. *Peptides* **26**, 1670-1675.
- Richert, M. M., Schwertfeger, K. L., Ryder, J. W. and Anderson, S. M.** (2000). An atlas of mouse mammary gland development. *Journal of Mammary Gland Biology and Neoplasia* **5**, 227-241.
- Ricken, A. M., Traenkner, A., Merkwitz, C., Hummitzsch, K., Grosche, J. and Spanel-Borowski, K.** (2007). The short prolactin receptor predominates in endothelial cells of micro- and macrovascular origin. *Journal of Vascular Research* **44**, 19-30.
- Risebro, C. A., Searles, R. G., Melville, A. A. D., Ehler, E., Jina, N., Shah, S., Pallas, J., Hubank, M., Dillard, M., Harvey, N. L. et al.** (2009). *Prox1* maintains muscle structure and growth in the developing heart. *Development* **136**, 495-505.
- Rissanen, T. T., Markkanen, J. E., Gruchala, M., Heikura, T., Puranen, A., Kettunen, M. I., Kholová, I., Kauppinen, R. A., Achen, M. G., Stacker, S. A. et al.** (2003). VEGF-D is the strongest angiogenic and lymphangiogenic effector among VEGFs delivered into skeletal muscle via adenoviruses. *Circulation Research* **92**, 1098-1106.
- Ristimäki, A., Narko, K., Enholm, B., Joukov, V. and Alitalo, K.** (1998). Proinflammatory cytokines regulate expression of the lymphatic endothelial mitogen vascular endothelial growth factor-C. *The Journal of Biological Chemistry* **273**, 8413-8418.
- Rockson, S.** (2001). Lymphedema. *The American Journal of Medicine* **110**, 288-295.

-
- Rodriguez-Niedenführ, M., Papoutsi, M., Christ, B., Nicolaides, K. H., von Kaisenberg, C. S., Tomarev, S. I. and Wilting, J.** (2001). Prox1 is a marker of ectodermal placodes, endodermal compartments, lymphatic endothelium and lymphangioblasts. *Anatomy and Embryology* **204**, 399-406.
- Rogers, P. A. W., Donoghue, J. F. and Girling, J. E.** (2008). Endometrial Lymphangiogenesis. *Placenta* **29**, S48-S54.
- Rossi, D. L., Hurst, S. D., Xu, Y., Wang, W., Menon, S., Coffman, R. L. and Zlotnik, A.** (1999). Lungkine, a novel CXC chemokine, specifically expressed by lung bronchoepithelial cells. *The Journal of Immunology* **162**, 5490-5497.
- Rossiter, H., Barresi, C., Ghannadan, M., Gruber, F., Mildner, M., Födinger, D. and Tschachler, E.** (2007). Inactivation of VEGF in mammary gland epithelium severely compromises mammary gland development and function. *The FASEB Journal* **21**, 3994-4004.
- Rozen, S. and Skaletsky, H. J.** (2000). Primer3 on the WWW for general users and for biologist programmers. In *Bioinformatics Methods and Protocols: Methods in Molecular Biology*, (ed. S. Krawetz and S. Misener), pp. 365-386. Totowa, NJ: Humana Press.
- Rutanen, J., Leppänen, P., Tuomisto, T. T., Rissanen, T. T., Hiltunen, M. O., Vajanto, I., Niemi, M., Häkkinen, T., Karkol, K., Stackner, S. A. et al.** (2003). Vascular endothelial growth factor-D expression in human atherosclerotic lesions. *Cardiovascular Research* **59**, 971-979.
- Rutkowski, J. M., Boardman, K. C. and Swartz, M. A.** (2006). Characterization of lymphangiogenesis in a model of adult skin regeneration. *American Journal of Physiology - Heart and Circulatory Physiology* **291**, H1402-H1410.
- Sabin, F. R.** (1902). On the origin of the lymphatic system from the veins, and the development of the lymph hearts and thoracic duct in the pig. *American Journal of Anatomy* **1**, 367-389.
- Saiki, A., Watanabe, F., Murano, T., Miyashita, Y. and Shirai, K.** (2006). Hepatocyte growth factor secreted by cultured adipocytes promotes tube formation of vascular endothelial cells *in vitro*. *International Journal of Obesity* **30**, 1676-1684.
- Sambrook, J. and Russel, D. W.** (2001). *Molecular Cloning: A Laboratory Manual*. New York: Cold Spring Harbour Laboratory Press.
- Scamuffa, N., Calvo, F., Chrétien, M., Seidah, N. G. and Khatib, A.-M.** (2006). Proprotein convertases: lessons from knockouts. *The FASEB Journal* **20**, 1954-1963.
- Schacht, V., Dadras, S. S., Johnson, L. A., Jackson, D. G., Hong, Y.-K. and Detmar, M.** (2005). Up-regulation of the lymphatic marker podoplanin, a mucin-type transmembrane glycoprotein, in human squamous cell carcinomas and germ cell tumors. *The American Journal of Pathology* **166**, 913-921.
- Schacht, V., Ramirez, M. I., Hong, Y.-K., Hirakawa, S., Feng, D., Harvey, N., Williams, M., Dvorak, A. M., Dvorak, H. F., Oliver, G. et al.** (2003). T1 α /podoplanin deficiency disrupts normal lymphatic vasculature formation and causes lymphedema. *The EMBO Journal* **22**, 3546-3556.
- Schäfer, G., Wissmann, C., Hertel, J., Lunyak, V. and Höcker, M.** (2008). Regulation of vascular endothelial growth factor D by orphan receptors hepatocyte nuclear factor-4 α and chicken ovalbumin upstream promoter transcription factors 1 and 2. *Cancer Research* **68**, 457-466.
-

- Schledzewski, K., Falkowski, M., Moldenhauer, G., Metharom, P., Kzhyshkowska, J., Ganss, R., Demory, A., Falkowska-Hansen, B., Kurzen, H., Ugurel, S. et al. (2006). Lymphatic endothelium-specific hyaluronan receptor LYVE-1 is expressed by stabilin-1+, F4/80+, CD11b+ macrophages in malignant tumours and wound healing tissue *in vivo* and in bone marrow cultures *in vitro*: implications for the assessment of lymphangiogenesis. *The Journal of Pathology* **209**, 67-77.
- Schmitz, J. M., McCracken, V. J., Dimmitt, R. A. and Lorenz, R. G. (2007). Expression of CXCL15 (Lungkine) in murine gastrointestinal, urogenital, and endocrine organs. *Journal of Histochemistry & Cytochemistry* **55**, 515-524.
- Schoppmann, S. F., Bayer, G., Aumayr, K., Taucher, S., Geleff, S., Rudas, M., Kubista, E., Hausmaninger, H., Samonigg, H., Gnant, M. et al. (2004). Prognostic value of lymphangiogenesis and lymphovascular invasion in invasive breast cancer. *Annals of Surgery* **240**, 306-312.
- Schoppmann, S. F., Birner, P., Stöckl, J., Kalt, R., Ullrich, R., Caucig, C., Kriehuber, E., Nagy, K., Alitalo, K. and Kerjaschki, D. (2002). Tumor-associated macrophages express lymphatic endothelial growth factors and are related to peritumoral lymphangiogenesis. *The American Journal of Pathology* **161**, 947-956.
- Schulz, B., Pruessmeyer, J., Maretzky, T., Ludwig, A., Blobel, C. P., Saftig, P. and Reiss, K. (2008). ADAM10 regulates endothelial permeability and T-cell transmigration by proteolysis of vascular endothelial cadherin. *Circulation Research* **102**, 1192-1201.
- Seaman, S., Stevens, J., Yang, M. Y., Logsdon, D., Graff-Cherry, C. and St. Croix, B. (2007). Genes that distinguish physiological and pathological angiogenesis. *Cancer Cell* **11**, 539-554.
- Sebzda, E., Hibbard, C., Sweeney, S., Abtahian, F., Bezman, N., Clemens, G., Maltzman, J. S., Cheng, L., Liu, F., Turner, M. et al. (2006). Syk and Slp-76 mutant mice reveal a cell-autonomous hematopoietic cell contribution to vascular development. *Developmental Cell* **11**, 349-361.
- Seidah, N. G., Mayer, G., Zaid, A., Rousselet, E., Nassoury, N., Poirier, S., Essalmani, R. and Prat, A. (2008). The activation and physiological functions of the proprotein convertases. *The International Journal of Biochemistry & Cell Biology* **40**, 1111-1125.
- Sentürk, A., Pfennig, S., Weiss, A., Burk, K. and Acker-Palmer, A. (2011). Ephrin Bs are essential components of the Reelin pathway to regulate neuronal migration. *Nature* **472**, 356-360.
- Sfiligoi, C., de Luca, A., Cascone, I., Sorbello, V., Fusco, L., Ponzzone, R., Biglia, N., Audero, E., Arisio, R., Bussolino, F. et al. (2003). Angiopoietin-2 expression in breast cancer correlates with lymph node invasion and short survival. *International Journal of Cancer* **103**, 466-474.
- Shackleton, M., Vaillant, F., Simpson, K. J., Stingl, J., Smyth, G. K., Asselin-Labat, M.-L., Wu, L., Lindeman, G. J. and Visvader, J. E. (2006). Generation of a functional mammary gland from a single stem cell. *Nature* **439**, 84-88.
- Shalaby, F., Rossant, J., Yamaguchi, T. P., Gertsenstein, M., Wu, X.-F., Breitman, M. L. and Schuh, A. C. (1995). Failure of blood-island formation and vasculogenesis in Flk-1-deficient mice. *Nature* **376**, 62-66.
- Shibata, M.-A., Ambati, J., Shibata, E., Albuquerque, R. J. C., Morimoto, J., Ito, Y. and Otsuki, Y. (2010). The endogenous soluble VEGF receptor-2 isoform suppresses lymph node metastasis in a mouse immunocompetent mammary cancer model. *BMC Medicine* **8**, 69-81.

- Shin, J. W., Min, M., Larrieu-Lahargue, F., Canron, X., Kunstfeld, R., Nguyen, L., Henderson, J. E., Bikfalvi, A., Detmar, M. and Hong, Y.-K.** (2006). Prox1 promotes lineage-specific expression of fibroblast growth factor (FGF) receptor-3 in lymphatic endothelium: a role for FGF signaling in lymphangiogenesis. *Molecular Biology of the Cell* **17**, 576-584.
- Siegfried, G., Basak, A., Cromlish, J. A., Benjannet, S., Marcinkiewicz, J., Chrétien, M., Seidah, N. G. and Khatib, A.-M.** (2003). The secretory proprotein convertases furin, PC5, and PC7 activate VEGF-C to induce tumorigenesis. *The Journal of Clinical Investigation* **111**, 1723-1732.
- Siegfried, G., Basak, A., Prichett-Pejic, W., Scamuffa, N., Ma, L., Benjannet, S., Veinot, J. P., Calvo, F., Seidah, N. and Khatib, A.-M.** (2005). Regulation of the stepwise proteolytic cleavage and secretion of PDGF-B by the proprotein convertases. *Oncogene* **24**, 6925-6935.
- Silberstein, G. B.** (2001). Postnatal mammary gland morphogenesis. *Microscopy Research and Technique* **52**, 155-162.
- Silberstein, G. B., Van Horn, K., Shyamala, G. and Daniel, C. W.** (1994). Essential role of endogenous estrogen in directly stimulating mammary growth demonstrated by implants containing pure antiestrogens. *Endocrinology* **134**, 84-90.
- Skalli, O., Pelte, M.-F., Pecllet, M.-C., Gabbiani, G., Gugliotta, P., Bussolati, G., Ravazzola, M. and Orci, L.** (1989). Alpha-smooth muscle actin, a differentiation marker of smooth muscle cells, is present in microfilamentous bundles of pericytes. *The Journal of Histochemistry & Cytochemistry* **37**, 315-321.
- Skaper, S. D.** (2008). The biology of neurotrophins, signalling pathways, and functional peptide mimetics of neurotrophins and their receptors. *CNS & Neurological Disorders - Drug Targets* **7**, 46-62.
- Skobe, M., Hawighorst, T., Jackson, D. G., Prevo, R., Janes, L., Velasco, P., Riccardi, L., Alitalo, K., Claffey, K. and Detmar, M.** (2001). Induction of tumor lymphangiogenesis by VEGF-C promotes breast cancer metastasis. *Nature Medicine* **7**, 192-198.
- Srinivasan, R. S., Dillard, M. E., Lagutin, O. V., Lin, F.-J., Tsai, S., Tsai, M.-J., Samokhvalov, I. M. and Oliver, G.** (2007). Lineage tracing demonstrates the venous origin of the mammalian lymphatic vasculature. *Genes & Development* **21**, 2422-2432.
- Srinivasan, R. S., Geng, X., Yang, Y., Wang, Y., Mukatira, S., Studer, M., Porto, M. P. R., Lagutin, O. and Oliver, G.** (2010). The nuclear hormone receptor Coup-TFII is required for the initiation and early maintenance of Prox1 expression in lymphatic endothelial cells. *Genes & Development* **24**, 696-707.
- Sriramarao, P., Mandler, M. and Bourdon, M. A.** (1993). Endothelial cell attachment and spreading on human tenascin is mediated by $\alpha_2\beta_1$ and $\alpha_v\beta_3$ integrins. *Journal of Cell Science* **105**, 1001-1012.
- St. Croix, B., Rago, C., Velculescu, V., Traverso, G., Romans, K. E., Montgomery, E., Lal, A., Riggins, G. J., Lengauer, C., Vogelstein, B. et al.** (2000). Genes expressed in human tumor endothelium. *Science* **289**, 1197-1202.
- Stacker, S. A., Baldwin, M. E. and Achen, M. G.** (2002). The role of tumor lymphangiogenesis in metastatic spread. *The FASEB Journal* **16**, 922-934.

-
- Stacker, S. A., Caesar, C., Baldwin, M. E., Thornton, G. E., Williams, R. A., Prevo, R., Jackson, D. G., Nishikawa, S.-i., Kubo, H. and Achen, M. G.** (2001). VEGF-D promotes the metastatic spread of tumor cells via the lymphatics. *Nature Medicine* **7**, 186-191.
- Stacker, S. A., Stenvers, K., Caesar, C., Vitali, A., Domagala, T., Nice, E., Roufail, S., Simpson, R. J., Moritz, R., Karpanen, T. et al.** (1999). Biosynthesis of vascular endothelial growth factor-D involves proteolytic processing which generates non-covalent homodimers. *The Journal of Biological Chemistry* **274**, 32127-32136.
- Stadtfeld, M. and Graf, T.** (2005). Assessing the role of hematopoietic plasticity for endothelial and hepatocyte development by non-invasive lineage tracing. *Development* **132**, 203-213.
- Sternlicht, M. D., Kouros-Mehr, H., Lu, P. and Werb, Z.** (2006). Hormonal and local control of mammary branching morphogenesis. *Differentiation* **74**, 365-381.
- Stingl, J., Eaves, C. J., Kuusk, U. and Emerman, J. T.** (1998). Phenotypic and functional characterization in vitro of a multipotent epithelial cell present in the normal adult human breast. *Differentiation* **63**, 201-213.
- Strickland, P., Shin, G. C., Plump, A., Tessier-Lavigne, M. and Hinck, L.** (2006). Slit2 and netrin 1 act synergistically as adhesive cues to generate tubular bi-layers during ductal morphogenesis. *Development* **133**, 823-832.
- Strieter, R. M., Burdick, M. D., Mestas, J., Gomperts, B., Keane, M. P. and Belperio, J. A.** (2006). Cancer CXC chemokine networks and tumour angiogenesis. *European Journal of Cancer* **42**, 768-778.
- Strieter, R. M., Polverini, P. J., Kunkel, S. L., Arenberg, D. A., Burdick, M. D., Kasper, J., Dzuiba, J., Van Damme, J., Walz, A., Marriott, D. et al.** (1995). The functional role of the ELR motif in CXC chemokine-mediated angiogenesis. *The Journal of Biological Chemistry* **270**, 27348-27357.
- Strongin, A. Y., Collier, I., Bannikov, G., Marmer, B. L., Grant, G. A. and Goldberg, G. I.** (1995). Mechanism of cell surface activation of 72-kDa type IV collagenase. Isolation of the activated form of the membrane metalloprotease. *The Journal of Biological Chemistry* **270**, 5331-5338.
- Struman, I., Bentzien, F., Lee, H., Mainfroid, V., D'Angelo, G., Goffin, V., Weiner, R. I. and Martial, J. A.** (1999). Opposing actions of intact and N-terminal fragments of the human prolactin/growth hormone family members on angiogenesis: an efficient mechanism for the regulation of angiogenesis. *Proceedings of the National Academy of Sciences of the United States of America* **96**, 1246-1251.
- Suami, H., Pan, W.-R., Mann, G. B. and Taylor, G. I.** (2008). The lymphatic anatomy of the breast and its implications for sentinel lymph node biopsy: a human cadaver study. *Annals of Surgical Oncology* **15**, 863-871.
- Suami, H., Pan, W.-R. and Taylor, G. I.** (2009). Historical review of breast lymphatic studies. *Clinical Anatomy* **22**, 531-536.
- Suchting, S., Freitas, C., le Noble, F., Benedito, R., Bréant, C., Duarte, A. and Eichmann, A.** (2007). The Notch ligand Delta-like 4 negatively regulates endothelial tip cell formation and vessel branching. *Proceedings of the National Academy of Sciences of the United States of America* **104**, 3225-3230.
-

- Suri, C., Jones, P. F., Patan, S., Bartunkova, S., Maisonpierre, P. C., Davis, S., Sato, T. N. and Yancopoulos, G. D. (1996). Requisite role of angiopoietin-1, a ligand for the TIE2 receptor, during embryonic angiogenesis. *Cell* **87**, 1171-1180.
- Suzuki-Inoue, K., Inoue, O., Ding, G., Nishimura, S., Hokamura, K., Eto, K., Kashiwagi, H., Tomiyama, Y., Yatomi, Y., Umemura, K. et al. (2010). Essential *in vivo* roles of the C-type lectin receptor CLEC-2: embryonic/neonatal lethality of CLEC-2-deficient mice by blood/lymphatic misconnections and impaired thrombus formation of CLEC-2-deficient platelets. *The Journal of Biological Chemistry* **285**, 24494-24507.
- Suzuki-Inoue, K., Kato, Y., Inoue, O., Kaneko, M. K., Mishima, K., Yutaka, Y., Yamazaki, Y., Narimatsu, H. and Ozaki, Y. (2007). Involvement of the snake toxin receptor CLEC-2, in podoplanin-mediated platelet activation, by cancer cells. *The Journal of Biological Chemistry* **282**, 25993-26001.
- Tammela, T. and Alitalo, K. (2010). Lymphangiogenesis: molecular mechanisms and future promise. *Cell* **140**, 460-476.
- Tammela, T., Saaristo, A., Holopainen, T., Lyytikä, J., Kotronen, A., Pitkonen, M., Abo-Ramadan, U., Ylä-Herttua, S., Petrova, T. V. and Alitalo, K. (2007). Therapeutic differentiation and maturation of lymphatic vessels after lymph node dissection and transplantation. *Nature Medicine* **13**, 1458-1466.
- Tammela, T., Saaristo, A., Lohela, M., Morisada, T., Tornberg, J., Normén, C., Oike, Y., Pajusola, K., Thurston, G., Suda, T. et al. (2005). Angiopoietin-1 promotes lymphatic sprouting and hyperplasia. *Blood* **105**, 4642-4628.
- Tammela, T., Zarkada, G., Wallgard, E., Murtomäki, A., Suchting, S., Wirzenius, M., Waltari, M., Hellström, M., Schomber, T., Peltonen, R. et al. (2008). Blocking VEGFR-3 suppresses angiogenic sprouting and vascular network formation. *Nature* **454**, 656-660.
- Toikkanen, S., Pylkkänen, L. and Joensuu, H. (1997). Invasive lobular carcinoma of the breast has better short- and long-term survival than invasive ductal carcinoma. *British Journal of Cancer* **76**, 1234-1240.
- Tremblay, A., Tremblay, G. B., Labrie, C., Labrie, F. and Giguère, V. (1998). EM-800, a novel antiestrogen, acts as a pure antagonist of the transcriptional functions of estrogen receptors α and β . *Endocrinology* **139**, 111-118.
- Uchino, S., Ichikawa, S., Okubo, M., Nakamura, Y. and Imura, A. (1987). Methods of detection of lymphatics and their changes with oestrous cycle. *International Angiology* **6**, 271-278.
- Uhrin, P., Zaujec, J., Breuss, J. M., Olcaydu, D., Chrenek, P., Stockinger, H., Fuertbauer, E., Moser, M., Haiko, P., Fässler, R. et al. (2010). Novel function for blood platelets and podoplanin in developmental separation of blood and lymphatic circulation. *Blood* **115**, 3997-4005.
- Valtola, R., Salven, P., Heikkilä, P., Taipale, J., Joensuu, H., Rehn, M., Pihlajaniemi, T., Weich, H., deWaal, R. and Alitalo, K. (1999). VEGFR-3 and its ligand VEGF-C are associated with angiogenesis in breast cancer. *The American Journal of Pathology* **154**, 1381-1390.
- van der Putte, S. C. J. (1975). The development of the lymphatic system in man. *Advances in Anatomy, Embryology and Cell Biology* **51**, 3-60.

-
- van Tetering, G., van Diest, P., Verlaan, I., van der Wall, E., Kopan, R. and Vooijs, M. (2009). Metalloprotease ADAM10 is required for Notch1 site 2 cleavage. *The Journal of Biological Chemistry* **284**, 31018-31027.
- Veikkola, T., Jussila, L., Mäkinen, T., Karpanen, T., Jeltsch, M., Petrova, T. V., Kubo, H., Thurston, G., McDonald, D. M., Achen, M. G. et al. (2001). Signalling via vascular endothelial growth factor receptor-3 is sufficient for lymphangiogenesis in transgenic mice. *The EMBO Journal* **20**, 1223-1231.
- Veltmaat, J. M., Mailloux, A. A., Thiery, J. P. and Bellusci, S. (2003). Mouse embryonic mammaryogenesis as a model for the molecular regulation of pattern formation. *Differentiation* **71**, 1-17.
- Volchek, M., Girling, J. E., Lash, G. E., Cann, L., Kumar, B., Robson, S. C., Bulmer, J. N. and Rogers, P. A. W. (2010). Lymphatics in the human endometrium disappear during decidualization. *Human Reproduction* **25**, 2455-2464.
- Voros, G., Maquoi, E., Demeulemeester, D., Clerx, N., Collen, D. and Lijnen, H. R. (2005). Modulation of angiogenesis during adipose tissue development in murine models of obesity. *Endocrinology* **146**, 4545-4554.
- Walker, N. I., Bennett, R. E. and Kerr, J. F. R. (1989). Cell death by apoptosis during involution of the lactating breast in mice and rats. *American Journal of Anatomy* **185**, 19-32.
- Walton, K. D., Wagner, K.-U., Rucker, E. B., Shillingford, J. M., Miyoshi, K. and Hennighausen, L. (2001). Conditional deletion of the *bcl-x* gene from mouse mammary epithelium results in accelerated apoptosis during involution but does not compromise cell function during lactation. *Mechanisms of Development* **109**, 281-293.
- Wang, H. U., Chen, Z.-F. and Anderson, D. J. (1998). Molecular distinction and angiogenic interaction between embryonic arteries and veins revealed by ephrin-B2 and its receptor Eph-B4. *Cell* **93**, 741-753.
- Wang, Z., Juttermann, R. and Soloway, P. D. (2000). TIMP-2 is required for efficient activation of proMMP-2 *in vivo*. *The Journal of Biological Chemistry* **275**, 26411-26415.
- Wasif, N., Maggard, M. A., Ko, C. Y. and Giuliano, A. E. (2010). Invasive lobular vs. ductal breast cancer: a stage-matched comparison of outcomes. *Annals of Surgical Oncology* **17**, 1862-1869.
- Watson, C. J. and Khaled, W. T. (2008). Mammary development in the embryo and adult: a journey of morphogenesis and commitment. *Development* **135**, 995-1003.
- Watt, S. M., Gschmeissner, S. E. and Bates, P. A. (1995). PECAM-1: its expression and function as a cell adhesion molecule on hemopoietic and endothelial cells. *Leukemia & Lymphoma* **17**, 229-244.
- Wetterwald, A., Hofstetter, W., Cecchini, M. G., Lanske, B., Wagner, C., Fleisch, H. and Atkinson, M. (1996). Characterization and cloning of the E11 antigen, a marker expressed by rat osteoblasts and osteocytes. *Bone* **18**, 125-132.
- Wigle, J. T., Chowdhury, K., Gruss, P. and Oliver, G. (1999). *Prox1* function is crucial for mouse lens-fibre elongation. *Nature Genetics* **21**, 318-322.
- Wigle, J. T., Harvey, N., Detmar, M., Lagutina, I., Grosveld, G., Gunn, M. D., Jackson, D. G. and Oliver, G. (2002). An essential role for *Prox1* in the induction of the lymphatic endothelial cell phenotype. *The EMBO Journal* **21**, 1505-1513.
-

-
- Wigle, J. T. and Oliver, G.** (1999). *Prox1* function is required for the development of the murine lymphatic system. *Cell* **98**, 769-778.
- Williams, M. C., Cao, Y., Hinds, A., Rishi, A. K. and Wetterwald, A.** (1996). T1 alpha protein is developmentally regulated and expressed by alveolar type I cells, choroid plexus, and ciliary epithelia of adult rats. *American Journal of Respiratory Cell and Molecular Biology* **14**, 577-585.
- Wilting, J., Aref, Y., Huang, R., Tomarev, S. I., Schweigerer, L., Christ, B., Valasek, P. and Papoutsis, M.** (2006). Dual origin of avian lymphatics. *Developmental Biology* **292**, 165-173.
- Wilting, J., Buttler, K., Schulte, I., Papoutsis, M., Schweigerer, L. and Männer, J.** (2007). The proepicardium delivers hemangioblasts but not lymphangioblasts to the developing heart. *Developmental Biology* **305**, 451-459.
- Witmer, A. N., van Blijswijk, B. C., Dai, J., Hofman, P., Partanen, T. A., Vrensen, G. F. J. M. and Schlingemann, R. O.** (2001). VEGFR-3 in adult angiogenesis. *The Journal of Pathology* **195**, 490-497.
- Witte, M. H., Bernas, M. J., Martin, C. P. and Witte, C. L.** (2001). Lymphangiogenesis and lymphangiodysplasia: from molecular to clinical lymphology. *Microscopy Research and Technique* **55**, 122-145.
- Wong, S. Y., Haack, H., Crowley, D., Barry, M., Bronson, R. T. and Hynes, R. O.** (2005). Tumor-secreted vascular endothelial growth factor-C is necessary for prostate cancer lymphangiogenesis, but lymphangiogenesis is unnecessary for lymph node metastasis. *Cancer Research* **65**, 9789-9798.
- Woo, C. S., Silberman, H., Nakamura, S. K., Ye, W., Sposto, R., Colburn, W., Waisman, J. R. and Silverstein, M. J.** (2002). Lymph node status combined with lymphovascular invasion creates a more powerful tool for predicting outcome in patients with invasive breast cancer. *The American Journal of Surgery* **184**, 337-340.
- Wu, J., Richer, J., Horwitz, K. B. and Hyder, S. M.** (2004). Progesterin-dependent induction of vascular endothelial growth factor in human breast cancer cells: preferential regulation by progesterone receptor B. *Cancer Research* **64**, 2238-2244.
- Xu, Y., Yuan, L., Mak, J., Pardanaud, L., Caunt, M., Kasman, I., Larrivée, B., del Toro, R., Suchting, S., Medvinsky, A. et al.** (2010). Neuropilin-2 mediates VEGF-C-induced lymphatic sprouting together with VEGFR3. *The Journal of Cell Biology* **188**, 115-130.
- Yang, Z., Strickland, D. K. and Bornstein, P.** (2001). Extracellular matrix metalloproteinase 2 levels are regulated by the low density lipoprotein-related scavenger receptor and thrombospondin 2. *The Journal of Biological Chemistry* **276**, 8403-8408.
- Yi, M. and Schnitzer, J. E.** (2009). Impaired tumor growth, metastasis, angiogenesis and wound healing in annexin A1-null mice. *Proceedings of the National Academy of Sciences of the United States of America* **106**, 17886-17891.
- Yuan, L., Moyon, D., Pardanaud, L., Bréant, C., Karkkainen, M. J., Alitalo, K. and Eichmann, A.** (2002). Abnormal lymphatic vessel development in neuropilin 2 mutant mice. *Development* **129**, 4797-4806.
-

-
- Zagzag, D., Friedlander, D. R., Dosik, J., Chikramane, S., Chan, W., Greco, M. A., Allen, J. C., Dorovini-Zis, K. and Grumet, M.** (1996). Tenascin-C expression by angiogenic vessels in human astrocytomas and by human brain endothelial cells *in vitro*. *Cancer Research* **56**, 182-189.
- Zagzag, D., Friedlander, D. R., Miller, D. C., Dosik, J., Cangiarella, J., Kostianovsky, M., Cohen, H., Grumet, M. and Greco, M. A.** (1995). Tenascin expression in astrocytomas correlates with angiogenesis. *Cancer Research* **55**, 907-914.
- Zagzag, D., Shiff, B., Jallo, G. I., Greco, M. A., Blanco, C., Cohen, H., Hukin, J., Allen, J. C. and Friedlander, D. R.** (2002). Tenascin-C promotes microvascular cell migration and phosphorylation of focal adhesion kinase. *Cancer Research* **62**, 2660-2668.
- Zawieja, D. C.** (2009). Contractile physiology of lymphatics. *Lymphatic Research and Biology* **7**, 87-96.
- Zeng, Y., Opeskin, K., Goad, J. and Williams, E. D.** (2006). Tumor-induced activation of lymphatic endothelial cells via vascular endothelial growth factor receptor-2 is critical for prostate cancer lymphatic metastasis. *Cancer Research* **66**, 9566-9575.
- Zeps, N., Bentel, J. M., Papadimitriou, J. M. and Dawkins, H. J. S.** (1999). Murine progesterone receptor expression in proliferating mammary epithelial cells during normal pubertal development and adult estrous cycle: association with ER α and ER β status. *Journal of Histochemistry & Cytochemistry* **47**, 1323-1330.
- Zhang, C., Tian, L., Chi, C., Wu, X., Yang, X., Han, M., Xu, T., Zhuang, Y. and Deng, K.** (2010). *Adam10* is essential for early embryonic cardiovascular development. *Developmental Dynamics* **239**, 2594-2602.
- Zhang, Q., Lu, Y., Proulx, S. T., Guo, R., Yao, Z., Schwarz, E. M., Boyce, B. F. and Xing, L.** (2007). Increased lymphangiogenesis in joints of mice with inflammatory arthritis. *Arthritis Research & Therapy* **9**, R118.
- Zheng, W., Tammela, T., Yamamoto, M., Anisimov, A., Holopainen, T., Kaijalainen, S., Karpanen, T., Lehti, K., Ylä-Herttuala, S. and Alitalo, K.** (2011). Notch restricts lymphatic vessel sprouting induced by vascular endothelial growth factor. *Blood* **118**, 1154-1162.